

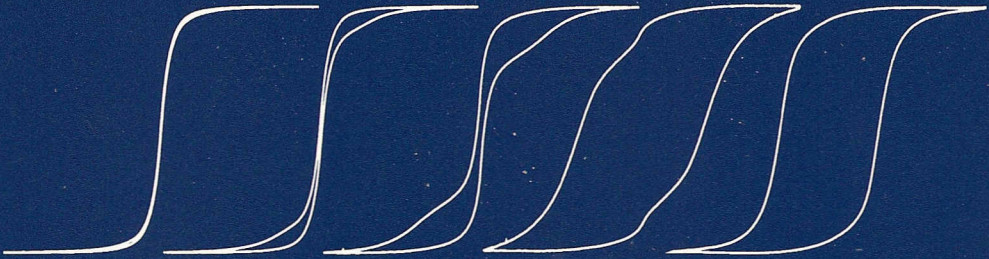
GEOLOGICA ULTRAIECTINA

Mededelingen van de
Faculteit Aardwetenschappen
Universiteit Utrecht

No. 177

**Rock-Magnetic Studies
on Hematite, Maghemite and
Combustion-Metamorphic Rocks**

The quest to understand the 'hidden attraction' of rocks



Cor B. de Boer

GEOLOGICA ULTRAIECTINA

Mededelingen van de
Faculteit Aardwetenschappen
Universiteit Utrecht

No. 177

**Rock-Magnetic Studies
on Hematite, Maghemite and
Combustion-Metamorphic Rocks**

The quest to understand the 'hidden attraction' of rocks

Cor B. de Boer

Cover: hysteresis loops of various mixtures of hematite and maghemite

Rock-Magnetic Studies on Hematite, Maghemite and Combustion-Metamorphic Rocks

Gesteentemagnetische eigenschappen van hematiet, maghemiet
en verbrandings-metamorfe gesteenten

(met samenvatting in het Nederlands)

PROEFSCHRIFT

TER VERKRIJGING VAN DE GRAAD VAN DOCTOR AAN DE
UNIVERSITEIT UTRECHT, OP GEZAG VAN DE RECTOR
MAGNIFICUS, PROF. DR. H.O. VOORMA, INGEVOLGE HET
BESLUIT VAN HET COLLEGE VOOR PROMOTIES IN HET
OPENBAAR TE VERDEDIGEN OP MAANDAG 11 OKTOBER 1999
DES MIDDAGS TE 14.30 UUR

DOOR

CORNELIS BAUKE DE BOER

geboren op 18 november 1966, te Leeuwarden

1999

Promotor: **PROF. DR. C.G. LANGEREIS**
Faculty of Earth Sciences,
Paleomagnetic Laboratory 'Fort Hoofddijk',
Utrecht University, Utrecht, The Netherlands

Co-Promotor: **DR. M.J. DEKKERS**
Faculty of Earth Sciences,
Paleomagnetic Laboratory 'Fort Hoofddijk',
Utrecht University, Utrecht, The Netherlands

Members of the dissertation committee:

Prof. Dr. S.K. Banerjee
Institute for Rock Magnetism and Department of Geology and Geophysics,
University of Minnesota, Minneapolis, USA

Prof. Dr. B.H.W.S. de Jong
Faculty of Earth Sciences, Petrology Group, Utrecht University, Utrecht,
The Netherlands

Dr. E. Petrovský
Geophysical Institute, Academy of Sciences of the Czech Republic,
Prague, Czech Republic

Prof. Dr. C.J. Spiers
Faculty of Earth Sciences, Experimental Rock Deformation Group,
Utrecht University, Utrecht, The Netherlands

The research for this thesis was carried out at:

*Paleomagnetic Laboratory 'Fort Hoofddijk', Faculty of Earth Sciences,
Utrecht University, Budapestlaan 17, 3584 CD Utrecht, The Netherlands.
The work was conducted under the programme of the Dutch national research school,
the Vening Meinesz Research School of Geodynamics.*

ISBN 90-5744-035-0

With more knowledge comes a deeper, more wonderful mystery, luring one on to penetrate deeper still. Never concerned that the answer may prove disappointing, with pleasure and confidence we turn over each new stone to find unimagined strangeness leading on to more wonderful questions and mysteries — certainly a grand adventure

Richard Feynman

(What Do You Care What Other People Think?)

*Voor mijn ouders en Janny
Ter nagedachtenis aan Anneke Tea
(You are the wind beneath my wings)*

Contents

Introduction

Rock magnetism	11
Outline and summary of this thesis	21

Part I : Hematite

Ch. 1: Review on hematite (α -Fe ₂ O ₃): rock-magnetic and other relevant properties	27
Ch. 2: Thermomagnetic behaviour of hematite and goethite as a function of grain size in various non-saturating magnetic fields	59
Ch. 3: Low-temperature behaviour of hematites: susceptibility and magnetization increase on cycling through the Morin transition	81
Ch. 4: Unusual thermomagnetic behaviour of hematites: neoformation of a highly magnetic spinel phase on heating in air	111

Part II : Maghemite

Ch. 5: Review on maghemite (γ -Fe ₂ O ₃): rock-magnetic and other relevant properties	137
Ch. 6: Grain-size dependence of the rock-magnetic properties for a natural maghemite	177

Part III : Combustion-Metamorphic Rocks

Ch. 7: Introduction to China's coal fire problem	189
Ch. 8: Pleistocene coal fires in Xinjiang, Northwest China	193
Ch. 9: Rock-magnetic properties of baked and molten rocks overlying burnt coal seams in Northwest China	207

References	227
Samenvatting in het Nederlands (Summary in Dutch)	247
Dankwoord (Acknowledgements)	253
Curriculum Vitae	255

*Magnes, the lodestone I,
your painted sheaths defy,
without my help on Indians seas,
the best of you might die.*

*I guide the Pilots course,
his helping hand I am,
the mariner delights in me,
so doeth the merchant man.*

*My virtues are unknown,
my secrets hidden are,
by me the Court and Common weal,
are pleased very far.*

*No ship could sail on seas,
her course to run aright,
nor compass show the ready way,
were Magnes not of might.*

(Robert Norman, 16th century instrument maker)

Introduction

*The Magnet's name the observing Grecians drew
From the Magnetic region where it grew*

(Lucretius, as quoted by William Gilbert, *De Magnete*)

Rock magnetism

Rock magnetism is the geophysical discipline concerning the magnetic properties of rocks and naturally occurring minerals, or their synthetic equivalents. In practice, these are the oxides, oxyhydroxides and some sulphides of iron together with the rocks they are part of. Rock magnetists investigate how the magnetic properties of these minerals depend on factors such as grain size, grain shape, crystallinity, chemical composition, temperature and pressure. Furthermore, this discipline studies the origin and characteristics of the different types of remanent magnetizations which rocks and magnetic minerals can acquire in nature and under conditions which approximate those in nature. These conditions are rather different from those of interest in fine-particle magnetism as applied in permanent-magnet and magnetic-recording technology. Nevertheless, these sciences all build on the same basic physical laws such as ferromagnetism and the magnetic domain theory. In this, rock magnetism is an informative and fundamental study in its own right. However, it is both a basic and applied science. The study of the magnetic properties of rocks and minerals has substantially contributed to several fields in the Earth sciences, and its applications continue to expand. They play an important role in furthering our understanding of geological, geophysical, geochemical and climatological processes, particularly when combined with other multidisciplinary information.

Rock magnetism historically developed from two other disciplines: solid-state physics and paleomagnetism. Rock-magnetic investigations and techniques are basically an extension to rocks and minerals of studies of the classical magnetic materials, namely iron and other transition elements, their alloys and oxides. The primary objective of paleomagnetic research is to obtain a record of past configurations of the geomagnetic field. From this perspective, rock magnetism was developed to provide the physical understanding of the magnetic memory of rocks over geological time, and to prove the reliability of the natural remanent magnetization (NRM). In other words, it serves as a direct link between theoretical aspects of the physics of magnetism and paleomagnetic applications. Nowadays, the use of rock- and mineral-magnetic measurement techniques is no longer restricted to paleomagnetism alone, but these techniques are being applied in a wide variety of (Earth) scientific disciplines.

A benefit of rock-magnetic methods is undoubtedly that they can be applied to all geological settings, because virtually every rock type and soil contains magnetic minerals in trace amounts or more. A major analytical advantage of the use of mineral-magnetic techniques is their high sensitivity. In general, detection limits are much lower for magnetic measurements than for conventional geochemical, mineralogical, or petrographic methods such as X-ray diffraction or optical reflectance. Thus, by using rock-magnetic techniques, high-precision data sets can be obtained. Other advantages of rock-magnetic techniques are that they require little sample preparation, are relatively rapid and inexpensive, usually non-destructive, and often grain-size indicative. Especially, this latter aspect is a major asset because no other analytical technique is able to give information about the size of the particles involved. Furthermore, these techniques involve 'bulk' properties, which makes them complementary to geochemical and microscopical micro-analytical techniques, where usually only a fraction of the sample can be analyzed.

Applications of rock- and mineral-magnetic properties

Rock magnetism, having its origin as a fundamental physics discipline, contributes to our understanding of one of nature's most intriguing phenomena, magnetism. Through rock- and mineral-magnetic research fundamental properties of magnetic minerals were discovered and new concepts were formulated. From the many new findings, two deserve special mention: the concept of magnetic domains as postulated by Weiss in 1907 and the discovery of ferrimagnetism and antiferromagnetism by Louis Néel in the 1940's that was awarded the Nobel Prize in 1970. The study of the magnetic properties of rocks and minerals, however, also has a variety of applications that are more focussed on Earth scientific processes. Before detailing some concepts of magnetism and the magnetic recording process, several applications of rock- and mineral-magnetic properties are described first.

Understanding the Earth's magnetic field

First of all the study of the remanent magnetization in ancient rocks (paleomagnetism) contributes to our understanding of geomagnetism through the derived history of the direction and intensity of the Earth's magnetic field. Historical observations are very short, so the remanent magnetizations of geological and archaeological materials provide the only direct quantitative records of the past behaviour of one of the Earth's most important physical properties. As mentioned, paleomagnetism is concerned with the isolation of the original remanent magnetization imparted in the rocks and minerals at the time of their formation, the so-called primary magnetization. From this remanent magnetization the direction and the (relative) intensity of the ancient geomagnetic field can be recovered that prevailed at the location and at the time of formation of the rock. By measuring the primary magnetization of rocks of different ages, a record of the Earth's magnetic field in the past can be obtained. Through observations of polarity

reversals of magnetization and their frequency during geological time, paleosecular variation and paleointensities, paleomagnetism is able to determine the long and short-term nature of the ancient geomagnetic field. Since the geomagnetic field originates within the Earth's core, these studies are critical to our understanding of the origin and evolution of both the field itself (i.e. physics of the geodynamo) and the Earth's interior.

Geophysical and geological processes

In addition, paleomagnetic studies, supported by rock-magnetic research, have also contributed significantly to large-scale and local geophysical and geological studies. The recognition of the irregular pattern of polarity changes of the geomagnetic field during geological time led to the construction of the geomagnetic polarity time scale (GPTS), which is based on the pattern of marine magnetic anomalies on each side of mid-ocean ridges. This 'fingerprint' pattern of reversals of the geomagnetic field plays a major role in establishing an accurate geological time scale, and magnetostratigraphy has become a very important tool in correlating and dating rocks.

The remanent magnetization provides also a history of the plate-tectonic motions of continents and oceans over millions of years. Deviations of the measured direction of the primary magnetization from the one expected from an axial geocentric dipole can be interpreted in terms of latitudinal translation and/or rotation. This principle contributed to our understanding of the tectonic evolution of the Earth. Paleomagnetic evidence confirmed the concept of continental drift, whereas magnetic anomalies of oceanic crust have served as the primary data in our understanding of the evolution of oceanic lithosphere, i.e. the concept of sea-floor spreading. A combination of both concepts has led to the revolutionary theory of plate tectonics, i.e. the Earth's lithosphere, including the continental and oceanic crust, is divided into several rigid plates that 'float' and 'ride' on the plastic, partially molten asthenosphere. Nowadays, the same paleomagnetic principle is used successfully in solving especially small-scale tectonic and structural problems.

Other rock-magnetic measurements, especially the analysis of the anisotropy of magnetic susceptibility (AMS), also proved its usefulness in structural geology. The AMS reflects the magnetic fabric of a rock, which in turn can be used to obtain the petrofabric of rocks so that their origin and structural evolution can be derived. For instance, an analysis of the magnetic fabric of rocks can be used to detect subtle effects of strain in rocks at the first stages of deformation, which are not or hardly 'visible' using other techniques. Other effects of directional processes, such as the paleocurrent in sediments, can also be detected with this method.

The magnetic properties of rocks, including their remanent magnetization, cannot only provide information on their formation but also on their history. Although secondary remanent magnetizations, which are acquired in the period between formation of the rock and the present time, are generally considered as undesired 'noise' obscuring the primary signal, they can sometimes be used to date important geological or geochemical events in the geological history of the rock. These secondary components are due to the partly or completely overprinting of an older NRM or due to the growth of new magnetic minerals,

for instance, caused by orogenic activity. The growing recognition of the need for identification, isolation and dating of secondary magnetizations requires far greater rock-magnetic input to paleomagnetic studies.

Geochemical processes

Rock-magnetic measurements are also increasingly used to understand the transformations in the iron oxide/oxyhydroxide systems and for tracing the dissolution, remobilization and reprecipitation of iron. These methods contributed to the characterization of numerous geochemical processes including weathering, soil chemistry, diagenesis and identification of fossil oxidation fronts in marine sediments. In soil science, the mineral magnetic parameters give valuable information about the soil formation process and the nature of the subsoil, and are used for magnetic characterization of soil profiles and types. Moreover, the type of magnetic minerals formed proves to be a good indicator of moisture, pH and redox conditions. Rock-magnetic measurements are thus a useful complementary technique when used in combination with conventional geochemical and other methods.

Environmental and climatological processes

Recently, there has been a vast increase in the use of magnetic techniques when it was recognized that variations in magnetic mineralogy, concentration and/or grain size are influenced by environmental and climate conditions prevailing over the sediment source and depositional area. Magnetic measurements have contributed to global-change reconstructions from marine and loess-paleosol sequences. The influence of climate change on magnetic-mineral records is demonstrated by comparing magnetic parameters to geochemical and biological proxies for climate, as well as by spectral analysis of magnetic-property records that establishes correlation with orbitally driven climate cycles. Hence, mineral-magnetic parameters provided by rock magnetism are increasingly used by other geodisciplines including climatology, paleoceanography, sedimentology, and soil science. This has led to the development of a new discipline called '*environmental magnetism*'. It involves the application of rock- and mineral-magnetic techniques to situations in which the transport, deposition or transformation of magnetic grains is influenced by environmental processes in the atmosphere, hydrosphere, and lithosphere. Here, the properties of magnetic minerals are used as proxy parameters for many purposes such as paleoclimate analysis, paleoceanographic studies, provenance studies of sediments, studies of anthropogenically-induced pollution, and archeological investigations. The subject has grown quickly as new measurement techniques, analytical equipment and applications have been developed. However, paleoclimatic interpretations of magnetic data still remain model-dependent and to some extent non-unique, both in the inversion of magnetic measurements for quantification of mineralogy and grain size, and in linking variations in these sediment characteristics to specific climatic changes.

Magnetism and magnetic recording

Magnetism is without doubt one of the most mysterious and elusive physical phenomena in nature. The recognition of this invisible force triggered much research in solid state physics and chemistry, and led to various applications of which the compass for navigation purposes was the first. Magnetism is created on different scales by the moving of electrically charged bodies. On a large-scale, convective fluid motions in the outer core of the Earth are responsible for the geomagnetic field. On the atomic scale, magnetism arises from the orbiting of electrons around a nucleus and from the spinning of the electrons around their axis, of which the latter is the most important. Especially the magnetic properties of the first transition metal series (Fe, Ni, Co), their alloys and compounds are the subject of classical magnetic research. Their uncompensated electron spins in the five *3d*-orbitals and the existence of (super)exchange interactions between atoms are responsible for the observed strong ferromagnetism. In addition to the strong intensity of their magnetization, some of these ferromagnetic materials show another very important physical phenomenon. They have the ability to record and thus 'remember' the direction of a previous applied magnetic field, the so-called hysteresis-effect or remanence acquisition. After removal of the field the induced magnetization does not return to zero but retains a memory of the previously applied field. The permanent magnetization that remains after the external field is removed is called the remanent magnetization. It is this unique property of ferromagnetism that makes these materials so important and even vital (e.g. computers) in modern society. It is used in a wide branch of sciences and technologies among which are the permanent-magnet industry, the magnetic-recording technology and, more confined to Earth sciences, last but not least paleomagnetism. In this perspective, paleomagnetism is the science of reading and interpreting the magnetic signal of rocks, while rock magnetism concerns the study of the actual recording process in rocks.

Magnetic recording processes

Rocks are by far the oldest magnetic-recording devices on Earth. Their constituent magnetic minerals have recorded ancient information of billions of years old, which can nowadays be decoded in the laboratory. Yet, in 1889, Valdemar Poulsen was able to successfully imitate nature by inventing the magnetic-recording technology. The principles of magnetic recording in paleomagnetism and magnetic-recording industry are actually the same but the physical parameters of recording are different. For instance, the strength of the Earth's magnetic field is much weaker (present geomagnetic field ~30–60 μT) than the magnetic fields involved in the magnetic-recording technology (typically ~30–80 mT bias fields in audio recording). Furthermore, in magnetic-recording technology the magnetic signal, e.g. music or data, is recorded by highly concentrated fine-grained magnetic particles of identical chemical composition, shape (needle-like) and grain size, and they are oriented in the same direction on the surface of a tape or disk. Rocks, on the other hand, only contain dilute suspensions of magnetic material. Their magnetic-recording particles usually have different compositions, shapes and sizes

and are generally oriented at random. In nature, the recording temperatures range from ambient temperatures up to $\sim 680^{\circ}\text{C}$, that is much higher than those used in technology. The most abundant ferromagnetic minerals present in terrestrial rocks that are capable of carrying a remanent magnetization are the iron(-titanium) oxides and some iron sulphides.

Like technology, nature also provides different recording mechanisms. The primary remanence can be acquired by one of three basic mechanisms: *thermoremanent magnetization* (TRM), *chemical remanent magnetization* (CRM) and *detrital remanent magnetization* (DRM). This respectively are thermodynamic, chemical and mechanical processes. Hence, the remanence acquisition mechanism depends upon the mode of formation of the rock. Sedimentary rocks and soils can acquire primary CRMs and DRMs, while the acquisition of a primary TRM is typically restricted to igneous rocks.

Igneous rocks, i.e. intrusives and volcanic lavas, which have been at high temperatures during their formation, acquire a TRM when the constituent magnetic minerals cool through their blocking temperature spectra in the ambient geomagnetic field. Below the Curie temperature (T_c) an exchange interaction (magnetostatic alignment forces) between atoms begins to dominate over the randomizing effect of thermal fluctuations. A strong spontaneous magnetization is developed within these crystals parallel (or, very rarely, antiparallel) to the ambient geomagnetic field provided that the rock is magnetically isotropic, i.e. the orientation of individual grains in a sample is random, or nearly random.

The response time of the magnetic moments of the grains to changes in the magnetic field (relaxation time) is very short (typically a few seconds) just below T_c . However, the relaxation time increases exponentially with decreasing temperature. At normal earth-surface temperature the relaxation time may be billions of years, even many times exceeding the age of the Earth. The stability of a signal recorded in this way can thus be that high that it cannot be erased by subsequent geomagnetic field changes and stays practically unchanged in the rock for millions or billions of years. This is the fundamental principle of paleo- and rock magnetism.

In sedimentary rocks a stable CRM can be acquired either by precipitation of a magnetic mineral out of solution or by alteration of one mineral to another. In sufficiently small magnetic particles (superparamagnetic grains) thermal fluctuations dominate at ambient temperatures. However, magnetostatic forces overcome thermal fluctuations if the particle grows through a critical value, i.e. its blocking volume. The concept of blocking volume is analogous to that of blocking temperature; the relaxation time increases exponentially with increasing grain volume as well. A stable remanence acquired in this way is aligned with the ambient geomagnetic field and its stability is similar to that of TRM.

A detrital remanent magnetization is another acquisition process that can occur in sediments that contain small magnetic particles. These grains, that were eroded from pre-existing rock formations, carry already a TRM or CRM and they will therefore act as small magnets. When they settle through the water column, they will become statistically aligned with a small preference for the direction of the ambient magnetic field. This orientation may be preserved during the depositional process, so that the resultant

sediment acquires a remanent magnetization that is parallel to the field at the time of deposition.

Stability of the signal

Subsequent to formation, the primary magnetization becomes a non-equilibrium state because of a change in recording conditions (e.g. a polarity reversal of the geomagnetic field). The original signal may decay either partly or completely, and further components may be added by a number of perturbation processes. These subsequent magnetizations are called *secondary magnetizations*. The resultant multi-component magnetization is referred to as *natural remanent magnetization* (NRM).

Just like the various magnetic tapes (e.g. ferri, chromium or metal) have different qualities, the different magnetic carriers in rocks also have their own characteristic properties and stability, i.e. their resistance to demagnetizing influences, also referred to as coercivity. Through observations of magnetic processes in natural or synthetic materials, rock magnetists are able to determine the optimal parameters and measurement procedure to discriminate between different carriers of remanence and different mechanisms of remanence acquisition.

The stability of the signal not only depends on the acquisition process and type of magnetic mineral involved, but also depends on the domain state of the magnetic particles. The magnetic domain state of a particle, i.e. the amount of uniformly magnetized domains present, is related to its grain size. Small grains are uniformly magnetized and consist only of one magnetic domain. These so-called single-domain (SD) grains are too small to accommodate a domain wall. The signal they carry is geologically very stable because it can only be changed by the simultaneous rotation of all the spin vectors. Larger grains are typically multidomain (MD), so are non-uniformly magnetized. The magnetization of these grains can change much easier by mobility of domain walls. Consequently, their remanence is less stable and thus they are less obviously suitable for retaining the paleomagnetic field. Hence, a major part of the research field of rock and mineral magnetism is concerned with the search for grain-size dependent parameters and methods, which are diagnostic for and can discriminate between single-domain and multidomain behaviour. The threshold size between SD and MD grains is different for different types of magnetic minerals.

Reading the signal

The technique of reading the paleomagnetic signal is in practice less simple than playing a tape in a cassette player or reading data from the hard disk in a computer. The paleomagnetic signal, for instance, is much weaker, much older (typically millions of years), and may be contaminated with noise from other geological or geochemical events which obscure the details of the original signal. The nucleus of paleomagnetic research is to recognize and eliminate secondary components, in order to isolate and characterize the primary NRM component. To distinguish between primary and secondary magnetizations

paleomagnetists use various demagnetization procedures on the NRM. The two most commonly employed 'cleaning' techniques are alternating field (AF) demagnetization and thermal demagnetization. In these cleaning procedures the remanence vector is step by step demagnetized by increasing temperature or alternating magnetic fields in order to selectively remove that part of the NRM with the shortest relaxation time. The most stable remanence component is often argued to be the primary magnetization, but this 'assumption' unfortunately does not always apply. A variety of more refined criteria for recognizing the primary NRM component have been developed in recent years, and must rely on sophisticated rock-magnetic techniques.

Rock-magnetic value of sediments

Already in the early days of paleomagnetism it was recognized that sediments potentially are an extremely valuable source of information for the paleomagnetic record. By their very nature, sediments may carry a continuous record of the ancient geomagnetic field. This in contrast to a pile of lava flows which represents a series of spot readings of the ancient geomagnetic field with varying and usually poorly defined time intervals between successive flows. Furthermore, sediments are more abundant compared to extrusive igneous rocks, are globally distributed and have an appropriate time control due to their fossil content and/or intercalated volcanic ash layers. However, the magnetic signal of sediments is generally much weaker than that carried by most igneous rocks, and until the early seventies it was not possible to 'read' the signal present in most sedimentary rocks. Moreover, the magnetic mineralogy and the acquisition processes of the NRM in sediments are more diverse and complex compared to those in igneous rocks. Consequently, most early paleomagnetic studies were confined to extrusive rocks because of their strong signal and relatively simple NRM acquisition process (TRM). The most important magnetic carriers in these rocks are magnetites containing different amounts of titanium, and hence most rock-magnetic research was focussed on the magnetic properties of these minerals and their magnetization process.

There have, however, been several developments to cause paleomagnetic data to be increasingly retrieved from sedimentary rocks. First, the development of much more sensitive spinner and cryogenic magnetometers (early 1970's) and improvements in the techniques for the removal of undesired magnetizations has enabled reliable measurements of the NRM of virtual every sediment. The 'rock-magnetic toolbox' became distinctly larger and much equipment has become adapted for the measurement of weakly magnetized material. This made a more precise identification of the various remanence carriers possible and led to a better understanding of the different remanence acquisition mechanisms in sediments, although the intricacies of all possible processes that may occur during and (soon) after sedimentation are still not sufficiently understood. The rock-magnetic value of sediments is also considerably increased because of the worldwide efforts to retrieve paleoclimate information from these types of rocks. Rock-magnetic data increasingly assist in the interpretation of these geological proxy records. Recent advances in measurement techniques and in studies of quantification,

calibration and/or modeling of magnetic properties enhanced the rock-magnetic value of sedimentary rocks even more.

Magnetic mineralogy of sediments: Ferric oxides

Clearly, for a scientifically sound paleomagnetic interpretation of sedimentary rocks the magnetic mineralogy and the various NRM acquisition processes must be understood in detail. So far, most rock-magnetic research was focussed on (titanium-substituted) magnetites because of their common occurrence in many rock types (e.g. ocean floor basalts) and their strong magnetization. However, in a wide variety of sedimentary rocks and soils, especially the iron oxides maghemite ($\gamma\text{-Fe}_2\text{O}_3$) and hematite ($\alpha\text{-Fe}_2\text{O}_3$) are important representatives of the remanence carrying particles. These ferric oxides are more stable under the oxidizing conditions that prevail during most sediment and soil formation processes than the ferrous oxide magnetite (Fe_3O_4). Hence, their importance for paleomagnetism and other geoscience disciplines is well recognized. Nevertheless, our understanding of their magnetic properties is still far from complete. To this end, more comprehensive rock-magnetic data from well-defined hematite and maghemite are badly needed.

Maghemite ($\gamma\text{-Fe}_2\text{O}_3$)

Maghemite is the fully oxidized equivalent of magnetite. It has the same chemical composition as hematite, but its crystal structure is essentially similar to magnetite. Consequently, the average magnetic hysteresis properties of maghemite resemble those of magnetite to a large extent. For this reason, maghemite was often confused with magnetite and its importance to paleomagnetism was longtime underestimated. It is now recognized that this ferrimagnetic remanence carrier has its own characteristic and distinguishable magnetic properties. Maghemite is only slightly less magnetic than magnetite, having room temperature saturation magnetizations of ~ 74 and $\sim 92 \text{ Am}^2 \text{ kg}^{-1}$, respectively. Its magnetic ordering temperature T_c is $\sim 645^\circ\text{C}$, higher than that of magnetite ($\sim 580^\circ\text{C}$). However, grain-size dependent rock-magnetic properties of maghemite are poorly known, which hinders a reliable paleomagnetic interpretation of maghemite-bearing rocks. Furthermore, $\gamma\text{-Fe}_2\text{O}_3$ is thermodynamically metastable and converts to weakly magnetic $\alpha\text{-Fe}_2\text{O}_3$ when heated in vacuum or in air. This may give rise to disturbing behaviour of the NRM during thermal demagnetization, an aspect which certainly warrants investigation. The conversion reaction is complex and may occur over a rather wide temperature range from $\sim 200^\circ\text{C}$ to over 700°C . The different conversion temperatures may be related to differences in grain size, crystallinity and isomorphous substitution.

Hematite ($\alpha\text{-Fe}_2\text{O}_3$)

Hematite has only a weak spontaneous magnetization, about 0.5 percent of that of magnetite. Nevertheless, the remarkably high coercivities of hematite (at least in small particles) ensure that this mineral is of importance in paleomagnetism because the NRM acquired by rocks containing hematite can be magnetically very stable. Furthermore, because of its block-shaped magnetization curve the (un)blocking temperatures of the NRM and other remanences are concentrated just below its Curie temperature ($\sim 680^\circ\text{C}$). These are the highest (un)blocking temperatures of all common natural magnetic carriers, and consequently it is the ultimate remanence isolated in thermal demagnetization. Moreover, these relatively high coercivities and blocking temperatures prevents the hematite remanence from being resetted during diagenesis or low-grade metamorphism.

However, unlike magnetite, the magnetism of hematite is not yet completely understood. Hematite is known for its complex and highly variable magnetic properties. Much of the difficulty is caused by the sensitivity of its magnetic properties to impurities and imperfections. These aspects have a much higher impact on the magnetic properties of relatively weakly magnetized hematite than they will have on those of the other, more strongly magnetized iron oxides.

Basically, two magnetic moments in hematite can be distinguished: the canted moment and the defect moment. The canted moment is caused by a very small deviation ($\sim 0.1^\circ$) from the ideal antiferromagnetic coupling, giving rise to a small ferrimagnetic moment. The defect moment is rather loosely defined as originating from 'defects' in the crystal structure, and it may be susceptible to heat treatment and applied stress. It is the interplay of different contributions of these canted and defect moments which gives rise to the observed variability of hematite's rock-magnetic parameters. However, some quantification of the relationships between both moments is, unfortunately not yet available.

Outline and summary of this thesis

This thesis is structured in three parts. Part I and II comprise fundamental research of the magnetic properties of hematite and maghemite, respectively, essential to improve the quality of paleomagnetic interpretations of sedimentary rocks in particular. The main purpose is to develop diagnostic rock-magnetic parameters of α -Fe₂O₃ and γ -Fe₂O₃ and to obtain more insight in the causes of their variation. Part III deals with thermally altered sediments associated with extensive subsurface coal fires in China. The combustion-metamorphic rocks are used to date paleo-coal fires magneto-stratigraphically and various applications of their magnetic properties are discussed.

Part I: Hematite

Chapter 1 reviews the complex magnetic properties of hematite and their dependence on variations in temperature, magnetic field, pressure, grain size and chemical composition. It builds on earlier reviews by *Fuller (1970)* and *O'Reilly (1984)* and supplements detailed information about relevant chemical and physical properties necessary for a proper understanding of hematite's magnetic properties. The review emphasizes the disproportionately high effect of the defect moment on the magnetic properties of hematite compared to that present in highly magnetic minerals such as magnetite and maghemite. In addition, it is argued that changes of magnetic properties within a synthesized series of hematites are often erroneously assigned to the change in one single parameter. Parameters such as grain size, degree of isomorphous substitution, crystallinity, internal stress as well as concentration and type of defects, generally are interconnected, have their own specific effect on hematite's magnetic properties and strongly depend on the mode of formation.

In **Chapter 2** the thermomagnetic behaviour of hematite and goethite are described as a function of grain size in various non-saturating magnetic fields. We were able to considerably enhance the interpretive value of thermomagnetic analysis of non-saturated magnetic minerals. The shape of the thermomagnetic heating curves of non-saturated minerals is shown to be dependent on the competitive interplay between the temperature dependence of the exchange energy and that of the coercive force with respect to the applied field. Stirring between subsequent runs is put forward as a tool to distinguish between temperature-induced chemical or structural changes and 'genuine' magnetic changes. Furthermore, based on their specific thermomagnetic behaviour, we could discriminate between hematites which magnetic properties are dominated by the canted moment only (defect-poor types) and those that are more affected by both the canted and defect moment (defect-rich types).

Chapter 3 examines the low-temperature behaviour of various hematite types. It is shown that the low-field susceptibility and the magnetization induced in non-saturating fields can be increased for coarse-grained hematite on cycling through the Morin transition. The observations are interpreted in terms of transdomain changes (i.e. increase in the number of magnetic domains) made possible by the low anisotropy at the Morin transition. In this way the magnetic state of large 'metastable' single-domain and pseudo-single-domain particles can be changed. Our findings may have serious implications for paleomagnetic results obtained from red beds, especially when the dominant remanence is carried by relatively pure specularite particles because their Morin transition temperature ($\sim -10^\circ\text{C}$) would lie within the range of Earth's surface temperatures.

Chapter 4 describes a new magnetic phase with a Curie point of $470\text{--}475^\circ\text{C}$. During heating in air above at least 400°C , it forms thin epitaxial outgrowths on the basal planes of specific hematite types with virtually no isomorphous substitution. The phase has a cubic spinel structure with a unit cell length similar to maghemite. The suggested structure is that of pure maghemite with part of the vacancies on tetrahedral interstices. A mechanism is proposed in which the structural rearrangement caused by the thermally activated release of tightly held structurally bound water may trigger the necessary redistribution of the oxygen framework from hexagonal-close-packed to cubic-close-packed in the outermost layers of hematite particles.

Part II: Maghemite

Chapter 5 presents a synopsis of current knowledge of the magnetic properties of maghemite, supplemented by relevant chemical and physical crystallographic data as well as an outline of maghemite's geological occurrence and general formation processes. No comprehensive review relating maghemite magnetic properties to provenance and mode of formation was yet available in literature. It appears that what is called maghemite actually is various different phases, characterized by a different positioning of the vacancies over the octahedral and/or tetrahedral interstices of the spinel lattice. The effect of these different vacancy arrangements on the magnetic properties is not known exactly yet.

In **Chapter 6** the grain-size dependence of the rock-magnetic properties for a natural maghemite is presented. They appear to be less prominent than those of magnetite of nominally the same size. The maghemite partly survives heating to 700°C allowing direct measurement of the Curie point at 610°C . It is made plausible that Al for Fe substitution stabilizes the maghemite structure, and the transformation degree of maghemite to hematite during a thermomagnetic run is shown to be grain-size dependent and thus kinetically related. Furthermore, it is suggested that the observed low-temperature behaviour of the induced anhysteretic remanent magnetization can be diagnostic of the presence of maghemite.

Part III: Combustion-metamorphic rocks

In 1997 the Paleomagnetic Laboratory '*Fort Hoofdijk*' became involved in the research and the efforts to control to subsurface coal fires in China by dating paleomagnetically the baked and molten rocks associated with the burnt coal seams. In the northern part of this country 55 coal fields suffer from extensive coal fires. Estimates of the annual loss of high-quality coal by spontaneous combustion range up to 200 million tons. Coal fires of this extent not only are an economic but also an environmental threat because of their significant contribution to the global CO₂ budget. It is estimated that the coal fires in Northern China produce 2–3% of the world's CO₂ emission resulting from the combustion of fossil fuels. **Chapter 7** outlines China's burning problem and reviews the causes of spontaneous combustion as well as the various subsurface coal fire spreading models.

The higher estimates for annual loss of coal and CO₂ output are essentially based on delineating coal fire boundaries from mapping burnt rocks recognized in remote sensing imagery and extending them underground using dip and thickness of the coal seams. Combined stratigraphic and paleomagnetic results presented in **Chapter 8**, show that the aforementioned estimates are greatly exaggerated, as over 85% of the burnt rocks in the studied area were formed during various stages in the Pleistocene. In the studied area, spontaneous combustion of coal fires is related to the creation of favourable outcrops by deformation, uplift and unroofing by erosion in combination with cyclic deposition and dissection related to climate change.

Chapter 9 addresses the magnetic properties of the combustion-metamorphic rocks. It is shown that the burnt rocks are high-quality geomagnetic field recorders with potential for paleointensity and paleosecular variation studies. Traces of native iron were detected in addition to various iron oxides indicating that the conditions during combustion can vary between effectively reducing to highly oxidizing. Furthermore, the thermally altered rocks appear to be substantially magnetically enhanced compared to their sedimentary protoliths. Magnetic anomaly modeling on burnt rocks has potential for coal exploration as well as for delineating areal extent and depth of (extinct) coal fires. This latter information can be used to refine the estimates of CO₂ emission and to further the understanding of the evolution and mechanism of coal fires.

Part I

Hematite ($\alpha\text{-Fe}_2\text{O}_3$)

*It is all very well to theorize,
but it is what we learn from experiment that really counts*

(Anonymous)

Chapter 1

Review on hematite (α -Fe₂O₃): rock-magnetic and other relevant properties

1.1 Introduction

Hematite (α -Fe₂O₃) is known for its highly variable and complex magnetic properties, which appear to be remarkably dependent on its mode of formation. Hematite is basically antiferromagnetic but it shows a weak ferromagnetic moment within the basal plane caused by a slight canting of the magnetic spins out of exact antiparallelism. Apart from this intrinsic or *canted moment*, hematite may have an additional weak magnetic moment caused by an ordered structure of chemical and/or structural defects in the lattice. This so-called *defect moment* is also present in other magnetic minerals. In weakly magnetic hematite, however, it affects the overall magnetic properties to a much higher extent compared to those of the highly magnetic iron oxides, magnetite (Fe₃O₄) and maghemite (γ -Fe₂O₃). The spontaneous magnetization of hematite due to the intrinsic moment is $\sim 0.4 \text{ Am}^2 \text{ kg}^{-1}$, which is two orders of magnitude lower than that of magnetite and maghemite, respectively ~ 92 and $\sim 74 \text{ Am}^2 \text{ kg}^{-1}$. Especially the defect moment is held responsible for hematite's highly variable magnetic properties. It is almost negligible in pure well-crystalline hematite, whereas it can be substantial in substituted and/or poorly ordered hematite. The relatively high influence of the defect moment also explains why the magnetic properties of hematite in particular are strongly dependent on the mode of formation.

As a consequence of its relatively low spontaneous magnetization, the natural remanent magnetization (NRM) carried by hematite is often weak compared to that carried by magnetite and maghemite. Hematite, however, is important in paleomagnetic research because its coercivity and unblocking temperature are relatively high, which generally ensures a highly stable remanence. In addition, hematite is thermodynamically the most stable iron oxide under ambient (oxidizing) conditions and it is the only or dominant magnetic carrier in several rock types, of which the so-called 'red beds' are the best known example. A short outline of the geological settings in which hematite can be an important NRM carrier is given in **Section 1.2**, together with a brief summary of the general processes by which hematite is formed in these particular environments.

For a proper understanding of hematite's magnetic properties some basic knowledge of its crystal chemistry and other relevant chemical and physical properties is required. In **Subsection 1.3.1** we review the crystal structure of pure 'ideal' hematite.

Natural hematites, however, often contain impurities. In **Subsection 1.3.2**, we describe how the unit cell of hematite is modified by cationic as well as anionic substitution. Hematite's magnetic properties may be directly affected by impurities through changes in the balance between the antiferromagnetic sublattices (isomorphous substitution of Fe by a cation of different atomic magnetic moment) and more indirectly through changes in interatomic distances and the possible inducement of substantial structural strain. In this section and subsequent sections on hematite's magnetic properties, we will focus on cationic substitution by diamagnetic Ti^{4+} and Al^{3+} and anionic substitution by $(OH)^-$ -groups (i.e. incorporation of structurally bound water), because these are the most widespread in nature. So far, anionic substitution has received surprisingly little attention in most rock- and mineral-magnetic investigations concerning hematite. It appears, however, to be inherent to most low-temperature formation processes of hematite. Hence, the observed variability in the magnetic properties of especially low-temperature hematites might be partly attributed to the incorporation of OH into the structure.

Subsection 1.3.3 is concerned with variations in microstructure, that is the crystal morphology, crystallinity, microporosity and crystallite and/or grain size. These parameters in turn may, once more, indirectly influence the magnetic properties of hematite. The microstructure strongly depends on the conditions under which the crystals were formed, such as temperature, oxygen fugacity, pH, etc. Impurities may also modify the microstructure of a material.

Apart from grain size it is not yet clear to what extent the other parameters modify the canted and particularly the defect moment of hematite. Nevertheless, they are important candidates for explaining the highly variable and sometimes even contradictory mineral-magnetic results obtained on hematites formed under virtually similar conditions. Moreover, parameters such as impurity content, degree of structural order, structural strain, porosity, and grain size are clearly interconnected and often simultaneously modified by formation conditions. Increasing incorporation of diamagnetic Al into the lattice of hematite, for instance, influences also the crystallinity and the grain size of the material; each parameter has its own specific effect on the magnetic properties. Thus, when dealing with hematite, it is difficult, and often even deceptive, to assign changes in

magnetic properties unequivocally to one parameter. Consequently, any meaningful study of the magnetic properties of hematite requires an exhaustive characterization of the sample material.

Transformations of magnetite, maghemite and goethite (α -FeOOH) to hematite are the subject of **Subsection 1.3.4**. Transformations between the various oxides and oxyhydroxydes of iron and titanium are common in nature. These processes are important for paleomagnetism, because they can destroy or obscure the primary NRM. On the other hand, the obtained secondary CRM can possible date major geological, geophysical or geochemical events during the history of the rock.

For elaborate reviews on the chemical and physical properties of hematite and the other iron(oxyhydr)oxides the reader is referred to *Schwertmann & Cornell* (1991) and *Cornell & Schwertmann* (1996).

The remainder of this chapter (**Section 1.4**) consists of a compilation of some specific rock- and mineral-magnetic properties of hematite, and how they depend on variations in temperature, pressure, magnetic field, grain size, chemical composition, etc. **Subsection 1.4.1** summarizes some general magnetic properties which may be diagnostic for hematite. In this subsection also some cautionary remarks are given concerning the magnetic properties of hematite reported in literature. **Subsection 1.4.2** deals with the canted and the defect magnetic moment of hematite. A detailed description is given of their origin, their characteristics at ambient temperature and their behaviour on heating and cooling. **Subsection 1.4.3** is concerned with the coercivity and the relative importance of the different types of magnetic anisotropy in hematite; possible origins of the high coercivities in SD hematite are discussed. In **Subsection 1.4.4** the temperature variation of hematite's characteristic magnetic transitions are given; i.e. the low-temperature Morin transition (isotropic point) and the high-temperature antiferromagnetic disordering point (Néel point). Finally, in **Subsection 1.4.5** the type and timing of remanence acquisition by hematite in sedimentary rocks is discussed. For earlier discussions or summaries on the magnetic properties of hematite the reader is referred to *Fuller* (1970), *Dunlop* (1971), *O'Reilly* (1984), *Morrish* (1994), and *Dunlop & Özdemir* (1997).

Hematite: What's in the Name

Hematite is the general name for the hexagonal alpha form of the ferric oxide polymorph, α -Fe₂O₃. The name is derived from the Greek '*haimatitis*' which means 'blood-like' and refers to its bright red colour in a finely dispersed state. Ancient superstition held that large deposits of hematite formed from battles that were fought and the subsequent blood that flowed into the ground. More massive crystals or dense crystal aggregates of hematite, however, are strongly absorbing and so appear black or sparkling grey. Hematite has several varieties, each with their own unique names referring to their physical appearance, grain size, precursor mineral, accompanying minerals, isomorphous substitution or the presence of structurally bound water (*cf. Morrish* 1994).

When hematite occurs in plates or scales as mica does and is steel gray with a brilliant metallic luster it is called micaceous hematite or '*specularite*' after the Latin word for mirror. Indeed, ancient people sometimes used hematite crystals as mirrors. Commercial deposits of small α - Fe_2O_3 particles in silica are called '*taconite*'. Large black compact specimens of reniform (botryoidal) modules are known as '*kidney ore*'. The fine-grained red earthy α - Fe_2O_3 ore is called '*red ochre*', and was largely used in the past as a paint pigment. Thin micaceous plates of hematite which form rosettes are referred to as '*iron rose*'. Hematite ores can be massive, earthy, oolitic, micaceous or botryoidal with a radial fibrous texture. These hematite ores might be regarded as unimportant from a paleomagnetic point of view; they, however, are successfully used in many fundamental rock- and mineral-magnetic studies. By crushing the ore and subsequent separation into well-defined grain-size fractions such natural hematites can be used to prepare artificial rock samples. These in turn can be subjected to various rock-magnetic measurements to determine the grain-size dependence of hematite's magnetic properties (e.g. *Dankers* 1978; *Hartstra* 1982).

Dispersed hematite grains found in various rock types are also known by different names. High-temperature hematite found as a primary mineral in igneous rocks often contains titanium, and therefore are called *titanohematites* or *hemoilmenites*. These Ti-containing minerals form a solid solution between the endmembers hematite and ilmenite (FeTiO_3). The relatively large ($\geq 1 \mu\text{m}$), black polycrystalline α - Fe_2O_3 particles found in various sediment types are called *specularite*, while the ultra-fine-grained reddish particles are known as *pigment*. The latter phase is ranging from brown through orange to red and purple and gives 'red' sediments their distinctive colour. Hematite pseudomorphs of magnetite (Fe_3O_4) and pyrite (FeS_2), formed by direct oxidation at ambient temperature, are called *martite*. Finally, α - Fe_2O_3 produced in aqueous solution or by thermal transformation of goethite often contains structurally bound water. These cation deficient hematite-like phases are known as '*protohematite*' and '*hydrohematite*' depending on the amount of incorporated OH-groups (*Wolska* 1981).

1.2 Geological occurrence and formation

1.2.1 Igneous and metamorphic rocks

High-temperature hematite may contain various amounts of titanium. Solid solution between the endmembers hematite and ilmenite is complete only at high temperatures ($\sim >1000^\circ\text{C}$); at lower temperatures ($\sim <700^\circ\text{C}$) a large miscibility gap exists. The titanohematites have compositions on the tie-line between Fe_2O_3 and FeTiO_3 and can be displayed on a TiO_2 - FeO - Fe_2O_3 ternary diagram (see *Fig. 5.2*, page 140); the general formula is $\text{Fe}^{3+}_{2-2x}\text{Fe}^{2+}_x\text{Ti}^{4+}_x\text{O}_3$. Primary titanohematites (THs) particularly crystallize in acidic (silica-rich) igneous melts because of their relatively high oxygen fugacity compared to mafic melts. Most primary THs in silicic rocks are Ti-poor, that is almost

pure hematite. Primary crystallizing THs in more mafic and intermediate igneous melts are relatively rare and mostly Ti-rich (*O'Reilly* 1984).

In general, the titanomagnetites (TMs) and their oxidized equivalents, the titanomaghemites (TMhs), magnetically dominate igneous rocks. There are, however, several circumstances in which the phases of the hematite-ilmenite series are the principal carrier of the NRM in these types of rocks. For instance, *Duff* (1979) reported hematite-rich phases to be the dominant magnetic carrier in some granites and other acid volcanics like syenites, rhyolites and trachytes. *Ade-Hall et al.* (1971) describe basalts with a substantial amount of hematite. They stated that (1) the highest levels of high-temperature oxidation (i.e. deuteric oxidation) during initial cooling of the melt and (2) reheating ('regional' hydrothermal alteration around 300°C) of igneous rocks are the two conditions which favour the replacement of primary TM and TMh by TH. Titanohematites of intermediate composition are found to magnetically dominate some dacitic and andesitic pyroclastics (e.g. *Uyeda* 1958; *Hoffmann & Fehr* 1996). Homogeneous THs of intermediate composition can only occur naturally in extremely rapidly cooled (quenched) rocks. Slow cooling of the magma promotes subsolvus exsolution because of the broad miscibility gap present at low temperatures. The single-phase THs then exsolve into intergrown iron-rich (near hematite) and titanium-rich (near ilmenite) phases. These microintergrowths in particular have attracted much attention because of their remarkable and complex (thermo)magnetic behaviour (e.g. *Heller et al.* 1986; *Hoffman* 1992; *Brown et al.* 1993). They have the property of acquiring a so-called self-reversed TRM. Although fascinating, the magnetic behaviour of these particular titanohematites lies beyond the scope of this review, and will not be treated. For a more detailed description of the formation, structure and properties of titanohematites and the other iron-titanium oxides, the reader is referred to *Haggerty* (1976), *Lindsley* (1976a & b), *O'Reilly* (1984) and *Dunlop & Özdemir* (1997).

Pure hematite has the highest unblocking temperatures of all common magnetic minerals. Hence, the primary NRM carried by hematite may survive low-grade metamorphism. During metamorphism, however, also secondary hematite can be formed and then carries a chemical remanent magnetization (CRM). In metamorphic rocks, hematite typically results from the prolonged heating of magnetite, maghemite, siderite (FeCO_3) and the hydrated iron oxides, provided the conditions are more or less oxidizing. Its existence is reported in metamorphosed iron formations, metabasites of low-grade metamorphism, aerobic clay rocks and metamorphosed manganese rocks (*cf. Cornell & Schwertmann* 1996).

1.2.2 Sediments

Sedimentary rocks may contain detrital as well as *in situ* formed hematite. The detrital particles contribute to a so-called detrital remanent magnetization (DRM), while the newly formed grains carry a CRM (see Subsection 1.4.5). Oxidizing conditions usually prevail during erosion, transportation and subsequent deposition. The high thermodynamic stability of hematite in such aerobic environments usually ensures that it remains unchanged over geological time spans, at least for as long as the aerobic

environment remains. Other magnetic minerals such as (Ti-)magnetite and the iron sulphides, however, are thermodynamically less stable in aerobic environments and tend to oxidize, with hematite usually being the stable endproduct. Other important processes that may generate hematite in sedimentary environments are the breakdown of iron-magnesium silicates and hydrous iron-bearing clays, the oxidation of magnetite, the inversion of maghemite, dehydration of goethite, and the precipitation of ultra-fine-grained hematite from iron-rich solutions as a coating on other matrix particles and in interstices in the rock. Once formed, hematite may, however, be redissolved by complexation with organic compounds or by reduction. All the reactions are slow at ambient temperature but accelerate with mild heating, e.g. during sediment burial.

Hematite is reported to be the dominant magnetic carrier in a variety of fine-grained red sediments, like red-coloured sandstones, shales and oolitic carbonates (e.g. *Van den Ende* 1977; *Tauxe et al.* 1980; *Walker et al.* 1981). These so-called 'red beds' owe their distinctive colour to finely divided hematite pigment. They are widespread all over the world and proved to be a particularly useful carrier of the paleomagnetic record. Red beds generally are more strongly magnetized than other types of sedimentary rocks. They typically have extremely hard and stable NRM's of 10^{-3} – 10^{-1} A/m (cf. *Dunlop & Özdemir* 1997). Accordingly, numerous paleomagnetic studies have been undertaken on red sediments; they are successfully used for paleopole calculations, paleo-reconstructions and magnetostratigraphy (e.g. *Creer* 1962b; *Douglass* 1988; *Channell et al.* 1992). A disadvantage of red beds is that they contain few or no fossils, being predominantly continental deposits laid down in high-energy depositional environments (cf. *Dunlop & Özdemir* 1997). They can be dated accurately only if interbedded with fossiliferous sediments or volcanic ash layers. Furthermore, the type (DRM and/or CRM) and timing of remanence acquisition is still controversial and seems to differ from one red bed to the next (see Subsection 1.4.5).

The hematite in these types of sediments often appears in various forms of diverse origins. *Walker et al.* (1981), for instance, recognized six different forms when studying the Moenkopi red beds (Triassic) of the Colorado Plateau. The particle size ranged from ultra-fine-grained red pigment ($\ll 1 \mu\text{m}$) to coarse-grained (2–40 μm) black crystalline hematite particles. Pigmentary hematite is translucent under transmitted light, while coarse-grained hematites are opaque and exhibit silvery anisotropic reflectance. *Walker et al.* (1981) divided the relatively coarse-grained hematite forms into four groups: crystals of specular hematite, polycrystalline and monocrystalline hematite grains pseudomorphing magnetite (martite), (partly) hematized ilmenite grains, and grains consisting of primary hematite-ilmenite intergrowths. In addition to an ultra-fine-grained, probably amorphous hematite type they recognized also a microcrystalline hematite form.

1.2.3 Soils

Rock- and mineral-magnetic measurement techniques are increasingly used to identify and characterize the different oxides and oxyhydroxides of iron present in soils and paleosols. Magnetic measurements may usually be interpreted in terms of the type of magnetic minerals present and frequently their size and shape. Since these parameters are

governed by various geochemical, climatological and environmental processes (e.g. *Fitzpatrick* 1988), magnetic measurements thus can provide valuable information on pedogenesis (e.g. *Mullins* 1977), (paleo)environment and (paleo)climate (e.g. *Maher* 1998). The loess/paleosols sequences from the Chinese Loess Plateau, for instance, preserved a continuous detailed record of Quaternary climate change spanning the last ~2.6 million years of Earth's history (e.g. *Maher & Thompson* 1992; *Verosub et al.* 1993). Rock-magnetic techniques are also used successfully to trace and determine human impact on soil profiles, i.e. archaeological landscapes, and to detect anthropogenically-induced pollution (e.g. *Thompson & Oldfield* 1986; *Strzyszcz* 1993; *Dalan & Banerjee* 1996; *Heller et al.* 1998). Most soils, however, are magnetically dominated by the various ferrimagnetic spinel-phases, and the reader is referred to Chapter 5 for a brief review on pedogenetic maghemite.

According to *Schwertmann* (1985), hematite occurs most abundantly in aerobic soils of subtropical, Mediterranean and humid to subhumid tropical regions (lateritic and plinthitic soils, red mediterranean soils, oxisols and utisols). Red hematitic soils, however, are also formed at two climatic extremes; extremely cold arid (e.g. Antarctica) and warm arid (e.g. deserts in Australia) regions, with a high rate of Fe-release during weathering and low content of soil organic matter. Hematite is usually absent in soils of temperate and cool regions. In soils it is almost always associated with its hydrated counterpart goethite. The presence of goethite (yellowish-brown), however, is often visually obscured because of the much higher pigmenting effect of hematite (reddish-brown).

Like in sediments, hematite in soils can be detrital or authigenic. Consequently, hematite present in paleosols can carry a DRM or CRM. In practice, the processes by which hematite is formed in soils are similar to those in sediments. From synthesis experiments under ambient conditions it is now well established that hematite in soils is not formed by dehydration of goethite, but by transformation (dehydration-rearrangement process) of ferrihydrite, which is therefore assumed to be a necessary precursor of hematite (*cf. Schwertmann* 1988b). Goethite, on the other hand, is believed to form directly from any Fe-source via solution. These two pathways are competitive and several environmental factors govern the rate at which the two reactions proceed. Factors that promote ferrihydrite formation and its transformation to hematite rather than the formation of goethite are: a high rate of Fe-release during weathering, good aeration, rapid decomposition of organic matter, relatively low Al-concentration in the system, a relatively high soil pH, a high soil temperature and low soil water activity. For soils these factors not only vary with climate, but also with topographic position (e.g. latitude, altitude, north- or south-facing slopes) and profile depth (e.g. *Fitzpatrick* 1988). Hematites produced from ferrihydrite usually have a typical granular texture (*cf. Schwertmann* 1988a). Comprehensive reviews on pedogenetic hematite and other Fe-minerals in soils can be found in Nato ASI Series C217: *Iron in Soils and Clay Minerals* edited by Stucki, Goodman and Schwertmann (1988), and *Cornell & Schwertmann* (1996).

1.3 Mineralogical and crystallographic characteristics

1.3.1 Crystal structure

Hematite crystallizes in the corundum structure which can be indexed in the four axis hexagonal crystal system or in the equivalent three axis rhombohedral system. For hexagonal symmetry, the Miller indices are $(hkil)$; i may be omitted (as in this thesis) as $h + k = -i$. Throughout this thesis we will use the triple primitive hexagonal unit cell instead of the twelve-fold (morphological) hexagonal unit cell (*cf. Hartman 1980*).

The crystal structure of $\alpha\text{-Fe}_2\text{O}_3$ was first determined by *Bragg & Bragg (1918)* using X-ray diffraction, and later refined by *Blake et al. (1966)*. A detailed review can be found in *Lindsley (1976a)*. Hematite has the space group $R\bar{3}c$, and the hexagonal unit cell parameters are $a_{\text{hex}} = 0.50340$ nm and $c_{\text{hex}} = 1.3752$ nm (*cf. Schwertmann & Cornell 1991*). A triply primitive hexagonal unit cell contains six formula units and thus consists of 18 O^{2-} anions forming an almost ideal hexagonal-close-packed (*hcp*) lattice. Between the oxygen layers, which are stacked in an ABAB-sequence parallel to the (001) basal plane, there are 18 sites for Fe^{3+} cations octahedrally coordinated by six oxygen ions. In hematite only two-thirds of these available cation sites are occupied; note that vacant sites are implicit in the stoichiometry, and should not be confused with vacancies. The arrangement of the occupied cation sites is in the form of connected hexagonal rings within each cation layer (*Fig. 1.1a*). The close-packed alternating cation layers are arranged in an ABCABC-sequence, that is planes of Fe atoms are shifted by one octahedral site in each successive layer along (001). The cation sequence along the c -axis normal to the basal plane layers is thus (Fe–Fe–vacant site–Fe–Fe–vacant site) n , giving a dioctahedral arrangement (*O'Reilly 1984*). The repeat layer distance comprises six anion and cation layers. *Table 1.1* lists the atomic coordinates of hematite.

Table 1.1 Atomic coordinates of hematite (*Blake et al. 1966*).

	x	y	z
Fe	0	0	0.3553
O	0.3059	0	0.25

The $\text{Fe}(\text{O})_6$ octahedra are connected by edge- and face-sharing. Each filled octahedron shares edges with three neighbouring octahedra in the same plane and one face with an occupied octahedron in an adjacent plane (*Fig. 1.1a*). Face-sharing thus occurs along the c -axis, forming pairs of Fe–Fe ions. Electrostatic repulsion of the Fe^{3+} ions across the shared face causes a displacement of the cations toward the unshared face (*Blake et al. 1966; Brown et al. 1993*). This distortion puckers the cation layers and leads to a distortion of the oxygen close-packing. In the shared face the O–O distance (0.2669 nm) is close to that of ideal *hcp*. In the unshared face, however, the O–O distance

is greater (0.3035 nm) than for ideal *hcp* (Blake *et al.* 1966; Lindsley 1976a). The distortion of the octahedral sheet and the absence of H bonds yield a compact structure which is responsible for the high density of 5.26 g cm^{-3} (Schwertmann & Cornell 1991). A hardness of $6\frac{1}{2}$ on Mohs scale is generally reported (*cf.* Cornell & Schwertmann 1996).

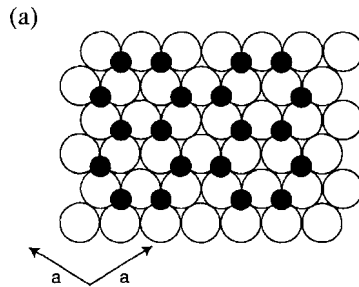
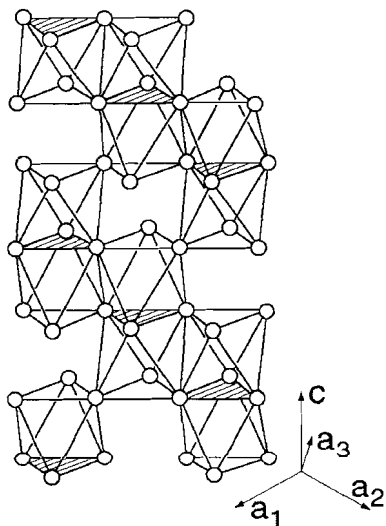
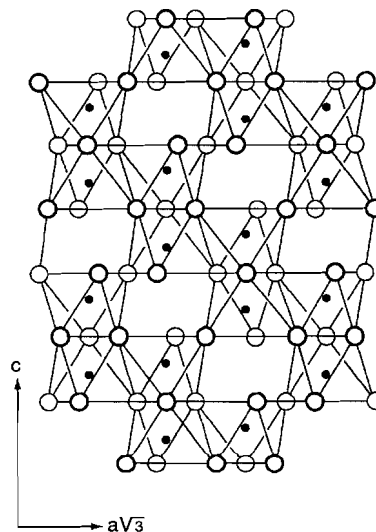


Figure 1.1: The crystal structure of hematite. (a) Close-packed model of ideal hematite showing the basal plane configuration of oxygen (large open circles) and Fe atoms (small solid circles). (b) Oxygen framework of hematite showing the stacking sequence of octahedra along the *c*-axis. Note their face-sharing (shaded planes). (c) The hematite structure projected onto $(11\bar{2}0)$ showing the puckering of the Fe atoms. Solid circles (Fe atoms) are in the plane, thin open circles (O atoms) are below the plane, and thick open circles (O atoms) are above the plane of the paper.

(b)



(c)



1.3.2 Cationic substitution and water in the structure

In α -Fe₂O₃, the Fe³⁺ cation may be partially replaced by other cations of similar size, thereby changing the physical properties of the hematite. Al³⁺ and Ti⁴⁺ are the best-known examples for this substitution, although other metals such as Cr, Mn, Co, Cu and Sn may also substitute for Fe. Ti-substitution is common in high-temperature hematite formed from igneous melts (e.g. *Brown et al.* 1993), while Al-substituted hematites are usually formed in sediments and soils at relatively low to moderate temperatures (e.g. *Schwertmann* 1988a).

Several investigators have synthesized (series of) Al- and Ti-substituted hematites by various procedures to attempt reproducing the natural formation and to determine the change in various (magnetic) properties as a function of substitution (e.g. *Morin* 1950; *Haigh* 1957b; *Schwertmann et al.* 1979; *Fysh & Clark* 1982; *Brown et al.* 1993; *Morrish* 1994 and references therein). The effect of small amounts of Al- and Ti-substitution on the magnetic properties of hematite will be examined in Section 1.4. Some caution must, however, be exercised in drawing conclusions from (magnetic) measurements on these synthetic materials (*cf.* *Morrish* 1994), because of aspects related to the synthesis of substituted single crystals or polycrystalline samples.

The substituted cations, for instance, are not always homogeneously distributed over the hematite lattice, and in sintered polycrystalline hematite samples the 'foreign' cations are often present at the grain boundaries instead of being really incorporated into the structure.

Another point which needs attention when dealing with low-temperature hematite, is the common incorporation of structurally bound water in the lattice. This relatively tightly held water is reported to remain into the hematite lattice even when heating up to 1000°C. The effect of this incorporated water was long time overlooked in fundamental magnetic studies on hematite, and as a consequence its influence on hematite magnetic properties is not yet clear. Some aspects of substitution of Ti, Al and structurally bound water will be discussed next.

Titanium Substitution

Above ~1000°C, a complete solid-solution series exists between the endmembers hematite and ilmenite. However, only relatively fast cooling can preserve intermediate compositions due to the existence of a broad miscibility gap at low temperatures. The hexagonal unit cell dimensions for ilmenite are $a = 0.50881$ nm and $c = 1.4080$ nm, compared with $a = 0.50340$ nm and $c = 1.3752$ nm for hematite. In the series Fe₂O₃-FeTiO₃ there is a steady increase in cell dimensions towards ilmenite. Vegard's Law (*Vegard* 1921) of linear variation of the unit cell parameter with chemical composition, however, is not obeyed strictly because of curvatures at either end of the line (*Banerjee* 1991).

Ionic substitution occurs with Ti⁴⁺ substituting for Fe³⁺ and one remaining Fe cation changing valence from Fe³⁺ to Fe²⁺. The generalized formula of these titanohematites is Fe_{2-x}Ti_xO₃, where x ranges from 0.0 for hematite to 1.0 for ilmenite, and with $(2-2x)\text{Fe}^{3+}$

and $x\text{Fe}^{2+}$ per formula unit (O'Reilly 1984). For hematite-rich solid-solution members, until approximately $x < 0.45$, the substitution ($\text{Fe}^{2+} + \text{Ti}^{4+}$) for 2Fe^{3+} takes place randomly. In these disordered $R\bar{3}c$ titanohematites the cation layers between the close-packed oxygen atoms are equivalent, implying an antiferromagnetic structure. At more ilmenite-rich compositions, i.e. for $x > 0.45$ at room temperature, however, the cations become ordered. The Ti cations preferentially occupy alternate cation layers in which the arrangement corresponds to layers with $(1-x)\text{Fe}^{3+}$ and $x\text{Ti}^{4+}$ adjacent to layers containing $(1-x)\text{Fe}^{3+}$ and $x\text{Fe}^{2+}$ *pfu* (O'Reilly 1984). This specific ordering implies a net ferrimagnetic moment, because, just as in hematite, the spin order is parallel within each layer and antiparallel between alternate layers. Cation ordering reduces the symmetry to the space group $R\bar{3}$ (Lindsley 1976a). The cation arrangement (ordered or disordered) of the intermediate members depends, however, on thermal history, because quench-cooled samples may retain the high-temperature disordered arrangement.

Aluminium Substitution

Corundum ($\alpha\text{-Al}_2\text{O}_3$) is isomorphous with $\alpha\text{-Fe}_2\text{O}_3$, but the range of solid solution between them is restricted. The extent of Al substitution in naturally occurring low-temperature (soil and sediment) hematite appears to be limited to $1/6$ of the possible octahedral positions. This is consistent with the observed maximum replacement of iron by aluminium in synthetic hematites prepared at low to moderate temperature (Schwertmann *et al.* 1979; Fysh & Clark 1982). Higher substitutions, ~32 mole %, can be achieved by heating Al-goethites to 500–700°C (e.g. De Grave *et al.* 1982). At even higher temperature (900–1000°C), however, considerable amounts of Al are expelled from the structure and crystallize as corundum. The limit of Al substitution falls again to 16 mole % or even lower (e.g. De Grave *et al.* 1982; Curi & Franzmeier 1984).

Unit cell dimensions of hematite decrease as Al-substitution increases because of the smaller diameter of the Al cation compared with Fe^{3+} , respectively 0.0535 and 0.0645 nm (Shannon & Prewitt 1969). Vegard's Law is, however, not strictly obeyed; the measured *d*-spacings are slightly larger than they would have been according to Vegard's Law of linear lattice contraction (e.g. De Grave *et al.* 1982; Schwertmann *et al.* 1979). The deviation is likely attributed to structural imperfections created by the incorporation of hydroxyl groups. For most synthesized Al-hematites series, the relationships between the amount of substitution and the unit cell dimension are substantially improved after heating to ~1000°C; i.e. they behave more according to Vegard's Law.

Structural Water

Most hematites produced in aqueous systems or by thermal dehydration of goethite at low temperature contain some structurally bound water (*sbw*) in the structure. This *sbw* is shown to exist in the form of hydroxyl groups replacing O^{2-} anions in the hematite crystal lattice (Wolska 1981; Wolska & Schwertmann 1989). The electroneutrality is preserved by Fe^{3+} deficiency in the cationic positions, rather than by changing the valence state of

some Fe^{3+} to Fe^{2+} . The incorporated hydroxyl groups expand the hematite structure slightly, especially along (001) and decreases the X-ray peak intensities (*cf. Cornell & Schwertmann 1996*). This allows the determination of $(\text{OH})^-$ by measurement of the X-ray peak intensities (*Stanjek & Schwertmann 1992*). There are no observations suggesting ordering of the cation vacancies or hydroxyls, but a complete refinement of the structure has not yet been done (*Waychunas 1991*).

Wolska & Schwertmann (1989) suggested the existence of two different transitional hematite-like phases which can be represented with the general formula $\alpha\text{-Fe}_{2-x/3}(\text{OH})_x\text{O}_{3-x}$ where $x = 9.07y/(51.15 + y)$ and $y = \% \text{H}_2\text{O}$. The two Fe-deficient phases, so-called 'protohematite' and 'hydrohematite', were recognized during the progressive thermal dehydration of goethite to hematite and display each their own distinct structural and compositional characteristics. When interpreting a series of X-ray diffractograms the authors recognized that while the crystallographic *c*-axis decreases steadily with progressing thermal dehydroxylation, the *a*-axis reaches a minimum at the temperature at which the typical non-uniform X-ray line broadening disappears. The differential line broadening arises from incomplete ordering of the cations in the structure. Protohematite ($1 \geq x > 0.5$) is represented by the largest unit cell of hematite phase after the goethite/hematite transition. This poorly crystalline hematite-like phase is characterized by a defect structure with ~6–3% H_2O , and broadened X-ray diffraction patterns. Hydrohematite, on the other hand, is characterized by the smallest unit cell after the disappearance of selected broadening of X-ray diffraction peaks. It appears when the crystalline phase still holds ~3% ($x \leq 0.5$) of structurally bound water. This *sbw* can be extremely persistent against heating. Complete removal may require temperatures up to ~1000 °C. *Wolska & Schwertmann (1989)* suggest that stoichiometric anhydrous hematite is thermodynamically less stable than hydrohematite with small *x* values.

The smallest unit cell representing the appearance of hydrohematite may already arise for $x \sim 0.66$ (~4% H_2O) when the phase is Al-substituted. It seems that Al^{3+} ions may specifically retain OH-groups in the structure of Al-hematite when OH associated with Fe has been lost during low temperature dehydroxylation, possible because of the higher ionic potential of Al^{3+} (*Fey & Dixon 1981; Schulze 1982; Schulze & Schwertmann 1984*).

1.3.3 Microstructure

Crystal Morphology

Hematite has (in contrast to, for instance, magnetite) widely different crystal forms in specimens of natural origin (*Kostov 1968*) as well as in synthetic crystals (e.g. *Schwertmann & Cornell 1991*). The usual habits of natural hematite crystals are platy, rhombohedral and rounded (*cf. Fig. 1.2*). The plates vary in thickness and can be round, hexagonal or of irregular shape (*Cornell & Schwertmann 1996*). Crystals formed from solution are predominantly thick plates or rhombohedral, whereas those grown from a vapour phase form thin plates (*Sunagawa 1987*). An example of the latter are the large crystals from the island of Elba which are often used in rock-magnetic investigations.

They probably formed by reaction of gaseous FeCl_3 with water vapour (cf. *Cornell & Schwertmann 1996*). Morphologies of synthetic hematite are more variable including plates, discs, rods, ellipsoids, double ellipsoids, spindles, stars, rhombohedra, cubes, spheres and bipyramids. However, in the absence of additives, hexagonal plates, often rounded, and rhombohedra predominate (*Cornell & Schwertmann 1996*). Hematite twins on the $\{001\}$ and the $\{102\}$ planes (*Kostov 1968*).

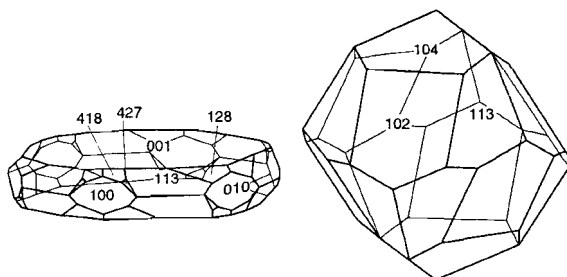


Figure 1.2: Crystal forms of platy and rhombohedral hematite (Redrawn from *Cornell & Schwertmann 1996*).

The shape of hematite (and other Fe-oxides as well) is governed principally by the arrangement of the $\text{Fe}(\text{O})_6$ octahedra in the structure. This arrangement determines the relative growth rate in the different crystallographic directions if the crystals can grow uninhibitedly (*Schwertmann & Cornell 1991*). The crystal structure of hematite, however, has a less directional effect on crystal habit than that of, for instance, goethite, and for this reason the habit of hematite is readily modified (*Cornell & Schwertmann 1996*).

As the fast growing faces are eliminated quite rapidly, it are the slow growing faces which dominate the morphology. Theoretically the growth habit of hematite should therefore be rhombohedral $\{012\}$, because this form appears to have the lowest attachment energy (E_{att}) and a positive correlation exists between the growth rate R of a crystal face and E_{att} (*Hartman & Bennema 1980; Hartman 1980; Reeves & Mann 1991*). In fact this form frequently occurs in nature but the platy habit $\{001\}$ clearly dominates. Because the attachment energies of the various faces in hematite are not that different, the order of stability of these faces may be altered quite easily by preferential adsorption of ionic species or by slight alterations in reaction conditions, and hence modify the crystal habit. *Hartman (1980)* showed that with respect to the other faces $\{001\}$ will have the strongest tendency to adsorption, because the density of unsaturated bonds is highest for this face. This adsorption will lower the growth rate of $\{001\}$, but increase the growth rates of all other forms. According to the author this explains the predominance of the platy $\{001\}$ habit in natural samples.

The shapes of synthetic hematites can significantly be modified, and hence be manipulated, by synthesis variables like temperature, pressure, pH, starting material (pseudomorphs), and type and concentration of formation additives (inorganic as well as

organic). *Cornell & Schwertmann* (1996) give a detailed review on morphologies of hematite and the conditions under which they were obtained.

The omnipresence of aluminium in weathering environments results in most newly formed hematites in sediments and soils being Al-substituted. When the cation Al is incorporated in the structure the crystal morphology of hematites is modified. Various synthesis experiments showed that Al substitution caused a change in morphology from rhombohedra to plates (e.g. *Schwertmann et al.* 1979; *Barrón & Torrent* 1984). With increasing Al content hematite plates become larger but thinner indicating that Al substitution hinders development in the crystallographic *c*-axis (*Schwertmann et al.* 1979).

Crystallinity, Grain size and Porosity

Crystallinity, size and also porosity of hematite particles depends strongly on the conditions under which the crystal growth takes place, i.e. the method of synthesis or, for natural hematite, on the environment of their formation. For example, high rates of crystal growth at low temperatures may lead to small poorly ordered crystals, whereas slow rates of formation and higher temperatures result in larger crystals. In natural environments, such extremes may exist in soils and some types of sediments on the one hand, and under hydrothermal conditions on the other (*Cornell & Schwertmann* 1996). In Section 1.4 we describe that even small changes in parameters such as crystallinity and grain size can already have a substantial effect on the magnetic properties of weakly magnetic hematite. The effect of porosity of hematite crystals on its magnetic properties is not yet known.

Synthetic methods allow crystal growth and thereby crystallinity and grain size to be manipulated to a certain extent. Numerous experiments have identified such factors as temperature, source of Fe (Fe^{2+} , Fe^{3+} , Fe-complexes), pH, presence of interfering or substituting ions such as Al, Mn, Si, and organics, as having a marked influence on growth (*Cornell & Schwertmann* 1996). *Schwertmann & Stanjek* (1998) showed that even a factor as stirring against not stirring during synthesis (or their natural equivalent; turbulent and non-turbulent systems) can significantly modify the crystallinity and grain size of particles. Particle size and crystallinity appear to be the result of interactions between all these factors. A small change in one of the factors can already affect the crystallinity and grain size of the resulting hematite in such a way that the magnetic properties will also be different and to some extent explain the highly variable magnetic properties of, in particular, synthetic hematites.

The crystallinity of synthetic hematite depends also on whether the oxide was produced by calcination or grown from solution. The latter procedure generally yields less crystalline material than the first. The crystallinity of poorly crystalline low-temperature hematite can be improved by annealing. Heating considerably affects the magnetic properties of those hematites and generally reduces their variability.

We already mentioned that various properties of hematite change as Al enters the structure; among them is also the crystallinity. The crystallinity of the Al hematite changes drastically with the level of Al in the structure; a maximum is often obtained at low to medium substitution, ~4 mole % (*Schwertmann et al.* 1979; *De Grave et al.* 1982).

Therefore, a certain extent of Al substitution may have a stabilizing effect on the structure of hematite probably by releasing structural strain (*Schwertmann 1988a*).

The nature of the anion in the system not only influences hematite morphology but also its grain size by retarding the crystallization process (*Barrón et al. 1997*). In particular those anions which have a stronger affinity for the Fe oxide surface, like silicate, organics and phosphate, prevent the crystals to develop. Such crystallization inhibitors are often present in the pore water of sediments and soils.

Microporous hematite is reported to result from the thermal transformation of oxyhydroxides like goethite and ferrihydrite (*Cornell & Schwertmann 1996; Weidler & Stanjek 1998*). The pores were created on progressive heating to allow escaping of the water vapour out of the precursor mineral. The degree of porosity of hematite depends on the annealing temperature. According to *Weidler & Stanjek (1998)*, the initial stage of the dehydration of ferrihydrite to hematite can be described as similar to the process of Ostwald ripening; i.e. increase in particle size and/or removal of smaller particles.

1.3.4 Transformations of iron(oxyhydr)oxides to hematite

Phase transformations between iron oxides and oxyhydroxides are, as a consequence of changing physico-chemical conditions, common in nature and may occur via many pathways. The main conversions between these minerals are discussed by *Cornell & Schwertmann (1996)*. As mentioned before, hematite is thermodynamically the most stable Fe-oxide under aerobic conditions, and during geological time the other Fe-oxides tend to transform to hematite, or to its oxyhydroxide counterpart goethite depending on a.o. $P_{\text{H}_2\text{O}}$ and temperature. This section concerns the transformations of magnetite, maghemite and goethite to hematite. These transformations are so-called topotactic reactions, that is one phase converts to another while preserving some of the original crystal planes and directions. From a paleomagnetic point of view the magnetic coupling between the two phases during hematitization is very important. It determines whether the CRM is coupled parallel (or antiparallel) to the NRM of the preexisting parent mineral, or the CRM tracks the ambient field at the time the hematite crystallite reaches its critical blocking size (e.g. *Hedley 1968; Porath 1968b; Heider & Dunlop 1987; Özdemir & Dunlop 1988; McClelland & Goss 1993*).

Transformation of Magnetite (Fe_3O_4) and Maghemite ($\gamma\text{-Fe}_2\text{O}_3$)

The transformation of magnetite to hematite proceeds either directly or via a maghemite stage. The inversion of $\gamma\text{-Fe}_2\text{O}_3$ to $\alpha\text{-Fe}_2\text{O}_3$ only implies a crystallographical change, while the hematitization of magnetite also requires a chemical change, i.e. oxidation. The transformation of maghemite to hematite occurs by restacking of close-packed oxygen layers (*ccp* to *hcp*) accompanied by displacement of interstitial ferric ions, rather than by wholesale recrystallization (*Kachi et al. 1963, 1971*). Plate-like hematite crystals, which are elongated in the basal (001) plane, grow in spinel (111) planes, and the hexagonal [001] and [110] axes coincide with the spinel [111] and [110] axes (*Feitknecht*

& Mannweiler 1967). Several important observations on transformation of trace element-substituted magnetite and maghemite to hematite are reported in literature. *Sidhu et al.* (1977) and *Sidhu* (1988) showed that the presence of trace elements (≤ 1 mole %) substantially reduced the oxidation rate of magnetite to maghemite and increased the inversion temperature of maghemite to hematite. *Sidhu et al.* (1980) showed in their dissolution studies that during the transformation of maghemite to hematite as much as ~60% of the Co, Ni, Zn and Cu present in the crystal structure of maghemite is ejected from the crystals to form a surface layer rich in these elements, whereas the Mn, Cr and Al present in maghemite are redistributed in hematite particles. For a more detailed description of this transformation process and the inversion temperature the reader is referred to Chapter 5 concerning the properties of maghemite.

Transformation of Goethite (α -FeOOH)

Transformation of goethite to hematite ($2\alpha\text{-FeOOH} \rightarrow \alpha\text{-Fe}_2\text{O}_3 + \text{H}_2\text{O}$) can take place in solution, usually under hydrothermal conditions. Thermal transformation of $\alpha\text{-FeOOH}$ is also widespread in natural environments under the influence of natural or man-made fires. Hematite, however, is only the endproduct of this reaction in the absence of large amounts of organic matter which produce reducing conditions during burning.

The common anion framework of goethite and hematite permits topological changes to take place relatively easily. In goethite, the O^{2-} and $(\text{OH})^-$ ions form approximately hexagonally close-packed layers, only half of the octahedral interstices are filled with Fe^{3+} . This oxyhydroxide consists of double bands of edge-sharing $\text{FeO}_3(\text{OH})_3$ octahedra; the double bands are linked by corner-sharing in such a way as to form 2×1 octahedra 'tunnels' crossed by hydrogen bridges (*Schwertmann & Cornell* 1991). During heating goethite transforms to hematite by removing the hydroxyl sheets and some of the oxygen in strips parallel to the c -axis to form water (*Francombe & Rooksby* 1959). The c -axis of hematite and the a -axis of goethite are equivalent in that they are perpendicular to the planes of hexagonal close packed O^{2-} anions that are preserved during the topotactic alteration of goethite to hematite (*Bernal et al.* 1959). The orthorhombic (001), (040), and (002) crystal planes of goethite become the hexagonal (003), (110) and (300) planes of hematite. Furthermore, the [100], [010] and [001] directions of goethite become the [001], [010] and [210] directions of hematite (*Van Oosterhout* 1960). The mechanism of hematite crystal transformation from goethite is essentially a nucleation process (*Watari et al.* 1983). The rearrangement of Fe results in nucleation and associated diffusion, creating voids parallel to the (100) plane of goethite which is the (001) plane of hematite, enabling the escape of water vapour (*Naono & Fujiwara* 1980; *Rendon et al.* 1983). As a result, the unit cell a dimension for goethite (*Schulze* 1984; *Schulze & Schwertmann* 1984) and the c dimension for hematite (*Stanjek & Schwertmann* 1992; *Ruan & Gilkes* 1995) are relatively more sensitive to the presence of structural OH.

1.4 Magnetic properties

This section is concerned with the magnetic properties of hematite and their dependence on parameters such as temperature, pressure, grain size, isomorphous substitution and crystallinity. Concerning the isomorphous substitution of Ti, we will focus only on small amounts of incorporated Ti. For a detailed description of the magnetic properties in the hematite-ilmenite series the reader is referred to *O'Reilly (1984)*, *Dunlop & Özdemir (1997)* and references in both books.

1.4.1 General

Hematite possesses a weak ferromagnetism ($\sim 0.2 - \sim 0.6 \text{ Am}^2 \text{ kg}^{-1}$) because of a slight canting of the magnetic spins out of exact antiparallelism (*canted moment*) and due to an ordered structure of chemical and/or structural defects causing a non-equivalence between the antiferromagnetically coupled sublattices (*defect moment*). Both, the weak ferromagnetism and the antiferromagnetic spin coupling, vanish at the same temperature of $\sim 680^\circ\text{C}$, which is the highest magnetic disordering temperature of all common magnetic minerals. Hematite appears to have highly variable magnetic properties which can be attributed to varying contributions of the two basic magnetization types. The variable expression of these two types yields a particularly elusive magnetic behaviour that is complex to interpret and is not yet entirely understood.

Between the Morin transition just below room temperature (*cf.* Subsection 1.4.4) and the Néel temperature at ca. 680°C , the magnetic spins are strongly pinned in the basal (001) plane, which is the 'easy' plane of magnetization. A substantial anisotropy field (H_a) of 3–4 T exists between the 'hard' *c*-axis and the 'easy' (001) plane, as indicated by resonance measurements (e.g. *Anderson et al. 1954*; *Kumagai et al. 1955*). As a consequence, the magnetization processes under the action of the Earth's magnetic field or of common laboratory fields are restricted to this plane causing hematite's magnetic properties to be highly dependent on crystallographic orientation. On cooling below room temperature, a characteristic discontinuity in several magnetic properties of hematite can be observed, due to a change in the direction of 'easy' magnetization from the basal plane to the hexagonal *c*-axis. For pure hematite, this so-called Morin transition (T_M) typically lies around -10°C , but its temperature and the range over which it occurs is dependent on grain size and impurity content.

Hematite is known for its relatively high coercivities (*cf.* Subsection 1.4.3), which can be several hundreds of mT for fine-grained particles (e.g. *Dankers 1978*; *Hartstra 1982*). Moreover, the low spontaneous magnetization (σ_s or M_s) of hematite results in a relatively high single-domain threshold size (d_0), since d_0 is inversely proportional to the square of σ_s (e.g. *Dunlop & Özdemir 1997*, page 129). The size of single-domain particles, which are paleomagnetically the most stable, may range between ~ 0.03 and $\sim 20 \mu\text{m}$ (theoretically even up to $\sim 100 \mu\text{m}$), compared to ~ 0.03 and $\sim 0.1 \mu\text{m}$ for magnetite. Halgedahl (1995), for instance, observed only a few domains in hematite platelets of $\sim 100 \mu\text{m}$, resulting in a pseudo-single-domain behaviour for these large

grains. Furthermore, the characteristic block-shaped magnetization curve causes remanent magnetization carried by hematite to become unblocked only in the vicinity of its Néel point at $\sim 680^\circ\text{C}$. These combined factors make hematite very important for paleomagnetism because they ensure an extremely high NRM stability during geological time which even may survive mild heating. Hematite, however, is notably stress-sensitive. The defect moment may be directly affected through mobility of dislocations in the lattice, and the canted moment is indirectly affected, since much of the basal plane anisotropy that pins its remanence is magnetoelastic (*cf. Dunlop & Özdemir 1997*).

At room temperature, the low-field mass susceptibility (χ_{lf}) of natural hematite samples is in the range $(10\text{--}750)\times 10^{-8} \text{ m}^3 \text{ kg}^{-1}$ (e.g. *Hunt et al. 1995*). It shows a dependence on grain size and crystallographic orientation; χ_{lf} values generally increase with increasing grain size in the SD to MD range (e.g. *Dankers 1978; Hartstra 1982; Soffel 1991*), and are higher when being measured in the ‘easy’ plane compared to the hard *c*-axis. The high-field or antiferromagnetic mass susceptibility (χ_{hf}), however, is almost isotropic above T_M , having a value of $\sim 25 \times 10^{-8} \text{ m}^3 \text{ kg}^{-1}$ (e.g. *Chevallier 1951; Néel & Pauthenet 1952; Pastrana & Hopstock 1977*). In being an intrinsic property it is independent of grain size and virtually constant for different hematite samples.

Some Cautionary Remarks

While reading the following sections one should bear several aspects in mind concerning the magnetic properties of hematite reported in literature. The first aspect concerns the change of magnetic properties within a (synthesized) series of hematites differing, for instance, in grain size or amount of isomorphous substitution. Especially for synthetically prepared hematites the trends observed seem to depend on the mode of formation. The main problem is that the changes observed in magnetic properties are often attributed to only one critical parameter, in this case the size of the grains or the degree of substitution. However, particularly the magnetic properties of hematite are readily influenced by parameters such as crystallinity, internal stress and structural imperfections, because of its low spontaneous magnetization. As seen in Section 1.3, these parameters may also change within the series, are often interconnected and highly dependent on the mode of formation. Hence, they easily bias the trend observed. As an example, the degree of Al substitution in hematite not only affects the magnetic properties by reducing the number of superexchange bonds and changing the lattice parameters, it also modifies the grain size, the grain shape, the crystallinity, the amount of incorporated water and the thermodynamic stability. Thus, observed changes of magnetic properties within a series can in most cases not be assigned unequivocally to the change in one single parameter but is more often due to the simultaneous change in different parameters with each their own specific effect; the individual relationships within a certain hematite series cannot be simply generalized.

Second, the influence of factors like the incorporation of structural bound water (*sbw*) and the morphology on hematite’s magnetic properties is not yet investigated. The importance of the first parameter is so far overlooked in most rock-magnetic studies dealing with low-temperature $\alpha\text{-Fe}_2\text{O}_3$. This type of hematite likely contains a substantial

amount of incorporated water (see Subsection 1.3.2). The incorporation of *sbw* causes an expansion of the unit cell, introduces structural disorder and results in a Fe-deficient structure. This will influence the magnetic properties of the hematite under investigation.

The extent to which a factor like morphology influences the magnetic properties of a weakly magnetic mineral is difficult to understand without further research. It is recognized, however, that a factor like grain shape is much more important when dealing with highly magnetic material because of the electrostatic forces developed on the surface. However, *Hartman* (1980), for instance, shows in a crystallographic study of the corundum structure that the basal (001) plane is a face where the uppermost layer consists of Fe atoms, while the uppermost layer of the (012) face consists of oxygen atoms. Consequently, in platy {001} forms of hematite relatively more surface Fe-atoms will be available to 'pin' the magnetization compared with rhombohedral {012} forms or acicular particles elongated along the *c*-axis. Furthermore, due to the highly directional dependence of hematite's magnetic properties, any preferred orientation of the grains may bias the magnetic measurements, especially when dealing with thin but large plates with (001) being the predominant face.

The third aspect concerns the possibly inhomogeneous distribution of substituted cations already mentioned in Subsection 1.3.2. Especially in some older literature the distribution is not always checked properly. *Morrish* (1994) discusses this problem and reports that more uniform substitution is usually achieved in polycrystalline samples made either by ceramic or by wet chemical methods than in single crystals grown by, for instance, the flux technique. But even for the first samples, caution must be exercised. Magnetic measurements by *Khalafalla & Morrish* (referred to in *Morrish* 1994, page 148), for example, show that single crystals with small amounts of Ti^{4+} (0.3 atom %) do not exhibit the Morin transition, at least down to 4.2 K. On the other hand, ceramic samples with as much as 4 atom % Ti have a Morin transition according to *Haigh* (1957). *Curry et al.* (1965) reported that many Ti-ions in these sintered samples must be suspected to be at the grain boundaries, and not in the lattice.

1.4.2 Canted and defect moment

Origin of the Magnetic moments

The magnetic structure of hematite was discovered by *Shull et al.* (1951) by means of neutron diffraction. At room temperature and above, the magnetic spins lie in the basal (001) plane orthogonal to the *c*-axis. The atomic Fe^{3+} moments are parallel coupled within (001) planes but antiparallel coupled between adjacent layers of cations, with sublattice magnetizations of 167–177 $\text{Am}^2 \text{kg}^{-1}$ at 0 K (e.g. *Iida & Mizushima* 1966; *Besser et al.* 1967). The magnetic and crystallographic unit cells appear to be the same. The cation arrangement in adjacent layers is equivalent so that an overall antiferromagnetic structure results. The sources of the main uniaxial magnetocrystalline anisotropy, which strongly confines the magnetic spins to the basal plane, are thought to be the magnetic-dipole anisotropy H_{MD} and the single-ion anisotropy H_{SI} (*Artman et al.* 1965). The two anisotropy fields have opposite signs, and at room temperature the first term dominates the second,

resulting in a negative value of the first magnetocrystalline anisotropy constant K_1 . *Dunlop & Özdemir* (1997; page 51) reported a K_1 of $-1.2 \times 10^6 \text{ J m}^{-3}$.

Symmetry considerations expect a triaxial crystalline anisotropy ('easy directions') to be present in the basal plane. This in-plane anisotropy (K_B), however, is relatively weak (cf. Subsection 1.4.3; $<1\text{--}400 \text{ J m}^{-3}$), and any stresses, internal or external, will cause the magnetic moment directions to be altered. More important in practice is an uniaxial magnetoelastic anisotropy governed by the stress due to, for instance, crystal twinning (*Dunlop & Özdemir* 1997).

Although basically antiferromagnetic, hematite, possesses a spontaneous magnetization at room temperature. *Dzyaloshinsky* (1958) showed in a theoretical study that a slight canting ($\sim 0.1^\circ$) of the magnetic moments within the basal plane is possible in the hematite structure without violating the magnetic symmetry. This imperfect antiferromagnetic coupling of the Fe^{3+} ions in the alternating A and B sublattices gives rise to a small net ferromagnetic moment, which lies in the basal plane nearly perpendicular to the sublattice magnetizations. *Moriya* (1960) demonstrated that anisotropic superexchange interaction is responsible for the spin canting in hematite. The principal superexchange pathways are summarized by *Morrish* (1994). *Searle & Wang* (1968) reported that the canting requires a canting field (H_D) of only 1–2 T. Spin canting thus appears to be an intrinsic property of hematite and the resulting moment is referred to as the canted, magnetocrystalline, fundamental, intrinsic or anisotropic moment. The weak spontaneous magnetization (σ_s) due to canting is generally reported to be $\sim 0.4 \text{ Am}^2 \text{ kg}^{-1}$ (e.g. *Haigh* 1957; *Flanders & Remeika* 1965), that is about three orders of magnitude smaller than the sublattice magnetizations.

In addition to this magnetic moment due to canting of the spins, hematite may have an additional weak, more variable magnetic moment referred to as the 'defect moment'. In perfect pure hematite crystals it is almost zero, while in substituted and/or poorly crystalline particles it may constitute a considerable part of the total magnetic moment. Part of it appears to be susceptible to heat-treatment and stress or can be changed by neutron irradiation. From these observations it is concluded that this defect moment is not an intrinsic property of hematite, and that its origin most probably lies in imperfections or impurities in the crystal lattice. These 'defects', however, should display some kind of ordering over the sublattices, otherwise no net moment would result due to an imbalance of the sublattice magnetizations. Consequently a distinction must be made between the anisotropic or spin-canted magnetic moment and the isotropic or defect magnetic moment in hematite. The precise connection between both moments is still not clear. Both moments are, however, coupled to the antiferromagnetic structure, but σ_s for the defect moment is parallel to the sublattice magnetization, whereas σ_s for the spin-canted moment is perpendicular (*Dunlop* 1971). Between the Morin transition and the Néel point both moments lie in the basal plane

Some kind of moment may also arise from residual epitaxial layers of Fe_3O_4 or $\gamma\text{-Fe}_2\text{O}_3$. Minute amounts of these highly magnetic contaminants already have a distorting effect on the magnetic properties of hematite samples. This type of moment would be sensitive to (heating-induced) oxidation and inversion, respectively.

The geometrical relationships between this moment and the canted and defect moments mentioned in the previous paragraph are described in Chapter 5, Subsection 5.4.6.

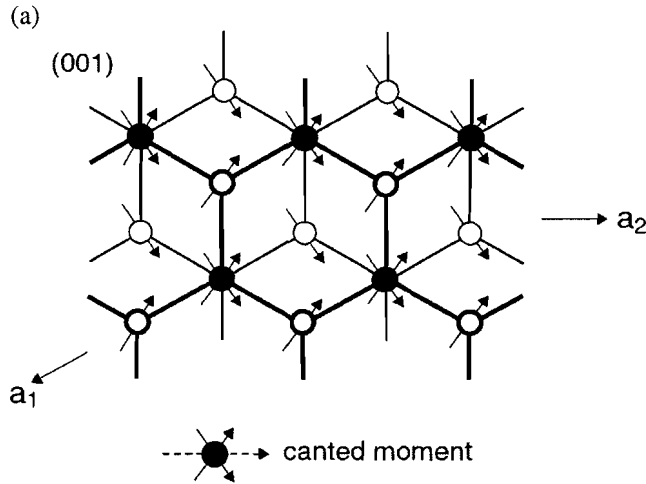
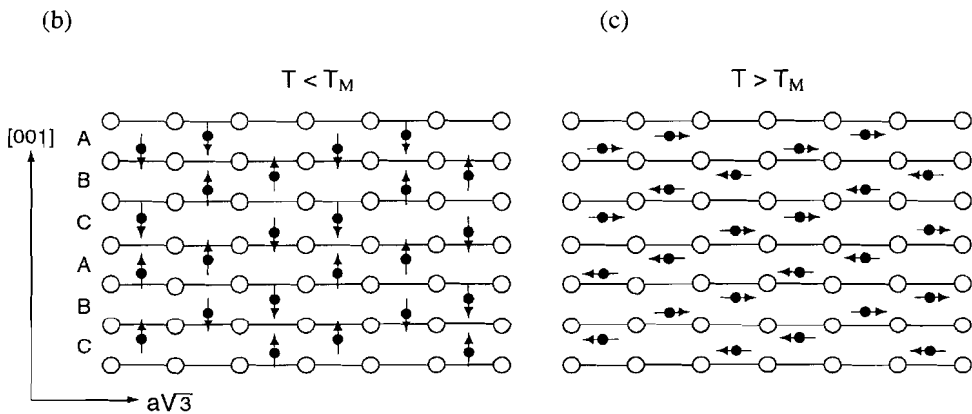


Figure 1.3: The magnetic structure of hematite. (a) Detail of the spin configuration in two adjacent basal planes. Fe atoms of the lower and upper basal plane are denoted by thin and thick open circles, respectively. Solid circles denote two overlying Fe atoms of adjacent layers. Coupling of the magnetic moments is parallel within a layer, whereas spin coupling is antiparallel between adjacent layers. Canting of the spins within in the basal plane is highly exaggerated. The dotted arrow denotes the canted moment resulting from coupling between canted spins of overlying Fe atoms. Panels (b) and (c) show the spin configuration below and above the Morin transition, respectively.



Behaviour on Heating

The magnetic interactions between Fe-atoms on alternating sublattices are strong and are reflected in hematite's high magnetic Néel temperature. The Néel temperature (T_N) of pure hematite is generally reported as $\sim 680^\circ\text{C} \pm 5^\circ\text{C}$ (e.g. *Morrish* 1994 and references therein). Above T_N the antiferromagnetic coupling disappears and hematite becomes a paramagnet. It is generally assumed that the canting of the sublattices and the antiferromagnetic ordering within the sublattice vanish simultaneously. Some data (e.g. *Smith & Fuller* 1967; *Schmidt* 1970; *Vincenz* 1975), however, might indicate that although the spin canting vanishes at $\sim 680^\circ\text{C} \pm 5^\circ\text{C}$, the spin coupling may persist up to higher temperatures ($\sim 725^\circ\text{C}$). The magnetic disordering temperature depends on chemical composition and crystal structure (e.g. interatomic distances) and hence can be affected by impurities (see Subsection 1.4.4). The loss of spin coupling is accompanied by a dilatation anomaly (e.g. *Chaudron & Forestier* 1924), and a specific heat anomaly (e.g. *Furnas* 1926; *Grønvold & Samuelsen* 1975).

The temperature dependence of σ_s for hematite has been reported by several authors (e.g. *Néel & Pauthenet* 1952; *Flanders & Schuele* 1964a; *Dunlop* 1971; *Pullaiah et al.* 1975, and references therein). It appears to be difficult to really saturate the hematite samples during thermal measurements. Consequently most σ_s - T curves are calculated or based on thermal demagnetization of a TRM with high blocking temperatures. In general these studies are based on 'model' hematite, that is the hematite is magnetically dominated by the canted moment. The σ_s - T curve of 'model' hematite has a characteristic block shape; starting from room temperature σ_s changes very slowly with temperature until just below T_N . The block-shaped σ_s - T curve of hematite is distinctive and quite different from that of the sublattice magnetizations $\sigma_A(T)$ and $\sigma_B(T)$. The latter magnetizations appear to drop more rapidly with increasing temperature, within reasonable accord with the Weiss molecular field theory for a spin quantum number $S = 5/2$ (e.g. *Ono & Ito* 1962; *Freier et al.* 1962). The fact that the magnetization due to canting decreases more slowly with temperature than predicted by Weiss theory may suggest that the canting angle increases at high temperature (*Flanders & Schuele* 1964a; *Dunlop* 1971). The possible influence of a superimposed defect moment on the temperature variation of the saturation magnetization is not exactly known. However, due to its origin the defect moment may be susceptible to heating, and affect in this way the σ_s - T behaviour. Structural defects, for instance, may be annealed out of the lattice, while chemical defects (e.g. isomorphously substituted Al) may become redistributed in the lattice on heating. In addition, heating-induced oxidation or inversion reactions will eliminate a chemical defect moment caused by residual Fe_3O_4 and $\gamma\text{-Fe}_2\text{O}_3$, respectively.

No data on the temperature dependence of K_1 between room temperature and T_N are, to the best of our knowledge, available in literature. *Callen & Callen* (1966), however, showed that according to theory, the magnetocrystalline anisotropy constants usually change much more rapidly with temperature than does σ_s . *Flanders & Schuele* (1964a) found a relation of $K_B(T) \propto \sigma_s^m(T)$ with $m = 10 \pm 1$ in for T between 20 and 500°C in one of their crystals. The high-field mass susceptibility or antiferromagnetic susceptibility hardly changes its value of $\sim 25 \times 10^{-8} \text{ m}^3 \text{ kg}^{-1}$, and stays almost isotropic (*Chevallier*

1951; Néel & Pauthenet 1952; Pastrana & Hopstock 1977). The temperature dependence of the coercivity of defect-poor hematite is not well known, but seems to be grain-size dependent. Dunlop (1971), for instance, suggested $H_c(T) \propto \sigma_s^8(T)$ for annealed fine hematite particles, while Flanders & Schuele (1964a) reported $H_c(T) \propto \sigma_s^3(T)$ for a relatively pure, large single crystal of hematite.

Behaviour on Cooling: the Morin transition

In general the magnetic properties of hematite undergo a transition when it is cooled from room temperature downward. In pure hematite crystals a sharp drop in susceptibility (Morin 1950), remanence (Néel & Pauthenet 1952), and saturation magnetization (Flanders & Schuele 1964) is observed around -10°C . This characteristic discontinuity in hematite's magnetic properties is called the Morin transition (T_M), and represents the magnetic isotropic point ($K_1 = 0$) for this mineral. The different temperature variations of the negative magnetic-dipole term and the positive single-ion term causes the change in sign of K_1 (Artman *et al.* 1965; Besser *et al.* 1967; Morrish 1994). As a consequence, the 'easy' directions of magnetization change, resulting in a reorientation of the antiferromagnetically coupled atomic spins from the basal plane for $T > T_M$ to the hexagonal c -axis for $T < T_M$ (e.g. Shull *et al.* 1951). Morrish *et al.* (1963) and later Krén *et al.* (1974) and Sváb & Krén (1979) concluded from neutron diffraction studies that the magnetic moments are likely inclined at an angle of $\sim 7^\circ$ to the [001] axis. Below the Morin transition, however, the antiparallel spin alignment is perfect; any canting would now violate the magnetic symmetry (Dzyaloshinsky 1958; Moriya 1960). Hence, the intrinsic canted moment is susceptible to the Morin transition, but the defect moment is not because the slight non-equivalence in the sublattice magnetic moments will remain. As a result, below T_M only the defect moment persists.

The (remanent) magnetization thus drops rapidly on cooling through T_M but generally does not go to zero because of a weak defect ferromagnetism. The high-field susceptibility becomes isotropic on cooling below T_M (e.g. Néel & Pauthenet 1952; Creer 1967). The susceptibility parallel to the c -axis decreases sharply from a fairly uniform value of $\sim 25 \times 10^{-8} \text{ m}^3 \text{ kg}^{-1}$ to $\sim (1-2.5) \times 10^{-8} \text{ m}^3 \text{ kg}^{-1}$. The susceptibility in the basal plane, however, shows no appreciable change except for a hump ($\sim 30 \times 10^{-8} \text{ m}^3 \text{ kg}^{-1}$) around T_M . Consequently, below T_M a sample of randomly oriented particles, with $1/3$ of the grains having their c -axis parallel to the applied field, has a χ_{hf} around $\sim 16.6 \times 10^{-8} \text{ m}^3 \text{ kg}^{-1}$.

Low-temperature 'Memory'

Hematite remanence cycled in zero field through the Morin transition decreases to low values on cooling, but exhibits 'memory': that is it partially recovers on rewarming through the critical temperature (e.g. Haigh 1957). It is shown that the original direction of remanence is recovered during cycling (e.g. Haigh 1957; Nagata *et al.* 1961). The origin of this 'memory' phenomenon is complex and not fully understood, for the

spin-canted remanence should vanish on cooling through T_m , along with the anisotropy that pins it (Dunlop & Özdemir 1997). There should be equal probability that the spins align themselves on reheating along either of the three possible 'easy' axes (minimum energy positions). Haigh (1957a) suggested that a field of the undemagnetized isotropic component could provide the aligning force. No indications were, however, found to support this argument. Memory is shown to be also present in crystals which do not possess an isotropic component of magnetization (Creer 1967). Most hematites show only a partial memory, but some natural single crystals exhibit an exact recovery of the initial remanence (e.g. Lin 1960; Gallon 1968). The latter author showed that in these particular crystals the low-temperature remanence still makes an angle of about 30° with the [001] axis.

The recovery appears to be dependent upon internal stress and impurities, and can consequently be influenced by heating (cf. Fuller 1970). Nagata *et al.* (1961) found that the recovery of the intensity of remanent magnetizations is closely dependent on the process leading to the remanent magnetization; the rate of recovery is generally large in the case of thermoremanent magnetization (TRM) compared with isothermal remanent magnetization (IRM). These authors also reported that in the case of TRM the larger the imparting magnetic field, the smaller the rate of recovery, while in the case of IRM the relation between the rate of recovery and the applied field is reversed.

Another unexplained feature of the memory is the zig-zag effect which is observed in some hematite samples subjected to repeated thermal cycles. Odd numbered cycles of low-temperature demagnetization give systematically smaller memories than following even cycles (Nagata *et al.* 1961; Borradaile 1994).

1.4.3 Coercivity and magnetic anisotropy

The (remanent) coercivity is the ability of a (remanent) magnetization of magnetic material to resist reorienting forces. The magnetic coercivity of hematite appears to be strongly dependent on grain size, stress, origin and thermal history. In general, coercivity increases with decreasing grain size reaching a maximum at the SD threshold size (e.g. Chevallier & Mathieu 1943; Dunlop 1971; Halgedahl 1995). In large multidomain (MD) grains the coercivity is controlled by wall motion, whereas in SD grains the magnetization reverses by rotation. Banerjee (1971) found, using data from Chevallier & Mathieu (1943), that H_c was proportional to $d^{-0.66}$ for grain sizes ranging between 15–300 μm . He stated that this power law behaviour is typical of MD grains. The paleomagnetic stabilities of the canted and defect moment appear to have a different grain-size dependence. There is evidence that in fine-grained hematite the canted moment has a higher coercivity than the defect moment (e.g. Haigh 1957a; Dunlop 1971), while for large single crystals the reverse is the case (e.g. Smith & Fuller 1967; Fuller 1970).

In contrast to the low coercivity of large MD hematite ($\sim 0.1 - \sim 10$ mT), the observed coercivity in single-domain hematite can be very high ranging $\sim 100 - \sim 1000$ mT (cf. O'Reilly 1984; Dunlop & Özdemir 1997 and references therein). H_c / H_{cr} ratios for fine-grained hematite are typically 1.5–2 (Dunlop 1971). There are two possible origins of the high coercivities observed in fine-grained hematites; the basal-plane anisotropy is

primarily of magnetocrystalline origin or of magnetoelastic origin. The latter is structure-sensitive and thus sensitive to annealing. In addition, coercivity is generally raised by foreign-ion substitution because the Fe^{3+} ion has a relatively low anisotropy (cf. Dunlop 1971). Shape anisotropy cannot be the origin of the required energy barriers in the basal plane of hematite since it is proportional to σ_s (Dunlop 1971). Soffel (1991) reported a H_c of only 1 mT due to shape anisotropy.

The in-plane triaxial magnetocrystalline anisotropy is relatively weak and hence difficult to determine. Reported K_b values are highly variable and dependent on the measurement technique and grain size. The most reliable estimates range between $<1\text{--}400 \text{ J m}^{-3}$ (cf. Dunlop 1971; Banerjee 1971 and references therein). The higher values represent the smaller grain sizes and can explain coercivities up to several hundreds of mT since for crystalline anisotropy $H_c \propto K_b / \sigma_s$ (cf. Banerjee 1971; Dunlop 1971; Soffel 1991). Porath (1968a), on the other hand, suggested that the primary source of the observed high coercivities in SD hematite must be magnetoelastic anisotropy due to internal stress. The author argued that internal stresses become more important in fine grains. The polycrystalline magnetostriction constant of hematite $\lambda_s \approx 8 \times 10^{-6}$ (Urquhart & Goldman 1956). This value is comparable to that of magnetite or maghemite, but the small value of M_s in hematite means that an internal stress (σ) of 100 MPa can produce a coercivity of ~ 500 mT, since $H_c = 3\lambda_s\sigma / 2\mu_0M_s$ (Dunlop 1971; Dunlop & Özdemir 1997, page 451). Since magnetoelastic anisotropy is sensitive to changes in internal structure, the coercivity due to uniaxial magnetostriction is sensitive to annealing in contrast to that of triaxial magnetocrystalline origin (Dunlop 1971).

1.4.4 Variations in T_N and T_M

The Dependence of T_N on Impurity content

The Néel temperature (T_N), like σ_s , is an intrinsic property of hematite depending only on chemical composition and crystal structure. The magnetic disordering temperature is thus susceptible to impurities when they may change the number of superexchange bounds and also affect the lattice parameters (Morrish 1994). T_N , which is determined by the product of the sublattice spin moments, is however relatively less sensitive to cation distribution variations than σ_s , which is the difference between A and B sublattice magnetic moments (Banerjee 1991).

Morrish (1994) summarizes some literature data on the variation of T_N with cation impurity. No reports on an increase in T_N for any impurity has appeared up to now, and hence all impurity cations are believed to reduce the Néel temperature. At least for small concentrations of impurity cations, the Néel temperature is observed to decrease roughly linearly with increasing substitution (e.g. Sváb & Krén 1979; Krén *et al.* 1965). Both, Al^{3+} and Ti^{4+} , are diamagnetic and their radius is smaller than that of the ferric ion. The effect of Al-substitution on the Néel temperature was measured by Hutchings (1964) and Krén *et al.* (1974). The latter authors found a relation between T_N and Al^{3+} of $T_N(x) = T_N(0) (1 - 0.54x)$ for $x \leq 0.22$. Nagata & Akimoto (1956) and Westcott-Lewis &

Parry (1971) reported a steady, almost linear, decrease of T_N with increasing Ti-substitution of $T_N(x) = 675 - 885x$ and $T_N(x) = 622 - 855x$ (for $0.3 < x < 1$), respectively.

The Dependence of T_M on Magnetic field, Pressure, Impurity content and Grain size

Variation with magnetic field and pressure: Before we review the dependence of the Morin temperature on impurity content and grain size one should be aware that the Morin transition is not only temperature induced but also magnetic-field or pressure driven (*cf. Morrish 1994*). The three variables are interdependent. By application of an external field the transition can be induced at lower temperatures; the critical field required to give the transition is dependent upon the temperature and the angle between the field and the crystal axis (e.g. *Morrish 1994* and references therein). A stress dependence of the low-temperature transition of ~ 4 K/kbar is reported by *Umebayashi et al. (1966)*, *Kawai & Ono (1966)* and *Kawai et al. (1968)*. In practice the pressure is usually close to one atmosphere and small (Earth's) magnetic fields may be present during the determination of T_M .

Variation with impurity content: For pure well-crystalline hematite the isotropic point typically lies around -10°C . The reorientation of the magnetic spins is very abrupt, in this case spanning only $\sim \leq 5^\circ$ (e.g. *Flanders & Remeika 1965*). However, particularly the parameters related to the Morin transition (H_{MD} and H_{SI}) are easily affected by small changes in the lattice. Their dependence on foreign-ion substitution is however different (*Artman et al. 1965; Besser et al. 1967*). Hence, the Morin transition is not only quite sensitive to externally applied pressure but also to the incorporation of small amounts of impurities. The sensitivity of the Morin transition to substituted cations has been studied by numerous workers (*cf. Morrish 1994* and references therein). Impurities not only cause a shift of the transition temperature but also tend to smear the reorientation of the magnetic spins over a larger temperature range. Smearred transitions are mostly described by the effective transition temperature T_M which is the temperature at which the change in moment with T of one-half the total change through the transition has occurred, and ΔT_M which is the temperature range over which the change in moment occurs (*Flanders & Remeika 1965*). Other authors, however, define T_M by the intersection of the two tangents along the moments obtained during and after the transition (*cf. Dunlop & Özdemir 1997*, page 70). Because of the hysteresis effect observed during a temperature cycle, the parameters are generally taken from the cooling curve.

Flanders & Remeika (1965) studied a variety of cations and found that the transition was most sensitive to the Sn extent. Most impurity cations investigated decrease the Morin transition, with Rh^+ , Ru^+ and Ir^{4+} being exceptions to this rule (*cf. Morrish 1994* and references therein). The influence of substituted cations on the Morin temperature is often more dramatic than on T_N . In sufficient quantities, the incorporated cation can completely suppress the Morin transition, at least down to the lowest temperatures measured (4.2 K). Hence, the weak ferromagnetic phase persists in these hematites over the entire temperature range (*Morrish 1994*). For hematites, only 1 atom % Ti-

substitution is already sufficient to completely suppress the transition below 4.2 K (e.g. Morin 1950; Besser *et al.* 1967; Morrish 1994). Haigh (1957b) however, reported a Morin transition in hematite substituted with ~4 atom % titanium. According to Curry *et al.* (1965) many Ti-ions in the sintered samples used must, however, be expected to be present at the grain boundaries, and not in the lattice. Aluminium, like copper and manganese appears to be less effective in reducing T_M than Ti (e.g. Flanders & Remeika 1965); full suppression of the Morin transition is reported for ~10 mole % Al (Hutchings 1964; Krén *et al.* 1974; Fysh & Clark 1982). Ishikawa & Akimoto (1957) found that 5 mole % of MgTiO₃ in the MgTiO₃-Fe₂O₃ system almost suppressed the transition. Natural hematite-bearing samples often contain more Ti, explaining the absence of the Morin transition in these samples.

The presence of Al and other impurity cations also tends to smear the Morin transition over a greater range in temperature (Srivastava & Sharma 1972; Krén *et al.* 1974; Fysh & Clark 1982). These authors found also indications for an increase in the angle between the [001] direction and the Fe³⁺ magnetic moment as non-iron atoms enter the lattice. Nininger & Schroerer (1978), and De Grave *et al.* (1982) showed that in a smeared transition both an antiferromagnetic and a weak ferromagnetic phase can coexist over a considerable temperature range. Furthermore, the electron spins of microcrystalline or Al-substituted hematites showing two phases, no longer change their direction spontaneously at the appropriate temperature, but rather execute a gradual and partial reorientation (De Grave *et al.* 1983). This continuous rotation of the spins out of the (001) plane to the [001] direction over a broad range from +80°C to -50°C was already reported by Lin (1960) for a natural hematite single-crystal from Elba.

Variation with grain size: A number of studies have demonstrated that the Morin transition is also lowered as particle size is reduced; it becomes even completely suppressed in pure hematite grains less than ~0.02 – ~0.03 μm (Bando *et al.* 1965; Kündig *et al.* 1966; Yamamoto 1968; Schroerer & Nininger 1967; Nininger & Schroerer 1978). Consequently, the basal-plane spin configuration is retained at least down to 4K. Creer (1962) reported that grinding first broadened and next suppressed the transition in some natural hematites.

Various explanations circulate in literature for the observed decrease in T_M with decreasing grain size. Schroerer & Nininger (1967) linked this observation to the lattice expansion which seems to be concomitant with a decrease in particle size due to surface effects. The resulting internal dilatational strain would then be responsible for the observed decrease in T_M . The authors argued that this lattice dilatation can be seen as equivalent to a negative pressure, and showed that the transition is found to be depressed under this negative 'equivalent pressure' at a rate comparable with the increase (~4 K/kbar) observed under hydrostatic pressures. From their experiments they conclude that the increase in the lattice parameter is homogeneous throughout the whole microcrystal volume. Burton & Godwin (1967) and Kündig *et al.* (1967), however, suggested that surface effects only distorted the first few surface atomic layers while not significantly affecting the bulk below. Yamamoto (1968) considers the decrease in the magnetic-dipole anisotropy field, induced by the *a*-axis dilatation as the source of the lowering of T_M . Gallagher & Gyorgy (1969) have suggested that the observed dilatation

in $\alpha\text{-Fe}_2\text{O}_3$ may be caused by the presence of structurally bound water in lattice due to insufficient heating of the initial solute. *Chadwich et al.* (1968) also argued that water in the hematite lattice appears to alter T_M . An other cause of decreasing T_M with smaller particle sizes may be the 'pinning' of atomic spins by the surface and inhibiting the Morin transition in this way (e.g. *Kündig et al.* 1967; *Yamamoto* 1968; *Nininger & Schroeer* 1978). Clearly, surface atoms constitute a greater fraction of the total as particle size decreases, and indeed ultrafine particles may be essentially all surface.

Other possibilities: Vacancies or defects produced by irradiation by fast neutrons are reported to cause also a slight decrease in T_M , a broadening of the transition, and an increase in low-temperature remanence (e.g. *Gallon* 1968a; *Zhetbaev et al.* 1990, 1992). Annealing appears to have just the opposite effect. *Kündig et al.* (1960), *Janot & Gilbert* (1970), and *Verbeeck et al.* (1986) have found indications that the morphology and degree of crystallinity can alter both T_M and the temperatures range over which the transition occurs (ΔT_M).

1.4.5 Mechanisms and timing of remanence acquisition in hematite-bearing sediments

Whether the hematite of sedimentary rocks is detrital or authigenic is not only important for the understanding of the genesis of these rocks, it also determines the type and timing of NRM acquisition. For paleomagnetism, the timing of the NRM is crucial.

Detrital hematite particles may become physically aligned with the geomagnetic field before dewatering and consolidation restricts motion of sedimentary particles. The remanence acquired during deposition is called a detrital remanent magnetization (DRM). A magnetization acquired because of physical alignment processes after deposition but before consolidation is referred to as post-depositional detrital remanent magnetization (PDRM). Depending on the size and remanence mechanisms of grains in the source rocks, DRM and PDRM may inherit the temperature and time stability and AF hardness of TRM, CRM, TCRM or VRM of SD, PSD, or MD grains (*Dunlop & Özdemir* 1997).

A true DRM reflects the geomagnetic field at the time of deposition. Such a primary component of the total NRM thus may provide useful information concerning polarity reversal mechanisms or secular variation. Estimates of PDRM 'lock-in' time, however, range up to 10^3 yr, depending on sedimentary environment (e.g. *Løvlie* 1976; *deMenocal et al.* 1990). Consequently, in the case of high lock-in times, field reversals may not be recorded as sharp events, short reversal events may be obscured and the record of paleosecular variation may be smoothed out. However, an important advantage of PDRM over DRM is that experimental evidence has shown that the former does not have an inclination error (*cf. Dunlop & Özdemir* 1997).

During growth of *in situ* formed hematite a so-called chemical remanent magnetization (CRM) may be acquired. As mentioned in Subsection 1.2.2, authigenic hematite may be formed by precipitation from iron-bearing solution or by alteration of pre-existing minerals. When the pre-existing mineral is magnetic, the direction of the

CRM acquired by the crystallizing daughter phase may be influenced by the magnetization of the parent phase through magnetostatic or exchange coupling across the moving phase boundary. Magnetic parent phases of hematite can be magnetite, maghemite or goethite. Each transformation reaction, however, implies substantial change of the crystal and magnetic structure, and therefore exchange-coupling between the two phases involved would not be expected (*cf. Dunlop & Özdemir 1997*). Indeed, phase-coupling seems not to be a general phenomenon in all three systems, and consequently a growth CRM controlled by the ambient field results. *Chevallier (1951)*, for instance, reported that dehydroxylation of goethite generally produces polycrystalline hematite that lacks hysteresis. According to *Dunlop & Özdemir (1997)*, the small crystallite size is probably the cause of superparamagnetic (*Creer 1961*) or incoherently magnetized (*Collinson 1969*) hematite in red beds, even in grains as large as $0.25\ \mu\text{m}$ (*Strangway et al. 1967*). Moreover, since all traces of goethite disappear before hematite crystallites grow to stable SD size, all memory of the NRM of goethite is lost (*cf. Dunlop & Özdemir 1997*). Goethite is antiferromagnetic but spin compensation is usually imperfect due to an ordered structure of impurities ($\sigma_s \sim 0.01\text{--}0.1\ \text{Am}^2\ \text{kg}^{-1}$). However, some controversy remains about the existence of exchange coupling across the magnetite–hematite and the maghemite–hematite phase boundary. *Heider & Dunlop (1987)*, for instance, oxidized synthetic magnetites to hematite and often found the CRM to appear in a spurious direction intermediate between the applied field H_0 ($= 50\text{--}200\ \mu\text{T}$) and a pre-existing ARM, M_{ar} . The CRM could be made parallel to either H_0 or M_{ar} by increasing one of these factors at the expense of the other. Also some type of phase-coupling seems to occur when polycrystalline maghemite produced by dehydrating acicular lepidocrocite crystals inverts towards hematite. This phenomenon is reviewed in Chapter 5, Subsection 5.4.6.

A remanence residing in grains chemically grown *in situ* may have formed at any time after deposition. A CRM carried by hematite thus may provide useful paleomagnetic information only if the time of acquisition is accurately known. Even then, the fine time-resolution of primary DRM is not likely obtained. However, a CRM formed within 10^5 yr of deposition could be applied to magnetic polarity stratigraphy, while a CRM formed over intervals up to perhaps 10^7 yr could still be used to determine paleomagnetic poles. The problems with determining the type and timing of remanence carried by hematite grains manifests itself in the ‘red bed controversy’.

The ‘Red Bed Controversy’

The ‘red bed controversy’ arises from the discussion whether the observed NRM (or one of its components) derives from a DRM acquired penecontemporaneously with deposition or from a CRM acquired during chemical processes that may occur up to 10 my after deposition. In extreme view, red bed sequences either provide high-fidelity records of the paleomagnetic field, or yield cautionary paleomagnetic results because the timing of the complex NRM components is poorly constrained.

Usually, various hematite forms of different origin are present in red beds (see Subsection 1.2.2), which may have acquired remanence by different mechanisms and at a different time. The respective contributions to the total NRM may vary considerably.

Often the multicomponent NRM can be unravelled and the predominance of either one or the other can be established by rock-magnetic and petrographic methods.

Pigmentary hematite (<1 μm) often forms the cement in red sediments and is clearly formed by post-depositional chemical processes. Because of the ultrafine grain size of many of the pigment crystals, the magnetization is often unstable over geological time, and these grains tend to acquire viscous magnetization (VRM). This VRM can be very hard because of the high intrinsic coercivities involved (*cf. Dunlop & Özdemir 1997*). Pigmentary hematite, however, can also acquire CRM because of prolonged grain growth (crystallite size $\sim >0.1 \mu\text{m}$) in the geomagnetic field. In general, its time of formation is difficult to constrain. Most studies, however, indicate that the CRM carried by pigmentary hematite is composed of multiple components of magnetization acquired during protracted chemical precipitation, perhaps millions of years after deposition (e.g. *Roy & Park 1972; Collinson 1974; Tauxe et al. 1980*). Consequently, the remanence residing in pigmentary hematite is commonly seen as an undesired secondary NRM component obscuring any possible ChRM carried by more coarse-grained (>1 μm) black crystalline hematite particles (specularite). In many cases the remanence carried by pigmentary hematite can selectively be removed by either chemical (acid leaching: e.g. *Roy & Park 1972*) or thermal demagnetization techniques (e.g. *Tauxe et al. 1980*). Pigmentary hematite usually has lower unblocking temperatures than specular hematite. However, very small temperature steps (5–10°C) are usually required to separate both components (e.g. *Lee et al. 1996*), because a strong grouping of unblocking temperatures for grains of all sizes in a 50°C range below T_c results from the 'blocky' nature of the σ_s - T curve of hematite (*cf. Dunlop & Özdemir 1997*).

For the majority of red sediments for which a high-stability ChRM can be isolated, the question of the timing of ChRM acquisition thus becomes a question of when the coarse-grained hematite varieties were actually formed. Detailed paleomagnetic, rock-magnetic and petrographic studies can often answer this question. For instance, the textural patterns of hematite particles or field tests of paleomagnetic stability applied to sedimentary structures may provide information about their origin.

For some red bed sequences the results seems to indicate the possibility of primary DRM or PDRM acquisition in detrital hematite particles (*Collinson 1966; Van den Ende 1977; Elston & Purucker 1979; Elmore & Van der Voo 1982; Steiner 1983; Douglass 1988*). High-fidelity records of paleosecular variation (*Baag & Helsley 1974*) and geomagnetic polarity transitions (*Herrero-Bervera & Helsley 1983; Shive et al. 1984*) obtained on these type of red beds require that the ChRM was acquired within $\sim 10^2$ yr of deposition. Especially, those red bed sequences in which the majority of the hematite derives from volcanic terrains seem to be magnetized by this mechanism (e.g. *Van den Ende 1977*).

Most evidence, however, seems to favour post-depositional formation of the majority of the specular varieties and thus the red bed remanence is largely CRM. *Roy & Park (1972)* and *Walker et al. (1981)*, for instance, concluded that the NRM in their red beds mainly consisted of several components of CRM. The authors argued that all authigenic hematite growth (CRM acquisition) must be considered to be a long-time process which may take many of thousands of years, making the use of red beds for geomagnetism and magnetostratigraphy questionable. From petrographical observation, *Walker et al. (1981)*

suggested that most hematite grains were formed by authigenesis resulting principally from intrastratal breakdown of iron-bearing detrital grains that require considerable geological time. In their red beds studied, they only found a small portion of hematite of unquestionable detrital origin, which hardly contributed to the total NRM. *Purucker et al.* (1980) and *Tauxe et al.* (1980) argued also that in their red beds the specular hematite remanent magnetizations were acquired as CRM. They, however, clearly showed that the CRM must be acquired during or shortly after deposition (early diagenesis), and thus represents a primary NRM perfectly useful for magnetostratigraphic studies.

Concluding, the controversy seems to stem mainly from the generalization of a particular red bed sequence to all red beds. Clearly, the paleomagnetic, rock-magnetic and chemical/petrographic history of each red bed sequence must be derived individually. Differences in type and timing of remanence acquisition between red bed sequences are likely caused by factors such as: mineralogical maturity of the sediment at deposition, grain-size of the sediment, presence of organic matter and the depositional environment and paleoclimate (*Turner* 1980). For comprehensive discussions on the genesis of red beds and on the type and timing of NRM acquisition, the reader is referred to *Blodgett et al.* (1993) and *Dunlop & Özdemir* (1997) respectively, and references in both.

Chapter 2

Thermomagnetic behaviour of hematite and goethite as a function of grain size in various non-saturating magnetic fields

Cor B. de Boer and Mark J. Dekkers

Paleomagnetic Laboratory 'Fort Hoofddijk', Utrecht University, Faculty of Earth Sciences, Budapestlaan 17, 3584 CD Utrecht, the Netherlands. E-mail: cdeboer@geo.uu.nl

Geophys. J. Int. (1998) 133, 541–552

SUMMARY

When interpreting thermomagnetic curves of non-saturated magnetic minerals, irreversible heating and cooling curves need not necessarily imply chemical or structural changes. Increased aligning of magnetic moments on heating in an applied magnetic field can also induce an irreversible cooling curve. The two processes can be distinguished by stirring of the sample between subsequent thermomagnetic runs. Sample redispersion considerably enhances the interpretative value of thermomagnetic analysis and is therefore strongly recommended, in particular when analysing non-saturated magnetic minerals.

Stirring between subsequent runs was extensively used in the analysis of the thermomagnetic behaviour of hematite and goethite as a function of grain size (i.e. coercivity) in various non-saturating magnetic fields (10 to 350 mT). The shape of the thermomagnetic heating curves of hematite is shown to be dependent on the competitive interplay between the temperature dependence of the exchange energy and that of the coercive force with respect to the applied field. On heating, pure, defect-poor hematite, which is magnetically dominated by the canted moment, has an initially increasing thermomagnetic heating curve. Further heating causes the magnetization to increase smoothly up to a certain temperature which depends critically on the applied

field and the coercivity of the sample. The irreversible block-shaped thermomagnetic cooling curve lies above the heating curve, and shows hardly any dependence on applied field and grain size. In contrast to the heating curve, the shape of the cooling curve depends only on the temperature variation of the exchange energy. Our data seem to indicate that for defect-poor hematites the domain configuration acquired at the maximum heating temperature is retained on cooling to room temperature. More defect-rich hematite has a gently decreasing thermomagnetic heating curve. On heating to increasingly elevated temperatures (800°C) the defects are annealed out of the lattice, because the thermomagnetic curves approach those of defect-poor hematite. The defect moment due to lattice defects seem to be additive to, but softer than, the canted moment. The canted and defect moment appear to have the same Néel (or Curie) temperature (~680°C), because no change in temperature was observed, whilst the relative contributions did change. The thermomagnetic behaviour of goethite is shown to be dependent on its coercivity and the amount of substituted ions.

2.1 Introduction

A Curie balance is a useful tool in magnetomineralogic research which is used to monitor the magnetization σ (σ_s when saturated) of a sample as a function of temperature. Thermomagnetic analysis not only provides mineral-specific Curie or Néel temperatures (T_c and T_N , respectively), but also yields essential information concerning changes in magnetic structure and chemical reactions involving ferromagnetic minerals. For saturated ferromagnetic minerals, the heating and cooling curves of one complete thermomagnetic cycle are reversible if no chemical, structural or textural changes occur as a consequence of heating. The shape of the thermomagnetic curves depends in this case only on the temperature variation of the exchange energy, which is a reversible process. Thermally induced chemical changes (e.g. dehydration, exsolution or, when measured in air, oxidation), structural changes (e.g. inversion, better ordering of the crystal lattice due to recrystallization or diffusion of lattice defects), and textural changes (e.g. sintering) may thus be detected by comparing the shape of heating and subsequent cooling curves.

The applied magnetic field in Curie balances, however, is often not sufficiently high to saturate hard magnetic minerals such as (ilmeno-)hematite, goethite, (oxidized) Titanomagnetites, some surficially oxidized greigites and fine-grained pyrrhotite. Consequently, in non-saturating fields the shape of the thermomagnetic curves also depends on the coercivity of the sample and its variation with temperature (*Day 1975; Duff 1979*). In this case, the irreversibility of the heating and subsequent cooling curve is not necessarily caused by chemical or structural changes of the mineral under investigation, but can also be caused by an irreversible magnetic 'aligning' process, as demonstrated by *Day (1975)* and *Duff (1979)* for synthetic titanomagnetite and natural hematite, respectively. Those observations, although acquired with rather insensitive Curie balances yielding noisy data, have received surprisingly little attention. Observed irreversible thermomagnetic behaviour is still often erroneously taken as evidence for thermally induced chemical or structural changes of non-saturated minerals.

Here, we present new data for two (synthetic and natural) submicron goethites and additional data for two natural hematites of different grain size, measured on a much more sensitive Curie balance (Mullender *et al.* 1993). It is shown that the shape of the thermomagnetic curves critically depends on the applied field and on the coercivity (i.e. grain size) of the sample. A pure, well-crystalline, 'defect-poor' hematite, which did not show any thermally induced chemical or structural changes, served as a reference for the measurement of field- and grain-size (i.e. coercivity) dependence of thermomagnetic curves. Deviations from this 'ideal' thermomagnetic behaviour are illustrated by the behaviour of a more 'defect-rich' hematite. For goethite, the difference between the thermomagnetic behaviour of a hard (synthetic) and a relatively soft (natural) sample is discussed. Redispersion of the sample followed by a repeated run to the same temperature is put forward as a tool for the detection of possible thermally induced chemical or structural changes.

2.2 Relevant rock-magnetic data

2.2.1 Hematite

Hematite (α -Fe₂O₃) is referred to as canted antiferromagnetic and has a saturation magnetization of $\sim 0.4 \text{ Am}^2 \text{ kg}^{-1}$ at room temperature (e.g. Stacey & Banerjee 1974; O'Reilly 1984). Reported σ_s -values vary between 0.2 and $0.5 \text{ Am}^2 \text{ kg}^{-1}$ (e.g. Néel & Pauthenet 1952; O'Reilly 1984). Above the Morin transition temperature ($T_M \sim -10^\circ\text{C}$) the antiferromagnetically coupled sublattice magnetizations lie in the basal plane orthogonal to the c -axis. A slight canting of the spin axis out of exact antiparallelism, however, results in a weak net ferromagnetic moment within the basal plane, perpendicular to the spin sublattices (Dzyaloshinsky 1958). In addition to this 'spin-canted moment', hematite may have a highly variable magnetization referred to as the 'defect moment'. Observed variations in σ_s are ascribed to this variable 'defect moment', which is thought to arise from (an ordered structure of) lattice defects or from substituted non-magnetic cations (e.g. Néel 1953; Dunlop 1971; O'Reilly 1984). The 'defect moment' is therefore negligible in perfect, pure crystals and large in strained or otherwise imperfect grains. Because hematite is weakly magnetic only, one has to be aware that the measured properties of hematite samples are susceptible to the distorting effect of minute amounts of magnetic contaminants such as magnetite and maghemite.

At the Morin transition the spin orientation is changed from perpendicular to parallel to the c -axis. The antiferromagnetic coupling is retained but spin alignment is now perfect; that is canting has disappeared, resulting in no net magnetic moment. The 'defect moment', however, would not be affected by this spin reorientation and therefore remains below T_M . The temperature at which the Morin transition occurs, as well as its extent, are shown to be dependent on crystallinity and the amount of substitution in the hematite (e.g. Flanders & Remeika 1965; De Grave *et al.* 1983). In pure hematite the Morin transition is completely suppressed in grains smaller than $\sim 0.03 \mu\text{m}$ (e.g. Bando *et al.*

1965; Schwertmann & Murad 1983). Dekkers & Linssen (1989) suggested that this grain-size limit may be larger for grains with sorbed silica and hydroxyl groups on their surface.

The Néel temperature of well-crystallized, pure hematite is generally reported to be $\sim 680^\circ\text{C}$. Substituted hematite has slightly lower values (e.g. Hutchings 1964). However, it is still debated whether or not the disappearance of the 'spin-canted moment' coincides with the antiferromagnetic T_N . Putnis (1992), for instance, reported that the spin canting vanishes around 675°C , but the antiferromagnetic coupling would persist up to $\sim 685^\circ\text{C}$. At higher temperatures the hematite is paramagnetic. This would imply that the 'defect moment' can be measured up to 685°C .

2.2.2 Goethite

Goethite ($\alpha\text{-FeOOH}$) is antiferromagnetic but the spin compensation is imperfect, allowing a small net moment (e.g. Van Oosterhout 1965; Banerjee 1970; Hedley 1971). Sublattice magnetizations as well as the weak ferromagnetism of goethite lie along the crystallographic c -axis. Özdemir & Dunlop (1996) showed for well-crystallized, natural goethite that the ferromagnetic T_c coincides with the antiferromagnetic T_N at $120^\circ\text{C} \pm 2^\circ\text{C}$. However, reliable values between 70°C to 130°C have been reported for T_N of goethite, depending on substitution, crystallinity, excess water and grain size (cf. Özdemir & Dunlop 1996 and references therein). Bocquet & Hill (1995), for instance, correlated reduced T_N values in fine-particle goethites with the concentration of iron vacancies, and proposed a cluster ordering model. Goethite can acquire a weak but very stable thermoremanent magnetization (TRM) with blocking temperatures up to 120°C (e.g. Strangway *et al.* 1967; Strangway *et al.* 1968; Banerjee 1970; Dekkers 1989a; Dekkers & Rochette 1992; Özdemir & Dunlop 1996). Observed saturation magnetizations are highly variable but are mostly in the range 10^{-2} to $10^{-1} \text{ Am}^2 \text{ kg}^{-1}$ (e.g. Bagin *et al.* 1976; Morris *et al.* 1985; Dekkers 1989b). Hedley (1971), however, reported σ_s -values increasing from 10^{-3} to $1 \text{ Am}^2 \text{ kg}^{-1}$ with rising aluminium content in the goethite.

2.2.3 Temperature dependence of the saturation magnetization

Hematites and goethites can show highly variable thermomagnetic behaviour. To explain observed differences between saturated and non-saturated behaviour and to distinguish different types of hematite and goethite by their thermomagnetic behaviour we need a reference σ_s - T curve typical of ideal crystals. In the case of hematite, calculated σ_s - T curves and curves based on thermal demagnetization of a TRM with high blocking temperatures of 'ideal' (pure and defect-poor) crystals are dispersed throughout the literature (e.g. Dunlop 1971; Pullaiah *et al.* 1975 and references therein). The reversible heating and cooling curves of saturated 'ideal' hematite are characterized by a typical block shape, with hardly any decrease in σ_s until $\sim 400^\circ\text{C}$ and a steep drop in magnetization after $\sim 650^\circ\text{C}$ to the Néel temperature. This characteristic shape indicates

that for 'ideal' hematite, which is dominated by the canted moment, any decrease in exchange energy is almost negligible up to $\sim 400^\circ\text{C}$.

The σ_s - T curves measured by *Rochette & Fillion* (1989) can be taken as more or less 'model' σ_s - T behaviour for saturated, relatively pure, fine goethite crystallites. The thermomagnetic behaviour is characterized by an almost linear decrease in magnetization from ~ 20 K to ~ 10 - 20° below T_N . Above this temperature, the magnetization decreases more rapidly up to T_N .

2.3 Samples and methods

Two relatively pure natural hematite samples and two (synthetic and natural) goethite samples were used for the experiments. The hematite samples, labelled LH4 and LH6, are described by *Hartstra* (1982). The sized LH4 and LH6 fractions were crushed by *Hartstra* from massive pure hematite aggregates in a copper mortar and yielded platy and rounded grains, respectively. No significant substitution was detected by microprobe analyses. The lamellar texture of the LH6 hematite suggests that it is a completely martitized magnetite. Very few exsolution lamellae, probably of maghemite ($\gamma\text{-Fe}_2\text{O}_3$), were detected in the finest grain-size fraction under reflected light (*cf. Hartstra* 1982). Using alternating gradient magnetometer (MicroMag) measurements on fresh, non-heated material (*Table 2.1*), we found that apart from the finest fraction ($< 5 \mu\text{m}$) of LH6 hematite, all grain-size fractions of LH4 hematite were also contaminated with a trace of a softer magnetic mineral. Consequently, data reported by *Hartstra* (1982) on these hematites are slightly biased by the magnetic contaminants. Test runs on the Curie balance indicated that the soft mineral in the LH6 sample was indeed maghemite (contribution to the signal $\leq 0.025 \text{ Am}^2 \text{ kg}^{-1}$ at room temperature, corresponding to ~ 0.03 weight per cent), and that this spinel phase can easily be removed (*i.e.* inverted to hematite) by heating above $\sim 400^\circ\text{C}$, essentially without affecting the hematite (*cf. Subsection 4.1.3; Fig. 2.2b*). Therefore, we preheated the $< 5 \mu\text{m}$ fraction to 700°C before measuring the field dependence of the thermomagnetic curves. The LH4 sample appeared to be contaminated with trace magnetite (contribution to the signal for the 30 - $40 \mu\text{m}$ fraction $\leq 0.05 \text{ Am}^2 \text{ kg}^{-1}$ at room temperature, corresponding to ~ 0.05 weight per cent) which was, however, minimized (*i.e.* oxidized to hematite) to an insignificant amount after heating to 700°C in air (*cf. Subsection 2.4.2*).

The synthetic goethite sample is described by *Dekkers & Rochette* (1992). It was precipitated from an aqueous ferric nitrate solution at 30°C . The more or less rectangular grains (0.3 - $5 \mu\text{m}$) have a granular texture with crystallite sizes ranging between 20 and 40 nm. The natural goethite was crushed from the massive outer rim of a rattle stone (museum piece). No concentric layering is visible in the sampled part. The sample contains a few percent of intergranular silica and clay (*J.J. van Loef*, personal communication). The individual goethite crystallites of rattle stones are generally reported to be in the nanometer size range, and the goethite is slightly Al-substituted (*Van der Horst et al.* 1994).

		B_c (mT)	B_{cr} (mT)	M_r / M_s
<i>LH6 fresh</i>	55–75 μm	182 ± 4	204 ± 2	0.79 ± 0.03
	<5 μm	279 ± 4	367 ± 1	0.74 ± 0.01
<i>LH6 800°C</i>	55–75 μm	180 ± 3	197 ± 3	0.84 ± 0.03
	<5 μm	324 ± 7	354 ± 1	0.92 ± 0.01
<i>LH4 fresh</i>	55–75 μm	70 ± 4	129 ± 1	0.54 ± 0.05
	<5 μm	100 ± 1	252 ± 1	0.57 ± 0.01
<i>LH4 800°C</i>	55–75 μm	174 ± 4	244 ± 5	0.73 ± 0.02
	<5 μm	277 ± 6	374 ± 5	0.76 ± 0.01

Table 2.1: Hysteresis parameters of the hematite samples measured at room temperature with an alternating gradient magnetometer. The coarser grain-size fractions of both hematites reach almost saturation in the maximum applied field (1 T), while saturation did not occur for the <5 μm fractions. Data of the fresh material is in some cases slightly biased by traces of a magnetically soft mineral (maghemite for the <5 μm grain-size fraction of LH6 hematite, and magnetite for both fractions of LH4 hematite). Cycling to 800°C ($\sim 6^\circ\text{C min}^{-1}$) in an oven minimized the influence of these minerals. After this treatment the hysteresis loops were no longer slightly dented and wasp-waisted for the LH6 and LH4 hematite samples, respectively.

The $\sigma(T)$ curves for this study were measured in air with a modified horizontal translation Curie balance, which uses a cycling field instead of a steady field (Mullender *et al.* 1993). By cycling between the field values B_{\min} and B_{\max} the output signal is amenable to Fourier analysis. This makes continuous drift correction possible and the output signal can be processed further with a transversal filtering programme that considerably improves the signal-to-noise ratio. In this way the sensitivity has been increased by two to three orders of magnitude compared to conventional systems. Routine heating and cooling rates were $10^\circ\text{C min}^{-1}$ and $2\text{--}4^\circ\text{C min}^{-1}$ for the hematite and goethite samples, respectively. Typically, 50–100 mg samples of material was weighed in the sample holder of the Curie balance.

With this ultrasensitive Curie balance the shape dependence of the thermomagnetic curves for non-saturated ‘ideal’ hematite on the applied field and on grain size (55–75 μm and <5 μm fraction) can be resolved accurately. The curves are measured at various non-saturating cycling fields ranging from 10 to 350 mT. Incremental runs to increasingly elevated temperatures up to T_N were measured to describe the magnetization process at temperatures lower than the T_N of the sample material. Sample redispersion between subsequent thermomagnetic runs was used to distinguish between genuine chemical and structural/textural changes of the sample on the one hand and field-induced changes in the magnetization on the other. After a thermomagnetic cycle, the sample was either redispersed with a copper stick inside the sample holder or it was taken out of the holder, redispersed, reweighed, and measured again under identical experimental conditions.

2.4 Results and discussion

2.4.1 Pure defect-poor hematite

Shape of the thermomagnetic heating curves

The thermomagnetic heating curves to 700°C measured as a function of applied cycling field are shown in *Figs 2.1(a & b)* for the 55–75 μm and <5 μm grain-size fractions, respectively, of LH6 hematite. In non-saturating fields, the shape of the thermomagnetic heating curves is obviously not only dependent on the temperature variation of the exchange energy, but also depends on the magnitude of the applied field. By comparing the results shown in *Figs 2.1(a & b)*, it appears that the effect of the field intensity on the shape of the heating curve, however, is also grain-size dependent.

For both grain-size fractions, the heating curves obtained show initially a gradual increase in magnetization with temperature, rather than having the block shape typical of saturated ‘ideal’ hematite (*cf.* Subsection 2.2.3). The initial increasing parts of the heating curves obtained in the lower applied cycling fields (<100–150 mT and <150–200 mT for the 55–75 μm and <5 μm grain-size fractions, respectively) have a more or less concave shape. With increasing field intensity the shape of the curves changes to convex. Once convex, the initial parts of the curves become increasingly horizontal, approaching the characteristic block shape typical of saturated ‘ideal’ hematite. From a specific temperature –referred to as peak temperature, T_p , and indicated in *Figs 2.1(a & b)* with solid circles– the magnetization starts to decrease up to the Néel point. The heating curve obtained in the lowest applied cycling field (10–30 mT) shows, for both grain-size fractions, a pronounced, relatively narrow maximum in magnetization close to the Néel temperature. With increasing field intensity, however, the peak in magnetization becomes broader and less apparent, and the maximum shifts to lower temperatures.

The high quality of the thermomagnetic curves allows the plotting of measured σ versus B_{max} of the applied cycling field to obtain the magnetization curve at any temperature between room temperature and 700°C. The resulting magnetization curves for room temperature, 300°C and 600°C are shown in *Fig. 2.1(c)* for the 55–75 μm grain-size fraction, and in *Fig. 2.1(d)* for the <5 μm fraction. Above the Néel temperature (~680°C) hematite is a paramagnet. Consequently, the $\sigma_{700^\circ\text{C}}-B_{\text{max}}$ curves obtained show the paramagnetic field dependence of hematite at this temperature, which is, as expected, linear with the field intensity and grain-size independent.

For both grain-size fractions, the starting points of the thermomagnetic heating curves are related to the field intensity (*Figs 2.1a & b*). In non-saturating fields more magnetic moments become aligned with the field as the field strength increases, resulting in a higher magnetization. The relation between the initial magnetization measured at room temperature ($\sigma_{i,\text{RT}}$) and B_{max} of the applied cycling field is clearly seen in *Figs 2.1(c & d)* from the S-shaped $\sigma_{i,\text{RT}}-B_{\text{max}}$ magnetization curves obtained. The $\sigma_{i,\text{RT}}$ values, however, appear to be higher for the 55–75 μm grains than for <5 μm grains in the same applied cycling field, illustrated by the steeper slope of the $\sigma_{i,\text{RT}}-B_{\text{max}}$ curve for the coarse grains

than for the fine grains. In the field range used, the difference becomes progressively larger with increasing field strength. The observed difference can be explained by the difference in coercivity between the grain-size fractions. Values of the coercive force (B_c) measured at room temperature with an alternating gradient magnetometer in fields up to 1 T are ~ 180 mT and ~ 280 mT for the 55–75 μm and < 5 μm fractions, respectively.

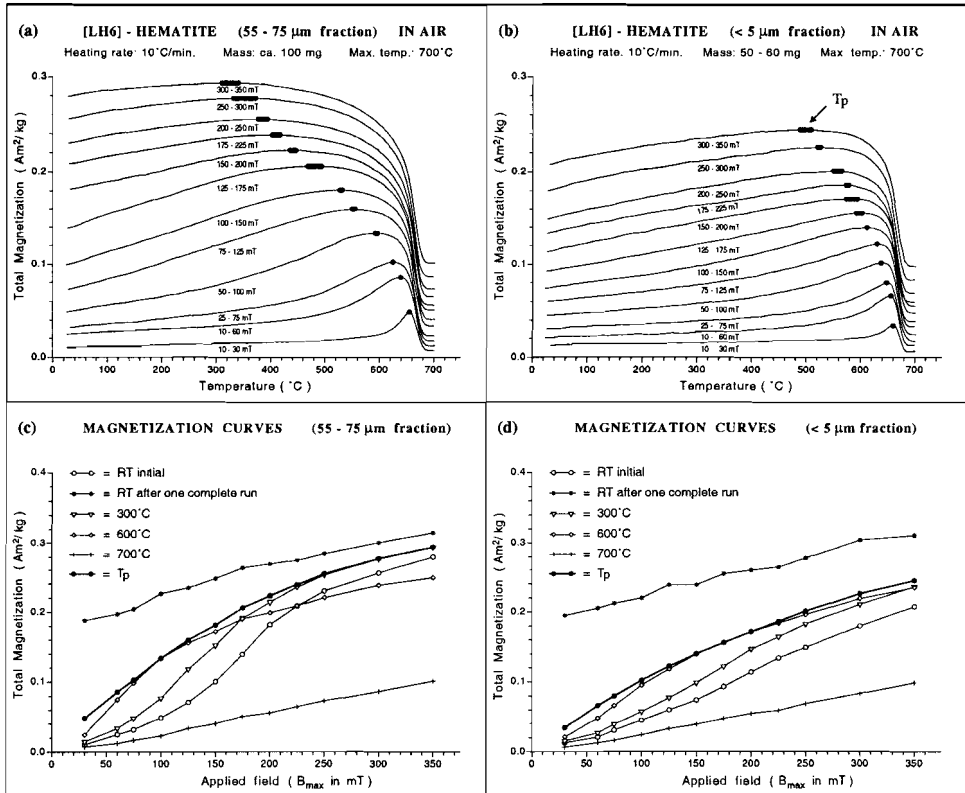


Figure 2.1: Thermomagnetic heating curves as a function of applied field for (a) the 55–75 μm and (b) the < 5 μm grain-size fractions of pure ‘defect-poor’ LH6 hematite, measured in non-saturating cycling fields ranging from 10–350 mT. Comparison of both figures indicates that the shape of the heating curves critically depends on grain size (i.e. coercive force) if the applied fields are not sufficiently high to saturate the sample. Temperature variation of the coercive force is responsible for the initial increasing magnetization. Solid circles correspond to the temperature range in which the highest magnetization is reached. Above this temperature the shape of the heating curves is dominated by the temperature variation of the exchange energy. Temperature variation of the magnetization curves for (c) the 55–75 μm fraction and (d) the < 5 μm fraction of LH6 hematite (room temperature: open circles; 300°C : triangles; 600°C : diamonds; 700°C :

pluses). Solid circles show the field-dependence of the maximum magnetization values, and asterisks correspond to the field dependence of the magnetization measured at room temperature after a complete thermomagnetic cycle to 700°C. The magnetization curves are derived from the thermomagnetic heating curves by plotting the measured magnetization versus B_{\max} values of the applied cycling fields. We may use B_{\max} values because the slopes of the asymmetric minor loops between B_{\min} and B_{\max} are very small, implying that the magnetic field actually acting can be equated to B_{\max} (cf. Mullender et al. 1993). The field dependence of the magnetization measured at room temperature after a complete thermomagnetic cycle to 700°C, together with the $\sigma_{i,RT}$, σ_{300C} , and T_p versus B_{\max} curves, allows an estimate of the saturation magnetization of this hematite. As a consequence of the block shape and the irreversible thermomagnetic behaviour, these four curves will all coincide when the hematite sample is saturated. If we visually extrapolate them to higher field intensities the curves appear to coincide at a magnetization value between 0.35 and 0.4 Am² kg⁻¹. This estimated σ_s value agrees with literature values for pure 'defect-poor' hematite (cf. Subsection 2.2.1).

On heating, however, the coercive force of the non-saturated hematite grains will decrease owing to the gain in thermal energy. Until saturation, a decreasing coercive force yields a magnetization increasingly aligned with the field. In non-saturating fields, the observed shape of the thermomagnetic heating curve thus results from the competitive interplay between the temperature dependence of the exchange energy and that of the coercive force. Consequently, in temperature intervals with an overall increasing magnetization, the decrease in coercivity with temperature outweighs the natural tendency of magnetization to decrease with temperature caused by the descending exchange energy. The overall initial increase in magnetization with temperature (Figs 2.1a & b) is also expressed by the steeper magnetization curves obtained for 300 °C compared to the $\sigma_{i,RT}$ - B_{\max} curves (Figs 2.1c & d). In hematite the microscopic coercivity is dominated by magnetoelastic effects. Contrary to the variation of the exchange energy with temperature (cf. Subsection 2.2.3), the temperature dependence of the coercivity of 'ideal' hematite is not well known, but seems to be grain-size dependent. Dunlop (1971), for instance, suggested $H_c(T) \propto \sigma_s^8(T)$ for fine hematite particles, while Flanders & Schuele (1964) reported $H_c(T) \propto \sigma_s^3(T)$ for a large single crystal of hematite.

The change in shape of the initial increasing part of the thermomagnetic heating curves from more or less concave to convex (Figs 2.1a & b) appears to be related to the inflection point of the S-shaped magnetization curves (Figs 2.1c & d). With increasing temperature this inflection point of the magnetization curves shifts to lower applied fields. Thus, during heating, the thermomagnetic curve obtained will have a concave shape as long as the applied field is lower than the field that coincides with this inflection point of the corresponding magnetization curve. Consequently, convex-shaped thermomagnetic heating curves of non-saturated hematite correspond to the convex top part of the magnetization curves. The difference between the concave and convex shape of the thermomagnetic curves is more pronounced for the coarse grains because the magnetization curves obtained are steeper than those for the fine grains.

Above the peak temperature (T_p) the decrease in exchange energy becomes the dominating parameter in determining the shape of the heating curve, actually causing the peak and the observed overall decrease in magnetization up to T_N . The sharp peak in magnetization observed in the lowest applied field may be interpreted as being a Hopkinson-like peak, while the broader and less pronounced peaks can be seen as its extension to higher applied fields (strictly speaking, only the peaking of the low-field susceptibility just before T_c or T_N is referred to as the Hopkinson effect; susceptibility goes to infinity at T_N). The T_p s show, for both grain-size fractions, a different but clearly negative correlation with the applied field (*Figs 2.1a & b*). The temperature shift of the magnetization peak with applied field is larger for the coarse grains than for the fine grains. Apparently, in the field interval used, the shape of the heating curves depends more on the initial difference in coercivity between the grain-size fractions than on their different temperature variations of the coercivity. In *Figs 2.1(c & d)* the T_p s are plotted against B_{\max} of the applied cycling field. Both fractions show an approximately logarithmic increase of the magnetization peak value with applied field, which is larger for the coarse grains. We are not certain how exactly to interpret this observed relation, but it clearly depends on the temperature variation of T_p which in turn is tied to the applied field and the coercivity of the sample.

Shape of the irreversible thermomagnetic cooling curves

The effect of the magnetic ‘aligning’ process on the shape of the thermomagnetic heating and subsequent cooling curve for temperatures lower than the Néel temperature of hematite is shown in *Fig. 2.2(a)*. Incremental runs to increasingly higher temperatures (maximum 700°C) are measured for the 55–75 μm fraction of LH6 hematite in a 50–100 mT cycling field. As a consequence of the field adjustment procedure (see *Fig. 2.2c* and its caption), the initial heating curve starts at a somewhat higher intensity than the corresponding curve in *Fig. 2.1(a)*. Already at moderate temperatures the thermomagnetic heating and cooling curves are irreversible. Instead of initially showing a reversible, gradual decrease in magnetization, the magnetization reached on heating to temperatures up to $\sim 400^\circ\text{C}$ is retained on cooling to room temperature, resulting in almost horizontal cooling curves. The subsequent cooling curves start to diverge more and more from being horizontal until they approach the block shape typical of saturated ‘ideal’ hematite.

When dealing with ‘ideal’ hematite, the observed irreversibility between the heating and subsequent cooling curves indicates that the magnetic ‘aligning’ process becomes irreversible on cooling. On heating to, for instance, 300°C , the part of the magnetic moments that became aligned with the field due to the decrease in coercivity stays aligned with the field on cooling, producing the observed horizontal cooling curve. First, this implies that the shape of the cooling curves of non-saturated ‘ideal’ hematite is thus hardly influenced by the reversible temperature variation of the coercive force. Instead, it is dominated by the temperature variation of the exchange energy only, which appeared, however, to be negligible in the room temperature– 300°C temperature interval.

Consequently, the observed cooling curve can be seen as equivalent to the horizontal low-temperature part of a block-shaped curve of saturated 'ideal' hematite. The difference between the heating and cooling parts can be seen as being the remanent part of the magnetization. The irreversible magnetic 'aligning' process is somewhat similar to the imparting of a partial TRM in a sample. Second, it apparently implies that for hematite the domain configuration at the maximum temperature (300°C in the example) is retained on cooling to room temperature, despite the decreasing thermal energy and the related increase in coercivity. Several authors (e.g. *McClelland & Shcherbakov* 1995; *McClelland et al.* 1996 and references therein) have published data relating to multiple changes in the domain structure of multidomain magnetites on cooling. Our observations indicate that this probably does not happen in hematite which is magnetically dominated by the canted moment. We realize that the domain state in the example is more likely to be single domain or few domain, so perhaps there are not many alternative local energy minima (LEM) states available. Grain-size fractions up to 250–425 μm , however, show similar behaviour.

On reheating to 400°C the cooling curve is reproduced until 300°C, because the maximum possible amount of aligned magnetic moments was already reached for that temperature in the applied field. Above 300°C, however, more magnetic moments become aligned with the field because of a further decrease in coercivity. The small divergence of the 500°C cooling curve from being horizontal indicates that at this temperature the change in exchange energy with temperature also becomes noticeable. After heating above T_N , the subsequent cooling curve approaches the block shape typical of saturated 'ideal' hematite. The part of the magnetic moments which stays aligned with the field during cooling from above T_N is a maximum for the field intensity used.

It appears that in the whole range of applied fields (10–350 mT) the cooling curves are almost identical and all approach the characteristic block shape. Typical thermomagnetic runs to 700°C obtained in two different applied fields for the 55–75 μm and <5 μm grain-size fraction are shown in *Fig. 2.2(b)*. Contrary to the heating curves, the shape of the cooling curves shows hardly any dependence on the applied cycling field and grain size. The cooling curves are strongly dominated by the temperature dependence of the exchange coupling, which in turn is almost independent on grain size and field strength. In the T_N –600°C interval, however, the curves obtained in the higher applied fields seem to be slightly steeper, that is they approach the block shape slightly more.

The magnetization values measured at room temperature after cooling from above T_N are plotted against B_{max} of the applied cycling fields (10–350 mT) in *Figs 2.1(c & d)* for, respectively, the 55–75 μm and <5 μm fractions. The parameters show a more or less linear relation, and the magnetization values obtained are almost the same for both grain-size fractions. Consequently, the maximum amount of magnetization which is retained in a certain field during cooling from above T_N is almost the same for both grain-size fractions, and thus more or less grain-size-independent in the interval used. This indicates that M_{rs}/M_s must also be almost identical for both grain-size fractions. This concurs with data from *Dankers* (1978; 1981) and *Haritstra* (1982), who reported that the isothermal saturation remanent magnetization is more or less grain-size-independent in a range from 250 μm down to 5 μm for LH6 hematite and some other natural hematite samples.

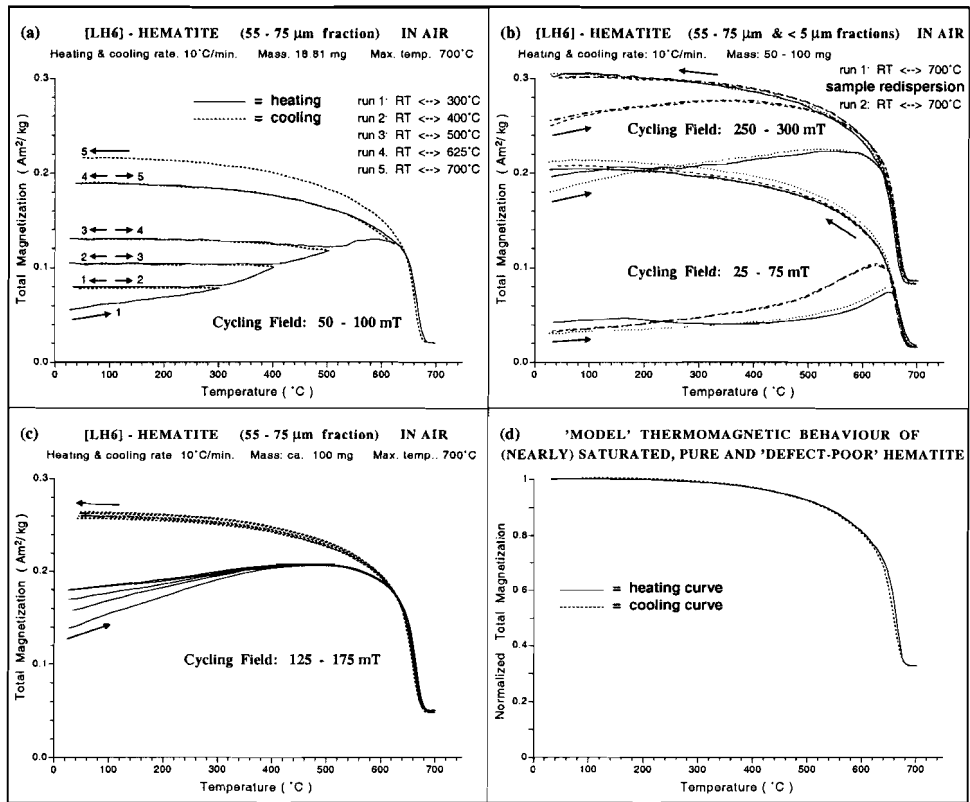


Figure 2.2: (a) Thermomagnetic behaviour for the 55–75 μm grain-size fraction of LH6 hematite in a 50–100 mT cycling magnetic field. Irreversibility between the heating curve and subsequent cooling curve is explained by field-induced changes in magnetization, rather than by thermally induced chemical or structural changes of the hematite. (b) Two subsequent thermomagnetic runs to 700°C for the 55–75 μm fraction and <5 μm fraction of LH6 hematite in a 25–75 mT and a 250–300 mT cycling magnetic field. Run 1 is denoted by solid and dot-dashed lines, while run 2 is denoted by dotted and dashed lines for the <5 μm and 55–75 μm grain-size fractions, respectively. Sample redispersion between the cycles is used to distinguish between chemical or structural changes of the hematite and field-induced changes of the magnetization. The fresh, non-heated, <5 μm fraction of LH6 hematite appeared to be contaminated with a trace of maghemite, which, however, completely inverts to hematite upon heating above 400°C. Apart from the removal of the trace maghemite, the thermomagnetic curves are fully recovered after sample redispersion, indicating that indeed only the magnetic ‘aligning’ process is responsible for the observed irreversible thermomagnetic behaviour. Cooling curves appear to be grain-size independent and show only a slight field dependence. (c) Various initial thermomagnetic curves for the 55–75 μm grain-size fraction of LH6 hematite measured in a 125–175 mT cycling field. This shows a potential problem when dealing with non-saturated minerals. The observed differences between the curves are inherent to the field adjustment procedure of the Curie balance. A small (≤ 25 mT)

but variable field overshoot is induced during the setting of the voltage. Apparently, the magnetization that became aligned during the field overshoot is retained in the desired field setting, which is (obviously) slightly lower. These variable starting points can be circumvented by setting the field range before suspending the sample in the measurement position. The heating curves coincide somewhere around 600°C, but the maximum in magnetization is shifted to somewhat lower temperatures for higher initial magnetization values. The cooling curves, however, are identical within the measurement error. (d) Normalized thermomagnetic curves for the 55–75 µm grain-size fraction of LH6 hematite measured in a 300–350 mT non-saturating cycling field. The curves are obtained during a second run to 700°C without sample redispersion in between. The thermomagnetic behaviour shown can be taken as representative for (nearly) saturated, pure and 'defect-poor' hematite, which is magnetically dominated by the canted moment. Note that the paramagnetic signal at 700°C is about 33 per cent of the initial total magnetization signal.

Sample redispersion

The observed irreversible thermomagnetic behaviour, however, might be erroneously taken as evidence for thermally induced chemical or structural changes of the hematite. Sample redispersion between subsequent cycles can be used to distinguish between these processes and field-induced changes in magnetization. If the observed irreversibility between the heating and cooling curves is caused only by the irreversible magnetic 'aligning' process, then the initial curves must be recovered after redispersion of the sample (Day 1975; Duff 1979). Fig. 2.2(b) shows two subsequent thermomagnetic cycles to 700°C for both grain-size fractions of LH6-hematite obtained in two different applied cycling fields (25–75 and 250–300 mT). After the first run to 700°C (which was performed on the fresh non-heated fractions) the sample was redispersed and remeasured under identical conditions. For the 55–75 µm fraction, the initial curves are fully recovered after sample redispersion. This indicates that the hematite grains of this fraction were not affected chemically, structurally or texturally by the heating. The observed irreversibility between the heating and cooling curves of each individual cycle is thus only caused by the magnetic 'aligning' process.

The initial heating curves of the <5 µm fraction, however, are not fully recovered after sample redispersion. It is reasonable, however, to ascribe the observed difference to the maghemite contamination present in this fine-grained fraction (cf. Section 2.3). The difference in $\sigma_{i,RT}$ of $\sim 0.025 \text{ Am}^2 \text{ kg}^{-1}$ between the heating curves of the subsequent runs corresponds to a maghemite ($\sigma_s = 74 \text{ Am}^2 \text{ kg}^{-1}$) contamination of only ~ 0.03 weight per cent. The marked drop in magnetization in the 180–350°C interval during the first run (solid lines in Fig. 2.2b) indicates the crystallographic inversion of $\gamma\text{-Fe}_2\text{O}_3$ to $\alpha\text{-Fe}_2\text{O}_3$ (e.g. de Boer & Dekkers 1996). Above 350°C, however, the heating curves of run 1 and 2 are almost reversible in both applied fields. This indicates that the inversion to hematite was complete and, moreover, that the hematite itself hardly changed due to the heating.

This redispersion experiment clearly illustrates that for non-saturated samples, irreversibility of heating and cooling curves of one complete thermomagnetic cycle does not automatically imply chemical alteration or structural change; it can also be caused by an irreversible magnetic ‘aligning’ process. Sample redispersion between subsequent cycles is thus mandatory to distinguish between these two processes when applied fields are not sufficiently high to saturate the material.

Simulated ‘model’ behaviour of saturated ‘ideal’ hematite

Up to now we have compared the thermomagnetic behaviour of LH6 hematite with the calculated or otherwise derived model σ_s - T curve for ‘ideal’ hematite (*cf.* Subsection 2.2.3). LH6 hematite does not alter on heating to 700°C, has an estimated σ_s close to reported values for pure ‘defect-poor’ hematite (*cf.* caption to *Fig. 2.1*), and moreover its thermomagnetic curves approach the block shape typical of ‘ideal’ hematite in the highest applied fields. Its thermomagnetic behaviour (*cf.* *Figs 2.1* and *2.2*) can be taken as representative of non-saturated pure and ‘defect-poor’ hematite, which is consequently dominated by the canted moment only.

Although the applied fields are not sufficiently high to saturate the sample, we can simulate saturated thermomagnetic behaviour by measuring two subsequent runs to 700°C in the highest non-saturating fields without sample redispersion in between. After the first run to 700°C the maximum magnetization is reached for the applied field. Consequently, the heating and cooling curves of the subsequent run are reversible and both have the typical block shape. As outlined in Subsection 2.4.1 (part 2), the shapes of the cooling curves obtained in the applied non-saturating fields only show a slight field dependence. The curves of the second run thus give a justified estimate of the shape of the σ_s - T curve for this hematite. *Fig. 2.2(d)* shows the normalized curves of LH6 hematite (55–75 μm fraction) measured during a second run to 700°C in a 300–350 mT cycling field without sample redispersion between the subsequent cycles. These measured curves have a similar shape to the calculated σ_s - T curves. These latter curves, however, apparently underestimate or do not take account of the paramagnetic contribution to the signal (~33% at 700°C). Consequently, the measured curves shown in *Fig. 2.2(d)* better represent the ‘model’ σ_s - T curves for (nearly) saturated, pure defect-poor hematite.

2.4.2 Pure defect-rich hematite

We now present a natural hematite which shows a thermomagnetic behaviour noticeably different from the general trend outlined for ‘ideal’ LH6 hematite. The slightly contaminated LH4 hematite sample chemically and structurally changes upon heating. The hematite itself appears to be typical of a pure, more ‘defect-rich’ hematite, thus magnetically typified by a combination of the canted moment and the defect moment. Incremental thermomagnetic runs to increasingly higher temperatures for the 30–40 μm fraction of the platy LH4 hematite are shown in 2.3.

All curves show a distinct initial increase in magnetization up to ~100°C. This characteristic maximum in magnetization cannot have the same origin as the maximums observed in the thermomagnetic heating curves of non-saturated LH6 hematite because it is also visible in the subsequent cooling curves. *Hartstra* (1982) reported that the TRM and isothermal saturation remanence (referred to as I_{sr} by *Hartstra*) also peak at the same temperature (100°C). He interpreted the initial increase in magnetization from room temperature to ~100°C as the onset of the Morin transition at this temperature, in contrast to commonly reported onsets of the Morin transition below room temperature (*cf.* Subsection 2.2.1). His low-temperature runs show that the decay in remanence (I_{sr} and TRM) takes place over a wide temperature interval starting already at room temperature, rather than having an initial interval of hardly decreasing remanence. He suggested that the Morin transition for LH4 hematite was probably an interval (spanning a temperature range -75°C to +100°C), rather than a well-defined transition.

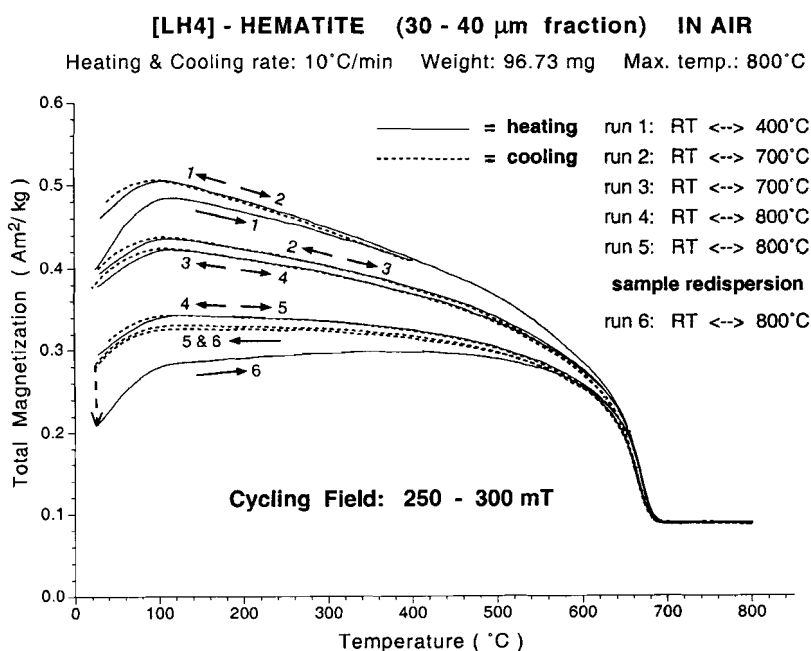


Figure 2.3: Thermomagnetic analysis of magnetite-contaminated 'defect-rich' LH4 hematite. On heating the magnetite is oxidized to hematite (run 2), and the defects are increasingly annealed out of the hematite lattice (run 2 to 5), until a pure defect-poor hematite resides. Sample redispersion between run 5 and 6 is denoted by the dashed arrow. The characteristic maximum in magnetization around 100°C is caused only by the canted moment, and can most probably be seen as the onset of the Morin transition at this temperature.

Apart from this remarkable initial increase, an overall decrease in magnetization with increasing temperature is observed, rather than the gradual initial increase in magnetization typical of non-saturated 'ideal' hematite. The initial magnetization at room temperature of LH4 hematite is significantly higher than the corresponding $\sigma_{i,RT}$ value of 'ideal' LH6 hematite measured in the same field. The first thermomagnetic cycle to 400°C (run 1) causes an increase in magnetization on cooling; the cooling curve lies above the corresponding heating curve. Sample redispersion (not shown here) recovers the initial curves, implying that the observed irreversibility is caused only by the irreversible magnetic 'aligning' process. A subsequent run to 700°C (run 2), however, results in a significant reduction of the magnetization. The cooling curve now lies below the corresponding heating curve. Sample redispersion (not shown here) no longer recovers the initial curves, indicating a thermally induced chemical and/or structural change of the hematite sample. Another run to 700°C (run 3) causes only a small additional decrease in magnetization. Cycling to even higher temperatures (run 4, 800°C), however, further reduces the magnetization. The cooling curve of this fourth run (*Fig. 2.3*) almost shows the block shape typical of pure 'defect-poor' hematite, apart from the onset of the Morin transition below 100°C. A second run to 800°C (run 5) reduces the magnetization only slightly more and induces minute further changes in the block shape. Once obtaining this characteristic shape, no further changes in magnetization are observed upon repeated thermomagnetic runs to 800°C (not shown here), and consequently the heating and cooling curves are now reversible. Sample redispersion (run 6, 800°C) reduces the magnetization and results in an upward-convex heating curve with a maximum (T_p) at ~360°C. The irreversible cooling curve, however, has a block shape identical to that of run 5. The thermomagnetic behaviour of LH4 hematite now resembles the behaviour typical of a pure 'defect-poor' hematite.

Apparently, above 400°C LH4 hematite starts to alter chemically and/or structurally to a pure 'defect-poor' hematite. MicroMag measurements detected a trace of a magnetically softer mineral in the grain-size fraction used (*cf.* Section 2.3). A hardly visible inflection between 550° and 600°C in the heating curve of run 2 points to magnetite (Fe_3O_4 , $T_c = 580^\circ\text{C}$) as being the magnetic contaminant. The inflection point can hardly be seen in the field range used because it is obscured by the overall decrease in magnetization. The magnetite part, however, can be made more visible by applying much lower cycling fields (e.g. 10–60 mT, not shown here). This indeed revealed a clear inflection point around 580°C, but more importantly, it also showed that the trace magnetite ($\sigma_s = 92 \text{ Am}^2 \text{ kg}^{-1}$: contribution to the signal at room temperature $\leq 0.05 \text{ Am}^2 \text{ kg}^{-1}$ corresponding to ≤ 0.05 weight per cent) was completely oxidized to hematite during the two runs to 700 °C. Progressive oxidation of magnetite to hematite on heating is thus only partly responsible for the observed decrease in magnetization (run 2–5); it cannot explain the irreversibility between the curves of run 3 and subsequent runs. Also, the magnetite contamination cannot account for the observed differences in magnetization between the curves in the 580–680°C temperature interval.

After run 2, the measured magnetization at room temperature is still high compared to LH6 hematite, and the curves obtained do not resemble the thermomagnetic behaviour indicative of 'defect-poor' hematite (canted moment only). A defect magnetic moment

superimposed on the canted moment is likely to be responsible for the relatively high initial magnetization. Several authors (e.g. *Dunlop* 1971, 1972; *Bucur* 1978) reported that the defect moment in particular is sensitive to heat treatment. The observed irreversible thermomagnetic behaviour may be explained by the presence of defects in the hematite lattice which are increasingly annealed out of the structure during heating. Heating to moderate temperatures (run 1, 400°C) obviously does not significantly affect the defects present in the lattice (or the magnetite contamination). However, on heating to higher temperatures (700° and 800°C), the defects are increasingly annealed out of the structure, that is heating diminishes the contribution of the defect moment to the signal. The magnetization decreases until the block shape typical of 'defect-poor' hematite remains. After sample redispersion (run 6) the slopes of the heating and cooling curves (apart from the first 100°C) as well as the differences in magnetization between them are almost identical to LH6 hematite measured in the same field. LH4 hematite, however, still has a somewhat higher overall magnetization than the LH6 hematite. Because the hematites are now both magnetically dominated by the canted moment, we suggest that the difference in absolute magnetization values is caused by a slightly different canting angle.

As mentioned before, the second run to 700°C (run 3) is not biased any more by the trace amount of magnetite. The heating and cooling curves differ slightly, indicating that only a small additional amount of defects is annealed out of the hematite lattice. Consequently, the shape of these curves is not affected by the removal of the defects from the hematite lattice; the curves thus reflect the temperature variation of the canted and defect moment. By subtracting the contribution of the canted moment to the signal (block-shaped cooling curve of run 6) from the curves of run 3, we get an impression of the temperature variation of the magnetization caused by the defect moment only. The resulting thermomagnetic behaviour shows a gradual decrease in magnetization up to T_N . Apparently, the defect moment has its highest magnetization at room temperature, implying that this moment is saturated –or at least is close to saturation– in the applied field. Therefore, the defect moment due to lattice defects must be (much) softer than the canted moment. The temperature variation of the exchange energy apparently has a different effect on the defect moment than on the canted moment, because a convex-downward curve results instead of the block-shaped curve typical of the canted moment. The overall effect of a decreasing defect moment on heating is that the hardness of the hematite increases, as was demonstrated by *Dunlop* (1971, 1972) for SD hematite grains.

With the ultrasensitive Curie balance used, no shift of the inflection point near 680°C to lower temperatures was observed upon continued cycling to 700°C and 800°C. This does not agree with earlier results (e.g. *Aharoni et al.* 1963; *Smith & Fuller* 1967), which suggested a difference between the temperature at which the spin canting vanishes (canted moment) and the temperature at which the antiferromagnetic coupling disappears (defect moment).

The characteristic maximum in magnetization around 100°C is still present after repeated cycling and is thus caused only by the canted moment. Our findings support the earlier suggestion by *Hartstra* (1982) of an onset of the Morin transition at a relatively high temperature in this sample.

2.4.3 Goethite

Synthetic goethite

The thermomagnetic analysis (four incremental runs up to 100°C) of a synthetic goethite is shown in Fig. 2.4(a). The fine goethite crystallites are reported to be pure (Dekkers & Rochette 1992). Therefore, the observed weakly ferromagnetic behaviour must have its origin in vacancies, crystal defects, excess structural (OH)⁻ or an odd number of spins, rather than in impurities. Heating this goethite sample to 40°C (run 1) in a non-saturating cycling field (200–300 mT) results in an almost linear decrease in magnetization. The heating curve is reproduced on cooling. This thermomagnetic behaviour resembles the behaviour of the ‘model’ σ_s - T curve for goethite described in Subsection 2.2.3, suggesting that the shape of the curves, in the room temperature–40°C temperature interval, is strongly dominated by the reversible temperature variation of the exchange energy. The start of a well-pronounced Hopkinson-like peak is observed on further heating (run 2, 60°C). The heating-induced decrease in coercivity evidently becomes important above ~50°C. Consequently, the magnetic moments can become increasingly aligned with the field, resulting in a sharp increase in magnetization. The heating and cooling curves of this second run are no longer reversible, implying that the magnetic ‘aligning’ process is also irreversible for goethite. However, on cooling from 60°C the magnetization first slightly decreases before it starts to increase at ~50°C according to the temperature variation of the exchange energy. The specific shape of the cooling curve indicates that, in the applied field, only part of the magnetic moments that became aligned with the field during heating to 60°C can stay aligned on cooling to room temperature. Heating to 80°C reveals the complete Hopkinson-like peak (T_p ~65°C), and results in an

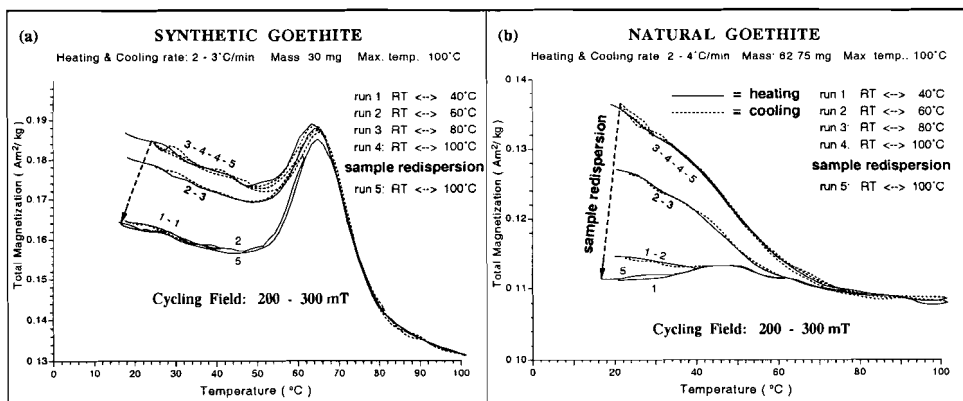


Figure 2.4: Thermomagnetic analysis of (a) a relatively hard synthetic goethite, and (b) a relatively soft, natural goethite.

additional increase in magnetization on cooling. The observation that the Hopkinson-like peak is partly preserved during cooling could imply the following two options: (1) some of the grains has very short relaxation times so that they essentially behave as superparamagnetic, or (2) the amount of acquired TRM (in the field of the Curie balance) is small compared to the height of the Hopkinson-like peak. In that case the peak will also be observable during the cooling run. A subsequent run to 100°C does not increase the magnetization; the heating and cooling curves are reversible. Consequently, the $T_c (= T_N)$ corresponding to the weak ferromagnetism must lie around 80°C. Sample redispersion (run 5, 100°C) recovers the initial heating curve, suggesting no major thermally induced chemical or structural changes in the goethite. Note that the T_p of ~65°C (Fig. 2.4a) corresponds to the maximum unblocking temperature of the CRM in Dekkers & Rochette (1992), while their measured maximum unblocking temperature of the TRM corresponds to the observed T_N of ~80°C.

Natural goethite

When the natural goethite sample is subjected to identical experimental conditions (same incremental runs in the same applied cycling field) to the synthetic goethite, a slightly different thermomagnetic behaviour results (Fig. 2.4b). The weak ferromagnetism of this natural goethite is, in contrast to the pure synthetic goethite, most probably dominated by impurities. In particular, Al-substitution is commonly reported in natural goethites (e.g. Fitzpatrick 1988; Van der Horst 1994). Heating the natural goethite to 40°C (run 1) results in a small increase in magnetization, rather than in an initial decrease in magnetization as is observed for the non-saturated synthetic goethite. On cooling the thermomagnetic behaviour is irreversible. Consequently, the shapes of the thermomagnetic curves for this natural goethite sample are influenced by the decrease in coercivity from room temperature upwards. Knowing that both goethite samples have comparable grain-size ranges, this suggests that the natural goethite is relatively softer than the synthetic sample. The slightly lower total magnetization values of the natural goethite are explained by a small amount of clay and quartz contamination. Heating to higher temperatures (run 2, 60°C, and run 3, 80°C) allows more magnetic moments to become aligned with the field. On cooling, the magnetization increases to values far above the magnetization corresponding to the Hopkinson-like peak. The less pronounced Hopkinson-like peak and lower T_p (~46°C) of the natural goethite compared with the synthetic goethite support the supposed relative softness of this goethite. It could be that goethites which have their origin of the weak ferromagnetism predominantly in substituted cations are relatively softer than those with another origin. This agrees with data of Dekkers (1989a), who also mentioned that dispersed silica between individual goethite crystallites making up a grain may have a similar effect. Heating above 80°C (run 4, 100°C) does not result in any additional increase in magnetization on cooling, indicating that T_N is passed. The heating and cooling curves are now reversible and consequently approach the shape of saturated goethite (cf. Subsection 2.2.3). Redispersion of the sample recovers the initial heating curve, indicating that the goethite

did not alter chemically during the thermal treatment. Despite the supposed different origin of the weak ferromagnetism and the different initial thermomagnetic behaviour, the heating-induced increase in magnetization (caused by the magnetic aligning process) for both goethites is almost the same ($\sim 0.025 \text{ Am}^2 \text{ kg}^{-1}$) after the complete experiment. Thus, on cooling from above T_N the same additional amount of magnetic moments is aligned with the field for both goethites, indicating that the remanence (specific 'TRM') for both goethites is similar.

2.5 Conclusions

The thermomagnetic behaviour of non-saturated minerals differs from that of saturated minerals in that it does not show reversible heating and cooling curves, in particular after heating above the T_N or T_C of the minerals. Apart from the temperature dependence of the exchange energy, the shape of the heating curve is shown to be dependent on the temperature variation of the coercivity with respect to the applied field. The cooling curves, however, show hardly any dependence on applied field and grain size (i.e. coercivity), and are dominated by the temperature dependence of the exchange energy. Thermomagnetic cycling thus results in a magnetization process if the applied field is not sufficiently high to saturate the sample. Consequently, in this case irreversible thermomagnetic behaviour does not automatically imply chemical or structural changes. Sample redispersion between subsequent runs is therefore mandatory to distinguish between field-induced changes on the one hand and chemical and/or structural changes on the other.

Initially increasing heating curves and block-shaped cooling curves appear to be indicative of non-saturated, pure and defect-poor hematite, which is magnetically dominated by the canted moment. The temperature which corresponds to the peak in magnetization observed on heating shows a negative correlation with the applied field. The temperature shift of the magnetization peak with applied field is larger for coarse grains than for fine grains due to the lower coercivity of the former. The domain configuration acquired at the maximum heating temperature is retained on cooling, suggesting that in multidomain defect-poor hematite no range of alternative local energy minima states is available.

Defects in the hematite lattice cause more gently decreasing heating curves. Annealing these more defect-rich hematites at increasingly elevated temperatures results in a thermomagnetic behaviour typical of defect-poor hematite. Our observations suggest that this particularly heat-sensitive defect moment is additive to the canted moment, and that it is distinctly softer than the canted moment. Furthermore, the temperature variation of the exchange energy seems to have a different effect on the defect moment due to lattice defects than on the canted moment. No difference is observed between the Néel temperature of the canted moment ($\sim 680^\circ\text{C}$) and the Curie point of the defect moment, as occasionally suggested in the literature.

The irreversible magnetic 'aligning' process acts on non-saturated goethite as well. The thermomagnetic behaviour of goethite is also shown to be dependent on coercivity.

ACKNOWLEDGEMENTS

We thank *Tom Mullender* for helpful discussions and for keeping the Curie balance in top running condition. We acknowledge *J.J. van Loef* for providing the rattle stone. Two anonymous reviewers are thanked for helping to improve the original manuscript. This work was conducted under the programme of the Dutch national research school, the Vening Meinesz Research School of Geodynamics.

Chapter 3

Low-temperature behaviour of hematites: susceptibility and magnetization increase on cycling through the Morin transition

Cor B. de Boer, Tom A.T. Mullender and Mark J. Dekkers

Paleomagnetic Laboratory 'Fort Hoofddijk', Utrecht University, Faculty of Earth Sciences, Budapestlaan 17, 3584 CD Utrecht, the Netherlands. E-mail: cdeboer@geo.uu.nl

Submitted to Geophys. J. Int.

SUMMARY

It has been realized before (e.g. *Borradaile* 1994) that cycling through the Morin transition (T_M , occurring in ideal α - Fe_2O_3 at -10°C) may have implications for the NRM of some hematite-bearing rocks. We investigated the behaviour of the low-field susceptibility (χ_{lf}), several magnetizations (in fields of 5, 25, 100, 1600 mT) and that of SIRM on cycling through T_M , of several well-characterized hematite types of varying crystallinity and particle shape. Before low-temperature treatment, χ_{lf} of the hematites varied between ~ 40 and $\sim 235 \times 10^{-8} \text{ m}^3 \text{ kg}^{-1}$. Below T_M , where only hematite's defect moment resides, χ_{lf} was much more uniform at ~ 19 to $\sim 28 \times 10^{-8} \text{ m}^3 \text{ kg}^{-1}$. After return to room temperature, increases in χ_{lf} up to $\sim 50\%$ were observed (when cycling in the Earth's magnetic field as well as in a field-free space), inferred to be a function of the domain state of the hematite. This was shown for one of the hematites (LH2 which is platy developed and particularly well crystalline) where a relation $y = (8.60 \pm 1.01)\ln(x) - 2.98$ was obtained with x being grain size (μm) and y the percentage of the susceptibility increase. We suggest that transdomain changes induce the change in χ_{lf} . The nucleation of (additional) domain walls in 'metastable' SD to PSD grains is made possible by the low anisotropy at the Morin transition. In view of this mechanism, small stable SD hematite particles would not be affected and the grain size corresponding to $y = 0$ ($\sim 1.5 \mu\text{m}$ for LH2) would represent the 'real' SD threshold size. Thermal cycling to over the Curie temperature (680°C) is needed to return to the original domain state before the LT treatment, as expressed by a return to the original χ_{lf} values. Measuring χ_{lf} between alternating field (AF) demagnetization steps shows that AF demagnetization gradually

removes the χ_{IF} increase which appears to be soft; 30 mT is already sufficient to erase 90%. Thermal cycling in a 5 mT field between temperatures above T_{M} showed that irreversible changes in domain structure are already noticeable before the isotropic point is passed. After cycling, magnetization is added to PSD and MD grains that intriguingly appeared to be remanence, likely induced by the broadening and subsequent irreversible displacement of loosely pinned domain walls. Complete cycling through the isotropic point considerably enhances the new remanence component in ‘metastable’ SD to MD particles by an increase in the number of domains. If this behaviour may be extrapolated to the intensity of the Earth’s magnetic field, this would imply that large ‘metastable’ SD to MD specularite crystals with a well-developed Morin transition are susceptible to acquire geologically irrelevant remanence components, when subjected to low ambient temperatures. Fine-grained hematite pigment, on the other hand, would not be affected. Thermal demagnetization alone would not be able to separate these two remanences as the new domain structure persists up to close to the Curie temperature. Our findings would indicate that a cleaning procedure consisting of an initial AF step followed by stepwise thermal demagnetization is preferable to properly isolate the original remanence component in hematite-bearing rocks.

Key words: *rock magnetism, hematite, Morin transition, low-field susceptibility, low-temperature magnetization.*

3.1 Introduction

In 1950 *Morin* described a low-temperature transition of hematite observed by measuring the magnetic susceptibility on a set of synthetic (Ti-substituted) hematite samples. This characteristic low-temperature transition of hematite, that typically occurs at $\sim -10^{\circ}\text{C}$ for pure samples, is now known as the Morin transition (T_{M}), although according to *Morrish* (1994) the transition was actually observed earlier by *Honda & Soné* (1914) and by *Charlesworth & Long* (1939). Nevertheless, it was *Morin’s* work that initiated much research on this transition. Similar discontinuities in the magnetic properties of hematite were later also observed by monitoring low-temperature cycling of the (saturation) magnetization (e.g. *Néel & Pauthenet* 1952; *Flanders & Remeika* 1965) and various remanent magnetizations (e.g. *Haigh* 1957; *Gallon* 1968), and low-temperature measurements have become a chemically non-destructive alternative to thermomagnetic analysis for the detection of hematite (e.g. *Fuller & Kobayashi* 1964). The Morin transition was also extensively studied using other techniques like Mössbauer spectroscopy (e.g. *Kündig et al.* 1966; *Van der Woude* 1966; *Nininger & Schroeer* 1978; *De Grave et al.* 1982) and neutron diffraction (e.g. *Shull et al.* 1951; *Besser et al.* 1967; *Sváb & Krén* 1979).

It is now well known that the Morin transition is actually hematite’s magnetic isotropic point and does not represent a crystallographic change like the Verwey transition of magnetite. At the isotropic point the first hexagonal magnetocrystalline anisotropy constant (K_1) of hematite becomes zero as it changes sign, being negative

above T_M and positive below it (e.g. *Morrish* 1994). As a consequence, the 'easy' directions of magnetization change, resulting in a reorientation of the antiferromagnetically-coupled atomic spins from the basal plane for $T > T_M$ to the hexagonal c -axis for $T < T_M$ (e.g. *Shull et al.* 1951). The observed fall in susceptibility and other magnetic parameters on cooling through T_M is caused by the accompanied change from a weak ferromagnetic state to an antiferromagnetic state of hematite (e.g. *Dzhalonshinsky* 1958; *Moriya* 1960): unlike the situation above the Morin transition, below T_M , canting of the spins out of exact antiparallelism is no longer possible due to magnetic symmetry considerations (*cf.* Section 3.2.2). As a result, below T_M the spin-canted remanence vanishes together with the anisotropy that pinned it, and only the isotropic defect remanence survives (*cf.* Section 3.2.2). However, for reasons unresolved to date, the spin-canted remanence partly remembers its original direction on reheating in zero field (e.g. *Haigh* 1957). *Gallon* (1968), however, showed that the memory of the spin-canted moment decreases when the defect moment is partially annealed out. Apparently, both moments are not entirely independent, and a defect moment seems to be necessary to renucleate the spin-canted moment during reheating (*cf.* *Dunlop & Özdemir* 1997). Thus, in contrast to cycling across the isotropic point and the Verwey transition in magnetite, cycling through the Morin transition is not recommended as a method of low-temperature cleaning because it enhances the defect moment at the expense of the probably more reliable intrinsic moment (*Borradaile* 1994; *Dunlop & Özdemir* 1997).

In nature, however, it is not unlikely that surface rocks have been repeatedly cycled through the Morin transition, especially hematite-bearing rocks occurring at high latitudes and altitudes. This process not only will partly erase the pre-existing remanence but, because cycling occurs in the Earth's magnetic field, it may even introduce also a secondary magnetization in the rock. *Borradaile* (1994) showed that stress effects caused by pore ice expanding on melting could even further reduce the memory of remanence on rearming through T_M . Moreover, *Halgedahl & Jarrard* (1995) observed that pseudo-single-domain (PSD) to multidomain (MD) magnetite particles might already lose part of their remanent magnetization in the temperature range before the actual isotropic point. In the neighbourhood of the isotropic point, when K_1 becomes very small, demagnetization could result from the broadening, unpinning and complete reorganization of domain walls (e.g. *Ozima et al.* 1964). For hematite particles, this would mean that they lose part of their NRM at common ambient Earth's surface temperatures. To this end, more insight in the physical mechanism by which the low-temperature transition of hematite occurs is necessary, in order to understand better which influence this process may have on the NRM.

In this paper we report on the effect of cycling through or approaching of the isotropic point on hematite's domain configuration, as deduced from changes in mineral-magnetic parameters. The results are obtained on a set of well-characterized, relatively pure hematites, spanning the single-domain (SD) to MD range. We measured the low-field mass susceptibility (χ_{lf}) before and after cycling through the isotropic point. Any irreversible change in the domain configuration caused by cooling and warming through T_M may be reflected in a change of the χ_{lf} value. Test runs showed χ_{lf} increases up to ~50% for coarse-grained MD hematites. Because it is likely that χ_{lf} of stable SD grains will not be affected by the low-temperature cycling, these measurements might

discriminate between SD and PSD to MD behaviour. Hence, these measurements might have potential as a grain-size indicator. The stability of the new domain configuration is tested against alternating field (AF) demagnetization and to temperatures up to 700°C, i.e. just above the Curie point. In addition, we checked for a possible field dependence of the irreversible change in domain configuration by monitoring cooling and warming runs of magnetization induced in various (non-)saturating magnetic fields, ranging from 5 to 1600 mT.

3.2 Relevant rock-magnetic data

3.2.1 General magnetic properties

Hematite is the alpha polymorph of ferric oxide ($\alpha\text{-Fe}_2\text{O}_3$). It crystallizes in the corundum structure (e.g. *Lindsley* 1979), which can be indexed in the four axes hexagonal or in the equivalent three axes rhombohedral crystal system. The crystallographic and magnetic unit cells are the same. The magnetic structure of hematite basically is antiferromagnetic, with a magnetic disordering temperature or Néel point (T_N) of $\sim 680^\circ\text{C}$. Neutron diffraction studies at room temperature (e.g. *Shull et al.* 1951) showed that the antiferromagnetically-coupled sublattice magnetizations lie in the basal plane of the crystal, orthogonal to the hexagonal c -axis. At room temperature, however, hematite possesses a spontaneous magnetization ($\sim 0.4 \text{ Am}^2 \text{ kg}^{-1}$) and is able to carry a remanence. The weak ferromagnetic moment is caused by a slight canting of the spin axes out of exact antiparallelism in the basal plane (*Dzyaloshinsky* 1958), and results from the anisotropic superexchange interaction in hematite (*Moriya* 1960). Hence, it is an intrinsic property of hematite and the moment is referred to as the canted moment (also known as intrinsic, fundamental, anisotropic or magnetocrystalline moment). In addition, hematite may have another, more variable magnetic moment that is believed to reside in an ordered structure of chemical and/or lattice defects, which cause an imbalance between the antiferromagnetically-coupled sublattices. This moment is referred to as defect moment (also known as isotropic moment), and is held responsible for the highly variable magnetic properties of hematite. The magnetization vector for the defect moment is parallel to the sublattice magnetizations and thus nearly perpendicular to the magnetization vector for the canted moment. Because of its origin, the defect moment can be structure-sensitive and thus be susceptible to applied stress or annealing; e.g. through mobility of dislocations. On heating, the canting of the spins vanish at the same temperature as the long-range antiferromagnetic ordering does (e.g. *De Boer & Dekkers* 1998); i.e. for hematite the Curie and Néel points are identical.

For $T_M < T < T_C$, the magnetocrystalline anisotropy of hematite can be expressed in terms of a first-order uniaxial constant (K_1) that determines the anisotropy between the 'hard' c -axis and the 'easy' basal plane (0001), and a triaxial constant (K_B) that determines the in-plane anisotropy (cf. *Hunt et al.* 1995 and references therein). However, to fit all experimental results, often a second-order anisotropy constant (K_2) is added

(*cf. Morrish 1994*). It is expected that $K_1 \gg K_2 \gg K_B$ (*cf. Morrish 1994*). The constants vary as a function of chemical composition, crystal structure, temperature and pressure, but are independent of grain size. *Flanders & Schuele (1964b)* found a relation (between 20 and 500°C) of $K_B(T) \propto \sigma_s^m(T)$ with $m = 10 \pm 1$ in one of their crystals. The sources of K_1 are the magnetic-dipole anisotropy and the magnetocrystalline anisotropy of the Fe^{3+} ion (*Artman et al. 1965*), while the origin of K_2 is solely a single-ion contribution (*cf. Morrish 1994*). The two microscopic origins of K_1 have opposite signs and different temperature dependencies. Above T_M , the negative magnetic-dipole term dominates the positive single-ion term. Resonance measurements (e.g. *Anderson et al. 1954; Kumagai et al. 1955*) indicated the anisotropy field between the c -axis and the 'easy' plane to be 3–4 T. *Dunlop & Özdemir (1997; page 51)* reported a K_1 of $-1.2 \times 10^6 \text{ J m}^{-3}$. As a consequence of the high value of the main magnetocrystalline anisotropy, for $T_M < T < T_C$, the magnetization process under the action of the Earth's magnetic field (remanence acquisition) or of common laboratory fields is restricted to the basal plane.

Hematite is important to paleomagnetism, mainly because of its highly stable remanences. Coercivities of fine-grained hematite up to several hundreds of mT are commonly reported (e.g. *Dankers 1978; Hartstra 1982*). The triaxial magnetocrystalline anisotropy within the basal plane, however, is relatively weak. Reported values are highly variable ranging between $<1 - 400 \text{ J m}^{-3}$ (*cf. Dunlop 1971; Banerjee 1971; and references therein*), but are not sufficiently high enough to account solely for the observed high coercivities. Shape anisotropy cannot be the origin of the required energy barriers in the basal plane of hematite since it is proportional to σ_s (*Dunlop 1971*). The same author showed that an uniaxial magnetoelastic anisotropy due to internal stress is the most likely candidate responsible for the high basal-plane anisotropy observed in fine-grained hematite. He calculated that a polycrystalline magnetostriction constant λ_s of $\sim 8 \times 10^{-6}$ (*Urquhart & Goldman 1956*) can produce a coercivity of $\sim 500 \text{ mT}$ for an internal stress of 100 MPa. Furthermore, *Porath (1968)* has argued that internal stress becomes more important in fine grains.

At room temperature, the low-field mass susceptibility of natural hematite samples is in the range $(10-750) \times 10^{-8} \text{ m}^3 \text{ kg}^{-1}$ (*Hunt et al. 1995*). The χ_{lf} values increase with increasing grain size (e.g. *Dankers 1978; Collinson 1983*). They also show a strong dependency on crystallographic orientation; χ_{lf} values being higher when measured in the 'easy' plane. For SD hematite grains, the in-plane or ferromagnetic susceptibility arises from the rotation of the spontaneous magnetization in the basal plane. It only exists between T_M and T_C , and its value depends on the type of basal-plane anisotropy, i.e. number of 'easy' axes (*Dunlop 1971*). If the basal-plane anisotropy is uniaxial, the susceptibility is inversely related to the coercive force H_c (*Stacey & Banerjee 1974*). The intrinsic initial susceptibility in large MD particles, however, is controlled primarily by reversible domain wall displacements. The high-field mass susceptibility (χ_{hf}) or antiferromagnetic susceptibility is due to the rotation of the spins by a field against the exchange forces. Above T_M it is almost anisotropic, has a value of $\sim 25 \times 10^{-8} \text{ m}^3 \text{ kg}^{-1}$, and shows only a slight temperature dependence (e.g. *Chevallier 1951; Néel & Pauthenet 1952; Pastrana & Hopstock 1977*). In being an intrinsic property, it is independent of grain-size and virtually constant for different hematite samples.

3.2.2 Morin transition

On cooling, pure well-crystalline hematite shows an abrupt drop in values for magnetic parameters around -10°C . At this temperature, the antiferromagnetically-coupled spins change their position from the basal plane to the hexagonal c -axis of the crystal. *Artman et al.* (1965) showed that the spin rotation is driven by the competition between the two main origins of K_1 having an essential different temperature dependence. The change in sign of the first magnetocrystalline anisotropy constant accounts for the observed Morin transition by changing the 'easy' axis of magnetization (*Besser et al.* 1967). Below T_M , the antiparallel spin alignment is perfect; any canting would now violate the magnetic symmetry (*Dzyaloshinsky* 1958). Hence, the intrinsic canted moment is susceptible to the Morin transition, but the defect moment is not. Consequently, below T_M only the defect moment persists.

The parameters related to the Morin transition, however, are affected in a significant way by small changes in the lattice. Impurity cations and reducing grain sizes are reported to shift T_M to lower temperatures and tend to smear the reorientation of the magnetic spins over a larger temperature range (*cf. Morrish* 1994 and references therein). The transition becomes even completely suppressed in pure hematite grains less than $\sim 0.02\text{--}0.03\ \mu\text{m}$ (e.g. *Bando et al.* 1965; *Kündig et al.* 1966), or due to the incorporation of critical quantities of impurity cations in the hematite lattice (e.g. *Morin* 1950; *Flanders & Remeika* 1965). Consequently, the weak ferromagnetic phase persists in these hematites over the whole temperature range measurable in the laboratory (down to 4 K). There have been found indications that vacancies or defects, morphology, degree of crystallinity and structurally bound water can also alter both T_M and the range of temperatures over which the transition occurs (*cf. Morrish* 1994 and references therein). *Nininger & Schroerer* (1978) and *De Grave et al.* (1982) showed that in a smeared transition both the antiferromagnetic and the weak ferromagnetic phase could coexist over a considerable temperature range.

One should be aware that the Morin transition is not only temperature-induced but also magnetic-field or pressure driven (*cf. Morrish* 1994). The three variables are interdependent. By application of an external field the transition occurs at lower temperatures; the critical field required to induce the transition is dependent on the temperature and the angle between the field and the crystal axis (e.g. *Morrish* 1994 and references therein).

The high-field susceptibility becomes isotropic on cooling below T_M (e.g. *Néel & Pauthenet* 1952; *Creer* 1967). The susceptibility parallel to the c -axis decreases sharply from a fairly uniform value of $\sim 25 \times 10^{-8}\ \text{m}^3\ \text{kg}^{-1}$ to $\sim (1\text{--}2.5) \times 10^{-8}\ \text{m}^3\ \text{kg}^{-1}$. The susceptibility in the basal plane, however, shows no appreciable change except for a hump ($\sim 30 \times 10^{-8}\ \text{m}^3\ \text{kg}^{-1}$) around T_M . Consequently, below T_M a sample of randomly oriented particles, with $\frac{1}{3}$ of the grains having their c -axis parallel to the applied field, has a χ_{hf} around $\sim 17 \times 10^{-8}\ \text{m}^3\ \text{kg}^{-1}$. The low-field susceptibility below T_M consists only of the antiferromagnetic susceptibility and a superimposed susceptibility in the direction of the c -axis arising from defects in the hematite lattice. Below the Morin transition, no or a small amount of domain walls are observed (*cf. Morrish* 1994 and references therein), thus displacement of domain walls in formerly PSD and MD grains no longer contribute

to the low-field susceptibility below T_M . So far, no data are available on the change of χ_{lf} values of PSD and MD hematite particles on cooling and rewarming through T_M .

3.3 Samples, methods and equipment

3.3.1 Samples

Seven well-characterized natural hematite samples and one sample of synthetic origin were used for the experiments. The synthetic sample was prepared by heating analytical grade iron(III)-nitrate [$\text{Fe}(\text{NO}_3)_3 \cdot 9\text{H}_2\text{O}$] to 800°C in an oven. The obtained material consists of fine-grained (<1 μm) dark-red particles.

The natural samples comprise one hematite-bearing rock sample (a so-called red bed) and six samples obtained by crushing macroscopic hematite crystals. They were all used in previous paleomagnetic and/or rock-magnetic studies on hematite. The red beds from Dôme de Barrot (France) were the subject of the PhD thesis by *Van den Ende* (1977), and some samples were also used in a rock-magnetic study by *Dekkers & Linszen* (1989). These Permian sediments consist of fine-grained dark red mudstones that are calcified or silicified, and are believed to originate from rhyolitic volcanic material. *Dankers* (1978, 1981) studied the hematite samples labelled LH2 (Kimberley, South Africa) and LH3 (Vosges, France), while those labelled LH4 (origin unknown), LH6 (Gellivara, Lapland), and LHC (origin unknown) were investigated by *Hartstra* (1982). The hematite material from the Kadaň locality in the Czech republic was previously studied by *Hejda et al.* (1992) and *Petrovský et al.* (1994, 1996).

The crushed natural hematite samples were characterized by the afore-mentioned authors using microprobe analyses (chemical composition), X-ray diffraction (unit-cell parameters and crystallinity) and optical microscopy (shape and lamellar twinning). Their findings are summarized in *Table 3.1*. Unfortunately, only from some of *Dankers'* and *Hartstra's* coarse-grained fractions enough sample material (>0.5 g) was left to measure reliably changes in χ_{lf} on cycling through T_M . Consequently, identical grain-size fractions of each hematite type were not available. In *Table 3.1* the particular grain-size fraction used in the present study is given together with some rock-magnetic parameters obtained by the afore-mentioned authors. *Dankers'* and *Hartstra's* results from various rock-magnetic experiments indicate that the particles of the grain-size fractions mentioned in *Table 3.1* are PSD or MD. For instance, remanent coercivities measured by *Dankers* and *Hartstra* for grain-size fractions ranging <5 μm to 150–250 μm don't show a peak diagnostic for the SD to PSD change, but decrease with increasing grain size over the whole range. The results from *Hejda et al.* (1992), however, might indicate that the Kadaň hematite is still SD for acicular particles between 75 and 100 μm .

Table 3.1 Some chemical and physical properties of the crushed natural hematite samples used in this study as determined by ⁽¹⁾Dankers (1978, 1981), ⁽²⁾Hartstra (1982) and ⁽³⁾Hejda et al. (1992).

	LH2 ⁽¹⁾	LH3 ⁽¹⁾	LH4 ⁽²⁾	LH6 ⁽²⁾	LHC ⁽²⁾	Kadaň ⁽³⁾
Fe₂O₃ (%)	98.2	98.2	97.9	98.1	99.9	~ 99
Al₂O₃ (%)	0.1	0.3	0.6	0.7	0.5	< 0.1
TiO₂ (%)	< d.l.	< d.l.	0.1	0.5	< d.l.	< 0.1
Unit cell a_o (Å)	5.050 ± 0.012	5.050 ± 0.012	5.038 ± 0.011	5.038 ± 0.011	5.038 ± 0.011	nd
Unit cell c_o (Å)	13.75 ± 0.04	13.75 ± 0.04	13.76 ± 0.031	13.76 ± 0.031	13.76 ± 0.031	nd
Shape	platy	platy	platy	rounded	platy	acicular (10:1)
Crystallinity	excellent	poor	excellent	good	excellent	excellent
Twinning	no	no	few	abundant	no	no
Fraction (μm)	55–75	25–30	40–55	40–55	75–100	75–100
σ_{sr} (Am² kg⁻¹)	0.218	0.200	0.167	~ 0.2	0.222	nd
B_{cr} (mT)	59	229	153	237	31	~ 256
B_{cr'} (mT)	55	225	179	223	29	~ 339
B_{1/2} (mT)	58	nd	100	220	75	~ 289

The rock-magnetic properties were determined for the grain-size fraction indicated. σ_{sr} is the isothermal 'saturation' remanence imparted at 2 T, B_{cr} is the remanent coercive force, $B_{cr'}$ is the remanent acquisition coercivity, $B_{1/2}$ is the median destructive field of the σ_{sr} , d.l. indicates detection limit; nd indicates not determined.

To be able to measure the grain-size dependence of changes in χ_{lf} on cycling through T_M and to get a suite of hematite particles spanning the SD to MD range, we prepared new fine-grained fractions from the 40–55 μm particles of sample LH2. The 30–40 μm, 25–30 μm, 20–25 μm, 15–20 μm, 10–15 μm, 5–10 μm, and <5 μm fractions were obtained by gently crushing the 40–55 μm grains followed by ultrasonic microsieving in propanon. The <5 μm fraction was further separated into two fractions by stirring the grains in propanon and decanting the particles remaining in suspension. This latter fraction consists of ultrafine red-coloured particles (pigment) which are all < ~1 μm, while the grey-coloured bottom material consists of particles roughly ranging between 1 and 5 μm, as was checked with reflected light microscopy. LH2 hematite was chosen not only because enough material was available to crush new fractions, but also because the grains of this hematite type clearly consist of only one or a few layers of non-twinned well-crystalline plates according to the basal plane and are not complex intergrowings of several particles as often is the case when grain-size fractions are obtained by crushing compact masses of hematite ore. Furthermore, Dankers' results on this hematite type showed clear grain-size dependent trends for various rock-magnetic parameters. Table 3.2 summarizes the hysteresis parameters of sample LH2 obtained on some of Dankers' original fractions and on the newly prepared fractions.

Table 3.2 Rock-magnetic properties of various grain-size fractions for hematite sample LH2 determined at room temperature by measurements on an alternating gradient magnetometer. The maximum field used was 1.6 T.

grain-size (μm)	B_{cr} (mT)	B_c (mT)	σ_{sr}/σ_s	saturated
75 – 100	40.96	33.49	0.626	yes
55 – 75	45.78	33.53	0.535	yes
40 – 55	50.44	40.57	0.622	yes
30 – 40	59.22	46.98	0.601	yes
25 – 30	107.3	82.59	0.680	yes
20 – 25	168.9	133.7	0.743	almost
15 – 20	197.7	158.3	0.757	no
10 – 15	270.3	204.3	0.746	no
5 – 10	340.5	261.5	0.769	no
1 – 5	565.8	365.8	0.709	no
< 1	873.6	469.0	0.586	no + SP

Complete saturation was achieved only for the five coarsest fractions. The <1 μm fraction revealed a slightly wasp-waisted hysteresis loop caused by superparamagnetic (SP) particles. The 75–100 μm , 55–75 μm and 40–55 μm fractions are the original fractions made by Dankers (1978, 1981), whereas the finer grain-size fractions were crushed by the present authors from Dankers' original 40–55 μm fraction. B_c is the coercive force: B_{cr} is the remanent coercive force: σ_{sr}/σ_s is the ratio between the remanent 'saturation' magnetization and the 'saturation' magnetization.

3.3.2 Experimental methods and instrumentation

Low-field magnetic susceptibility measurements

A CS-2 furnace apparatus and low-temperature unit connected to a low-field KLY-2 kappabridge (all AGICO, Brno, Czech Republic) was used to record the temperature variation of χ_{lf} between -196°C and $+700^\circ\text{C}$. Operating conditions of the instrument are a measuring frequency of 720 Hz with a rms fieldstrength of 0.377 mT (corresponding to a peak fieldstrength of ~ 0.5 mT). Demagnetizing fields are negligible in hematite, and thus it is the intrinsic initial susceptibility that is measured (Collinson 1983). Between high- (HT) and low-temperature (LT) measurements switching of furnace type and temperature sensor is necessary. Unfortunately, only the warming run from -196°C back to room temperature can be monitored during the LT-experiment. Typically 0.5 to 0.8 g was inserted in the quartz-glass sample tube. All χ_{lf} – T measurements were afterwards corrected for the temperature variation of the empty furnace (*cf. AGICO manual*).

The following measuring procedure was used to obtain the $\chi_{lf} - T$ curves plotted in Figs 3.1 and 3.2. First, the sample was cycled between room temperature and $+150^\circ\text{C}$ at a rate of $\sim 5^\circ\text{C min}^{-1}$ to determine whether mild heating causes any change in χ_{lf} . Then the sample was cooled to liquid-nitrogen temperature and χ_{lf} was monitored on warming back to 0°C or room temperature. A complete warming run from -196°C to 0°C takes about 40 minutes; warming rates decrease gradually with increasing temperature. Afterwards, the sample was again cycled between room temperature and $+150^\circ\text{C}$ to study how the possibly changed domain structure (as deduced from changes in χ_{lf}) reacts to mild heating.

Two hematite samples (LH2 and LHC) were afterwards also cycled to 700°C at a rate of $\sim 10^\circ\text{C min}^{-1}$ to determine the effect of high temperatures and cycling through T_c ($\sim 680^\circ\text{C}$) on the new magnetic state. These two samples were chosen because they have the highest susceptibility and revealed the highest change in χ_{lf} on cycling through T_M . Furthermore, test runs to 700°C with a non-treated LH2 sample showed identical heating and cooling curves. The complete recovery of the initial magnetic state on cooling implies that no heating-induced chemical or physical changes (e.g. grain growth or reordering of the lattice) occur in this hematite type when heated up to 700°C . This means that for LT-treated LH2 hematite any irreversible behaviour between the heating and cooling curves can be interpreted as a heating-induced change in the new magnetic state as obtained after cycling through T_M . Non-treated LHC hematite, on the other hand, does show a slight susceptibility increase after cycling to 700°C . This hematite type will be used to determine whether heating-induced chemical or physical changes affect the χ_{lf} increase obtained on cycling through T_M .

As mentioned in Section 3.2.1, the magnetic properties of hematite show a strong directional dependence; χ_{lf} measured in the basal plane will be much higher than in the direction of the hexagonal c -axis. It was realized that some degree of magnetic anisotropy may exist in our samples, i.e. the particles are not likely to be oriented fully randomly in the sample tube. As a result, the measured absolute χ_{lf} values will in essence only be representative of that particular orientation of the grains. Moreover, the orientation of the particles may possibly also affect the χ_{lf} change obtained after cycling through T_M . Furthermore, it was recognized that the orientation of the grains might have changed during the experiment because of the required change in sample set-up between HT and LT runs. This once more could affect the difference obtained in χ_{lf} measured before and after cycling through T_M , and might be misinterpreted as a change in domain configuration.

We checked in several ways whether or not these orientational effects seriously affect our results. First, the absolute χ_{lf} values measured initially at room temperature for LHC and LH2 hematite indeed depend on the orientation of the grains in a particular batch. Absolute differences in χ_{lf} up to $\sim 50 \times 10^{-8} \text{ m}^3 \text{ kg}^{-1}$ due to stirring and/or ultrasonic vibrating of the grains in the sample tube were possible for LHC and LH2 hematite, respectively. Differences in the other hematite samples, however, appeared to be marginal, possible due to their finer grain size or different shape. LH4 hematite,

for instance, consists just like LHC and LH2 of well-crystallized plates, but the former grains are thicker being comprised of a larger number of plates.

Second, the change in χ_{lf} was also determined without monitoring the low-temperature warming run on the KLY-2/CS-2 device, i.e. no change of sample set-up was required in this way. For this purpose the quartz-glass sample tube with the connected temperature sensor were taken out of the furnace of the kappabridge after an initial measurement at room temperature. Then the sample was placed in liquid nitrogen and measured again after warming to room temperature. In this way possible movement of the hematite particles was minimized to barely noticeable proportions. Still χ_{lf} increases were measured after a LT treatment implying that changes in particle orientation are not responsible for the effects observed. It also appeared that absolute χ_{lf} increases after a LT treatment might depend on the orientation of the grains in the sample tube (e.g. depending on the grain-size and the thickness of the platy grains), whereas the χ_{lf} increases normalized to their initial value measured at room temperature were independent on the particle orientation within a particular batch. Normalization thus provides an orientation-independent parameter. The afore-mentioned procedure without changing the sample set-up was used to measure the grain-size dependence of the normalized χ_{lf} change for sample LH2 (see *Fig. 3.3*). During the course of the measurements it became also possible to carry out a cooling and warming cycle in a field-free space by placing the sample tube in a set of Helmholtz coils. Warming through hematite's Morin transition in the Earth's magnetic field or in a field-free space appear not to affect the χ_{lf} increase obtained.

Third, the anisotropy of magnetic susceptibility (AMS) was measured on a KLY-3 kappabridge (AGICO, Brno) before and after a complete cooling and warming cycle through the Morin transition. Any significant change in AMS would imply that the χ_{lf} is changed preferentially in a specific direction. The AMS measurement was carried out on a standard-size, cylindrical artificial sample consisting of five thin layers of highly oriented hematite particles in an epoxy-resin matrix (Araldit D with hardener HY 956, Ciba-Geigy). The thin hematite platelets of the 40–55 μm grain-size fraction of sample LH2 were positioned in such a way that they had a preferred orientation in the basal plane of the sample. No significant changes in the AMS ellipsoid orientation (directions of the three principal susceptibility axes) were detected. The extremely high anisotropy factors F (k_2/k_3) and P (k_1/k_3) change from 3.10 and 3.12 to 3.58 and 3.60 before and after the LT treatment, respectively. The measurements were corrected for the isotropic diamagnetic moment of the matrix. Furthermore, the normalized χ_{lf} increase (26%) obtained for these highly oriented grains falls within the range (24–33%) obtained during experiments on the same grain-size fraction using the powders (see *Fig. 3.3*). This experiment indicates as well that a possible (slight) movement of the grains between the high- and low-temperature measurements does not cause the observed gain in χ_{lf} . Furthermore, it can be concluded that χ_{lf} becomes higher irrespective of the orientation of the grains and no relation exists between the orientation of the hematite grains in the sample and the found changes in bulk susceptibility normalized to its initial value.

Measurements on a similar non-treated sample showed that changes in bulk susceptibility due to AF demagnetization (300 mT) of the initial state are negligible (<1%). Warming this sample from -196°C to room temperature in a field-free space again yield similar increases in normalized bulk susceptibility (31%) compared to warming in the Earth's magnetic field. Afterwards, the stability of the new magnetic state against increasing AF demagnetizing fields was tested on this sample. This experiment resulted in a full recovery of the original mean susceptibility value (see Section 3.4.1 and Fig. 3.4).

MicroMag measurements

A Princeton alternating gradient magnetometer (MicroMag 2900) equipped with a helium (or nitrogen) flow-through cryostat was used to monitor low-temperature cooling ($+80$ to -100°C) and warming (-100 to $+80^{\circ}\text{C}$) runs of induced magnetic moments (σ in various fields and σ_{rs}), and to measure hysteresis loops at various temperatures between $+80^{\circ}\text{C}$ and -170°C . This specific temperature range was chosen, because $+80^{\circ}\text{C}$ lies fully above the onset of the Morin transition, whereas -100°C is fully below T_{M} . Cooling and warming rates were $\sim 3^{\circ}\text{C min}^{-1}$. All measurements were done on the same sample, which was demagnetized between the different experiments by the MicroMag routine using 5% decrement in magnetization per iteration starting at 300 mT. The sample consisted of 2.85 mg of the 75–100 μm grain-size fraction of LHC hematite. This particular hematite type was used because it yielded the highest χ_{if} increase on cycling through T_{M} and also showed the most pronounced and abrupt Morin transition with the largest difference between the magnetic states above and below T_{M} . The grains were stuck to a small quartz-glass platelet by using double-sided tape and subsequently fixated with transparent lacquer spray. A slight preferred orientation of hematite's basal plane parallel to the applied field might exist as a consequence of this procedure. All results were afterwards corrected by subtracting the values obtained by measuring a blank (quartz-glass platelet with tape and lacquer spray only).

The low-temperature $\sigma - T$ cycles were recorded in various applied magnetic fields (5, 25, 100 and 1600 mT), to determine the field dependence of the magnetization increase on cycling through the Morin transition. The highest applied field appears to be sufficient to completely saturate LHC hematite. Hysteresis loops were measured at various temperatures to follow its change in shape by cooling through the Morin transition. The saturation remanence (1.6 T) obtained at $+80^{\circ}\text{C}$ was also cycled through T_{M} to determine its memory.

Repeated cooling and warming cycles to increasingly lower temperatures were recorded in a 5 mT field to determine the onset of the irreversible change in magnetization (i.e. domain configuration) related to T_{M} . After each cycle the field was momentarily turned off to determine which part of the magnetization increase could be considered as being remanence.

Minor hysteresis loops (5 mT) were measured at various temperatures to determine the change in shape of the loops obtained in a non-saturating applied field. A first minor

loop was obtained at +80°C starting from a demagnetized state. Then the sample was cooled to -30°C within a 5 mT field and two subsequent minor loops were measured at this temperature. Next, the sample was warmed back to +80°C, demagnetized at this temperature, and then cycled between +80°C and -100°C in a 5 mT field before measuring the two subsequent minor loops back at +80°C. Additional runs were carried out to obtain the B_{cr} values at the afore-mentioned temperatures.

3.4 Experimental results

3.4.1 Low-field susceptibility measurements

Coarse-grained hematites

The $\chi_{lf} - T$ behaviour between +150°C and -196°C is shown in *Fig. 3.1(a-f)* for six coarse-grained hematites, respectively LHC, LH2, LH3, LH4, LH6 and Kadaň. The χ_{lf} values initially measured at room temperature (starting point of cycle 1) differ widely between the various hematite types, ranging between $(40-235) \times 10^{-8} \text{ m}^3 \text{ kg}^{-1}$. They fall within the range reported in literature (*cf.* Section 3.2.1). Platy-developed hematite particles (LHC, LH2, LH4 and LH3) appear to have the highest χ_{lf} values, while the rounded (LH6) and acicular (Kadaň) hematite grains represent the lowest values, irrespective of orientational effects and differences in grain size.

A first heating to 150°C (solid line of cycle 1) results in all cases in a slight gradual increase in χ_{lf} , likely caused by a small decrease in coercivity. The break in slope at ~50°C and ~100°C for sample LH3 and LH4, respectively, represents the high-temperature onset of the Morin transition for these hematites (*cf.* Hartstra 1982; De Boer & Dekkers 1998). The cooling curves of these first cycles (dotted lines) are reversible with respect to the heating curve, indicating that the initial magnetic state is recovered on cooling to room temperature. This part of the experiment thus shows that mild heating does not change neither the initial magnetic state of the coarse-grained hematites nor causes any chemical and/or physical changes.

After cooling to liquid-nitrogen temperature, the χ_{lf} recorded at the beginning of the warming curve (run 2) is almost identical for all hematite samples and ranges between $(19-28) \times 10^{-8} \text{ m}^3 \text{ kg}^{-1}$, except for sample LH4 which has a value of $\sim 65 \times 10^{-8} \text{ m}^3 \text{ kg}^{-1}$. The former χ_{lf} values are only slightly higher than that reported for randomly oriented hematite particles. Here, the susceptibility below T_M consists only of the antiferromagnetic susceptibility ($\sim 16.6 \times 10^{-8} \text{ m}^3 \text{ kg}^{-1}$, *cf.* Section 3.2.2). This indicates that the superimposed susceptibility due to ordered defects is not very significant in our hematite samples. The higher value of sample LH4 can be explained by a minute magnetite contamination (*cf.* De Boer & Dekkers 1998). The increase in χ_{lf} on warming from -196°C and the characteristic hump around -160°C are typical of respectively the Verwey transition and the magnetic isotropic point of slightly oxidized or substituted magnetite.

COARSE-GRAINED NATURAL HEMATITES

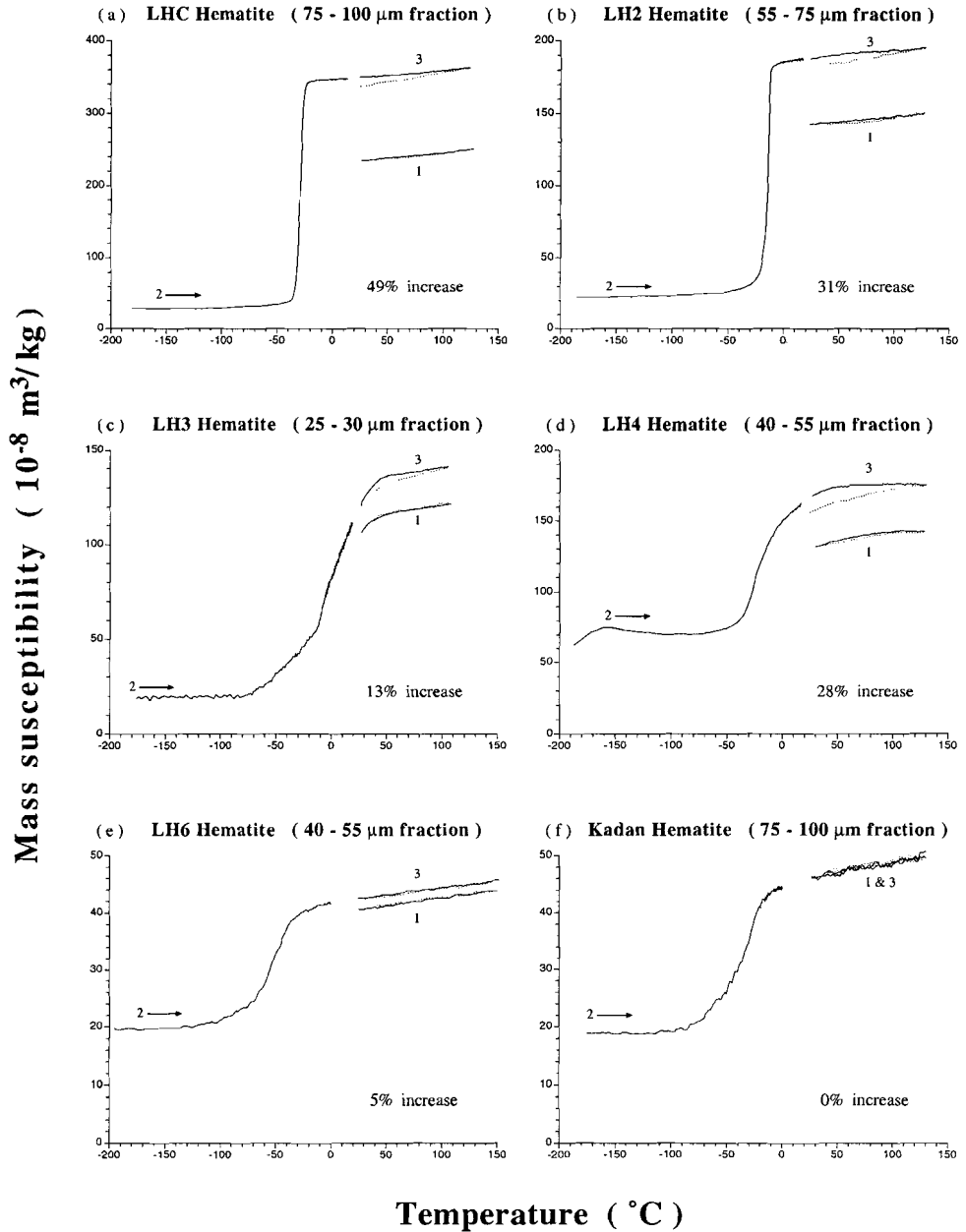


Figure 3.1 (left): Low-field susceptibility vs temperature runs for various coarse-grained natural hematites. 1 and 3 refer to cycles between room temperature and 150°C, while 2 is a warming run from -196°C to room temperature. Cycle 3 is measured after run 2. An increase in χ_{lf} after cycling through the Morin transition (i.e. isotropic point) is observed for platy (LHC, LH2, LH3, LH4) and rounded (LH6) particles but not for acicular Kadaň hematite. Solid and dotted lines denote heating and cooling runs, respectively.

All coarse-grained hematites show a well-developed Morin transition. These hematites can be divided into three groups (I, II and III) on basis of the shape of the Morin transition. Group I hematites (LHC & LH2) are characterized by a sharp ($<10^\circ$) transition with hardly any tail at the low-temperature end. The switch of the 'easy' axis of magnetization, resulting in the change between the antiferromagnetic and the weak ferromagnetic state, must be very abrupt. The complete Morin transition may lie within the range of Earth's surface temperatures, especially during colder geological periods. Group II hematites (LH3 & LH4) have, apart from the effect caused by the magnetite contamination (LH4), a more smeared transition ($>50^\circ\text{C}$) with its high-temperature onset above room temperature. The rotation of the magnetic spins is thus more gradually, but starts already (far) above normal Earth's surface temperatures. Group III hematites (LH6 & Kadaň) also have a smeared transition ($>50^\circ\text{C}$), but with its high-temperature onset below 0°C and with a relatively large low-temperature tail. For this type of hematite, the rotation of the magnetic spins will not even be fully completed within an extreme range of Earth's surface temperatures.

All coarse-grained hematites, which are PSD or MD according to previous rock-magnetic studies (cf. Dankers 1978, 1981; Hartstra 1982), show a distinct increase in χ_{lf} when comparing the values measured at room temperature before and after cycling through T_M . The absolute χ_{lf} increase ranges between 2×10^{-8} and $115 \times 10^{-8} \text{ m}^3 \text{ kg}^{-1}$, and between 5 and 49% when normalized to its initial value. Samples with comparable grain sizes (LHC–Kadaň and LH4–LH6) show different percentages of susceptibility increase. Evidently, the increase in susceptibility is dependent on the hematite type under investigation. The acicular Kadaň sample, which despite its coarse grains is most likely SD (cf. Hejda *et al.* 1992), shows no increase in χ_{lf} on cycling through T_M . The existence of a Morin transition is apparently necessary to have a χ_{lf} increase, but not automatically implies an increase. Several times repeating of the low-temperature experiment, before doing the second high-temperature cycle to 150°C, yields similar-shaped warming curves and thus identical χ_{lf} increases.

The heating curve of the second χ_{lf} – T cycle to 150°C (cycle 3, solid lines) has a similar shape and inclination as the heating curve of the first run. On cooling back to room temperature, however, some cooling curves now become irreversible with respect to the heating curve. This indicates that mild heating is able to neutralize a portion of total χ_{lf} increase gained on cycling through T_M . This portion is ~15% for samples LHC and LH2, ~35% for samples LH3 and LH4, and ~0% for hematite LH6, although this latter value cannot be determined very accurately. The relatively high losses obtained for sample LH3 and LH4 are because these hematites pass the high-temperature onset of their Morin transition on cooling back to room temperature.

Fine-grained hematites

The $\chi_{lf}-T$ curves obtained for the fine-grained synthetic hematite and the red bed sample are shown in Figs 3.2(a & b), respectively. Both hematites, which most likely are SD, do not show any χ_{lf} increase after the LT treatment. The warming curve of the synthetic hematite from -196°C back to room temperature (run 2) reveals a more or less two-step Morin transition, likely indicating the presence of two distinct grain-size distributions. In this view, the steep part of the warming curve between $\sim -30^{\circ}\text{C}$ and -10°C represents the relatively coarse, well-crystalline fraction with grains up to $\sim 1\ \mu\text{m}$, whereas the smeared low-temperature tail of the curve represents the ultrafine, possibly less crystalline particles of the sample. The high-temperature onset of the Morin transition at $\sim -10^{\circ}\text{C}$ indicates that the particles consist of pure $\alpha\text{-Fe}_2\text{O}_3$.

On warming from -196°C , the red bed sample does not show the characteristic increase in susceptibility related to a switch of ‘easy’ axes of magnetization, but rather shows a hyperbolic temperature dependence of χ_{lf} . This specific $\chi_{lf}-T$ behaviour can either be caused by ultrafine hematite grains being superparamagnetic over the whole temperature range or by the paramagnetic minerals of the sediment. A rock-magnetic study by Dekkers & Linssen (1989) on samples from the same locality, however, showed that the first possibility is highly unlikely because their isothermal remanent magnetization (IRM) was not viscous. LT-cycling of their induced IRM did also not reveal a clear Morin transition. In view of the assumed volcanic origin of the hematite, it is quite plausible to explain the persistence of the weak ferromagnetic phase down to -196°C by a small amount of incorporated Ti (*cf.* Section 3.2.1).

FINE-GRAINED HEMATITES

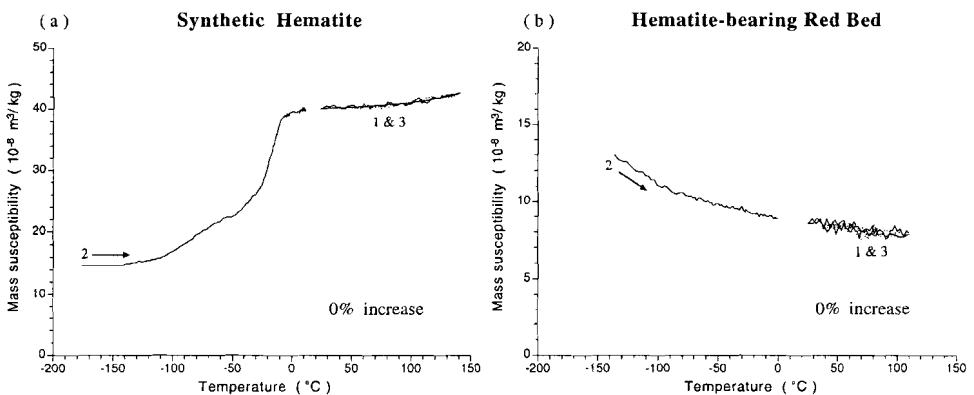


Figure 3.2: Low-field susceptibility vs temperature runs for fine-grained hematites, curve numbering as in Fig. 3.1. (a) Synthetic hematite prepared by thermal decomposition of hydrated ferric nitrate salt at 800°C , and (b) hematite-bearing red bed from Dôme de Barrot (France). No difference in χ_{lf} is obtained before and after a low-temperature run.

Grain-size dependence of the χ_{lf} increase caused by cycling through T_M

The percentage χ_{lf} increase caused by cycling through T_M is plotted in Fig. 3.3 for several grain-size fractions of LH2 hematite. The χ_{lf} increase (y), normalized to its initial value, clearly increases with the logarithm of grain size (x). A linear fit results in $y = (8.60 \pm 1.01) \ln(x) - 2.98$ with $R^2 = 0.82$, implying that for this particular hematite no increase in χ_{lf} can be observed in grains smaller than $\sim 1.5 \mu\text{m}$. The results plotted in this figure also illustrate that normalized χ_{lf} increases obtained in a field-free space (indicated with solid dots) fall in the same range as those obtained on identical grain-size fractions in the Earth's magnetic field.

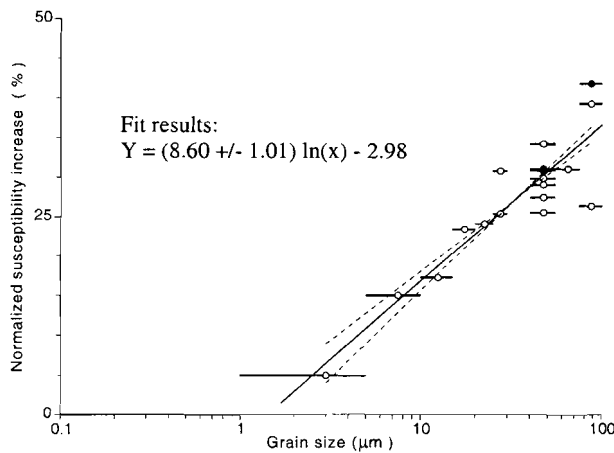


Figure 3.3: Percentage susceptibility increase after cycling through the Morin transition for various grain-size fractions of well crystalline, platy LH2 hematite. Open and solid circles denote measurements in the Earth's magnetic field and in a field-free space, respectively. Solid lines through the circles denote the grain-size fraction used.

High-temperature and AF stability of the new magnetic state

Figures 3.4(a & b) show the HT-behaviour of the initial magnetic state and the new magnetic state as obtained by cycling through T_M for LH2 and LHC hematite, respectively. For LH2 hematite, a high-temperature $\chi_{lf} - T$ cycle to 700°C starting from the initial state revealed complete reversible behaviour (Fig. 3.4a, cycle 1). No heating-induced changes in χ_{lf} caused by irreversible chemical and/or physical changes were detected after cycling. Next, the new magnetic state, characterized by the higher χ_{lf} value, is obtained by cooling to -196°C and subsequent warming to room temperature (run 2). Subsequent heating to 700°C (cycle 3) shows that the heating curve of the new magnetic

state resembles that of the initial magnetic state in shape, but lies entirely above it until the Curie point is reached at $\sim 685^\circ\text{C}$, indicating that the new magnetic state remains up to T_c . The cooling curve of cycle 3, on the other hand, is irreversible with respect to the heating curve, but perfectly matches the curves obtained during cycle 1, indicating that after cycling through T_c the initial magnetic state is recovered. A subsequent LT-treatment (not shown here) yielded a warming curve similar to run 2.

Unlike the procedure followed for LH2 hematite, the treatment on LHC hematite was not started with an initial cycle to 700°C . Instead, cycle 1 and warming run 2 shown in Fig. 3.4(b) are identical to those plotted in Fig. 3.1(a), and represent the initial magnetic state and the new magnetic state obtained after cycling through the Morin transition, respectively. A subsequent HT cycle to 700°C does not recover the initial magnetic state on cooling but produces a further increase in susceptibility. Preceding test runs on an untreated sample (see Section 3.3.2) revealed that this increase in susceptibility is most probably caused by a heating-induced structural change of the hematite (e.g. recrystallization or better ordering). A subsequent test cycle to 700°C showed no further irreversible χ_{lf} changes and the heating and cooling curves were identical. From this perspective, the magnetic state of the better-ordered hematite can be regarded as a new 'initial' state. A low-temperature treatment (run 4) on this structurally-improved hematite, increases its χ_{lf} value with $\sim 15\%$. Cycling to 700°C (cycle 5) fully neutralizes this increase and recovers the 'initial' state of the better-ordered hematite, i.e. the one after cycle 3.

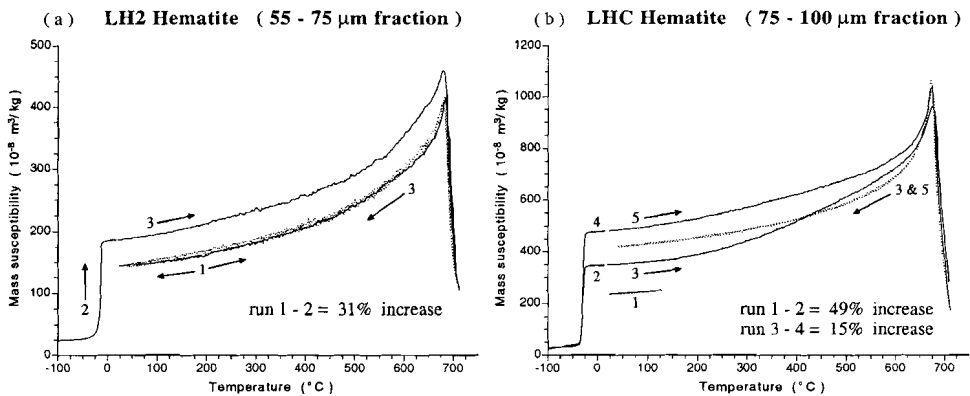


Figure 3.4: Low-field susceptibility vs temperature runs for coarse-grained (a) LH2 and (b) LHC hematite. See text for explanation of curve numbers. The susceptibility increase obtained after cycling through the Morin transition is fully neutralized after heating above the Curie point recovering the initial magnetic state.

Figure 3.5 shows that the increase in bulk susceptibility obtained on cycling through T_M can also be neutralized to its initial value before the LT experiment by AF demagnetization. This involves measurement of χ_{hf} between subsequent AF steps. For the 40–55 μm fraction of LH2 hematite, 50% of the increase is already lost in an AF demagnetizing field of 7.5 mT, while peak fields up to ~ 100 mT are required for a full recovery of the initial bulk susceptibility.

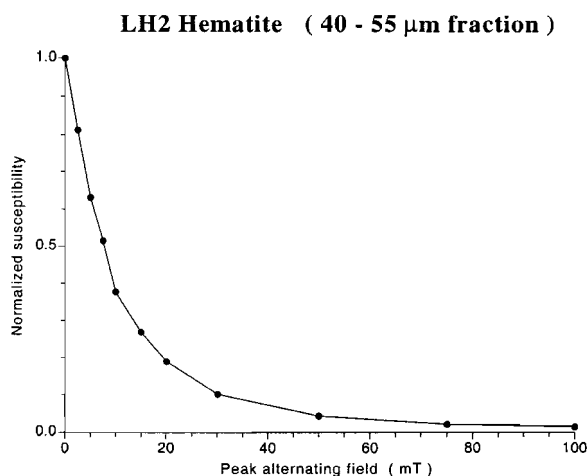


Figure 3.5: Measurements of χ_{hf} between alternating field demagnetization steps of sample LH2 after being cycled through T_M , showing the gradual neutralization of the χ_{hf} increase to its initial value.

3.4.2 MicroMag measurements

Figure 3.6 shows the changing shape of the hysteresis loops obtained in a 1.6 T field when passing through the Morin transition. The 75–100 μm grain-size fraction of sample LHC appears to be fully saturated at temperatures above T_M . At temperatures during and below the Morin transition, however, the 1.6 T field is no longer sufficient to saturate the sample. Below T_M , still some hysteresis can be seen indicating the presence of a small defect moment. Hysteresis parameters measured at $+20^\circ\text{C}$ are: $\sigma_s = 0.316 \text{ Am}^2 \text{ kg}^{-1}$, $\sigma_{rs} = 0.218 \text{ Am}^2 \text{ kg}^{-1}$, $B_c = 23.4 \text{ mT}$ and $B_{cr} = 28.9 \text{ mT}$. The high-field susceptibility at 20°C deduced from the hysteresis loop is $26.76 \times 10^{-8} \text{ m}^3 \text{ kg}^{-1}$. This is in good accordance with published data on χ_{hf} . Using $26.76 \times 10^{-8} \text{ m}^3 \text{ kg}^{-1}$, this would yield a χ_{hf} value of $\sim 18.5 \times 10^{-8} \text{ m}^3 \text{ kg}^{-1}$ below T_M for randomly oriented particles with $1/3$ of the grains having their c -axis parallel to the applied field (*cf.* Section 3.2). We measured a high-field susceptibility of $22.8 \times 10^{-8} \text{ m}^3 \text{ kg}^{-1}$ at -170°C , indicating that in our sample the grains

have a preferred orientation with their basal plane parallel to the applied field (~85%), something which can hardly be avoided due to the sample holder. It must thus be realized that all our MicroMag measurements are preferentially related to hematite's basal plane and not to a randomly dispersed sample.

The hysteresis values obtained at 20°C, together with the shape of the curve, are diagnostic of multidomain hematite. The slight wasp-waistedness of the hysteresis loops might be explained by the preferred orientation of the grains. The saturation remanence, for instance, will be higher than that of a randomly oriented sample, while the B_c and B_{cr} values will also be slightly biased. Another explanation could be the difference in coercivity between the canted and defect moment. The existence of SP grains or a magnetic contaminant are less likely explanations, because no adhering ultrafine hematite particles were observed under an optical microscope and other magnetic measurements (e.g. $\chi_{if} - T$ curves) revealed no indication for a magnetic impurity. A similar hysteresis loop is obtained by *Flanders & Schuele* (1964) on a large natural hematite crystal.

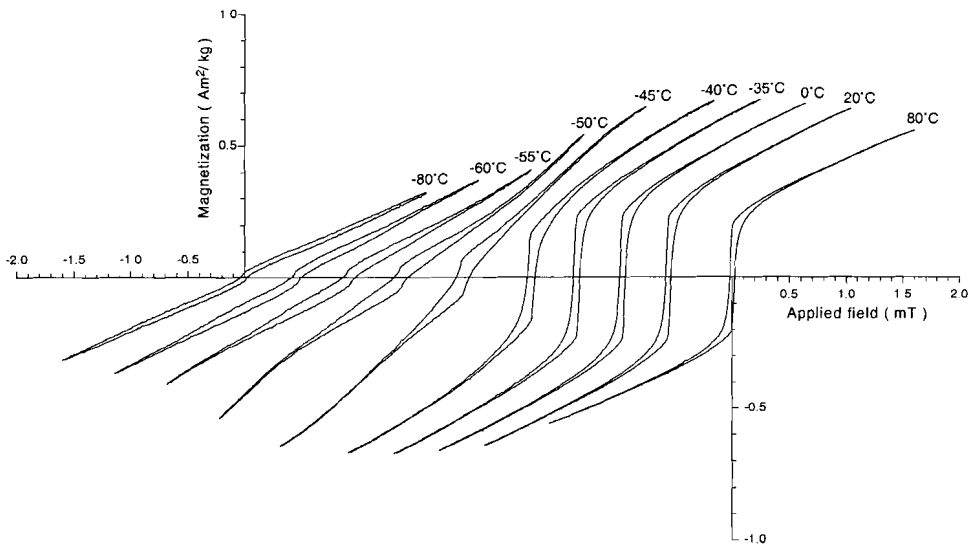


Figure 3.6: Hysteresis loops (maximum applied field 1.6 T) measured at various temperatures for LHC hematite (75–100 μm), showing the changing shape on passing through the Morin transition.

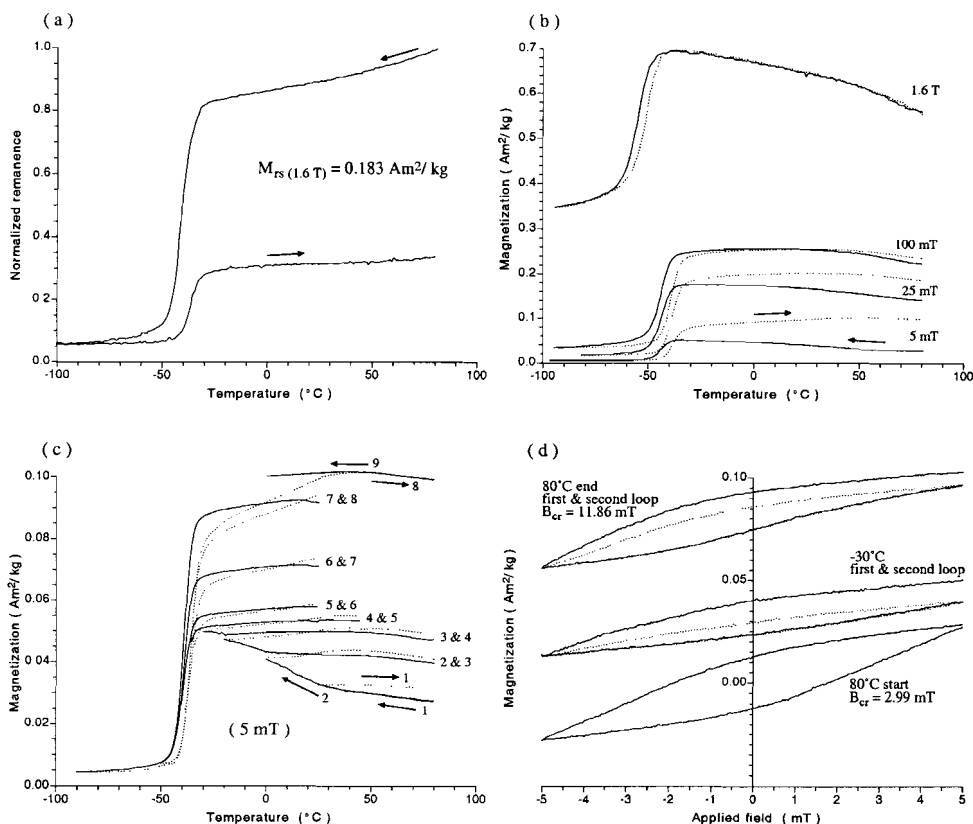


Figure 3.7: Various low-temperature MicroMag measurements obtained on LHC hematite (75–100 μm). (a) LT-cycle of the saturation remanence (1.6 T), (b) LT-cycles in various applied fields, (c) repeated in-field cycling (5 mT) to increasingly lower temperatures, (d) minor hysteresis loops (5 mT) obtained at different temperatures during a LT-cycle through the Morin transition.

A low-temperature cycle of the saturation remanence imparted at +80°C ($\sigma_{rs} = 0.183\text{ Am}^2\text{ kg}^{-1}$) is shown in Fig. 3.7(a). Apart from effects due to the preferred orientation of the grains, it should be realized that LT cycling of σ_{rs} using a MicroMag without applying a magnetic field is not completely identical to LT cycling in zero field. First, no correction for the vertical component of the Earth’s magnetic field is possible, and second, a small magnetic gradient exists between the edges of the sample due to the measuring technique.

Above T_M , the remanence vector lies in the ‘easy’ basal plane of hematite, and thus along the measuring direction for most of the grains. During cooling to the high-temperature onset of the actual Morin transition at -30°C, already ~18% of the initial remanence is destroyed. At -100°C, well below T_M , only ~6% of the original remanence is

left, which resides in hematite's defect moment. For temperatures below T_M , the remanence vector of this moment lies orthogonal to the basal plane and thus also orthogonal to the measurement direction for the largest fraction of the grains. For these oriented grains the remanence measured below T_M will thus be lower than that of randomly oriented grains. *Hartstra* (1982) reported that ca. 33% of an initial σ_{rs} (2 T) imparted at 0°C was left after cooling to -150°C for randomly oriented samples of LHC hematite, whereas ca. 75% of the initial remanence was recovered after rewarming. Rewarming our sample to +80°C recovered only ~33% of the initial remanence. The discrepancy may be caused by the influence of the vertical component of the Earth's magnetic field. On warming through the Morin transition part of the domains will orient themselves along this component which lies in the basal plane but orthogonal to the measuring direction. Only the most strongly pinned domains can recover their initial direction. In the warming curve a slight break in slope is recognizable at ca. +40°C. Warming above this temperature tends to recover the remanence more faster than during the temperature range between T_M and +40°C. For the cooling curve a similar break in slope at the same temperature might be recognized.

Figure 3.7(b) shows low-temperature $\sigma - T$ runs measured in various applied magnetic fields (5, 25, 100 and 1600 mT). Cycling in a 1.6 T field, which is a saturating field down to the high-temperature onset of the Morin transition, results in reversible cooling and heating curves except for some temperature hysteresis observed in the temperature range in which the actual switch of axis happens. An increase in magnetization, however, is observed on cycling through the Morin transition in the other three, non-saturating fields. The gain in magnetization decreases with increasing field strength; it is 200, 25 and 5% for 5, 25, and 100 mT fields, respectively. *Figure 3.7(b)* also illustrates that the Morin transition is shifted to slightly lower temperatures with increasing field strength. By applying a magnetic field in the direction of the basal plane the rotation of the magnetic spins from this plane to the hexagonal c -axis is hampered (see Section 3.2.2). For all applied fields again a break in slope around +40°C is visible in both the cooling and warming curves.

The characteristic break in slope at ca. +40°C is even better visible in *Fig. 3.7(c)*. This figure shows repeated cooling and warming cycles to increasingly lower temperatures in a 5 mT field. The warming curves (dotted lines) are already irreversible compared with the corresponding cooling curves (solid lines) long before the actual Morin transition starts. Cycling between +80°C and +25°C results in a ~15% increase in magnetization measured back at +80°C. After this first cycle, the sample was demagnetized using the MicroMag routine with a starting field of 30 mT. This procedure resulted in the full recovery of the initial demagnetized state, and an identical magnetization was obtained when reapplying the 5 mT field. Between subsequent cycles, the sample was not demagnetized anymore. The magnetic field, however, was switched off before the next run was started. Only small differences in magnetization were observed, implying that the increase in magnetization caused by thermal cycling is for the greater part a remanent magnetization. The remanent magnetization values are not plotted

in this figure but are clearly illustrated in *Fig. 3.7(d)* for three different temperatures. The small discrepancies observed between the starting point of the cooling curve and the end point of the warming curve of the foregoing run (*Fig. 3.7c*) must be explained as follows. When the magnetic field is switched off, a small negative field overshoot occurs that slightly demagnetizes the gained remanent magnetization. When reapplying the field, the original value is not fully recovered due to this effect. Differences between the remanent magnetization values obtained and the starting points of the new cooling curve are marginal, not exceeding 2% (the points are not shown because they are beyond the plotting resolution). Between the last cycle (no. 8) and the partial cooling run to 0°C (no. 9) the field was not switched off.

Cycling down to -30°C (cycle 1-4), i.e. to just before reaching T_M , already increases the magnetization with ~95% of the initial value; which is ~35% of the total increase after the entire experiment. By far the largest part of this 95% increase is gained during cycling to temperatures below the break in slope around +40°C. Complete cycling through the Morin transition (cycle 8) results in a ca. 260% gain in magnetization when compared to the initial value at +80°C.

In the temperature range between T_M and +40°C, thus at the low-temperature side of the break in slope, the warming curve of a particular cycle differs in shape from the cooling curve of a subsequent cycle; i.e. in this particular temperature range, the magnetization increases more rapidly with temperature during warming than it decreases with temperature during the next cooling run. Above the break in slope, however, the warming and subsequent cooling curves are colinear.

Figure 3.7(d) shows some minor hysteresis loops obtained in a 5 mT magnetic field at different temperatures during cycling through T_M . Note that the curves shown have the same ordinate axis; they are not displaced with respect to each other. The minor loop of the initial demagnetized state at +80°C is closed at both sides. A partial B_c and B_{cr} of 2 mT and 2.99 mT are measured, respectively. The minor loop measured at -30°C, however, is no longer closed at the right-hand side, indicating that a portion (~50%) of the magnetization gained on cooling is demagnetized by a backfield of only -5 mT. A subsequent minor loop measured at the same temperature is again closed. Before measuring the following minor loop, the sample was warmed back to +80°C, demagnetized, and next cycled to the desired temperature. The minor loop measured when returned to +80°C after a complete cycle through the Morin transition (-100°C) is not closed as well. However, now only ~10% of the gained magnetization is demagnetized by a 5 mT backfield. The partial B_{cr} value is increased to 11.86 mT.

3.5 Discussion

3.5.1 Domain reorganization as deduced from mineral-magnetic measurements

Low-field susceptibility measurements

For PSD and MD grains, the number of magnetic domains and the mobility of the domain walls determine the susceptibility, whereas for SD grains it is determined by the elastic simultaneous rotation of the spins. Wall motion usually requires lower fields than domain rotation. Consequently, it may be stated that SD grains have lower susceptibility than MD grains. This especially holds for antiferromagnetic substances because wall displacements are not limited by any demagnetizing field, as is the case for ferrimagnetic substances (*cf. Dunlop & Özdemir 1997, page 139*). Irreversible changes in susceptibility caused by a particular treatment that does not chemically or physically (e.g. grain growth) change the material under investigation, may thus be interpreted in terms of domain reorganization.

It is known that low-temperature cycling may change the domain configuration of hematite. The saturation remanence of hematite, for instance, is usually only partly recovered upon cycling. Domain structure observations on hematites in a saturation remanent state (*Eaton & Morrish 1969; Morrish 1994, and references in both*) show that most crystals lose their domain pattern on cooling. Below T_M often a single-domain state is observed, and if they are warmed to room temperature again, a new pattern is seen. In some crystals, however, the walls, or part of the walls, persist below T_M and act as nucleating centers for the configuration which is achieved upon warming the sample back to room temperature (*cf. Fuller 1970*). The latter situation can give an almost perfect recovery of the initial domain configuration.

We showed that thermal cycling through hematite's magnetic isotropic point appears to increase the initial low-field susceptibility of large (at least $>1.5 \mu\text{m}$) platy and rounded grains, whereas fine to ultrafine grains and large acicular grains that likely are SD, do not show this irreversible behaviour. Moreover, the percentage χ_{lf} increase obtained on cycling through the Morin transition increases linearly with the logarithm of grain size.

Dankers (1978) showed that the susceptibility of hematites could be changed considerably by the imparting of a saturation remanence. Consequently, the χ_{lf} increase observed on cycling through T_M might be caused by the destroying of an old remanence or the development of a new remanence. However, for three reasons, this explanation is unlikely. First, our initial state and the magnetic state obtained after AF demagnetization yield identical bulk susceptibilities and thus have comparable domain configurations. Second, χ_{lf} increases are independent on the crystallographic orientation of the hematite grains (at least within the basal plane). Third, cycling in the Earth's magnetic field or in a field-free space yield similar increases.

In our opinion, the results observed must rather be explained by an increased number of magnetic domains induced by thermal cycling through T_M . The fact that AF

demagnetization of the new magnetic state is able to recover the bulk susceptibility value related to the initial magnetic state seems to support this assumption. Our suggestion is also supported by results of *Boyd et al.* (1984), who have reported that low-temperature cycling does trigger the nucleation of walls in large magnetite particles that initially appear to be saturated at room temperature.

The renucleation of domain walls on warming through T_M obviously happens under different conditions as those appear at room temperature or above. Near the isotropic point the magnetocrystalline anisotropy constant K_1 is almost zero resulting in a relatively low domain wall energy, $\gamma_w \approx (K_{\text{tot}})^{1/2}$ (where K_{tot} = total anisotropy energy), and nucleation field, $2K_{\text{tot}}/\sigma_s$ (cf. *Dunlop & Özdemir* 1997, Chapter 5). According to *Halgedahl & Jarrard* (1995), the net result is an increasing accessibility of equilibrium domain states and the addition of energetically favourable walls in some grains. Consequently, the increase in susceptibility likely reflects the nucleation of (additional) domain walls in hematite grains that initially had 'metastable' SD or PSD domain configurations. This also suggests that these so-called transdomain changes could contribute substantially to the observed loss of remanence during zero-field cycling through T_M , even for originally SD hematite particles.

Transdomain changes will have the biggest effect on susceptibility when a relatively large area of uniform magnetization becomes subdivided by an elastic domain wall. The low spontaneous magnetization of hematite makes that even large grains should have only a few broad domains because the equilibrium number and average width of lamellar domains are proportional to $(\sigma_s^2)^{1/2}$ and $(1/\sigma_s^2)^{1/2}$, respectively (cf. *Dunlop & Özdemir* 1997, Chapter 5). Indeed, *Halgedahl* (1995) observed only very few domains in $\sim 100 \mu\text{m}$ sized hematite platelets and reported typical PSD behaviour. This suggests that the coarsest grain-size fractions consist of an assemblage of relatively soft MD particles and metastable PSD particles with only a few large domains and possibly even a small portion of large metastable SD particles. The relation obtained between the grain size and the normalized susceptibility increase for sized fractions of LH2 hematite thus might reflect the increasing size of the metastable uniformly magnetized parts of the grains, rather than a fast increase in the number of domains as observed for ferrimagnetic substances like magnetite, Ti-magnetite and pyrrhotite (*Dunlop & Özdemir* 1997; *Figs 5.10 & 6.7*, and references therein). If the suggested mechanism of transdomain changes due to thermal cycling through T_M is correct, then the intercept of the fitted line drawn in *Fig. 3.5* gives the approximate value for the 'true' critical SD threshold size d_0 for LH2 hematite. Evidently, below a grain size of $\sim 1.5 \mu\text{m}$ walls cannot be nucleated, even in the more favourable conditions at the transition, so the χ_{lf} is unaffected. Above this size, however, nucleation can take place and becomes increasingly easy with increasing grain size (cf. *Boyd et al.* 1984). The determined value of $d_0 = \sim 1.5 \mu\text{m}$ is much lower than the value predicted by domain theory ($\sim 10\text{--}100 \mu\text{m}$), possibly due to crystal imperfections, but better agrees with the size range of $0.5\text{--}1 \mu\text{m}$ suggested for d_0 by *Dekkers & Linssen* (1989).

Repeated thermal cycling through T_M of the same sample yielded identical warming curves and χ_{lf} values back at room temperature. The reproducibility of the results suggests that only one final domain configuration, i.e. a so-called local energy minimum (LEM) state, is obtained by cycling. The AF stability of the new magnetic state is not very high;

30 mT is already sufficient to erase 90% of the χ_{lf} increase, whereas a complete recovery of the initial LEM state is achieved in AF demagnetizing fields up to ~ 100 mT. On the other hand, temperatures up to $\sim 680^\circ\text{C}$ are necessary before the new LEM state with the higher amount of walls returns to the initial LEM state. The $\chi_{lf} - T$ heating curves obtained for the new and the initial magnetic state are identical in shape almost up to T_c . This agrees with *Dunlop & Özdemir (1997, page 197)* who stated that only at temperatures close to the Curie point, the exchange energy drops to such an extent that energy barriers between LEM states can be taken by thermal energy alone. The fact that the initial magnetic state and the ones obtained after AF demagnetization and thermal cycling through the Curie point all yield identical values suggests that these states represent identical LEM states and that only thermal cycling may cause a different LEM state in hematite. The assumption that hematite has far fewer LEM states and that switching between them is much more difficult compared to ferrimagnetic substances, possibly results from the fact that even large grains of weakly magnetic hematite can only contain a small amount of domains.

MicroMag measurements

The MicroMag measurements show that 75–100 μm hematite particles can gain magnetization when they are thermally cycled through the Morin transition in non-saturating fields. Lower applied fields appear to induce higher magnetization increases upon cycling. Even more important is the observation that this gain in magnetization appears to be remanence. This is clearly demonstrated by the shift of the minor hysteresis loops obtained at different temperatures during cycling in a non-saturating 5 mT field. Moreover, for the hematite under investigation, the irreversible displacement of domains started already $\sim 70^\circ\text{C}$ before the actual Morin transition is reached.

The gain in magnetization caused by thermal cycling between 80°C and temperatures above the high-temperature onset of the Morin transition could be explained by the transdomain mechanism described before. In this case both the metastable SD and PSD fraction of the hematite grains could be responsible for the observed behaviour. This explanation, however, is not likely. As mentioned, domain structure observations on hematites report a decrease rather than an increase in the number of domains upon cooling in the vicinity of the Morin transition. This phenomenon can possibly be explained as follows. On approaching hematite's isotropic point, the vanishing of K_1 will result in a considerable broadening of the domain walls because wall width is proportional to $K_1^{-1/2}$ (cf. *Dunlop & Özdemir 1997, Chapter 5*). *Xu & Merrill (1989)* and *Moskowitz (1993)* showed that broad walls are less effectively pinned by localized defects and eventually escape. Domain wall thickness also varies with temperature but this probably is a less important factor in the temperature range mentioned. Consequently, a non-saturating field that is not sufficiently strong to overcome a certain energy barrier, i.e. to move a particular domain wall, may surmount the decreasing energy barrier on cooling, resulting in the displacement of a relatively loosely pinned domain wall. Consequently, more domains can become aligned with the field. Evidently, the unpinned or vanished domain walls do not return to their initial position on rewarming in a non-saturating field.

If this is the correct mechanism then the metastable SD fractions of the hematite grains could not take part in this mechanism, simply because they do not contain a domain wall.

On passing through the isotropic point, all or at least the greater part of the most rigid domain walls will now become unpinned due to the switch of the 'easy' axis. On warming back, instantly a number of broad domain walls will nucleate. The considerable increase in magnetization compared to the situation before cycling must be caused by distinct domain reorganization. In our opinion, a substantial part or even the total increase compared to the magnetization achieved just before the actual Morin transition is caused by the nucleation of (additional) domain walls in formerly metastable SD and/or PSD grains. A minor additional increase in magnetization is achieved on further warming. It might be caused by the decreasing wall thickness and some repositioning of the domain walls on energetically more favourable positions. Another explanation may be that some tiny nuclei of walls were already formed instantly at the Morin transition but could only escape from the nucleation site and traverse the particle at somewhat higher temperatures (*cf. Boyd et al. 1984*). Whatever the exact reason may be, fact is that the behaviour becomes irreversible on subsequent cooling between +40°C and the high-temperature on-set of the Morin transition. Cycling above the break in slope at +40°C, however, yields reversible cooling and warming behaviour.

Which particular role the characteristic break in slope at +40°C plays in the whole process is not clear at present. It could represent a change in exchange energy or some sort of critical point below which K_1 becomes sufficiently low to be no longer the most important anisotropy constant. Another suggestion may be that the canting angle of the atomic spins slightly changes in the vicinity of the isotropic point. No explanation is found in literature. A similar break in slope, however, is observed in the σ_3 - T curves obtained by *Néel & Pauthenet (1954)*.

3.5.2 Possible paleomagnetic implications

Large (>1 μm) black hematite particles (specularite) are often believed to carry a stable primary DRM or CRM in red sediments, whereas the fine-grained red pigment carries a secondary CRM. Our LT experiments suggest that the interpretation of remanences residing in specularite in particular, should be done with some caution, especially in areas of high altitude or latitude. Variations in Earth's surface temperature might possibly induce secondary remanence components in these large hematite grains which may partially or totally overprint the primary remanence. Moreover, our experiments also seem to indicate that separation of an original remanence and the remanence induced by cycling through the Morin transition will be difficult to achieve by means of standard thermal demagnetization. However, stepwise thermal demagnetization in combination with an initial AF demagnetizing step of a few tens of mT might solve this problem; 95% of the χ_{lf} increase obtained on cycling through T_M was already neutralized in a 50 mT AF field.

Necessary conditions for the induction of such a secondary remanence are that the hematite grains must at least be >1.5 μm and that they exhibit a well-pronounced Morin transition with its high-temperature onset in reach of (extreme) Earth's surface

temperatures; i.e. not to far below 0°C. In-situ formed specularite often fulfils these conditions because it usually consists of relatively pure platy-developed particles. Detrital specularite, on the other hand, often are Ti-substituted because of their high-temperature origin (e.g. Dôme de Barrot red beds) and already small amounts of Ti successfully shift the Morin transition to lower temperatures.

Although complete passing of the Morin transition on LT cycling is required for relatively large 'metastable' SD grains, thermal cycling in the vicinity of the Morin transition may already be sufficient to induce a secondary remanence in PSD and MD grains. It is, however, realized that the in-field LT runs were recorded in magnetic fields many times that of the Earth's magnetic field, and our experimental results may not be projected unambiguously to the natural situation. On the other hand, $\chi_{if} - T$ runs in zero-field did also show the susceptibility increase, and the saturation remanence did lose part of its intensity on cooling in zero field before the actual high-temperature onset of the Morin transition was reached.

We plan to test these suggestions on a set of artificial samples with a DRM carried by hematite particles. The samples will be thermally cycled through the Morin transition in various magnetic fields with a direction perpendicular to the original DRM. Afterwards the samples will be AF and thermally demagnetized.

3.6 Conclusions

The low-field susceptibility of large ($>1.5 \mu\text{m}$) hematite particles can be increased by low-temperature cycling through their Morin transition. We suggest that transdomain changes are responsible for this irreversible behaviour. The nucleation of additional domain walls in formerly 'metastable' SD and PSD grains is triggered on rewarming through the isotropic point when the crystalline anisotropy and thus the nucleation energy is relatively low. The new LEM state with a greater number of domains can only be obtained by cycling through the isotropic point; AF demagnetization and high-temperature thermal cycling recover the initial LEM state. A 'true' critical SD threshold size of $\sim 1.5 \mu\text{m}$ is obtained for a well-crystalline platy hematite. Below this grain size walls cannot be nucleated, even in the more favourable conditions at the transition. Because of the same mechanism, a new remanence component can be induced in large SD and PSD hematite grains on cycling through the Morin transition in non-saturating fields, at least for field strengths as low as 5 mT. Thermal cycling in the vicinity of T_M achieved already irreversibly changes in the domain configuration of PSD and MD hematite grains when cycling was done in a 5 mT field. Consequently, paleomagnetic results obtained from red beds in which the remanence is dominantly carried by low-temperature specularite exhibiting a well-pronounced Morin transition with a high-temperature onset near -10°C must be regarded with some caution, the more so as it seems to be difficult to separate the original and the cycling-induced remanences by standard thermal demagnetization. A procedure with an initial AF demagnetizing step of a few tens of mT is recommended for cleaning the mentioned red bed varieties.

ACKNOWLEDGEMENTS

We gratefully acknowledge the assistance given by *Adry van Velzen* with the low-temperature measurements on the MicroMag. *Eduard Petrovský* kindly made available a high purity hematite rock sample of the Kadaň hydrothermal ore deposit. This work was conducted under the programme of the Dutch national research school, the Vening Meinesz Research School of Geodynamics (VMSG).

Chapter 4

Unusual thermomagnetic behaviour of hematites: neof ormation of a highly magnetic spinel phase on heating in air

Cor B. de Boer and Mark J. Dekkers

Paleomagnetic Laboratory 'Fort Hoofddijk', Utrecht University, Faculty of Earth Sciences, Budapestlaan 17, 3584 CD Utrecht, the Netherlands. E-mail: cdeboer@geo.uu.nl

Submitted to Geophys. J. Int.

SUMMARY

The formation of traces of a magnetic phase with a Curie point of 470–475°C is detected during standard thermomagnetic analysis of various hematite types without significant isomorphous substitution. Using heating and cooling rates of 10°/min, the formation temperature can be 400°C for synthetic hematite samples, whereas higher temperatures, 700 to 800°C, are required for natural samples. The new phase appears to be persistent to prolonged heating at 1000°C. It appears to form thin epitaxial outgrowths preferentially on (0001) planes of hematite, and has a cubic spinel structure with a unit cell length $a = 0.0835 \pm 0.0005$ nm similar to pure maghemite. This suggests that the reverse of the $\gamma\text{-Fe}_2\text{O}_3 \rightarrow \alpha\text{-Fe}_2\text{O}_3$ transformation can occur under appropriate conditions on certain specific substrates. The relatively low T_C of this specific maghemite variety suggests that the vacancy (and/or cation) ordering over the magnetic sublattices is different in thin epitaxial outgrowth compared to distinct particles, at least when the parent phase is hematite. In accordance with *Takei & Chiba (1966)*, who also reported on a pure maghemite variety with identical T_C , a cation-deficient spinel structure with part of the vacancies on tetrahedral sites is adopted. A mechanism in which the thermally activated release of structurally bound water triggers the formation of maghemite traces on the surface of hematite (0001) planes is put forward. The formation of traces of this highly magnetic mineral during routine stepwise thermal demagnetization or during annealing hematite at high temperatures may seriously affect the NRM measurements or may be erroneously be taken as hematite's defect moment.

Key words: *hematite, maghemite, thermomagnetic analysis, rock magnetism.*

4.1 Introduction

It is generally accepted that under oxidizing conditions and ambient pressure, hematite ($\alpha\text{-Fe}_2\text{O}_3$), the hexagonal polymorph of ferric oxide, is thermodynamically the most stable of all naturally occurring pure iron oxide phases over a broad temperature range. A dissociation temperature in an air atmosphere of $\sim 1450^\circ\text{C}$ is commonly quoted for hematite (cf. Zdujic *et al.* 1998). Its melting point is ca. 1565°C (cf. Morrish 1994). The $\alpha\text{-Fe}_2\text{O}_3$ phase diagram at 1 atm suggests 1000°C as the lowest temperature at which local reduction in air can occur (cf. Dunlop 1971). Gardner *et al.* (1963) measured the electrical conductivity of hematites and reported that molecular oxygen loss, leading to the formation of metal excess, occurred upon firing stoichiometric $\alpha\text{-Fe}_2\text{O}_3$ in air above 1000°C . Below about 1000°C , however, no oxygen loss was detected. Indeed, beside minor structural improvements and possible grain-size and shape changes due to sintering, generally no phase alterations are reported after annealing pure hematites at high temperatures ($900\text{--}1100^\circ\text{C}$) in air; a procedure often used in rock-magnetic studies to improve the crystallinity of low-temperature synthesized hematites and to anneal out the defect moment introduced in freshly crushed hematite particles (e.g. Dunlop 1971; Bucur 1978; Fysh & Clark 1982).

Although being metastable, the other common iron oxide forms can usually persist for long time at normal subaerial conditions (even on a geological time scale), because of sluggish kinetics. The oxidation rate of the Fe^{2+} containing iron oxides (magnetite, Fe_3O_4 , and the cation-deficient spinels of the $\text{Fe}_{1-z}^{2+}\text{Fe}_{2+z}^{3+}\text{O}_{4+0.5z}$ series with $0 < z < 1$), however, increases with temperature. In addition, the inversion of the cubic $\gamma\text{-Fe}_2\text{O}_3$ polymorph, maghemite, to the stable hexagonal form is a thermally activated process. Consequently, laboratory heating in air of mineral concentrates of all known naturally occurring pure iron oxides (and thus also of all pure iron sulfides and oxyhydroxides) eventually results in the formation of stable $\alpha\text{-Fe}_2\text{O}_3$.

On a laboratory time scale, in the dry state and at ambient pressure, metastable $\gamma\text{-Fe}_2\text{O}_3$ typically inverts to stable $\alpha\text{-Fe}_2\text{O}_3$ around 350°C . Reported inversion temperatures, however, are highly variable and may range from ~ 250 up to 900°C (e.g. Bernal *et al.* 1957; Wilson 1961; Kachi *et al.* 1963; Özdemir & Banerjee 1984; Özdemir & Dunlop 1988; Özdemir 1990; Dunlop & Özdemir 1997), depending on the origin of the maghemite, its crystallinity, impurity content, degree of residual Fe^{2+} , and morphological properties such as particle size and shape.

In general, the crystallographical $\gamma\text{-Fe}_2\text{O}_3 \rightarrow \alpha\text{-Fe}_2\text{O}_3$ transformation has been held to be irreversible. Meillon *et al.* (1995), however, reported the existence of a direct phase transformation from hematite to maghemite by the mechanical action of prolonged (>25 days) wet grinding in ethanol. The grinding process was characterized by the presence of a shearing component exerted on the $\alpha\text{-Fe}_2\text{O}_3$ particles. According to the authors, the necessary change in oxygen framework (hexagonal close-packing to cubic close-packing) was accomplished by a periodic sequence shear, where two oxygen planes move together with the same shearing stress. X-ray diffraction patterns obtained on the resulting $\gamma\text{-Fe}_2\text{O}_3$ phase showed superstructure reflections diagnostic for long-range

ordering of vacancies over octahedral interstices (see Section 4.2). The inversion temperature lies around 425°C.

Finch & Sinha (1957) detected the $\alpha \rightarrow \gamma$ transformation under conditions somewhat more realistic from a rock-magnetic point of view. These authors observed in an electron-diffraction study the formation of epitaxial maghemite outgrowths on pure hematite particles on heating above $\sim 700^\circ\text{C}$. According to the authors, the $\gamma\text{-Fe}_2\text{O}_3$ form was created via an intermediate metastable hematite-like phase (named $\beta\text{-Fe}_2\text{O}_3$ by the authors) previously formed at 500°C . This rare β -phase should be characterized by additional reflections which are forbidden for the space group of hematite. It has, however, an oxygen-ion framework and unit cell identical to $\alpha\text{-Fe}_2\text{O}_3$, but probably differs from normal hematite by having some cations on tetrahedral interstices similar to the $\beta\text{-Al}_2\text{O}_3$ (bixbyite) structure as observed by *Bragg et al.* (1931) and *Hendricks & Pauling* (1926). *Finch & Sinha* (1957) showed that the proposed structure of $\beta\text{-Fe}_2\text{O}_3$ results in a ferrimagnetic phase. *Blackman & Kaye* (1960), however, seriously questioned the existence of such an intermediate phase. The $\gamma\text{-Fe}_2\text{O}_3$ phase formed during the experiments of *Finch & Sinha* (1957) showed an unusual high thermal stability as it persisted even prolonged heating at 900°C . Their results showed that the $\alpha\text{-Fe}_2\text{O}_3$ to $\gamma\text{-Fe}_2\text{O}_3$ transformation may occur under suitable conditions, but an appropriate mechanism to explain the unusual phase transition could not be revealed. Moreover, the vacancy distribution (see Section 4.2) and magnetic properties of this maghemite type were not determined.

From a paleomagnetic point of view, the possible formation of even a small amount of these ferrimagnetic phases is a matter of serious concern in studies of hematite-bearing sediments and rocks. The formation of the β -phase during a standard thermal demagnetization treatment before reaching the crucial unblocking temperature segment of NRM's residing in hematite could be an important source of noise, hampering the determination of the characteristic remanent magnetization carried by hematite. Furthermore, the magnetic properties of minute traces of the γ -phase developed during annealing hematite at high temperatures may erroneously be described to the defect moment of hematite. To this end, a description is needed of those hematite types which are susceptible to the $\alpha \rightarrow \gamma$ transition, together with a magnetic characterization of the reaction products, in order to recognize the occurrence of the process.

We measured the thermomagnetic behaviour of various hematite types with basically no isomorphous substitution, to induce the unusual $\alpha \rightarrow \gamma$ transformation and to get a better insight in the appropriate conditions necessary to cause this phase transition. The technique used, i.e. the monitoring of the (saturation) magnetization of a sample as a function of temperature, is very sensitive to heating-induced chemical and/or structural changes especially if magnetic changes from a weak antiferromagnetic phase ($\alpha\text{-Fe}_2\text{O}_3$) to strong ferrimagnetic phases ($\beta\text{-Fe}_2\text{O}_3$ and $\gamma\text{-Fe}_2\text{O}_3$) are involved. The detection limit of the $M_{(s)}$ monitoring technique is much lower than other structure-sensitive analyzing techniques; the creation of minute traces, at least $\sim 0.05\%$ for $\gamma\text{-Fe}_2\text{O}_3$, are readily reflected in irreversible thermomagnetic behaviour. Moreover, the specific Curie temperature of the newly created phase may reveal important information about the vacancy ordering over the octahedral and tetrahedral lattice interstices.

4.2 Crystal structure and rock-magnetic background

4.2.1 Hematite

Hematite crystallizes in the corundum structure which can be indexed in the rhombohedral as well as in the hexagonal system (e.g. *Blake et al.* 1966; *Lindsley* 1976a). Usually quoted hexagonal unit cell parameters are $a_{hex} = 0.50340$ nm and $c_{hex} = 1.3752$ nm (cf. *Schwertmann & Cornell* 1991). The space group is $R\bar{3}c$. In the corundum structure, the oxygen layers are stacked in an AB-sequence parallel to the (0001) basal plane forming an almost ideal hexagonal-close-packed (*hcp*) lattice. The O^{2-} layers alternate with layers of octahedrally coordinated Fe^{3+} cations. In hematite only two-thirds of the available cation sites are occupied because of charge balance considerations (note that vacant sites are implicit in the stoichiometry, and should not be confused with vacancies). The iron atoms are arranged regularly with two filled sites being followed by one vacant site in the (0001) plane thereby forming sixfold rings (cf. *Cornell & Schwertmann* 1996). The close-packed alternating cation layers are arranged in an ABC-sequence, that is planes of Fe atoms are shifted by one octahedral site in each successive layer along (0001).

The room-temperature spin configuration of hematite is basically antiferromagnetic. The magnetic moments of the Fe^{3+} ions lie in the basal (0001) plane orthogonal to the *c*-axis (e.g. *Shull et al.* 1951). Within these (0001) planes the magnetic spins are coupled parallel but antiparallel coupling exists between adjacent layers of cations. The cation arrangement in adjacent layers is equivalent so that an overall antiferromagnetic structure results. Hematite, however, possesses a weak ferromagnetic moment due to a slight canting of the atomic spins out of exact antiparallelism (*Dzyaloshinsky* 1958). This so-called canted moment lies in the basal plane perpendicular to the sublattice magnetizations (*Shull et al.* 1951), and is generally reported to be $\sim 0.3\text{--}0.4$ Am² kg⁻¹ (e.g. *Haigh* 1957; *Flanders & Remeika* 1965). In addition, hematite may have another weak magnetic moment referred to as the 'defect moment'. This more variable moment is thought to reside, at least partly, in an ordered structure of imperfections or impurities in the crystal lattice. Because of its origin, part of this moment is susceptible to heat-treatment.

The strong magnetic interactions between Fe-atoms on alternating sublattices are reflected in hematite's high magnetic disordering temperature. The Néel temperature (T_N) of pure hematite is commonly reported as $\sim 680^\circ\text{C} \pm 5^\circ\text{C}$ (e.g. *Morrish* 1994 and references therein). It is generally assumed that the canting of the sublattices and the antiferromagnetic ordering within the sublattice vanish simultaneously. The shape of the thermomagnetic curves for different types of hematite are described in *De Boer & Dekkers* (1998).

4.2.2 Maghemite

Maghemite has the same chemical composition as hematite but like magnetite it crystallizes in the spinel structure, which generally has a $Fd\bar{3}m$ space group. In fact, maghemite can be considered as a non-stoichiometric defect magnetite with incomplete spinel cation site occupancy (Waychunas 1991). A cubic unit cell parameter of $a \approx 0.833\text{--}0.835$ nm is usually quoted for maghemite, compared to $a = 0.8396$ nm for magnetite (Lindsley 1976a).

The spinel structure consists of a framework of cubic close-packed (*ccp*) anion layers (cf. O'Reilly 1984). The O^{2-} layers may be seen forming (111) planes of a face-centered cubic (*fcc*) lattice stacked orthogonal to the cube diagonal [111] direction in an ABC-sequence. The oxygen framework encloses octahedral (sixfold coordination) as well as slightly smaller tetrahedral (fourfold coordination) interstices for cations, often referred to as A and B positions respectively. In a spinel structure, normally 1/3 of the occupied interstices are tetrahedrally coordinated with oxygen and 2/3 are octahedrally coordinated. In the *cation-deficient* spinel structure of maghemite, however, only 5/6 of the total available positions are filled by Fe^{3+} , the rest are vacant. The chemical formula for maghemite written as spinel thus is $Fe_{2.67}\square_{0.33}O_4$, where \square denotes the vacancies.

The arrangement of the vacancies in the spinel-like lattice of maghemite appears to be very variable, and is still somewhat controversial. The exact positioning of the vacancies determines the final symmetry of the substance. Hence, for structure-dependent physical properties, what is called 'maghemite' actually is indeed various different phases, characterized by a different positioning of the vacancies (Pecharrómán *et al.* 1995; Eggleton *et al.* 1988). The vacancies could occur in either octahedral sites or mixed over both tetrahedral and octahedral sites. The presence of a stable maghemite with only tetrahedral vacancies has been discounted by Lindsley (1976a & b).

Most experimental evidence supports the tendency for the vacancies to occupy octahedral sites only (e.g. Armstrong *et al.* 1966; Haneda & Morrish 1977a; Greaves 1983; Boudeulle *et al.* 1983; Coey 1987; Collyer *et al.* 1988). Three different varieties of maghemite with completely filled tetrahedral spinel sites are yet generally accepted. The structures are characterized by a different degree of long-range crystal order of the vacancies (Braun 1952; Van Oosterhout & Rooijmans 1958; Haneda & Morrish 1977a; Smith 1979; Greaves 1983; Boudeulle *et al.* 1983; Collyer *et al.* 1988; Eggleton *et al.* 1988; Pecharrómán *et al.* 1995). The atomic coordinates of these three idealized crystal structures are summarized by Pecharrómán *et al.* (1995; Table 1, page 22). The maghemite varieties characterized by a totally random, a partly ordered and a totally ordered vacancy distribution have a face-centered cubic, a primitive cubic and a tetragonal structure, respectively. The respective space groups are $Fd\bar{3}m$, $P4_132$ and $P4_32_12$. Vacancy ordering can be particularly evident in X-ray diffraction, where maghemites with vacancy ordering show typical superstructure lines (extra reflections) that are inconsistent with the face-centered cubic system, and thus can be used to distinguish between maghemite and magnetite.

Takei & Chiba (1966) concluded from their high saturation magnetization value obtained on epitaxially-grown single crystals of maghemite (MgO substrate) that part of the vacancies should occupy tetrahedral interstices. *Weber & Hafner* (1971), *Annersten & Hafner* (1973) and *Ramdani et al.* (1987) found also some indication that part of the vacancies could be on A sites as well.

The magnetic structure of $\gamma\text{-Fe}_2\text{O}_3$ basically consists of an alternation of two opposed but unequal magnetic sublattices, i.e. the ferrimagnetic structure (*Néel* 1948). The atomic Fe^{3+} moments within each sublattice are coupled parallel, whereas those of the A and B sublattices are coupled antiparallel through an intervening O^{2-} anion. Because of the non-equivalence of the sublattice magnetizations a strong net ferrimagnetic moment results in maghemite. For the most common maghemite varieties with only octahedral vacancies, an average excess of $\frac{1}{2}\text{Fe}^{3+}$ exists on the B sublattice per formula unit (*pfu*) $\gamma\text{-Fe}_2\text{O}_3$. This corresponds to a net magnetic moment *pfu* of $2.5\mu_{\text{B}}$, implying a theoretical saturation magnetization of $\sim 87 \text{ Am}^2 \text{ kg}^{-1}$, adjusted to zero thermal energy at 0 K. A typical room temperature value of $74 \text{ Am}^2 \text{ kg}^{-1}$ is often found for this maghemite type (e.g. *Johnson & Merrill* 1974; *Bate* 1980; *Goss* 1988; *Özdemir & Dunlop* 1988; *Özdemir* 1990; *Moskowitz* 1993). The presence of part of the vacancies on tetrahedral interstices would result in a higher net magnetic moment. *Takei & Chiba* (1966) obtained a net magnetic moment *pfu* Fe_2O_3 of $2.9\mu_{\text{B}}$ for their synthetic maghemite variety, which would imply that nearly 20% of the total amount of vacancies occupy tetrahedral interstices.

Direct measuring of the Curie point of pure maghemite is often not possible, because of its inversion to hematite at lower temperatures, i.e. $T_{\text{inv}} < T_{\text{C}}$. Determination of T_{C} by indirect methods or by calculations yielded values between ~ 590 and 770°C (e.g. *Michel & Chaudron* 1935; *Maxwell et al.* 1949; *Aharoni et al.* 1962; *Frölich & Vollstädt* 1967; *O'Reilly* 1968; *Readmann & O'Reilly* 1972; *Da Costa et al.* 1995). The few direct measurements reported in literature indicate a T_{C} around $640\text{--}645^\circ\text{C}$ for tetragonally ordered $\gamma\text{-Fe}_2\text{O}_3$ (*Özdemir & Banerjee* 1984; *Heider & Dunlop* 1987; *Van Oorschot & Dekkers* (1999), see also *Fig. 5.1b* of this thesis). However, the effect of different ordering of vacancies or cations over the two magnetic sublattices is not yet known exactly. *Takei & Chiba* (1966), for instance, measured a T_{C} of 470°C for their pure maghemite with suggested tetrahedral vacancies.

4.2.3 Crystallographic relations between $\gamma\text{-Fe}_2\text{O}_3$ and $\alpha\text{-Fe}_2\text{O}_3$

The transformation of $\gamma\text{-Fe}_2\text{O}_3$ to $\alpha\text{-Fe}_2\text{O}_3$ is considered to be topotactic, occurring by restacking of close-packed oxygen ion layers (*ccp* to *hcp*) accompanied by displacement of interstitial ferric ions rather than by wholesale recrystallization (e.g. *Bernal et al.* 1957, 1959; *Kachi et al.* 1963). Plate-like hematite crystals grow with its (0001) planes in the (111) planes of the maghemite, and with the [111] and [110] axes of maghemite corresponding to the [0001] and $[10\bar{1}0]$ axes of hematite, respectively (*cf. Cornell & Schwertmann* 1996).

4.3 Samples and equipment

4.3.1 Samples

The hematites used in this contribution comprise six natural samples and three samples of synthetic origin. The natural samples were upgraded from various raw hematite ores or macroscopic hematite crystals (museum pieces). They were all used in previous rock-magnetic studies. *Dankers* (1978, 1981) studied the hematite samples labeled LH2 (Kimberley, South Africa) and LH3 (Framont, France), while those labeled LH4 (origin unknown), LH6 (Gellivara, Lapland) and LHC (origin unknown) were investigated by *Hartstra* (1982). The hematite material from the Kadaň locality in the Czech republic was previously studied by *Hejda et al.* (1992) and *Petrovský et al.* (1994, 1996). The low-temperature behaviour of these natural samples was described in *De Boer et al.* (1999, Chapter 3 of this thesis). *Table 4.1* shows the chemical composition of these hematites as determined by Microprobe analysis; no significant isomorphous substitution was detected.

Table 4.1: Chemical composition of the natural hematite samples used in this study as determined by ⁽¹⁾*Dankers* (1978, 1981), ⁽²⁾*Hartstra* (1982) and ⁽³⁾*Hejda et al.* (1992) using Microprobe analysis. <d.l. = lower than detection limit; nd = not determined.

	LH2 ⁽¹⁾	LH3 ⁽¹⁾	LH4 ⁽²⁾	LH6 ⁽²⁾	LHC ⁽²⁾	Kadaň ⁽³⁾
Fe ₂ O ₃ (%)	98.2	98.2	97.9	98.1	99.9	~ 99
Al ₂ O ₃ (%)	0.1	0.3	0.6	0.7	0.5	< 0.1
TiO ₂ (%)	< d.l.	< d.l.	0.1	0.5	< d.l.	< 0.1
Cr ₂ O ₃ (%)	< d.l.	< d.l.	0.3	0.2	< d.l.	< 0.1
SiO ₂ (%)	0.4	0.4	0.9	< d.l.	0.1	< 0.1
V ₂ O ₃ (%)	nd	nd	0.7	0.5	< d.l.	< 0.1
MnO (%)	< d.l.	< d.l.	0.1	0.2	0.1	< 0.1
MgO (%)	< d.l.	< d.l.	nd	nd	nd	< 0.1

For our investigations, we used the mineral concentrates made by *Dankers* and *Hartstra*, whereas new grain size fractions of the Kadaň hematite were prepared. The high purity hematite concentrates of *Dankers* and *Hartstra* were separated by a procedure which briefly comprises of crushing the raw ore in a copper mortar followed by further separation according to hematite's specific weight and magnetic properties by means of a heavy liquid overflow-centrifuge and a Frantz isodynamic magnetic separator, respectively. We obtained sized fractions of the Kadaň hematite by crushing crystal fragments in a copper mortar followed by sieving. The fragments were cut from macroscopic acicular crystals (~10 cm long) using a small diamond drill. Only fresh pure hematite from the inner part of the needles was selected. Except for traces of quartz, no

minerals other than hematite were detected in the mineral concentrates using X-ray diffraction analysis and optical microscopy. Examples of X-ray diffraction analyses are shown in Figs 4.3(a & c) for Kadaň and LH3 hematite, respectively. Traces (<0.05 % by weight) of spinel-type magnetic contaminants were detected in grain size fractions of some of the hematite samples by means of magnetic measurements (cf. De Boer & Dekkers 1998, Chapter 2 of this thesis).

The synthetic hematite samples were prepared either by transformation of (2-line) ferrihydrite in aqueous solution and by thermal decomposition of either a synthetic goethite or of commercial hydrated ferric nitrate salts (analytical grade, Merck). For the hematite synthesis from solution a procedure described by Schwertmann & Cornell (1991; Method 4 page 103) was used. In brief, several well-cleaned glass bottles filled with ~250 ml of a 0.1 molar ferric nitrate solution were heated at 97°C for 48 hours in a water bath. In this way hematite is precipitated via a ferrihydrite intermediate stage; i.e. a poorly-ordered iron oxyhydroxide. After termination of the synthesis the samples were washed salt-free, centrifuged and the excess solution was removed before the material was dried in a stove for 1 day at ca. 40°C. A sample, previously (~1 year) made under identical conditions by Thomas Pick and stored in the mother solution was also available for thermomagnetic analysis. The synthesis product is a dark reddish-brown powder consisting primarily of hematite, although some goethite and ferrihydrite traces are usually present. The major part of the hematite occurs in anhedral crystals being smaller than ~0.1 µm, although also some coarser (0.1 to 10 µm) hexagonal crystals may be present (cf. Schwertmann & Cornell 1991). Stocking & Tauxe (1990) synthesized α -Fe₂O₃ under similar conditions and describe similar features of the hematite.

The hematite synthesis by dehydroxylation of a goethite precursor (~35 mg) was done in air in the open-ended furnace of the Curie balance by repeated heating and cooling cycles to increasingly higher temperatures using heating and cooling rates between 1 and 10 °C min⁻¹. In this way, the thermal decomposition of the goethite could be followed and the creation of a possible ferrimagnetic phase could be detected instantly. The synthetic goethite used was prepared and described by Dekkers & Rochette (1992).

The other synthetic α -Fe₂O₃ sample was prepared by heating analytical grade iron(III)-nitrate [Fe(NO₃)₃ · 9H₂O] to 800°C in a Curie balance and in a bigger furnace as well, using ~50 mg and 10 g starting material, respectively. The synthesis in the Curie balance was either done by one thermal cycle to 800°C or by repeated cycles to increasingly higher temperatures using heating and cooling rates of 10°C min⁻¹. In the bigger furnace, the Fe nitrate salt was heated with 10°C min⁻¹ to ~350°C. The sample was held at this temperature for almost 30 minutes. During this time the furnace was opened to let the yellowish-brown gas (NO₂) escape. Some amount of the brownish-red material formed was sampled before the other portion was heated to 800°C. Every 100° the furnace was opened for a short period allowing the possibly newly produced gas escape. Cooling was done in an uncontrolled way by just opening the furnace. The obtained material consists of fine-grained (<1 µm) dark-red particles and some grey-coloured clusters of fused hematite particles. Nininger & Schroerer (1978) also prepared hematite by thermal decomposition of ferric-nitrate salts. They found that the size of the particles was dependent on both the temperature and the duration of the heating. They obtained a

particle size of $500 \pm 30 \text{ \AA}$ for a sample heated at 347°C for 30 min. The low-temperature behaviour of the $\alpha\text{-Fe}_2\text{O}_3$ heated to 800°C in the big furnace was described in *De Boer et al.* (1999, Chapter 3 of this thesis).

4.3.2 Equipment used

Thermomagnetic analyses were performed in air using a modified horizontal translation Curie balance that makes use of a cycling field (*Mullender et al.* 1993). Previous measurements showed that the atmosphere inside the open-ended furnace unit stays oxidizing up to the highest possible temperature of 800°C . Step-scanned X-ray diffractograms were recorded with a Philips PW 1700 diffractometer using Cu-K α radiation and Si as internal standard. Thermogravimetric analysis, a method that measures the change in weight as a sample is heated with a specified rate, was performed in air. A Princeton alternating gradient magnetometer (MicroMag 2900) equipped with a helium flow-through cryostat was used to monitor low-temperature (room temperature to -230°C) cooling and warming runs of induced remanence (2 T), and to measure hysteresis loops at room temperature. Cooling and warming rates were $\sim 5^\circ\text{C min}^{-1}$.

4.4 Experimental results and discussion

4.4.1 Natural hematite samples

Thermomagnetic analyses

Figure 4.1(a-f) shows the thermomagnetic behaviour of various natural hematites. The four uppermost panels (a-d) illustrate behaviour commonly encountered for pure hematite. Samples LHC, LH2 and LH6 show behaviour characteristic of non-saturated, pure defect-poor hematite magnetically dominated by the canted moment (*cf. De Boer & Dekkers* 1998; Chapter 2). The gradual increase in magnetization observed during initial heating is caused by the decrease in coercivity allowing an increasing portion of the magnetic domains to become aligned with the field. Heating above the Curie point (700°C cycle) results in the typical irreversible block-shaped cooling curve which shape only depends on the temperature variation of the exchange energy. Heating to 800°C slightly improves the crystallinity as can be deduced from the small gain in magnetization compared to that after the 700°C cycle, but no creation of an additional magnetic phase is observed. The behaviour shown by LH4 hematite (*Fig. 4.1c*) is characteristic of $\alpha\text{-Fe}_2\text{O}_3$ rich in structural defects. On heating to 800°C the defects are progressively annealed out of the lattice resulting in the block-shaped curve typical for defect-poor hematite (*cf. De Boer & Dekkers* 1998). The removal of this specific type of internal defects obviously does not trigger the formation of a new magnetic phase. The break in slope at $\sim 100^\circ\text{C}$ is the high-temperature onset of the Morin-transition.

NATURAL HEMATITES

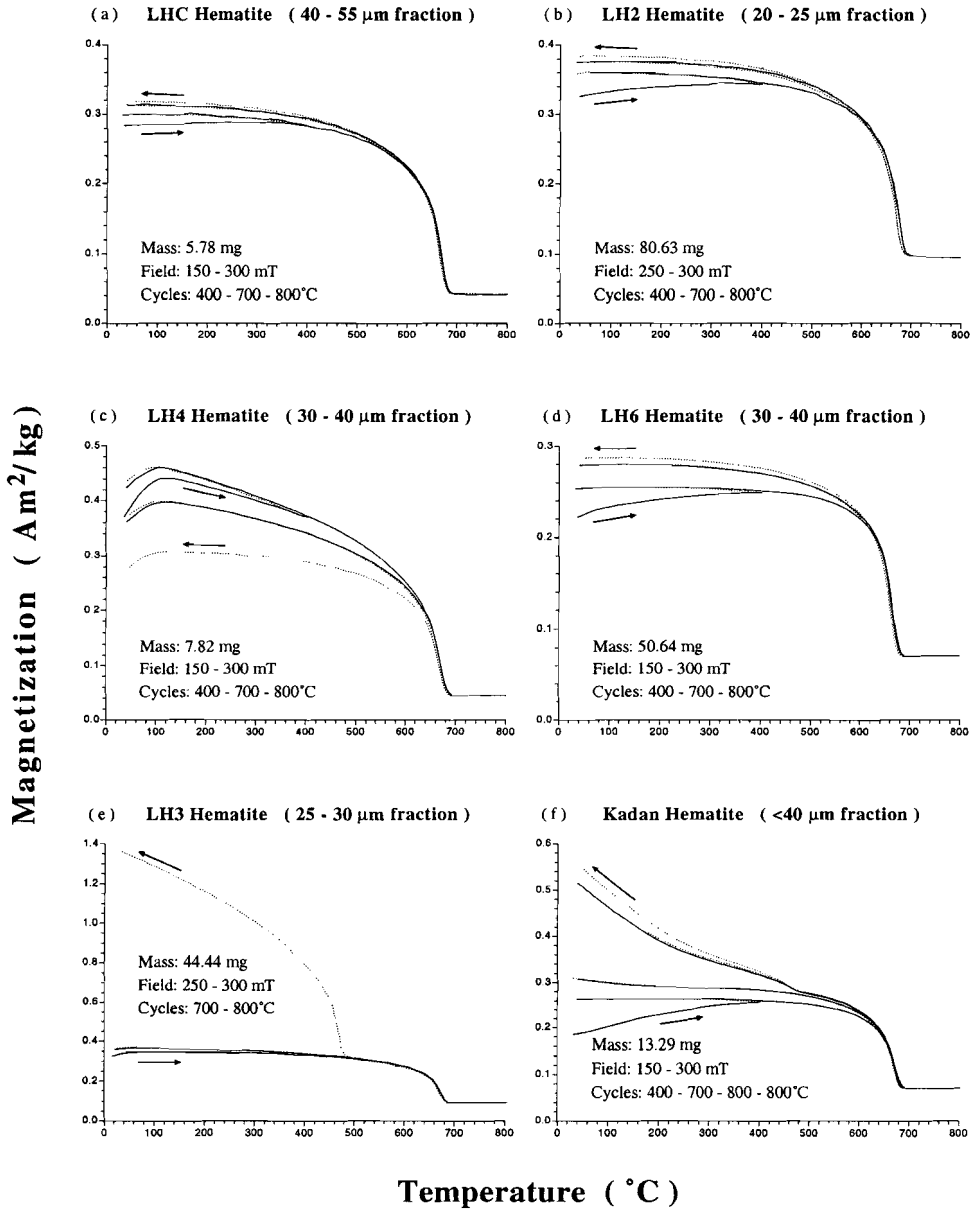


Figure 4.1 (left): Thermomagnetic behaviour of various natural hematite samples. Solid and dotted lines denote heating and cooling curves, respectively. Figs (a), (b) and (d) illustrate thermomagnetic behaviour typical of non-saturated defect-poor hematite magnetically dominated by the canted moment, whereas the behaviour shown in panel (c) is characteristic of a more defect-rich hematite whose defect moment becomes progressively reduced on heating. The specific break in slope at $\sim 100^\circ\text{C}$ represents the high-temperature onset of the Morin transition. Figs (e) and (f) show the formation of traces of a new magnetic phase from hematite after heating to $\sim 700\text{--}800^\circ\text{C}$. This new magnetic phase is characterized by a Curie temperature of $\sim 470\text{--}475^\circ\text{C}$.

In contrast, Figs 4.1(e & f), show thermomagnetic behaviour noticeably different from that described above. Both figures illustrate that the formation of a magnetic phase from hematite on heating is possible. At first, until cycling to $\sim 700^\circ\text{C}$, Kadaň and LH3 hematite show thermomagnetic behaviour similar to that observed for non-saturated, defect-poor hematite. Mass-specific magnetization values and Curie temperatures are typical of pure hematite. For Kadaň hematite, the small tail of increasing magnetization observed at the end of the cooling curve of the 700°C cycle, however, is a first indication for the development of a new magnetic phase though a distinct Curie temperature is not yet visible. On cooling from 800°C , the thermomagnetic curves of both samples, however, clearly reveal the presence of an additional magnetic phase which is characterized by a magnetic ordering temperature of $\sim 470\text{--}475^\circ\text{C}$. No noticeable shift in Curie temperature of the hematite phase itself is observed.

For sample LH3, the part of the cooling curve representing the new magnetic phase is identical in shape to that usually observed for ferrimagnetic magnetite and maghemite (see Fig. 5.1 of this thesis). Furthermore, its specific shape suggests that the major part of the grain sizes of the new phase lie above the single-domain threshold size, whereas the exponential shape observed for the Kadaň sample suggests a high contribution of ultra-fine superparamagnetic particles. In addition, the differences in mass specific magnetization obtained after the 800°C cycle indicate that a considerably higher amount of the new magnetic phase is created from platy-developed LH3 hematite compared to acicular Kadaň hematite particles that are elongated in the c -direction. These findings suggest that the new magnetic phase is a spinel outgrowth preferentially forming on hematite basal (0001) planes. The fact that no magnetic phase is created from relatively large uncrushed ore chips of Kadaň hematite treated under identical conditions (*cf. Petrovský et al.* 1996) supports this suggestion; i.e. in this case simply not enough basal planes are available to grow the spinel phase on.

The observed behaviour may represent the crystallographic $\alpha \rightarrow \gamma$ transformation described by Finch & Sinha (1957). The Curie point of the new phase, however, does not concur with T_c ($\sim 640\text{--}645^\circ\text{C}$) reported for the most common maghemite type with octahedrally coordinated vacancies only. On the other hand, it is identical to the T_c reported by Takei & Chiba (1966) for an epitaxially grown maghemite type with a suggested portion ($\sim 20\%$) of its vacancies on tetrahedrally interstices.

Other possibilities to explain the T_c found are the presence of newly formed varieties of substituted magnetite or maghemite. If these phases are formed from hematite,

this would imply that certain foreign cations present in the hematite structure become incompatible on heating and are expelled from the lattice forming a spinel surface layer rich in these elements. Following the molecular-field approximation for ferrimagnetism, most impurity cations in the spinel lattice will cause a more or less linear decrease in T_c with increasing substitution. To get a T_c of 470°C, for instance, magnetite must be substituted with ~20 mole% Ti (e.g. *Readman & O'Reilly* 1972), whereas for maghemite a substitution of ~50% Ti (e.g. *Readman & O'Reilly* 1972) or ~20% Al (e.g. *Da Costa et al.* 1995) is needed. Other spinel phases with reported Curie points in the mentioned temperature range are CoFe_2O_4 (520°C), CuFe_2O_4 (455°C), MgFe_2O_4 (440°C) and MnFe_2O_4 (300°C) (e.g. *Smit & Wijn* 1959). In this view, it, however, is remarkable that the other hematite types with similar or even higher traces of foreign cations in their lattice do not show comparable behaviour. Moreover, it would be highly coincident that from both hematites a substituted spinel is created with exactly the same Curie point.

MicroMag measurements

The Kadaň sample was heated to temperatures above 800°C in a furnace different from the Curie balance, first to investigate its thermal stability and second to get a higher yield of the new magnetic phase necessary for a proper X-ray diffraction analysis. In this closed furnace, heating rates were similar to that in the Curie balance but cooling was done in an uncontrolled way by turning off the power supply. Cooling to room temperature commonly lasted for ~12 hours. The results of these heatings are shown in *Fig. 4.2*, together with additional magnetic measurements of the original material and material heated in the furnace at 600°C.

The hysteresis loop obtained for the original Kadaň hematite is typical of a high coercivity mineral. No trace of a low coercivity mineral was detected in this sample. The hysteresis loops measured on the heated material, however, clearly demonstrate the progressive development of a low-coercivity phase from the hematite sample with increasing temperature, i.e. the loops become increasingly wasp-waisted. The first traces of the new magnetic phase are now already detected after heating to 600°C probably because of the longer exposure to this temperature compared to the Curie balance measurements. The magnetic characteristics of the material being heated to temperatures above 800°C not only show that the new magnetic phase is persistent to these high temperatures but also that the formation process was not yet fully completed. Furthermore, the progressive change in shape of the thermomagnetic curves from concave for the material preheated at 600 to 900°C to convex for the material preheated at 1000°C, indicate an increase in grain size of the new magnetic phase. After the heating at 1000°C almost all of the material was attracted to a hand magnet indicating that we most likely are dealing with epitaxial outgrowings of the magnetic phase on the hematite parent rather than some isolated contamination.

KADAN HEMATITE

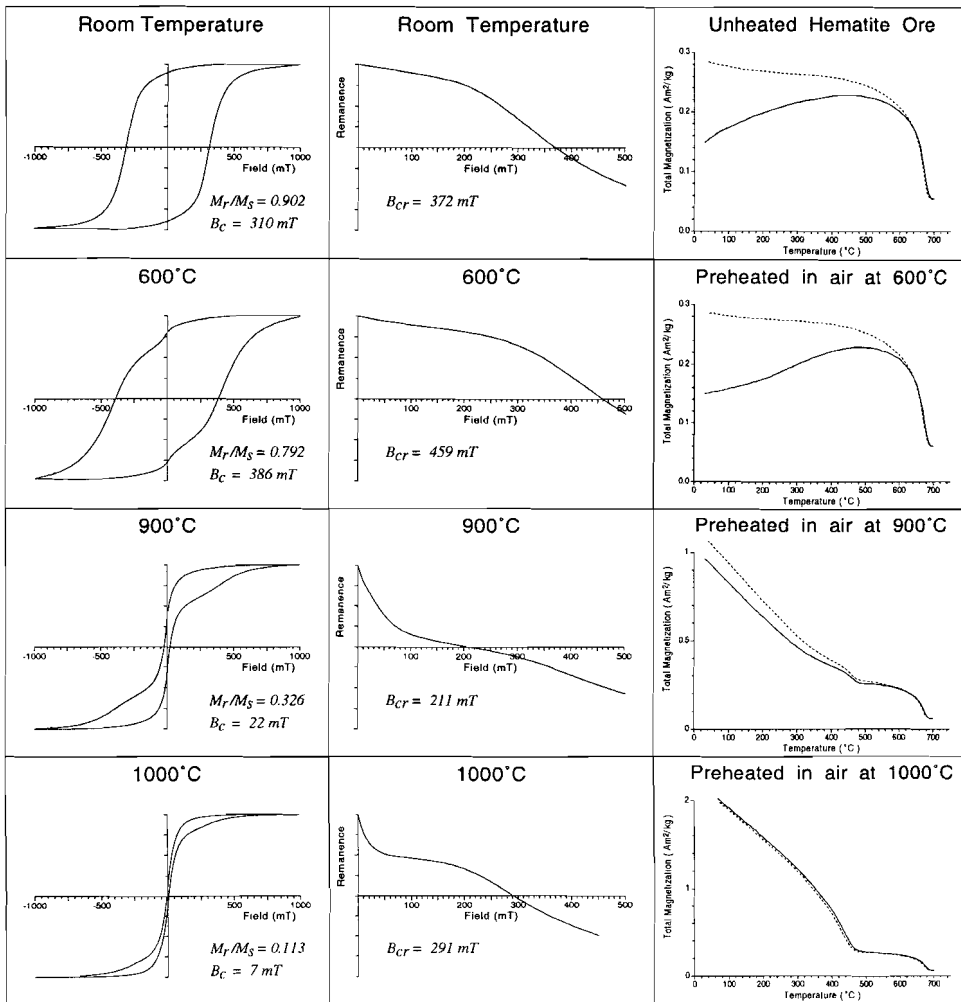


Figure 4.2: *MicroMag measurements at room temperature and thermomagnetic analysis of original Kadaň hematite and samples heated in a furnace to 600, 900 and 1000°C, clearly showing the progressive development of a highly magnetic low-coercivity phase from pure hematite with temperature. Hysteresis loops are slope corrected.*

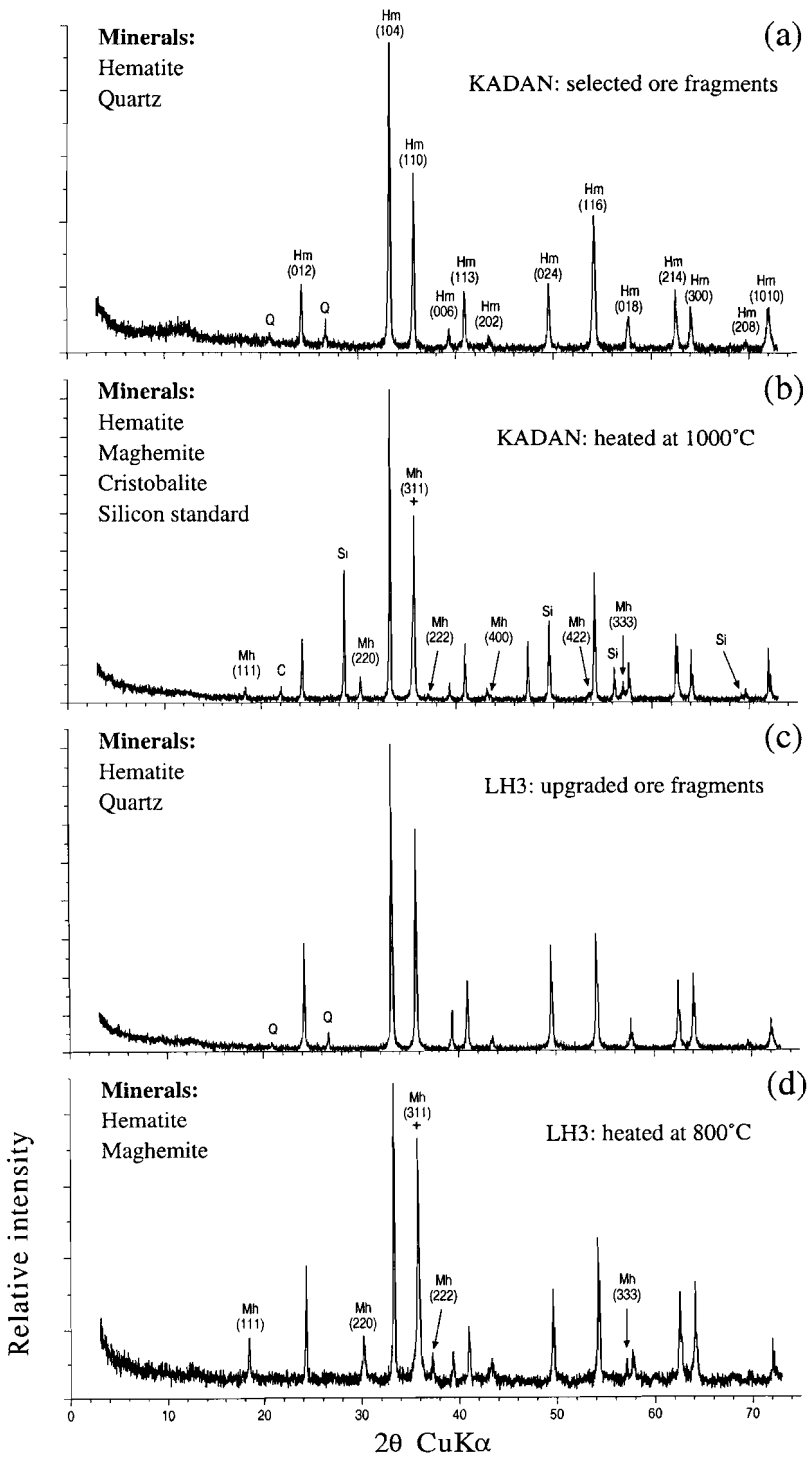
Figure 4.3 (right): X-ray diffraction patterns of (a) original Kadaň hematite and (c) original LH3 hematite and after heating the material to (b) 1000°C and (d) 800°C, respectively. The heated samples clearly show additional peaks belonging to the cubic spinel structure of maghemite. Reflections of hematite, maghemite, quartz, cristobalite and the silicon standard are denoted with Hm, Mh, Q, C and Si, respectively.

X-ray diffraction analysis

The X-ray diffraction patterns obtained for the original Kadaň (Fig. 4.3a) and LH3 (Fig. 4.3c) samples show beside strong hematite reflections only some minor peaks revealing the presence of traces of quartz. No other impurities were recognized. For both samples, the positions of the hematite peaks and their relative intensities concur well with those reported for pure α -Fe₂O₃. The diffractograms of heated Kadaň (Fig. 4.3b) and LH3 (Fig. 4.3d) samples clearly reveal additional reflections characteristic of a cubic spinel phase. The high relative intensities of the peaks representing the (111), (222) and (333) planes again strongly suggest that the spinel phase forms epitaxial outgrowths on the basal plane of hematite. Cubic unit cell dimensions found for the spinel phase grown on Kadaň and LH3 hematite both are $a = 0.8350.005$ nm. This value falls in the range commonly reported for pure maghemite, and it is also similar to the cell dimension of the maghemite described by *Takei & Chiba* (1966). On the other hand, the same unit cell length will be obtained for a magnetite substituted with a certain amount of an ion smaller in size than the iron ion, such as, for instance, Al³⁺ (e.g. *Schwertmann & Murad* 1990), something we regard as unlikely. No shift in the positions of the XRD peaks belonging to hematite is observed after heating.

Low-temperature behaviour of imparted remanence

Figure 4.4 shows a low-temperature cycle between 0°C and -230°C of imparted remanence (2T) for sample LH3 preheated in a Curie balance to 800°C. After cooling to ca. -50°C, i.e. below the Morin transition of hematite, still ~85% of the initial remanence remains. This indicates that, as suggested earlier, at least part of the spinel phase particles lie above the SD threshold size of ~25–30 nm. On further cooling hardly any change in remanence is observed, whereas on warming back to room temperature a gradual decrease in intensity occurs until ~75% of the initial IRM. No indication of a Verwey transition is observed, which excludes the possibility that the spinel phase is a slightly substituted or slightly oxidized magnetite. On the other hand, the specific behaviour observed concurs well with the behaviour described earlier for maghemite by *Dankers* (1978) and *De Boer & Dekkers* (1996, Chapter 6 of this thesis).



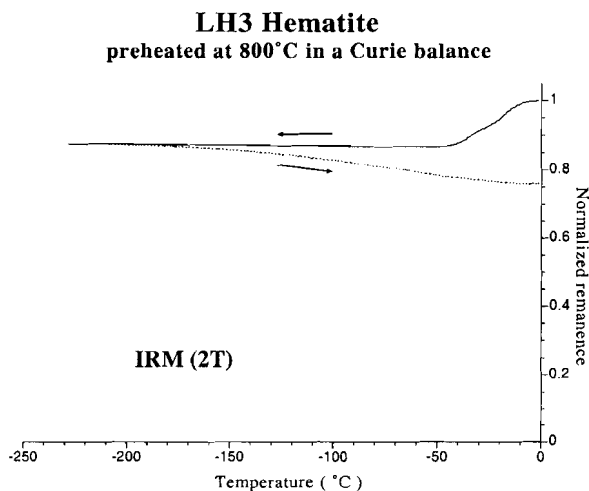


Figure 4.4: Low-temperature cycling of a 2 T IRM imparted at room temperature for sample LH3 after a thermal cycle to 800°C in a Curie balance.

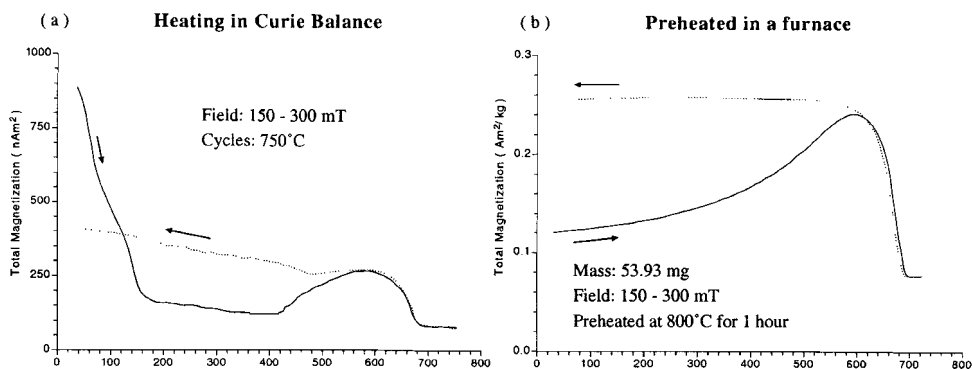
4.4.2 Synthetic hematite samples

Fe(III)nitrate and ferrihydrite precursors

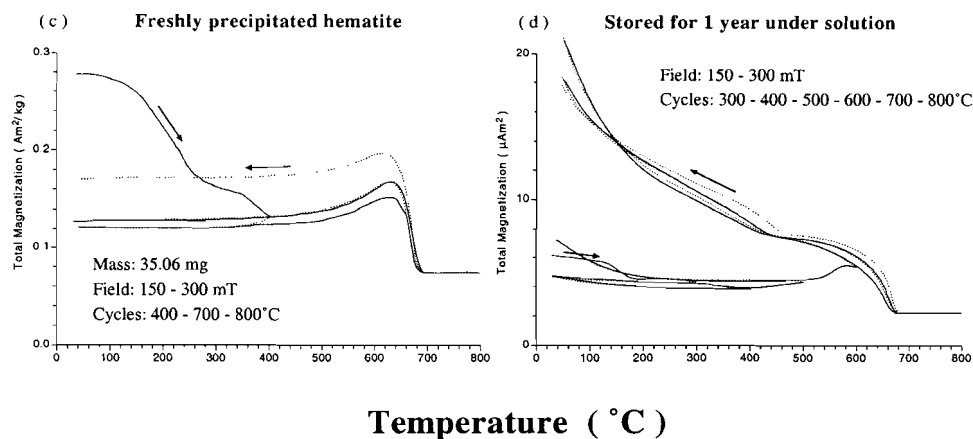
Figure 4.5 shows the thermomagnetic behaviour of synthetic hematite samples prepared from a hydrated ferric nitrate precursor (*a* & *b*) and a ferrihydrite precursor (*c* & *d*). Evidently, a magnetic spinel phase with $T_c \sim 470\text{--}475^\circ\text{C}$ similar to the one described earlier for the natural hematite samples can be created from both synthetic hematites (*a* & *d*) on thermal cycling. The conditions during and after the formation of the hematite phase, however, seem to be a crucial factor determining whether the additional magnetic phase is created on heating or not.

The thermal decomposition of highly pure $\text{Fe}(\text{NO}_3)_3 \cdot 9\text{H}_2\text{O}$ to hematite is monitored during a standard thermomagnetic analysis in a Curie balance using heating and cooling rates of $10^\circ\text{C min}^{-1}$ (Fig. 4.5a). The initial decrease in magnetization on heating agrees reasonably well with reported melting and boiling (i.e. decomposing) points of the monoclinic nitrate salt, being 47.2 and 125°C , respectively (*CRC Handbook of Chemistry and Physics*). Obviously, an appropriate hematite type necessary to create the magnetic phase can be formed when applying one single heating cycle between room temperature and $\sim 750^\circ\text{C}$ (Fig. 4.5a). Subsequent heating to 800°C and annealing for 30 minutes (not shown here) causes almost reversible thermomagnetic behaviour indicating that the maghemite-like phase is persistent to this high temperature and that no additional amount was formed.

Hydrated Ferric Nitrate Salt Precursor



Ferrihydrite Precursor



Temperature ($^{\circ}\text{C}$)

Figure 4.5: Thermomagnetic behaviour of synthetic hematites prepared from different precursor minerals. Panel (a) shows the thermal decomposition of a hydrated ferric nitrate salt to hematite and the subsequent formation of an additional magnetic phase with a T_c of $\sim 470^{\circ}\text{C}$. Panel (b) shows a thermomagnetic analysis of a hematite sample prepared from the same starting material which was preheated to 800 $^{\circ}\text{C}$ in a furnace with a 30 minutes intermediate heating step at 350 $^{\circ}\text{C}$. (c) Thermomagnetic behaviour of a synthetic hematite freshly precipitated from a ferric nitrate solution via a ferrihydrite stage. (d) Hematite sample synthesized under identical conditions as (c) after ~ 1 year storage in the mother solution.

On the other hand, stepwise cycling to increasingly higher temperatures (not shown here) or keeping the sample for a certain time at an intermediate temperature (e.g. 200 or 350°C) before further heating to 750 or 800°C does not favour the formation of the appropriate hematite type; i.e. no additional magnetic phase is created on heating. *Fig. 4.5(b)*, for instance, shows the thermomagnetic analysis of a hematite sample produced by heating the nitrate salt to 350°C in a furnace and keeping the sample at this temperature for half an hour before it was heated to 800°C where it was annealed for 1 h.

When dealing with a Fe(III)nitrate precursor, the specific thermal cycling procedure used thus seems to determine whether an appropriate hematite type is formed from which a maghemite-like phase can be created on heating or not. Again, these observations do not support any suggestion that the spinel phase is created by diffusion of impurity cations toward the surface, because this process is not likely dependable on the heating procedure used but rather on the height of the temperature reached; i.e. cations incompatible with the hematite structure will be expelled from the crystal lattice irrespective of the heating procedure. Consequently, the formation of the spinel phase must rather be associated with another type of internal defects of which the concentration varies with the preparation method.

Figures 4.5(c & d) show the thermomagnetic analysis of a hematite sample freshly precipitated from an iron nitrate solution via an intermediate ferrihydrite stage and a sample synthesized under identical conditions, left for almost one year in the mother solution, respectively. A magnetic phase with a Curie temperature of 470–475°C is created only from the second sample during thermal cycling. The first appearance of the maghemite-like phase can already be deduced from the tail of increasing magnetization after the 400°C cycle. A distinct Curie point, however, can only be recognized after the 600°C cycle. The spinel-phase does not survive annealing at 1000°C (not shown here).

The initial two-step decrease in magnetization observed for both samples can be attributed to two different goethite phases with distinct grain-size ranges similar to the hematite particles or due to a goethite and a ferrihydrite impurity with different dehydration temperatures. Because both samples show this initial behaviour it is not likely that these impurities are responsible for the creation of the magnetic phase, also because the natural hematite samples described earlier did not have these contaminations. Consequently, changes in the precipitated hematite during storage must thus be responsible for the different thermomagnetic behaviour. The thermomagnetic behaviour representative of the hematite phase gives several clues for these changes. The Hopkinson-like peak in magnetization lies at a lower temperature for the stored sample and it shows a block-shaped cooling curve after heating above the Curie point, whereas the cooling curve of the freshly precipitated sample still shows the Hopkinson-like peak. According to *De Boer & Dekkers* (1998), both observations likely indicate that the stored sample is magnetically a little bit softer, in this case presumably caused by an improved crystallinity and/or an increase in grain size. A plausible explanation for these changes is Ostwald ripening; i.e. the growth of large particles in a suspension at the expense of the smaller ones which redissolve. In addition, unstable phases such as ferrihydrite will convert to more stable hematite, which explains the lower contribution to the signal of these impurity minerals for the stored sample.

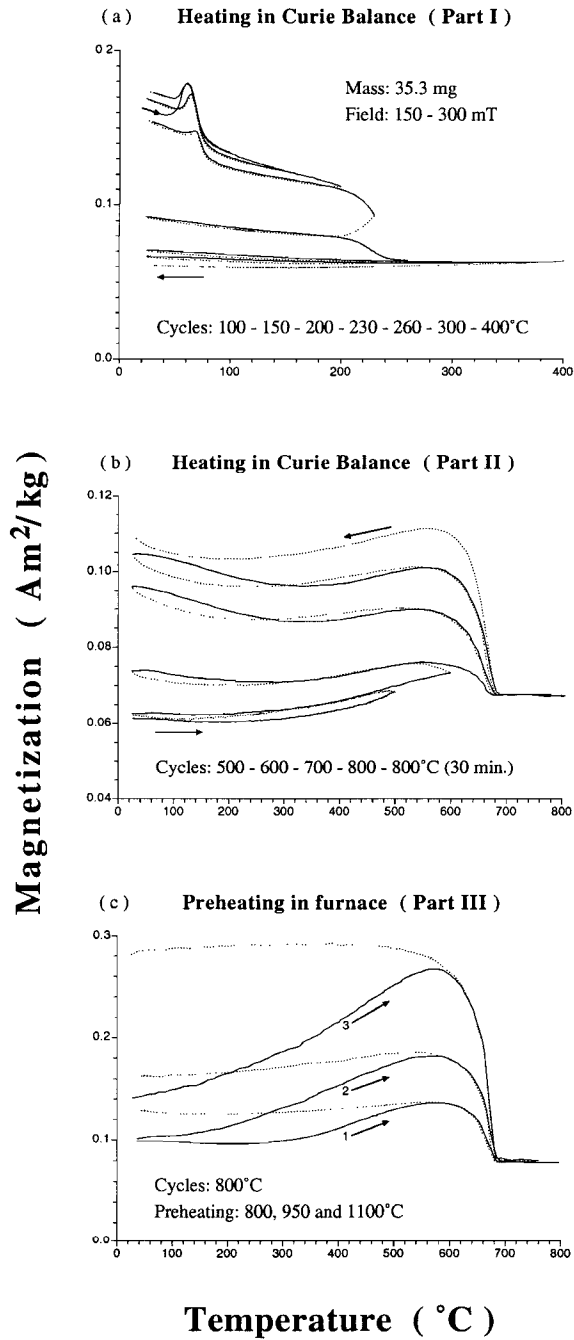
Goethite precursor

Figures 4.6(a-c) show the changes in magnetization during the thermal decomposition of a synthetic goethite to hematite and the subsequent heating-induced crystal structure improvement and grain-size increase. The thermomagnetic behaviour of this synthetic goethite is described in *De Boer & Dekkers* (1998) for cycling up to 100°C. Subsequent cycling to 150 and 200°C slightly alters the goethite phase as can be deduced from the irreversibility of the curves (i.e. decrease in magnetization) and the shift of the Hopkinson-like peak to higher temperatures. The latter also indicates that the magnetic hardness of the goethite increases. On further cycling, the distinct drop in magnetization between 200 and 250°C marks the major dehydroxylation step of the goethite phase to hematite. During the 400°C cycle the transformation to hematite is completed. Using this technique, no indication for the existence of a spinel phase is found. Other authors (e.g. *Özdemir* 1998), however, have reported the possible formation of intermediate magnetite during the transformation reaction.

Hematite formed in this way is reported (e.g. *Chevallier* 1951) to be extremely fine-grained and generally is superparamagnetic; i.e. $<0.03 \mu\text{m}$. The $\alpha\text{-Fe}_2\text{O}_3$ particles just above the SD threshold size appear to be extremely hard (e.g. *Dekkers* 1990), implying that they are far from being saturated in the magnetic fields possible in the Curie balance. The progressive gain in magnetization on repeated cycling to increasingly higher temperatures (*Fig. 4.6b*) shows that the particles become magnetically increasingly softer; i.e. illustrates the continued heating-induced growth of the hematite crystallites. Obviously, during this process no spinel phase with a distinct Curie point is created on the $\alpha\text{-Fe}_2\text{O}_3$ particles. Although the typical tail in magnetization at the low temperature side of the curves may indicate the presence of ultrafine-grained spinel particles, it is more likely explained by very small SD hematite particles which already become SP on mild heating ($<300^\circ\text{C}$). The temperature hysteresis between a cooling curve and the heating curve of the subsequent cycle may represent some sort of hard VTRM. The mentioned behaviour resides up to 950°C (*Fig. 4.6c*). Only after annealing at 1100°C, the sample shows a block-shaped cooling curve characteristic of well-ordered defect-poor hematite.

Figure 4.6 (next page): *Thermal decomposition of a synthetic goethite sample as observed in a Curie balance during repeated runs to increasingly higher temperatures. Figure (a) shows the dehydroxylation to poorly-ordered fine-grained hematite, whereas panel (b) illustrates the subsequent heating-induced crystallinity improvement and crystallite growth. The exponential tail in the magnetization curves observed at their low temperature side most likely represent the ultrafine-grained part of the hematite crystallites becoming SP on heating, rather than it indicates the possible existence of traces of an additional magnetic phase. Figure (c) shows the thermomagnetic behaviour of the sample after annealing in a furnace for several hours at 800⁽¹⁾, 950⁽²⁾ and 1100°C⁽³⁾, respectively. Annealing at 1100°C resulted in a perfectly ordered defect-poor hematite whose thermomagnetic behaviour is similar to that observed for the natural samples in Figs 4.1(a,b & d).*

Goethite Precursor



4.4.3 Possible formation mechanism of the spinel phase

Experimental evidence seems to favour the possibility that the low-coercivity phase with a characteristic T_c of 470–475°C is a relatively pure ferric oxide form with a maghemite-like spinel structure that preferentially grows on basal planes of a hematite parent when being heated at least above 400°C. This interpretation supports earlier studies by *Finch & Sinha* (1957) and *Meillon et al.* (1995) who concluded that the $\gamma\text{-Fe}_2\text{O}_3 \rightarrow \alpha\text{-Fe}_2\text{O}_3$ transformation is not strictly irreversible but may proceed under appropriate conditions. The relatively low Curie point, however, indicates that the superexchange bonds existing in the specific maghemite form created during our experiments must be less in amount or less strong compared to the bonds present in the most common maghemite varieties with all vacancies on octahedral sites and a characteristic T_c at ~645°C. The difference may be explained by an odd arrangement of the vacancies and/or cations over the octahedral and tetrahedral sites. The epitaxially grown maghemite variety described by *Takei & Chiba* (1966), for instance, has an identical T_c of 470°C. Various analyses performed by these authors clearly showed that it was a pure ferric oxide form, discounting the possibility that any impurity cation was responsible for the lowering of the T_c . Moreover, their measured value for the first cubic magnetocrystalline anisotropy constant K_1 of -4.60^3 J m^{-3} agrees closely with the value $K_1 = -4.70^3 \text{ J m}^{-3}$ calculated by *Birks* (1950) based on measurements of initial permeability for polycrystalline maghemite (*cf. Dunlop & Özdemir* 1997). Combining our findings with results of *Finch & Sinha* (1957) and *Takei & Chiba* (1966) seem to suggest that the arrangement of vacancies and/or cations in thin epitaxial outgrowths of maghemite on certain specific substrates can be different from that usually encountered in distinct maghemite particles. The suggested structure by *Takei & Chiba* (1966) with ca. 20% of the vacancies on tetrahedral sites may also be adopted in our case, especially when one takes into consideration that all Fe^{3+} ions in the hematite parent are octahedrally coordinated.

The fact that the $\alpha\text{-Fe}_2\text{O}_3 \rightarrow \gamma\text{-Fe}_2\text{O}_3$ transformation takes place at the surface of the hematite particles strongly suggests that, in our case, a thermally activated outward migration of some specific type of internal defects forces the necessary structural rearrangement from a thermodynamically stable *hcp* to a less stable *ccp* stacking of the oxygen layers. The thermomagnetic behaviour of sample LH4, however, showed that not every type of internal defect can trigger this process. The hematites from which the spinel phase is created must thus have a specific type of defects in common. These defects must be in sufficient concentration and must migrate to grain edges on heating.

In general, the type and concentration of internal defects is highly determined by the mode of formation. It is known from literature that most hematites produced in aqueous systems or by thermal dehydration of either hydrated nitrate salts or goethite often retain some incorporated water in the structure (e.g. *Gallagher & Gyorgy* 1969; *Wolska* 1981; *Šubrt et al.* 1984; *Wolska & Schwertmann* 1989; *Schwertmann & Cornell* 1991; *Waychunas* 1991; *Stanjek & Schwertmann* 1992). This structurally bound water (*sbw*) is shown to exist in the form of hydroxyl groups replacing O^{2-} anions in the hematite crystal lattice (*Wolska* 1981; *Wolska & Schwertmann* 1989). The electroneutrality is preserved by Fe^{3+} deficiency in the cationic positions, rather than by changing the valence state of

some Fe^{3+} to Fe^{2+} . Moreover, *Wolska & Schwertmann (1989)* showed that such structurally bound water can be extremely persistent against heating. Complete removal may require temperatures up to ca. 1000°C . The release of this *sbw* on heating implies some rearrangement of the hematite structure and when present in appropriate concentration it may possibly trigger the formation of the maghemite-like phase on the surface of the particles. Thus, at least for the synthetic samples, the presence of structurally bound water in the lattices of the hematites might be a suitable candidate explaining the behaviour observed.

The Kadaň hematite is reported to be of hydrothermal origin ($<200^\circ\text{C}$) and its genesis is associated with a Tertiary fluorite-barite mineralization. *Figure 4.7* shows the typical weight loss pattern of a Kadaň hematite sample ($<40\ \mu\text{m}$) measured during continuous heating from room temperature up to 1000°C using a constant rate of $10^\circ\text{C}\ \text{min}^{-1}$. The thermogravimetric curve shows three distinct steps starting around 400°C , 700°C and 900°C , respectively. The weight losses at these high temperatures most probably correspond to the release of tightly held structurally bound water, whereas the initial decrease in weight up to $\sim 200^\circ\text{C}$ can be explained by the release of more weakly bound adsorbed water. This specific thermogravimetric behaviour seems to support our hypothesis that the release of *sbw* triggers the formation of a spinel phase from pure hematite.

The genesis of LH3 hematite is not known, and unfortunately, not enough sample material was left to perform thermogravimetric analysis. However, the brief description of the original ore by *Dankers (1978)* suggests that it was formed at relatively low temperatures because of the relative poor crystallinity compared to the other ores described by *Dankers (1978)* and *Hartstra (1982)*. Furthermore, no textural indications were found for the creation from a ‘waterless’ precursor mineral like magnetite. Our hypothesis can thus not be rejected by these findings.

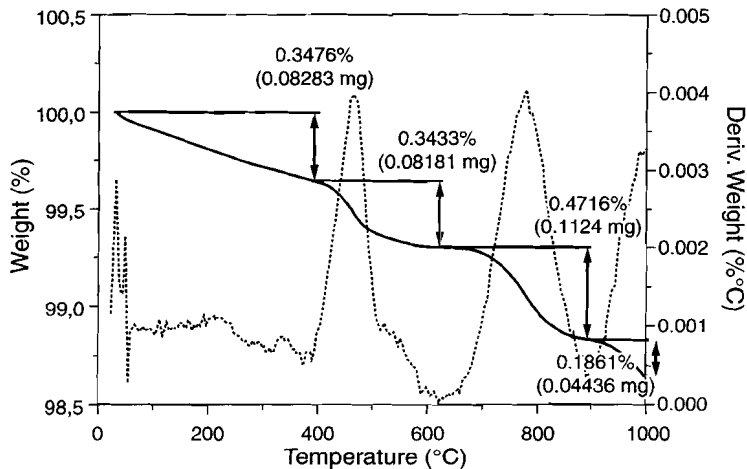


Figure 4.7: Thermogravimetric analysis of Kadaň hematite showing the typical stepwise release of tightly held structurally bound water.

The results obtained on the various natural and synthetic samples, however, imply that the release of incorporated water is not the only condition necessary for the creation of the magnetic phase to take place. Obviously, some other conditions need to be fulfilled at the same time otherwise no maghemite-like phase is formed. For instance, no or hardly any magnetic phase is created on ~1 cm large ore fragments of Kadaň hematite, whereas a spinel did form on particles crushed below ~250 μm . This most likely has to do with the availability of appropriate planes to grow on. As mentioned, Kadaň hematite is acicular, developed along the crystallographic *c*-axis, so the amount of suitable basal planes is very low in relatively large ore fragments. On crushing, however, the length to width ratios of the individual particles substantially improves and more basal planes become available by subdividing larger particles. This may also explain why considerable more of the new magnetic phase is created on platy developed LH3 hematite compared to acicular Kadaň hematite. Thus, in the temperature range the structurally bound water is expelled, enough and sufficiently large basal planes of hematite must be available, otherwise no maghemite-like phase can be created.

The same principle likely underlies the differences in thermomagnetic behaviour obtained on the various synthetically prepared hematite samples. The individual hematite crystallites prepared from goethite, for instance, stay low in crystal perfection and size even at high temperatures. Likely, most of the incorporated water will already be released before well-crystallized basal planes of hematite become available in sufficient size to grow the maghemite on. Similar considerations hold for the fine-grained poorly crystalline hematite particles freshly precipitated from solution. On the other hand, the crystallinity and grain size of the sample stored for a long period in the mother solution would have been increased because of Ostwald ripening; the creation of the maghemite phase is now possible. For the hematite created from the hydrated ferric nitrate salt our hypothesis would imply that a higher concentration of internal defects (i.e. structural water) becomes incorporated during a single heating step compared to repeated heating steps to increasingly higher temperatures or annealing at temperatures close to the decomposition temperature of the precursor mineral before completing the heating procedure.

4.5 Conclusions

Trace amounts of a magnetic spinel with a characteristic T_c of 470–475°C can be created on the surface of relatively pure hematite during a standard heating procedure in air. The spinel has a cubic structure with a unit cell length of $a = 0.0835.0005$ nm. It is argued that the newly created phase is a pure ferric oxide polymorph rather than an isomorphously substituted spinel. The suggested structure is that of pure maghemite with a peculiar distribution of its vacancies (and/or cations) over the two magnetic sublattices; i.e. with part of the vacancies on tetrahedral interstices. A mechanism is proposed in which the structural rearrangement caused by the thermally activated release of tightly held structurally bound water may trigger the necessary redistribution of the oxygen

framework from *hcp* to *ccp* in the outermost layers of hematite particles. The availability of well-crystallized hematite (0001) planes of appropriate size, however, seems to be an explicit condition for the epitaxial maghemite growth to take place.

ACKNOWLEDGEMENTS

We gratefully acknowledge the assistance of *Tom Mullender* and *Adry van Velzen* with the low-temperature measurements on the MicroMag. *Eduard Petrovský* kindly made available a high purity hematite rock sample of the Kadaň hydrothermal ore deposit. This work was conducted under the programme of the Dutch national research school, the Vening Meinesz Research School of Geodynamics (VMSG).

Part II

Maghemite ($\gamma\text{-Fe}_2\text{O}_3$)

How can I know what I think until I see what I say?

(Karl E. Weick)

Chapter 5

Review on maghemite ($\gamma\text{-Fe}_2\text{O}_3$): rock-magnetic and other relevant properties

5.1 Introduction

Maghemite is a strong ferrimagnetic mineral. Apart from its technological importance as a material for data storage systems, maghemite is of considerable paleomagnetical interest, since it is able to carry a stable remanence over geological time and occurs naturally in a wide variety of rock types and soils. In addition, maghemite is lately getting increased attention as being a significant constituent of the reddish-brown, magnetic dust on Mars. It typically forms by weathering or low-temperature oxidation of fine-grained magnetite and an entire solid-solution series exists between both end members. The transformation involves oxidation of ferrous iron and production of (ordered) cation vacancies. Oxidation of large magnetites ($>1\ \mu\text{m}$) generally results in a two-phase grain of intergrown maghemite and hematite. The name maghemite is derived from the first syllables of *magnetite* and *hematite*, in allusion to the mineral's magnetism and composition. Maghemite ($\gamma\text{-Fe}^{3+}_2\text{O}_3$) has the same chemical composition as hematite ($\alpha\text{-Fe}^{3+}_2\text{O}_3$), but its Fe-deficient spinel structure is similar to that of magnetite, ($\text{Fe}^{2+}\text{Fe}^{3+}_2\text{O}_4$). Having a structure essentially similar to that of magnetite, its magnetic hysteresis properties resemble those of magnetite to a large extent. For this reason maghemite was often confused with magnetite. It is, however, now well recognized that most magnetic properties show a clear trend throughout the solid-solution series, and that $\gamma\text{-Fe}_2\text{O}_3$ has distinct magnetic characteristics (*Figs 5.1a & b*). On oxidation of magnetite, the saturation magnetization decreases by about 15% from ~ 92 to $\sim 74\ \text{Am}^2\ \text{kg}^{-1}$, while the Curie temperature increases steadily from 580°C to about 645°C for pure maghemite. Maghemite, however, is a metastable cubic phase which inverts irreversibly to its hexagonal polymorph hematite when heated sufficiently, resulting in a very large decrease ($\sim 99.6\%$) in spontaneous magnetization. The activation energy of the phase transition is relatively high and at ambient temperature and pressure maghemite is able to persist during geological time. During laboratory heating, inversion typically starts at ca. 350°C .

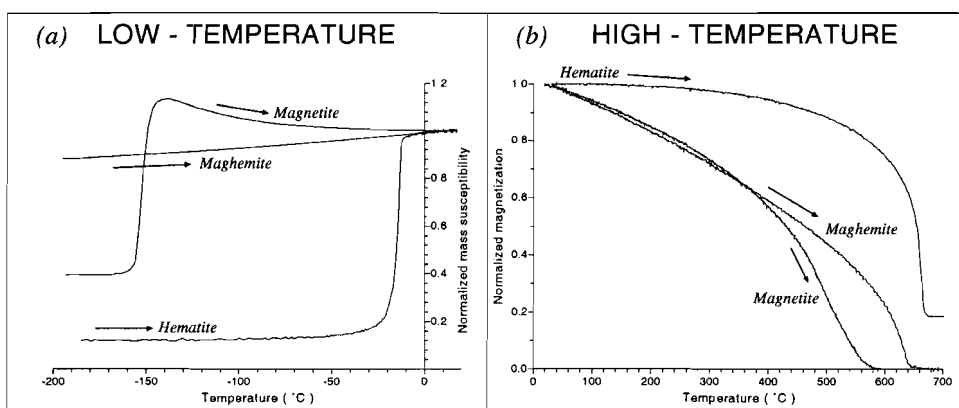


Figure 5.1: Typical (a) low-temperature and (b) high-temperature magnetic behaviour (heating in air) of different iron oxides. Magnetite: 55–75 μm fraction of sample HM4 described by Hartstra (1982). Hematite: 55–75 μm fraction of sample LH2 described by Dankers (1978, 1981). Maghemite: synthetic sample (0.05 – 0.2 μm) described by Van Oorschot & Dekkers (1999). (A) Characteristic increases in low-field susceptibility at -150°C and -15°C represent the Verwey transition of magnetite and the Morin transition of hematite, respectively. (b) On heating, the saturation magnetization of hematite decreases less fast compared to that of magnetite and maghemite, resulting in a more block-shaped thermomagnetic heating curve for hematite. The relatively high paramagnetic contribution to the signal remaining after passing the Néel point of hematite ($\sim 675^\circ\text{C}$) results from the normalization: the spontaneous magnetization of hematite is two orders of magnitude lower than that of magnetite and maghemite.

Natural maghemites quite often contain some residual ferrous iron, i.e. are incomplete reaction products of magnetite. In the magnetite–maghemite solid-solution series ($\text{Fe}_{1-z}^{2+}\text{Fe}_{2+z}^{3+}\text{O}_{4+0.5z}^{2-}$), the degree of oxidation is given by the oxidation parameter z , ranging between 0 for magnetite and 1 for maghemite (O’Reilly & Banerjee 1967). In literature, however, no definite boundary can be said to exist between maghemite and non-stoichiometric magnetite. Partially oxidized magnetites are usually called ‘maghemites’, although maghemite ($\gamma\text{-Fe}_2\text{O}_3$) itself is the *fully* oxidized daughter of magnetite. In addition, the oxidized equivalents of the widespread Ti-substituted magnetites are usually called titanomaghemites even at the earliest stages of oxidation ($z > 0.1$). To our opinion, *cation-deficient (titano)magnetite* is a more accurate term to denote the intermediate phases with $0.1 < z < 1$, nevertheless it is only used sporadically in literature.

The geological occurrence of maghemite and cation-deficient (CD) magnetite in various rock types and soils is given in **Section 5.2**, together with a description of the most common formation processes in these geological settings. In sediments and soils, maghemites and CD magnetites may occur together with other magnetic minerals such as hematite, goethite ($\alpha\text{-FeOOH}$) or lepidocrocite ($\gamma\text{-FeOOH}$). The phases may be intimately

intergrown (*cf.* Annersten & Hafner 1973). In both settings, the concentration of ferrimagnetic phases of the magnetite–maghemite series, the extent of oxidation of magnetite and the assemblage of associated magnetic minerals are generally influenced by environmental and/or climatic factors. Hence, apart from its importance for paleomagnetism, maghemite showed its usefulness in environmental science and paleoclimatic reconstructions (e.g. Kent & Lowrie 1974; Kodama 1982; Heller *et al.* 1993; Verosub *et al.* 1993). In addition, maghemite has also proved to be important to soil science because it gives valuable information about the soil formation process and the nature of the subsoil (e.g. Le Borgne 1955; Mullins 1977; Tice & Oliphant 1984; Maher 1986). This secondary soil mineral, for example, is held responsible for the magnetic enhancement of most surface soils. Furthermore, the purity or the type of isomorphous substitution of maghemite provides information about its precursor minerals and the weathering environment in which these phases were formed. Maghemites formed by low-temperature oxidation of primary magnetites usually contain substantial amounts of Ti in their lattice. This is a solid-state process not involving any dissolution-precipitation step. In contrast, maghemites formed from secondary magnetites or from other secondary Fe-containing minerals such as goethite, lepidocrocite and hematite usually are more pure or are Al-substituted instead of Ti-substituted. These precursor minerals most likely are formed in an aqueous environment by oxidation of dissolved Fe^{2+} . Al for Fe substitution is common in these secondary minerals because of the omnipresence of Al in the weathering environment. This diagnostic value, for instance, is used to reveal whether the maghemites present in the *Martian* dust are inherited from the underlying bedrock by a still ongoing solid-state weathering process or were formed long ago in an aqueous weathering environment and thus furnish proof of the warm and watery past of the Red Planet.

Section 5.3 reviews the mineralogical and crystallographic characteristics of maghemite necessary to understand its magnetic structure and rock-magnetic properties. Maghemite was first reported as a natural mineral by Sosman & Posnjak (1925), who also noted the similarity of its X-ray powder-diffraction pattern to that of magnetite (*cf.* Collyer *et al.* 1988). Both minerals indeed possess the same inverse spinel structure with cations on both tetrahedral and octahedral sites, but maghemite has additional cation-deficient sites –*vacancies*– compared to magnetite. The arrangement of these vacancies in the maghemite lattice, however, appears to be highly variable and may affect the magnetic properties. Conversely, information about the positioning of vacancies and cations in the maghemite structure may be inferred from magnetic measurements. Furthermore, long-range ordering of vacancies may sometimes be observed in maghemite. This phenomenon leads to the formation of a superstructure that produces additional diagnostic reflection peaks in X-ray diffraction patterns of this type of maghemite. The various maghemite structures suggested in literature are reviewed in **Subsection 5.3.1**, preceded by a brief description of the general spinel lattice and the magnetite structure.

Subsection 5.3.2 describes the structural implications of the common Ti- and Al-substitution in maghemite and the possible incorporation of structurally bound water. It was once believed that incorporated water in the form of $(\text{OH})^-$ was implicit in the maghemite structure and was considered a prerequisite for stabilizing the metastable

structure. More recent experimental evidence, however, refuted this suggestion. Nevertheless, small amounts of structural water may become incorporated when formation takes place in an aqueous environment or when the precursor mineral has an excess of structural water.

The usual natural formation processes of maghemite are the oxidation or weathering of magnetites and to a lesser extent the dehydroxylation of lepidocrocite. Both processes generally result in fine-grained, submicron particles. The resulting maghemite frequently pseudomorphs the precursor minerals, leading to cubic and acicular particles, respectively. The latter particles are often microporous. The microstructure of maghemite is the subject of **Subsection 5.3.3**, while the mentioned transformation mechanisms of Fe_3O_4 and $\gamma\text{-FeOOH}$ to maghemite together with the inversion of metastable $\gamma\text{-Fe}_2\text{O}_3$ to thermodynamically stable $\alpha\text{-Fe}_2\text{O}_3$ are the subject of **Subsection 5.3.4**.

The remainder of this chapter (**Section 5.4**) concerns the magnetic properties of $\gamma\text{-Fe}_2\text{O}_3$ and the trends observed throughout the magnetite–maghemite solid-solution series. The ferrimagnetic structure is discussed in detail with particular emphasis on the magnetic properties most diagnostic to distinguish between magnetite and maghemite. These are the saturation magnetization and its behaviour on heating, the Curie temperature and the low-temperature behaviour of induced magnetization. The magnetic properties of the titanomaghemites lie beyond the scope of this review and will only be touched upon at appropriate places. For comprehensive reviews on these minerals the reader is referred to *Haggerty* (1976), *Lindsley* (1976a & b, 1991), *O'Reilly* (1984), *Dunlop & Özdemir* (1997), and references therein.

In paleomagnetism, the presence of maghemite indicates a NRM that is mainly a CRM and occasionally a DRM in origin (*cf. Dunlop & Özdemir* 1997). As maghemite is formed from magnetite, it is important to know whether the CRM remembers the original NRM direction carried by the magnetite precursor or tracks the then ambient geomagnetic field. The same holds for the so-called two-phase CRM produced during the inversion of ferrimagnetic maghemite to canted antiferromagnetic hematite. Both processes will be discussed in **Subsection 5.4.6**.

Cautionary remarks: Because of difficulties in obtaining pure natural material, studies on maghemite have been largely restricted to synthetic samples. Crystal-chemical properties of maghemite such as crystal habit and cation and vacancy ordering appear to depend on the mode of formation, and are often difficult to characterize because of the typical small grain sizes. It remains uncertain to which extent the properties of synthetic samples resemble those of natural material. The magnetic properties of maghemite, however, are directly related to these properties. Caution should therefore be used when synthetic phases are treated as analogues to naturally occurring magnetic oxides. In addition, the maghemitization process has also been studied almost exclusively in the laboratory. Most experiments involve heating in air to promote oxidation, a process that presumably is based on the 'addition of oxygen' mechanism (*cf. Subsection. 5.3.4*) Maghemitization in nature, however, most often occurs according to the 'iron removal' mechanism because of the presence of (pore) water. It is not unlikely that some differences in crystal-chemical properties exist between the products obtained. Heating in

fluid is infrequently used to simulate the maghemitization process. This process, however, appears to involve dissolution and neocrystallization rather than diffusion of Fe.

5.2 Geological occurrence and formation

5.2.1 Igneous and metamorphic rocks

Fine-grained maghemites are relatively common in a wide variety of subaqueous or subaerial oxidized igneous rocks, but especially are widespread in basic extrusives, like basalts. The high concentration of magnetic minerals (~1–5 vol. %) and small grain sizes of these basic volcanic rocks make them excellent recorders of the paleomagnetic field. In these rock types, however, 'maghemites' are seldom fully oxidized and generally contain variable amounts of Ti in their lattice. These CD titanomagnetites are either formed at high temperatures during original cooling of an igneous rock (typically >600°C), or at lower temperatures by weathering or hydrothermal alteration (typically <250°C) of primary titanomagnetites. These two formation processes of maghemite are called *deuteric oxidation* and *maghemitization*, respectively. *O'Reilly* (1984) discussed both processes and argued that Ti-magnetite crystallizing from an igneous melt and cooling from high temperature can sustain only a limited degree of non-stoichiometry before breaking up into an intergrowth of phases. This deuteric oxidation process is related to volatile accumulation and oxygen fugacity of the melt. Oxidative alteration at low temperatures, on the other hand, can produce high or the maximum possible degree of non-stoichiometry. Maghemitization appears to proceed either by the so-called '*addition of oxygen*' mechanism, i.e. building new unit cells at the surface, or by the alternative '*iron removal*' mechanism (*O'Reilly* 1984). In the latter case, which occurs under submarine conditions, oxygen is not present at the surface and iron is leached by the seawater (cf. *Dunlop & Özdemir* 1997; *Xu et al.* 1997). This low-temperature transformation process of $\text{Fe}_3\text{O}_4 \rightarrow \gamma\text{-Fe}_2\text{O}_3$ is described in more detail in Subsection 5.3.4.

At high temperatures iron oxides commonly contain titanium and form solid-solution series. The composition of these FeTi-oxides can be displayed on the $\text{TiO}_2\text{-FeO-Fe}_2\text{O}_3$ ternary diagram (*Fig. 5.2*), in which the titanomaghemites are represented by the compositions inside the quadrilateral $\text{Fe}_2\text{O}_3\text{-Fe}_3\text{O}_4\text{-Fe}_2\text{TiO}_4\text{-FeTiO}_5$. Their chemical composition and hence their location on the ternary diagram can be conveniently expressed in terms of two parameters. The composition parameter x expresses the mole % Ti^{4+} present, while the oxidation parameter z indicates the degree of oxidation. Unoxidized titanomagnetites on the magnetite–ulvöspinel join have $z = 0$, while fully oxidized titanomaghemites with $z = 1$ lie on the maghemite–pseudobrookite join. Progressive maghemitization according to the 'addition of oxygen' mechanism involves no change in Fe/Ti ratio, i.e. the bulk composition follows horizontal oxidation lines (see *Fig. 5.2*), whereas in the 'iron removal' case the Fe/Ti ratio falls as oxidation

proceeds and the oxidation lines on the ternary diagram slope upwards to the right (cf. O'Reilly 1984; Dunlop & Özdemir 1997).

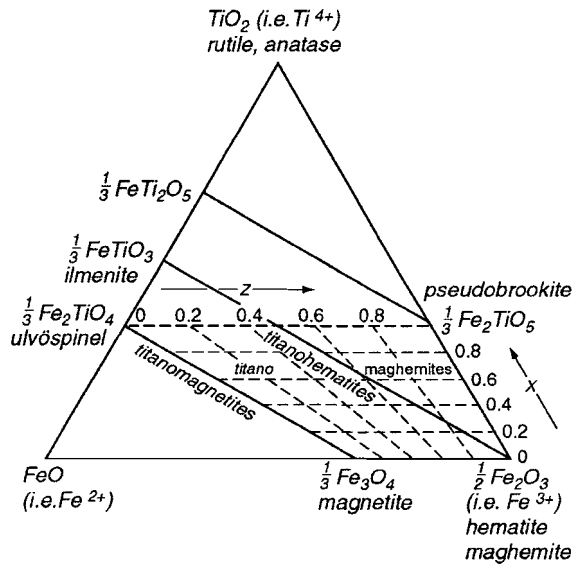


Figure 5.2: $\text{TiO}_2\text{-FeO-Fe}_2\text{O}_3$ ternary diagram representing the compositions of important iron-titanium oxides. Positions from left to right indicate increasing ratios of ferric (Fe^{3+}) to ferrous (Fe^{2+}) iron while positions from bottom to top indicate increasing Ti content (Ti^{4+} : total Fe). Using $\frac{1}{2}\text{Fe}_2\text{O}_3$ as the parameter for the Fe^{3+} corner normalizes the diagram to one cation, producing the convenient effect that lines of oxidation (increasing the $\text{Fe}^{3+}:\text{Fe}^{2+}$ ratio) according to the 'addition of oxygen' mechanism are parallel to the base of the diagram (Butler 1992).

Especially the titanomaghemites present in rapidly quench-cooled ocean-floor basalts have been investigated thoroughly, because of the possible effect of the maghemitization process on observed linear marine magnetic anomalies (e.g. Ryall & Ade-Hall 1975; Prevot *et al.* 1981). The dominant primary magnetic mineral in the newly created ocean-floor pillow basalts at the spreading ridges is a fine-grained homogeneous, single-phase Ti-magnetite, $\text{Fe}_{3-x}\text{Ti}_x\text{O}_4$, with $x \sim 0.6$ (TM60), often containing Al and Mg as impurities (cf. Dunlop & Özdemir 1997). In this particular environment, deuteric oxidation of titanomagnetite during initial cooling is prevented by rapid quenching and by the excess of sulphur over oxygen once the oxides and silicates have crystallized. Rapid cooling also prevented subsolvus exsolution to take place. Submarine conditions, however, appear to

promote the maghemitization process. The quenched basalts in the upper 1–2 km of the oceanic crust are penetrated by seawater and warmed through burial beneath later eruptions (*cf. Dunlop & Özdemir 1997*). Under these low-grade metamorphic conditions the fine-grained Ti-magnetites oxidize rapidly to CD Ti-magnetites, certainly within 0.5 Myr (*Irving 1970; Ozima 1971; Johnson & Pariso 1993*), and perhaps within 20 kyr (*Gee & Kent 1994*). Samples of ocean-floor basalts described by *Xu et al. (1997)* indicated that the maghemitization process is completed between 26 and 70 Myr. Consequently, (near-)end-member titanomaghemite produced during seafloor weathering is one of the most abundant FeTi-oxides in the Earth's crust. Fortunately, the secondary CRM carried by daughter titanomaghemites resembles the primary TRM direction carried by parent single-domain titanomagnetites because of exchange coupling between both phases. The NRM intensity, however, slightly decreases during the maghemitization process because of the lower spontaneous magnetization of Ti-maghemite compared to Ti-magnetite (see Subsection 5.4.4); indeed a systematic decrease in NRM with increasing age of ocean-floor basalts, –that is, with increasing distance from spreading ridges– is observed (e.g. *Irving 1970*).

The conditions under which subaerial lavas form and subsequently alter, differ in several ways from the submarine environment, leading to different, often complex magnetic end products (*cf. Dunlop & Özdemir 1997*). Subaerial basalts, in contrast to submarine basalts, are commonly deuterically oxidized because the oxygen fugacity of the melt is frequently high. This high-temperature oxidation generally results in intergrown spinel (near-magnetite) and hexagonal (near-ilmenite) phases. Furthermore, instead of quenched pillow basalts, massive lava flows with slowly cooling interiors are common under subaerial conditions. Consequently, the few homogeneous primary titanomagnetites of intermediate composition that escaped deuteritic oxidation tend to exsolve into intergrown iron-rich (near-magnetite) and titanium-rich (near ulvöspinel) cubic phases. The Ti-poor spinel phases produced by both processes may become oxidized to relatively pure maghemites during subsequent hydrothermal alteration. Maghemitization of subaerial lava flows, however, is relatively slow because there is less external water available. For a more detailed description of the possible products formed during progressive deuteritic oxidation and the changes involved with increasing regional hydrothermal alteration the reader is referred to *Wilson & Watkins (1967)*, *Watkins & Haggerty (1967)*, *Ade-Hall et al. (1971)*, *O'Reilly (1984)*, *Dunlop & Özdemir (1997)*, and references therein.

5.2.2 Sediments

Maghemite has been reported as one of the dominant magnetic minerals in some deep-sea sediments, like oceanic muds (*Collinson 1983*) and pelagic red clays that occur widely in the middle latitudes of the Pacific (e.g. *Yamazaki 1995*) and in the North Pacific (e.g. *Kent & Lowrie 1974; Johnson et al. 1975*). *Freeman (1986)* observed detrital skeletal titanomaghemite in several pelagic limestones and *Kodama (1982)* described maghemite as the carrier of a stable NRM in marine siltstones and mudstones deposited

on the shelf and slope. Maghemite is also a constituent of oolitic or pisolitic ironstones and laterites (e.g. Harms & Morgan 1964; Singh & Gilkes 1995). Umeorah (1987), for instance, reported maghemite as an abundant component of a sedimentary oolitic ironstone formation in Nigeria. Furthermore, it appears as a colloidal component in many iron-bearing clays (cf. Pecharromán *et al.* 1995), and $\gamma\text{-Fe}_2\text{O}_3$ has also been identified in a wide range of red sandstones. In these so-called red beds, which are deposited in shallow-water flood plains, hematite, however, is usually the main magnetic carrier (see Section 1.2). Ultrafine maghemite particles ($<1\ \mu\text{m}$) have recently also been identified in loess deposits of Central Europe and in the extensive Chinese loess-paleosol sequences (e.g. Heller *et al.* 1993; Verosub *et al.* 1993; Eyre & Shaw 1994; Evans & Heller 1994).

The main mechanism by which maghemite is formed in sedimentary environments is the low-temperature oxidation process of precursor magnetite. Because oxidizing conditions usually prevail during pre-depositional processes such as weathering and transport, most magnetites become already oxidized to some extent before the actual deposition takes place. Kodama (1982), for instance, made it plausible that in his studied marine sediments maghemitization took place before deposition and the maghemite therefore carries a DRM. Extensive chemical weathering in the provenance area, however, appears to favour the production of the more stable iron oxide hematite or the hydrated iron oxides goethite and lepidocrocite over maghemite (Taylor & Schwertmann 1974b). Kent & Lowrie (1974) noted an increased maghemitization of deep-sea sediments of 1.5–0.9 Ma in age, which they attributed to the Pleistocene glaciation of the northern hemisphere and the associated increased ratio of mechanical to chemical weathering. The results of Kodama (1982) on sediments of the same age seem to support this conclusion.

In addition to detrital maghemite, authigenic maghemite commonly forms *in situ* when oxidizing conditions are available during deposition. This post-depositional low-temperature oxidation of magnetite is often related to variables such as accumulation rate and organic content, which in turn are often controlled by climatic variations (cf. Thompson & Oldfield 1986). Maghemitization of (Ti)magnetites is particularly frequent in slowly deposited oxic sediments with little organic input, that, for instance, may occur in pelagic and hemipelagic environments. The low sedimentation rates in these deep-sea sediments increase the exposure time of sedimenting particles to oxidizing bottom waters and permit oxidation near the sediment/water interface before burial occurs (cf. Thompson & Oldfield 1986). The widespread occurrence of maghemite in the slowly deposited, non-fossiliferous, 'red clay' deep-sea sediments ($<3\ \mu\text{m}/\text{yr}$) is explained in this way (Kent & Lowrie 1974). Johnson *et al.* (1975) found that non-fossiliferous cores of deep-sea sediments contained clearly more heavily oxidized authigenic magnetic minerals compared to the fossiliferous equivalents.

Maghemitization may continue to some extent after burial, in any case as long as the conditions remain oxic. Furthermore, maghemite can also form diagenetically from a lepidocrocite precursor (Taylor & Schwertmann 1974b). Lepidocrocite is common in some deep-sea sediments where it, like goethite, might have formed authigenically or by direct or indirect precipitation from seawater (Murray 1979; Henshaw & Merrill 1980). In addition, the alteration of iron containing carbonates such as siderite (FeCO_3) and ankerite ($[\text{Ca},\text{Mg},\text{Fe}]\text{CO}_3$), may also produce maghemite. These common authigenic

constituents of sedimentary rocks may decompose by either weathering or by diagenetic or metamorphic processes, to form an iron oxide or oxyhydroxide depending on the conditions during alteration (O'Reilly 1984). Hus (1990) oxidized several siderite concretions at different temperatures and found maghemite as one of the reaction products.

5.2.3 Soils

Maghemite is widespread in aerobic soils of subtropical and tropical areas such as Australia, Brazil, Hawaii, India and Africa (e.g. Adetoy 1970; Taylor & Schwertmann 1974a; Fitzpatrick 1978; Coventry *et al.* 1983; Anand & Gilkes 1987a; Fontes & Weed 1991), and has also been reported in soils of humid temperate regions like Japan, Germany, The Netherlands, Canada and the United States (e.g. Van der Marel 1951; Schwertmann & Heinemann 1959; Kojima 1964; Pawluck 1971; Sadiq & Lindsay 1988), and in weathered basalts from Greenland. Maghemite may be distributed throughout the soil profile, but is often accumulated in the surface soil (e.g. Le Borgne 1955; Singer & Fine 1989). Furthermore, $\gamma\text{-Fe}_2\text{O}_3$ may be finely dispersed in the soil matrix or concentrated in different kinds of pedogenic materials, such as saprolites, geodes, magnetic bands, glaeboles, ferricretes, and red-brown hard-pans (Fitzpatrick 1988).

Iron oxides and oxyhydroxides play an important role in soil science. Magnetic measurements are increasingly used to describe soil profiles and to further our understanding of pedogenic processes. Virtually all soils are magnetically dominated by maghemite and the other, less oxidized and/or Ti-substituted, ferrimagnetic spinel-phases. Hence, magnetic property profiles measured on soils mainly reflect concentration and/or grain-size variations of these minerals (see Subsection 5.4.1). The mentioned variations in turn may provide valuable information on soil-formation processes. Magnetic susceptibility measurements, for instance, revealed that the upper horizon of many soils is enhanced in ferrimagnetic minerals; particularly maghemite. Several pedogenic mechanisms have been proposed to explain these findings (see below). Furthermore, Özdemir & Banerjee (1982) showed that the evolution from rock through subsoil to soil is reflected in magnetic properties as it involves changes in grain size of the ferrimagnetic iron oxides. The magnetic record of soils may also reflect (changing) climatic conditions. Magnetic susceptibility variations in loess/paleosol sequences, for instance, correlate well with oceanic oxygen isotope stages (Dunlop & Özdemir 1997), and thus are climatically controlled. In addition, spatial patterns of magnetic susceptibility variations in soils can also be used to reveal human impact (e.g. Thompson & Oldfield 1986; Dalan & Banerjee 1996). Local disturbance of magnetic soil profiles may provide additional evidence for the presence of man on archaeological sites. Ploughing, for instance, can cause such disturbance, while man-made fires, like natural fires, usually cause magnetic anomalies because this process transforms weakly magnetic soil hematites and goethites to strong ferrimagnetic maghemite. Furthermore, the extent of anthropogenically-induced pollution in industrialized areas can also be detected by means of magnetic measurements. Industrially-derived dust and fly ashes usually contain ferrimagnetic spinel-phases, and

thus causes a distinct magnetic enhancement of the topsoil (e.g. *Strzyszcz* 1993; *Heller et al.* 1998).

Formation Processes of Maghemite in Soils

Maghemites concentrated in the surface layers of soils are frequently Al-substituted, whereas the more homogeneously distributed maghemites often appear to be titaniferous. The specific distribution throughout the soil profile and the different impurity cation does not suggest a common origin for these two maghemites. *Mullins* (1977) and *Schwertmann* (1988b) identified various mechanisms by which maghemite can be formed in soil.

1. *Low-temperature oxidation of magnetite.* Magnetite present in soils may be of either **lithogenic origin** (i.e. magnetite inherited from the parent rock by weathering), **detrital origin** (i.e. water- or wind-transported erosion products) or of **authigenic origin** (i.e. fine-grained magnetite formed in situ biogenically or by organic or inorganic pedogenesis). The omnipresence of maghemite in soils developed on highly weathered basic and ultrabasic igneous rocks is explained by the oxidation of inherited primary magnetites (e.g. *Schwertmann & Latham* 1986; *Fontes & Weed* 1991; *Trolard et al.* 1995). The Ti typically present in these magnetites is retained in the structure during oxidation. Oxidation of lithogenic magnetite usually causes a relative homogeneous distribution of titaniferous maghemite during progressive pedogenesis. For relatively mature soils with large contents of inherited ferrimagnetic minerals, *Fine et al.* (1989), however, proposed a mechanism for preferential accumulation of oxidized lithogenic magnetites in the topsoil. They suggested that leaching of easily weatherable minerals and the subsequent dilution of relatively weathering-resistant ferrimagnetic minerals in illuvial horizons, may produce and intensify magnetic enhancement of eluvial horizons. Detrital and authigenic magnetites typically are accumulated in the topsoil. Oxidized detrital magnetites may be Ti-substituted depending on their origin. Authigenic magnetites typically are more pure and are not Ti-substituted.

2. *Dehydration of lepidocrocite.* γ -FeOOH can dehydrate directly to form maghemite. During laboratory heating, dehydration typically occurs around 250°C (see Subsection 5.3.4). Natural dehydration on a pedogenic time scale, however, may occur at substantial lower temperatures. Lepidocrocite is generally less widespread than its polymorph, goethite. This mechanism is restricted to some specific soil types and cannot account for the common occurrence of maghemite in soils. Lepidocrocite usually is not Al-substituted, because Al in the system favors the formation of goethite (*Taylor & Schwertmann* 1978a; *Schwertmann* 1988).

3. *Natural burning in the presence of organic matter.* In (sub)tropical areas, accumulation of maghemites in the topsoil is frequently attributed to heating (ca. 300–800°C) of other, often Al-substituted, pedogenetic Fe-oxides in the presence of organic matter during fires. It can be envisaged as a two-stage process. First, the combined influence of heat and reducing conditions causes the transformation of finely divided Fe-oxides and oxyhydroxides to magnetite, which is then subsequently oxidized to maghemite on cooling under the less reducing conditions which may follow after the combustion of the soil organic matter. The amount of maghemite formed is a function of

the degree (i.e. rate) and duration of heating, the type and amount of ferruginous material, the mineralo-chemical properties of the source mineral, as well as the type of organic matter initially present (Fitzpatrick 1988; Schwertmann & Fechter 1984). Pedogenic goethites and hematites are the most appropriate precursor minerals because of their abundance and their usual Al for Fe substitution in soil environments. This mechanism may explain the occurrence of high amounts of maghemite in soils developed on rocks low in magnetite. Since most soils in tropical and subtropical regions have at some stage in the last thousand years been subject to natural or man-made fires this mechanism may be of considerable importance, especially when vegetated soils with limited air access are set on fire (Mullins 1977). The close positive relationship between the abundance of maghemite in those regions and that of corundum ($\alpha\text{-Al}_2\text{O}_3$) is a strong indication for the reliability of this process because corundum is clearly a heating product of Al compounds (Anand & Gilkes 1987b). Furthermore, the common presence of charcoal in localized maghemite-bearing soils in temperate areas also points to their association with fires.

4. *Repeated oxidation-reduction cycles.* Another mechanism that magnetically enhances the topsoil is the formation of microcrystalline ($\ll 1 \mu\text{m}$) maghemite from iron oxides or oxyhydroxides by repeated oxidation-reduction cycles. Alternate wetting and drying of the surface soil is thought to provide the necessary change in redox conditions. The processes involved in this mechanism are complex and poorly understood. However, the decay of organic matter under anaerobic conditions prevailing during wet periods (i.e. fermentation) seems to provide the reducing conditions and chelating agents needed to bring into solution the iron formerly present in weakly magnetic oxides and oxyhydroxides (Taylor & Schwertmann 1974b; Schwertmann & Taylor 1977; Mullins 1977). Oxidation of the formed products occurs during subsequent dry aerobic conditions. Taylor & Schwertmann (1974b) and Taylor (1980) simulated these reductomorphic conditions in the laboratory and suggested that greenish-blue $\text{Fe}^{2+}(\text{Fe}^{3+} \text{Al}^{3+})$ hydroxysalts, so-called green rusts, can be an intermediate phase in these processes. According to the authors, maghemite appears to be the typical product of slow oxidation of this green rust at pH around 7–8. Cycles of oxidation and reduction may thus record variations in rainfall (Mullins 1977). This process is particularly evident in Mediterranean soils formed on a permeable limestone substratum (Tite & Linington 1975).

5.3 Mineralogical and crystallographic characteristics

5.3.1 Crystal structure

The minerals of the solid-solution series between the end members magnetite and maghemite crystallize in the inverse spinel structure, which can be indexed in the cubic crystal system. In principle, magnetite as well as the non-stoichiometric oxidized spinels all have the space group $Fd\bar{3}m$. On oxidation, magnetite transforms to maghemite by changing the valence state of two third of the original Fe^{2+} to Fe^{3+} , while simultaneously removing one third of the original Fe^{2+} , necessary for charge balance: $3\text{Fe}^{2+} \rightarrow 2\text{Fe}^{3+} + \square$.

This removal occurs by solid-state diffusion producing *vacancies* (\square) in the spinel structure where a Fe^{2+} cation had previously resided. These vacancies account for the name *cation-deficient spinel*, and cause the density to decrease from $\sim 5.18 \text{ g cm}^{-3}$ for magnetite to $\sim 4.87 \text{ g cm}^{-3}$ for maghemite (cf. Cornell & Schwertmann 1996). In addition, progressive maghemitization cause the X-ray diffraction peaks characteristic of the cubic spinel lattice to shift to lower d -values, and an approximately linear decrease in the cubic unit cell parameters from $a = 0.8396 \text{ nm}$ for magnetite to $a \approx 0.833\text{--}0.835 \text{ nm}$ for maghemite is reported (Lindsley 1976a, Fig. L-9). The oxidation parameter z thus can be estimated using the measured cell parameter, provided the mineral is pure or the effects of solid solution of components such as Ti and Al are known. Furthermore, on oxidation, the black colour of magnetite changes to the red-brown of maghemite.

As maghemite can be considered as a non-stoichiometric defect magnetite with incomplete spinel cation site occupancy (Waychunas 1991), its structure can be thought of as derived from magnetite. The maghemite structure, however, is more complex and appears to have many variants mainly characterized by a different positioning of the vacancies. Therefore, before reviewing the various possible maghemite structures, a description of the general spinel and magnetite structure is given first.

The Spinel Structure

The spinel structure consists of a framework of cubic close-packed (*ccp*) anion layers (cf. O'Reilly 1984). The O^{2-} layers may be seen forming (111) planes of a face-centered cubic (*fcc*) lattice stacked orthogonal to the cube diagonal [111] direction in an ABCABC-sequence (Fig. 5.3a). The oxygen framework encloses octahedral (sixfold coordination) as well as slightly smaller tetrahedral (fourfold coordination) interstices for cations, often referred to as A and B positions respectively (Fig. 5.3b). In general, the cations are slightly larger than the interstices. The flexibility of the oxygen framework, however, allows a wide range of cations to become incorporated in the spinel lattice. The inter-layer spacing as well as the intra-layer spacing (O–O distance) is relative easily adapted to the specific size of the cations (Waychunas 1991). The anion displacements appear to introduce a corrugation into the anion layers (Zoltai & Stout 1984).

In spinel oxides only 1/8 of the available tetrahedral interstices and 1/2 of the octahedral interstices are occupied due to charge balance considerations. The general chemical formula for ideal stoichiometric spinels is XY_2O_4 , where X and Y are cations of different valence. Various valence combinations are possible but for stoichiometric spinels the average valence of the cations must always be 8/3. The spinel *fcc* unit cell contains eight formula units. Layers of cations alternate with the oxygen layers along the triad axis [111]; cation layers in which all the cations are in six-fold coordination alternate with others in which the cations are distributed among A and B positions. Spinel is classified as *normal* or *inverse*, depending on the distribution of cations among the A and B positions. The specific distribution of cations is of great importance for rock and mineral magnetism as it defines the magnetic properties of the mineral. In the *normal* spinel structure all octahedral sites are occupied by identical cations. That is, 16 trivalent cations occupy the 16 octahedral sites and 8 divalent cations occupy the 8 tetrahedral

sites, giving the structural formula $R^{2+}[R^{3+}]O_4$, where brackets denote cations in octahedral sites. In *inverse* spinels, however, the octahedral sites are shared by two different cations; i.e. 8 of the 16 trivalent cations occupy the 8 tetrahedral sites, giving the structural formula $R^{3+}[R^{3+} R^{2+}]O_4$.

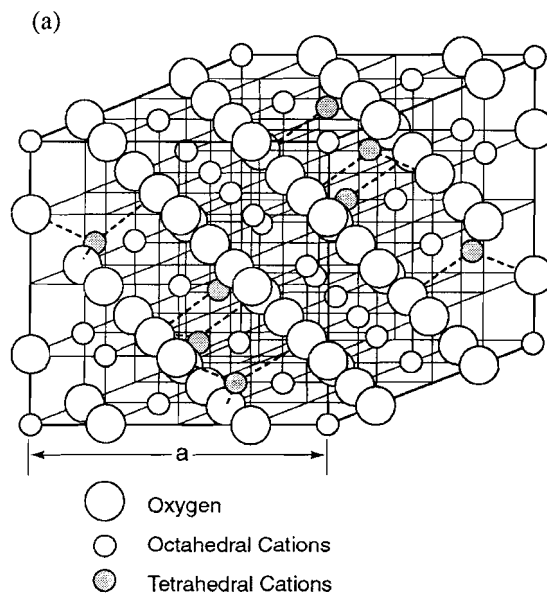
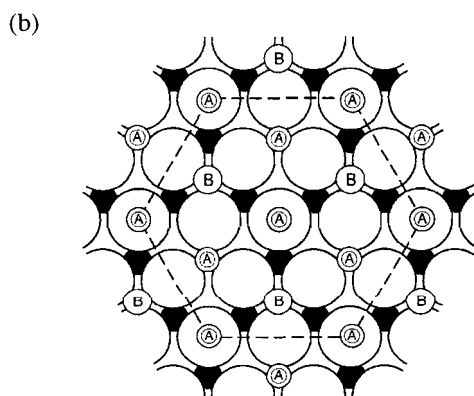


Figure 5.3: (a) The spinel unit cell positioned to achieve a optimal view of the (111) planes (Redrawn from Lindsley 1976). (b) Occupation of the octahedral and tetrahedral interstices in magnetite. Solid circles denote Fe atoms in octahedral interstices below the oxygen layer (large open circles). Small open circles denote Fe atoms in tetrahedral (A) and octahedral (B) interstices above the oxygen layer.



The Structure of Magnetite (Fe₃O₄)

The crystal structure of magnetite was first described by Bragg (1915) and Nishikawa (1915) using X-ray diffraction. In the inverse spinel structure of magnetite the tetrahedrally coordinated site per formula unit (*pfu*) is occupied exclusively by Fe³⁺ (ionic radius 0.67 Å), while the two octahedrally coordinated sites are randomly occupied by the larger Fe²⁺ (ionic radius 0.83 Å) and the remaining Fe³⁺ ion, i.e. Fe³⁺[Fe³⁺ Fe²⁺]₂O₄ (Lindsley 1976a & b).

The random distribution of B site Fe³⁺ and Fe²⁺ ions at room temperature makes 'electron-hopping' possible, which causes the relatively high electrical conductivity of magnetite. At this temperature the hopping mechanism (small polaron model) has a small activation energy of only 0.065 eV (*cf. Waychunas* 1991). Due to the fast electron transfer, the individual Fe ions at the octahedral positions appear to have an intermediate valence of 2.5 (*cf. Waychunas* 1991). However, as magnetite is cooled the hopping rate slows, until at about -155°C the conductivity decreases abruptly. This is the onset of the crystallographical Verwey transition (*T_v*), and signals the ordering of the octahedral cations resulting in a large increase in activation energy for polaron conduction. This first order transition is also accompanied by a sharp change in magnetocrystalline anisotropy (see Subsection 5.4.4). Below *T_v*, where magnetite behaves as an insulator, the magnetite structure is now believed monoclinic or even triclinic and not orthorhombic, as was believed before (*Miyamoto & Chikazumi* 1988).

The Structure of Maghemite (γ-Fe₂O₃)

Maghemite has a structure comparable to that of magnetite as can easily be deduced from the similarity of their X-ray diffraction patterns. The vacancies in the cation-deficient spinel lattice of maghemite, however, cause the structure to be more open compared to that of stoichiometric spinels. The formula for maghemite can also be written as Fe_{2.67}□_{0.33}O₄; the unit cell thus contains 2²/₃ vacancies, 21¹/₃ Fe³⁺ ions and 32 O²⁻ ions.

Vacancy distribution: The arrangement of the vacancies in the spinel-like lattice of maghemite appears to be very variable, and is still somewhat controversial. The exact positioning of the vacancies determines the final symmetry of the substance. Hence, for structure-dependent physical properties, what is called maghemite actually is indeed various different phases, characterized by a different positioning of the vacancies (*Pecharromán et al.* 1995; *Eggleton et al.* 1988). The vacancies could occur in either octahedral sites or mixed over both tetrahedral and octahedral sites. The presence of a stable maghemite with only tetrahedral vacancies has been discounted by *Lindsley* (1976a & b). In addition, the arrangement of the vacancies in maghemite appears to be affected by the crystallite size and the mode of formation.

Octahedral sites only: Most experimental evidence supports the tendency for the vacancies to occupy octahedral sites only (e.g. *Armstrong et al.* 1966; *Haneda & Morrish* 1977a; *Greaves* 1983; *Boudeulle et al.* 1983; *Coey* 1987; *Collyer et al.* 1988), leading to

the structural formula $\text{Fe}^{3+}[\text{Fe}^{3+} \text{Fe}^{3+}_{2/3} \square_{1/3}]_4\text{O}_4$. Three different varieties of maghemite with completely filled tetrahedral spinel sites are yet generally accepted. The structures can be thought of as derived from magnetite, by replacing the eight Fe^{2+} ions on octahedral sites by the charge equivalent of $5\frac{1}{3}$ Fe^{3+} ions plus $2\frac{2}{3}$ cation vacancies, and are characterized by a different degree of long-range crystal order of the vacancies (Pecharrómán *et al.* 1995; Eggleton *et al.* 1988). The atomic coordinates of these three idealized crystal structures are summarized by Pecharrómán *et al.* (1995; Table 1, page 22).

1) If the vacancy distribution is totally random, all octahedral spinel positions are statistically equivalent and the material has a face-centered cubic structure with an average $Fd\bar{3}m$ symmetry, i.e. the same as in the fully occupied stoichiometric ideal spinel. If the vacancies, however, tend to be placed in some particular position, the symmetry of the structure reduces. 2) Partial ordering of the vacancies in maghemite leads to a primitive cubic structure (space group $P4_132$ or the enantiomorphous $P4_332$) similar to that of ordered lithium ferrite $\text{Fe}_8[\text{Li}_4\text{Fe}_{12}]\text{O}_{32}$, with the vacancies taking the place of the Li atoms (e.g. Braun 1952; Van Oosterhout & Rooijmans 1958; Smith 1979; Collyer *et al.* 1988). 3) Total ordering of the vacancies, i.e. vacancies order along a fourfold screw axis with a translation of $\frac{1}{4}c$ on the Li^+ sites in lithium ferrite, causes a tetragonal superstructure with space group $P4_32_12$ (e.g. Van Oosterhout & Rooijmans 1958; Haneda & Morrish 1977a; Greaves 1983; Boudeulle *et al.* 1983). The tetragonal unit cell is three times as large as in the c direction as that of spinel, i.e. $c = 3a$. Vacancy ordering can be particularly evident in X-ray diffraction, where maghemites with vacancy ordering show typical superstructure lines (extra reflections) that are inconsistent with the face-centered cubic system, and thus can be used to distinguish between maghemite and magnetite.

The usually quoted unit cell dimension for *fcc* maghemite is $a \approx 0.834$ nm (cf. Schwertmann & Cornell 1991). Goss (1988) describes a face-centered maghemite with $a = 0.83419 \pm 0.00006$ nm, which changes upon heating to a primitive cubic maghemite with $a = 0.83505 \pm 0.00005$ nm. Van Oosterhout & Rooijmans (1958) firstly reported maghemites with a tetragonal symmetry superlattice; $a = 0.8330$ nm and $c \approx 3a$. More recently, Greaves (1983) concluded from powder neutron diffraction data that these tetragonally ordered maghemites have a unit cell with $a = 0.83396$ nm and $c = 2.4996$ nm. Schwertmann & Cornell (1991) quoted $a = 0.8338$ nm and $c = 2.5014$ nm for the tetragonal unit cell.

Other ordering schemes of the vacancies and cations in maghemite: Takei & Chiba (1966) concluded from their high saturation magnetization value obtained on epitaxially-grown single crystals of maghemite (MgO substrate) that nearly 20% of the total amount of vacancies should occupy tetrahedral interstices. Weber & Hafner (1971), Annersten & Hafner (1973) and Ramdani *et al.* (1987) found also some indication that part of the vacancies could be on A sites as well, at least for those maghemites prepared by oxidation of magnetite. Goss (1988) proposed a slight increase in tetrahedral Fe^{3+} ions together with a related increase in octahedral vacancies to explain the reduced saturation magnetization obtained for his maghemite samples.

Effect of crystallite size and mode of formation on the vacancy distribution: Feitknecht (1964) oxidized synthetic magnetite crystals (ca. 200 nm) and found that intermediate compositions ($\text{Fe}^{2+}/(\text{Fe}^{2+} + \text{Fe}^{3+}) = 0.30\text{--}0.19$) had a primitive cubic structure while on further oxidation ($\text{Fe}^{2+}/(\text{Fe}^{2+} + \text{Fe}^{3+}) < 0.13$) the tetragonal superstructure appears. For magnetite particles smaller than 100 nm, however, no vacancy ordering was observed in the resultant maghemite. Haneda & Morrish (1977) also reported the degree of vacancy ordering to decrease with decreasing particle size; ordering of the vacancies was prohibited in maghemites smaller than about 20 nm. Goss (1988) found that synthetic colloidal magnetite oxidizes to hematite via at least two metastable maghemites. The first of these, created through low-temperature oxidation by the formation of a magnetite/maghemite solid solution, is a face-centered cubic maghemite (fully oxidized end member $\sim 500^\circ\text{C}$). Before this maghemite transforms to hematite the vacancies in the structure order ($\sim 600\text{--}800^\circ\text{C}$) to give the second maghemite with a primitive cubic structure. A study by Xu *et al.* (1997) on coarse-grained ($\sim 1\text{--}10\ \mu\text{m}$) FeTi-oxides present in ocean-floor basalts of different ages (i.e. different oxidation degrees) indicated that long-range ordering of vacancies occurs only at the final stages of oxidation and hence is at least in part a separate process. Furthermore, commercial acicular maghemite particles ($\sim 200\ \text{nm}$) made from hematite by a reduction-oxidation process generally have the tetragonal unit cell, while maghemite particles of similar size obtained by dehydroxylation of lepidocrocite show no superstructure (cf. Cornell & Schwertmann 1996). During dehydroxylation, the water molecules leave the lepidocrocite crystals causing the host structure to break up and as a result, only tiny crystallites of maghemite form in which no ordering of vacancies can take place.

5.3.2 Cationic substitution and water in the structure

The Fe-atoms in the spinel structure of magnetite and maghemite can easily be replaced by a large range of other cations mainly because of the flexibility of their oxygen framework. Partial replacement of iron with titanium and to a lesser extent with aluminium are by far the most common examples of isomorphous substitution reported for natural maghemites. Ubiquitous Ti-substituted maghemites have primary high-temperature Ti-magnetites as their precursor, while Al-substitution is a common phenomenon in soil maghemites produced from other secondary iron oxides and oxyhydroxides during pedogenesis. On the other hand, Al^{3+} is also the most frequent impurity cation in natural intermediate titanomagnetites (TM60) present in submarine basalts (e.g. Özdemir & Moskowitz 1992). In addition, other metals such as Ni, Cr, Co, Zn, Mn, Mg, V and Cu may also substitute for Fe in magnetites and maghemites (e.g. Deer *et al.* 1980; Schwertmann & Cornell 1991; Trolard *et al.* 1995). Spinel phases present in industrially-derived dust, such as fly ash, generally contain a wide variety of these impurity cations (e.g. Dekkers & Pietersen 1992; Heller *et al.* 1998). Synthetic maghemites for magnetic recording devices are often doped with up to 5% Co to improve coercivity and storage capacity (cf. Cornell & Schwertmann 1996).

Sidhu et al. (1980) followed the behavior of some isomorphously substituted trace elements (<1 mole %) in magnetite during the alteration to maghemite. Co, Ni and Zn were randomly distributed within the magnetite structure and replaced octahedral Fe²⁺. In contrast, dissolution curves indicated that Cu, Mn and Cd appear to be concentrated near the surface of the crystals. The trace elements were retained within the maghemite. However, after complete conversion an outer zone free from trace elements was formed around the crystal indicating that oxidized Fe had migrated outwards and formed a new maghemite layer leaving the trace elements in the core.

Titanium Substitution

Primary magnetites crystallized from igneous melts generally contain significant amounts of Ti, and these titanomagnetites form a complete solid-solution series between the end members magnetite and ulvöspinel. The general formula for ideal stoichiometric titanomagnetite is Fe_{3-x}Ti_xO₄ (0 < x < 1). The Fe for Ti substitution causes the titanomagnetite unit cell to increase from ~0.8396 nm for magnetite to ~0.8535 nm for ulvöspinel (e.g. *O'Reilly* 1984 and references therein). In the oxidized equivalents of the titanomagnetite series, both Fe for Ti substitution and the substitution of vacancies for Fe-atoms occurs (cf. *Collyer et al.* 1988). The principle in going from the pure Fe-oxide to the Ti-containing phase is to replace two Fe³⁺ by one Fe²⁺ and one Ti⁴⁺. Hence, every Ti-substituted maghemite also contains some divalent iron in its lattice because of charge balance considerations. The generalized chemical formula for Ti-maghemites produced according to the 'addition of oxygen' model is: Fe_{(3-x)R}Ti_{xR}□_{3(1-R)}O₄ with 0 < x < 1 and R between 1 and 8/(9 + x), or more explicitly Fe_{(1-z)(1+x)R}²⁺ Fe_{(2-2x+z+zR)R}³⁺ Ti_{xR}⁴⁺ □_{3(1-R)} O₄²⁻ where R = 4/{4 + (z/2)(1 + x)} (*O'Reilly* 1984). Titanomagnetites are conventionally defined to have 0 ≤ z ≤ 0.1. Any Fe-Ti spinel oxide outside this range is referred to as titanomaghemite (cf. *Waychunas* 1991). *O'Reilly & Readman* (1971) and *Nishitani & Kono* (1983) determined the unit cell parameter for titanomaghemites synthesized by the 'addition of oxygen' mechanism. The cell edge appear not to be very sensitive to cation distribution and it is probable that no great differences would result from maghemitization by alternative mechanisms (*O'Reilly* 1984).

The structure and the cation and vacancy distributions in titanomaghemites remain uncertain. The distribution of cations and vacancies between the sublattices of the titanomaghemites most likely depends on both the cation distribution in the initial titanomagnetite and the maghemitization mechanism, i.e. 'addition of oxygen' or 'removal of metals' (cf. *O'Reilly* 1984). Various models are presented in literature to predict the cation distribution in magnetites and maghemites with increasing Ti for Fe substitution (e.g. *Néel* 1955; *Chevallier et al.* 1955; *O'Reilly & Banerjee* 1965; *Readman & O'Reilly* 1971). All models assume a high preference of Ti⁴⁺ for the octahedral sites (*Waychunas* 1991), which is in agreement with neutron-diffraction studies (e.g. *Ishikawa et al.* 1971) and magnetic measurements (*O'Reilly & Banerjee* 1965; *Stephenson* 1969). The arrangement of Fe²⁺, Fe³⁺ and vacancies, however, varies per model and appears to

depend on the amount of substituted Ti. More recently, *Collyer et al.* (1988) studied the crystal structure and crystal chemistry of a natural single crystal of an intermediate ($x = 0.47$, $z = 0.82$) titanomaghemite, and discussed his results in the light of the previously published models. A crystal-structure parameter refinement of the mineral indicated a primitive cubic lattice with $a = 0.8341$ nm and space group $P4_332$. According to these authors, divalent iron and titanium are restricted to octahedral sites in this intermediate titanomaghemite. Cation vacancies, however, appear on both tetrahedral and octahedral sites, the majority being on the octahedral sites. Combined single-crystal X-ray studies and Mössbauer spectroscopy of the titanomaghemite gave the following structural formula: $\text{Fe}_{0.96}^{3+} \square_{0.04} (\text{Fe}_{0.23}^{2+} \text{Fe}_{0.99}^{3+} \text{Ti}_{0.42}^{4+} \square_{0.37}) \text{O}_4$. This distribution was consistent with the *Chevallier et al.* (1955) model of precursor titanomagnetite spinel cation distribution, and, except for the small amount of tetrahedral vacancies, with the model of *Readman & O'Reilly* (1971) for titanomagnetite oxidation (*cf. Waychunas* 1991). For more comprehensive reviews on this subject the reader is referred to *Lindsley* (1976a) and *Waychunas* (1991), and references in both.

Aluminium Substitution

Aluminium is commonly present in authigenic soil hematites and goethites, and is (partly) retained in the lattice during their heating-induced transformation to maghemite. The extent of aluminium substitution in soil goethites appears to be limited to $\frac{1}{3}$ (33 mole %) and in soil hematites to $\frac{1}{6}$ (16 mole %) of the possible octahedral positions (*Schwertmann & Cornell* 1991). Al-substitution up to 15 mole % has been reported for maghemites found in tropical soils (*Schwertmann & Fechter* 1984; *Schwertmann & Latham* 1986; *Fontes & Weed* 1991). This value seems to be the solubility limit of Al in maghemites produced in the soil environment during a fire in the presence of organic matter.

Experiments on synthetic minerals suggest a dependence of the Al solubility limit in maghemite on its precursor mineral. *Da Costa et al.* (1994, 1995), for example, produced Al-maghemites by heating a mixture of synthetic Al-hematite and an organic compound (sucrose) followed by oxidation of the reaction product. Their data seem to indicate that the solubility limit of Al for this type of maghemite is at least 15 mole %. *Wolska & Schwertmann* (1989), on the other hand, reported a solubility limit of ca. 10 mole % for Al-maghemites produced by sequentially heating Al-ferrihydrite, reducing the product to magnetite and reoxidizing the magnetite to maghemite. For maghemites formed by firing goethite, *Schwertmann & Fechter* (1984) suggest that Al-substituted maghemites are only the dominant phase if the Al-substitution was <10 mole % in the parent goethite, otherwise hematite will be dominant.

Several recent studies have shown that Al has no site preference, its location being dependent on the synthesis procedure and on its concentration. However, there are reports in which all Al are located exclusively on the tetrahedral sites (*Da Costa et al.* 1994; *Goulart et al.* 1998), on the octahedral sites (*Allan et al.* 1989; *De Jesus Filho et al.* 1992; *Bowen et al.* 1994) or on both sites (*Wolska & Schwertmann* 1989; *Da Costa et al.* 1995).

The diameter of the Al cation is smaller than that of the Fe^{3+} cation by ca. 16% (Eggleton *et al.* 1988). As a result, the dimension of the unit cell will decrease upon progressive Al-substitution, illustrated by a shift of the X-ray line positions to lower d-values. Both Schwertmann & Fechter (1984) and Da Costa *et al.* (1995) reported a linear relation between the unit cell length and the substitution by Al at least upto 10 mole %. The first authors determined a calibration curve with $a = 8.343 \text{ \AA} - 2.22 \times 10^{-3} \text{ Al}$ (mole %).

'Hydrogen' Maghemite

The fact that an aqueous environment does promote maghemitization rather than direct oxidation of magnetite to hematite, together with the observed metastability of maghemite upon heating led different authors to suggest that the structure may require bonded water for stabilization (Braun 1952; David & Welch 1956; Van Oosterhout & Rooijmans 1958; Elder 1965; Rao *et al.* 1974). The presence of this combined water is thought to be due to protons (H^+) replacing Fe^{3+} in the structure leading to the formation of $(\text{OH})^-$. However, neutron diffraction investigations by Greaves (1983) showed no evidence for the presence of structural H^+ ions, and the kinetic studies of Giovanoli & Brüttsch (1975) also conclude that H^+ is absent from the structure (*cf.* Goss 1988). The absolute necessity of H^+ ions for stabilizing the maghemite structure is thus quite unlikely, but it is not excluded that hydrogen might become incorporated into the maghemite structure during formation in an aqueous environment or due to the presence of structurally bound water in the precursor mineral. Braun (1952) and Swaddle & Oltmann (1980), for example, reported that their maghemite contains ca. 2% water which is partly exchangeable with Na^+ and K^+ . Sidhu (1988) transformed several trace element-substituted synthetic maghemites to hematite. During heating all maghemites showed a diffuse endothermic peak at about 350°C accompanied by a slight loss in weight which according to the author might represent the loss of 1% of combined water. De Bakker *et al.* (1991) found the inversion temperature of $\gamma\text{-Fe}_2\text{O}_3 \rightarrow \alpha\text{-Fe}_2\text{O}_3$ to decrease with the amount of excess water molecules present in the lepidocrocite precursor of the maghemite. The authors proposed the incorporation of $(\text{OH})^-$ ions in the maghemite lattice to explain the observed relation. Wolska & Baszynski (1986) suggested the presence of residual hydroxyl groups in the lattice of their maghemites from the measured IR spectrum.

For this 'hydrogen' maghemite a structure analog to lithium ferrite $\text{Fe}[\text{Li}_{0.5}\text{Fe}_{1.5}]\text{O}_4$ is suggested, i.e. $\text{Fe}[(\text{H}_{(1-x)/2}\text{Fe}_{x/6}\square_{x/3})\text{Fe}_{3/2}]\text{O}_4$, where the () brackets denote cations on lithium sites (Braun 1952; Van Oosterhout & Rooijmans 1958). If existing, this structure would have a primitive cubic lattice. In this perspective it is necessary to mention that the maghemites investigated by Greaves (1983) possessed a tetragonal superstructure. The primitive cubic maghemite obtained by Goss (1988), however, most likely does not contain any H^+ ions.

5.3.3 Microstructure

Crystal Morphology

Maghemite is usually formed by solid-state transformations from another iron oxide or iron compound and as a result virtually always adopts the morphology of its precursor. In practice this means that natural maghemite most abundantly forms pseudomorphs after magnetite and to a lesser extent after lepidocrocite.

When formed by oxidation of magnetite, either cubic or irregular maghemite particles occur. The typical shape of natural magnetites observed in well-crystalline samples are cubes, octahedra, dodecahedral, or quasi-spheres (*Schwertmann & Cornell* 1991). Magnetites in lavas quenched from the melt may have skeletal, cruciform, dendritic or other irregular forms (e.g. *Xu et al.* 1997), while secondary magnetites in metamorphic rocks usually conform the space available. Detrital oxidized magnetites present in sediments and soils often have an equidimensional subrounded shape due to transport (*Schwertmann & Taylor* 1977). Maghemite formed by dehydroxylation of lepidocrocite predominantly forms laths elongated in the [110] direction. Less common tabular lepidocrocite dehydrates to more platy-developed maghemite. *Abreu & Robert* (1985) identified needle-like particles of maghemite in the sandy fractions of a soil. The needles were arranged in star-like patterns on the surface of quartz grains. They postulated that the formation of this typical maghemite morphology would be catalysed by quartz surfaces.

Certain maghemite morphologies are desirable for industrial applications. Needles of maghemite, for example, are required for magnetic tapes because they can be orientated in a strong magnetic field during the manufacturing process and display a high magnetization and coercivity, i.e. high magnetic stability. On the other hand, maghemite pigments for the use in paints should be equant because otherwise they tend to orient themselves with the brush stroke. Considerable effort has, therefore, been directed towards producing maghemites with a well-defined habit and, where possible, uniform size distribution (*cf. Cornell & Schwertmann* 1996).

The usual procedure to obtain a specific maghemite habit is by selecting a suitable precursor mineral and eventually modifying its morphology by appropriate additives during synthesis. Commercial needle-shaped maghemite crystals for magnetic recording devices are produced in a series of steps from acicular goethite. This process involves the dehydroxylation of goethite to hematite (200–300°C), then reduction to magnetite in a H₂ atmosphere and finally reoxidation to maghemite in air at 250 to 400°C (*Berkowitz et al.* 1985). Spindle-shaped hematites are also often used as a precursor mineral in this manufacturing process mainly to avoid the initial dehydration step and hence pore formation (*Maeda* 1978; *Ozaki & Matijevic* 1985). The starting material is stabilized against sintering during the thermal treatment by being coated with silicate or phosphate (*cf. Cornell & Schwertmann* 1996).

Morales et al. (1989) produced a variety of platy maghemites. Porous platy crystals with extensive development of the (110) planes were produced by transformation of FeOOCH₃, while more finely divided plates were obtained by decomposition of N₂H₅Fe-(N₂H₃COO)₃. *Batis-Landoulis & Vergnon* (1983) precipitated twinned,

monodisperse maghemite crystals bounded by {110} and {111} faces directly from a vapour phase reaction in a O₂/H₂ flame.

Crystallinity, Grain size and Porosity

The crystallinity of maghemite particles is highly affected by the crystallinity of its precursor mineral and the temperature involved. The crystallinity of commercial maghemites is generally improved by annealing the precursor mineral if possible, or by repeating the oxidation–reduction steps several times.

Unlike incompletely oxidized (Ti)magnetites, pure maghemite single crystals larger than ≈1 μm can rarely be found in nature and appear extremely difficult to synthesize (Stacey & Banerjee 1974). The reason is inherent to the formation process of maghemite, i.e. the oxidation mechanism of magnetite and the dehydroxylation process of lepidocrocite (for detailed description see Subsection 5.3.4).

Since oxidation of magnetite to maghemite is controlled by diffusion, it mainly is a surface process. Only in relatively small magnetite grains, diffusion pathways are short enough for complete transformation of Fe₃O₄ → γ-Fe₂O₃ to take place (e.g. Feitknecht 1964; Gallagher *et al.* 1968; Gillot *et al.* 1978). In coarse magnetite grains, on the other hand, an initially formed outer rim of maghemite generally blocks further conversion. Due to the lattice mismatch between both phases, structural strain builds up between the oxidized surface layer and the less –or even unoxidized magnetite– core, which often results in the development of contractional microcracks in the surface layer (e.g. Johnson & Hall 1978; Petersen & Vali 1987). This process effectively subdivides the original particle, causes a reduction in the effective grain size of the maghemite phase and promotes further oxidation. Finally it may lead to a total disintegration of the original grain into several fine-grained maghemite particles.

During dehydroxylation of γ-FeOOH, the original needle- or plate-like morphology of the lepidocrocite crystals is preserved and relatively large, generally micro- to mesoporous maghemite grains seem to be obtainable in this way. The large maghemite particles, however, in fact are polycrystalline aggregates of perfectly oriented crystallites with an average diameter of about 10 nm (e.g. Giovanoli & Brüttsch 1975). The effective maghemite grain size is therefore extremely fine. The transformation is thus pseudomorphic, rather than genuinely topotactic (*cf.* Cornell & Schwertmann 1996). Giovanoli & Brüttsch (1975) showed that the crystallite size cannot be increased by a longer reaction time.

5.3.4 Transformation processes

Low-temperature Oxidation of Magnetite

Low-temperature oxidation of (Ti)magnetite occurring during subaerial and subaqueous weathering at ambient temperatures, or hydrothermal alteration can lead to the production of single-phase (Ti)maghemite (Lindsley 1991). This process is also referred to as

maghemitization and typically occurs below 250°C. *Lindsley* (1976a & b), however, points out that such non-equilibrium single-phase oxidation can occur at temperatures as high as 600°C (*cf. Dunlop* 1990). This oxidation can take place in stages and miscibility is complete along the join $\text{Fe}_3\text{O}_4 - \gamma\text{-Fe}_2\text{O}_3$ (*Fig. 5.2*).

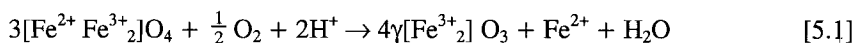
Solid-state diffusion, ferrous iron oxidation and vacancy ordering: As shown in Subsection 5.3.1, transformation of magnetite to maghemite involves a reduction in the number of Fe atoms per unit cell. The Fe/O ratio may be changed by one or both of the mechanisms of ‘addition of oxygen’ or ‘removal of iron’ (*cf. O’Reilly* 1984). The mechanisms essentially appear to occur by solid-state diffusion of Fe^{2+} to crystal boundaries, leaving disordered lattice vacancies, and the surface Fe^{2+} then oxidizes to Fe^{3+} (e.g. *Feitknecht* 1964; *Gallagher et al.* 1968). Long-range ordering of vacancies may occur as a (partly) independent process at intermediate to final stages of the transformation, at least in grains $>0.1 \mu\text{m}$ (*Feitknecht* 1964; *Xu et al.* 1997).

Being controlled by Fe^{2+} diffusion rates and distance to the surface, the $\text{Fe}_3\text{O}_4 \rightarrow \gamma\text{-Fe}_2\text{O}_3$ transformation proceeds much more rapidly in small crystals than in larger ones (*Nishitani & Kono* 1982). Because of their shorter diffusion pathways and larger specific surface area the smaller grains will become oxidized faster and more thoroughly than the larger grains (*Gallagher et al.* 1968). Ultrafine crystals of magnetite change over years from black to the brown of maghemite even at room temperature (*Murad & Schwertmann* 1993). *Haneda & Morrish* (1977) found 10 nm particles to be 95% oxidized to maghemite already after 50 days at room temperature.

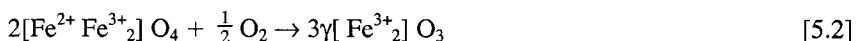
Cornell & Schwertmann (1996) reported a diffusion coefficient at room temperature for cation migration of $1\text{--}2 \times 10^{-15} \text{ cm}^2 \text{ s}^{-1}$. *Van Velzen & Zijdeveld* (1995) quoted that the diffusion rate at 150°C is 12 orders of magnitude higher than that at 30°C. *Sidhu et al.* (1977) showed that substitution of <1 mole % of heavy metals (Co, Ni and Zn) reduces the cation diffusion coefficient.

Activation energies for this transformation of between 83.6 kJ mol^{-1} (*Sidhu et al.* 1977) and 137 kJ mol^{-1} (*Gillot et al.* 1978) have been reported, depending on sample surface area and on whether or not there is Al substitution (*cf. Cornell & Schwertmann* 1996). Other factors that may promote oxidation are crystalline imperfection (*Colombo et al.* 1964), and adsorbed or incorporated water (*Sidhu et al.* 1977).

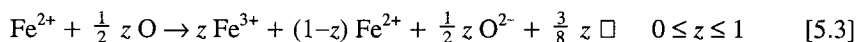
The ‘removal of iron’ and ‘addition of oxygen’ mechanisms: Cations reaching the surface may either be removed (topotactic transformation according to the ‘removal of iron’ mechanism), if the oxidation takes place in the presence of water or hydrothermal solutions, or may nucleate new unit cells of the cation-deficient phase (epitaxial oxid alteration according to the ‘addition of oxygen’ mechanism) (*cf. O’Reilly* 1984; *White et al.* 1994). In the former case, the usual one in nature, the crystal shrinks and may crack (*Petersen & Vali* 1987), leading to finer effective grain size and increased coercive force. This topotactic transformation of magnetite to maghemite under oxid conditions has been experimentally demonstrated at ambient temperatures (*Gallagher et al.* 1968). Such a reaction (eq. 5.1), involves electron exchange with dissolved O_2 to produce ferrous ion and water (*White et al.* 1994).



Epitaxial oxidic alteration occurs when adsorbed oxygen is reduced at the surface by electrons derived from oxidation of structural ferrous atoms within the magnetite structure (Lindsley 1976a & b). Oxygen cannot be added to the cubic-close packed anion framework. Rather, oxygen reacts with ferric atoms which diffuse to the surface, depositing an epitaxial rim of maghemite. The corresponding reaction (eq. 5.2), involves the incorporation of additional oxygen into the newly formed oxide structure (White *et al.* 1994). In this case, the crystal grows, which in a confining matrix may increase the coercive force (Dunlop 1990).



The degree of maghemitization (by oxygen addition) is usually defined by the oxidation parameter labelled 'z' (O'Reilly 1984). It refers to the fraction of Fe^{2+} ions per unit magnetite molecule that has undergone low-temperature oxidation to Fe^{3+} . Hence, for charge balance (O'Reilly & Banerjee 1967; Readman & O'Reilly 1972):



For measuring aqueous oxidation degree, O'Reilly (1984) has proposed a similar parameter z^1 , based on a proposed 'iron removal' mechanism.

Grain-size dependent reaction products: Most laboratory experiments investigating the maghemitization process involve the dry heating of (synthetic) magnetite in air, i.e. oxidation according to the 'addition of oxygen' mechanism. These experiments indicate that initially a mixed phase, $\text{Fe}^{2+}_{1-z} \text{Fe}^{3+}_{2+z} \text{O}_{4+0.5z}$, with less Fe^{2+} , more Fe^{3+} and more cation vacancies than magnetite, forms. This phase then oxidizes further (e.g. Feitknecht 1965). A very important feature of this transformation is the influence of the magnetite crystal size on the nature of the reaction products, at least on a laboratory time scale. Pure, single-phase maghemite only appears to be the end product when dealing with submicron magnetite precursors, (Feitknecht 1964; Gallagher *et al.* 1968; Feitknecht & Gallagher 1970; Readman & O'Reilly 1970; Gillot *et al.* 1978). At 200–250°C, equidimensional magnetite grains with diameters <0.3 μm transformed via the mixed phase to maghemite which in turn transformed to hematite at temperatures above 500°C. In these small crystals, the diffusion pathways are short and reaction rates, therefore, fast, so that complete oxidation is achieved rapidly (*cf.* Cornell & Schwertmann 1996). For slightly larger grains and small z, the mixed cation-deficient spinel is also formed on oxidation, but when z is increased by raising the temperature, nuclei of hematite arise. At 220°C, the outer layer of maghemite that formed initially, blocks further conversion. The spontaneous nucleation of $\alpha\text{-Fe}_2\text{O}_3$ nuclei in the maghemite layer at somewhat higher temperatures (320°C) seems to be related to structural strain developed because of the

large gradient in vacancy concentration (Gallagher *et al.* 1968; Gillot *et al.* 1978). Following this, the remainder of the intermediate mixed phase underlying the maghemite rim disproportionates to a mixture of magnetite and hematite. At temperatures greater than 400°C, the remainder of the magnetite transforms to hematite. In the larger grains only an inversion from Fe_3O_4 to $\alpha\text{-Fe}_2\text{O}_3$ is observed (Gillot *et al.* 1978).

Dehydration of Lepidocrocite ($\gamma\text{-FeOOH}$)

Orthorhombic lepidocrocite ($\gamma\text{-FeOOH}$) dehydrates upon dry heating to cubic maghemite. The transformation temperature on a laboratory time scale is reported to range between 200–280°C when heated in air (e.g. Bernal *et al.* 1957). The name lepidocrocite is derived from the Greek words for scale or flake and saffron-coloured, i.e. *lepidos* and *krokoeis* respectively.

The orthorhombic unit cell of $\gamma\text{-FeOOH}$ contains four formula units and its dimensions are $a = 0.388$ nm, $b = 1.254$ nm and $c = 0.307$ nm (Ewing 1935; Oles *et al.* 1970; Christensen & Nørnlund-Christensen 1978). The structure consists of arrays of *ccp* anions (O^{2-}/OH) stacked along the [051] direction with Fe^{3+} ions occupying the octahedral interstices (Fasiska 1967). The [051] direction of the orthorhombic unit cell corresponds to the [111] direction of a distorted cubic cell and this relationship facilitates dehydroxylation to a spinel phase. Like goethite ($\alpha\text{-FeOOH}$), lepidocrocite consists of double chains of $\text{Fe}(\text{O},\text{OH})_6$ octahedra running parallel to the *c*-axis. The double chains share edges with adjacent double chains and each chain is displaced by half, with respect to its neighbour, thus forming corrugated sheets of octahedra. These sheets are stacked perpendicular to the [010] direction and are separated by double rows of empty octahedral sites. The sheets are held together solely by hydrogen (OH–H) bonds (cf. Cornell & Schwertmann 1996).

TEM observations by Giovanoli & Brüttsch (1975) showed that maghemite nuclei ca. 10 nm across form in a random manner, initially at defects and crystal edges. Further strings of nuclei are then generated along the direction of the lepidocrocite lath axis. Eventually, the original single crystal of lepidocrocite is replaced by a highly ordered aggregate of small maghemite crystals. The morphology of the original crystal is still maintained with the [001] axis and (100) plane of lepidocrocite corresponding to the [110] axis and the (001) plane of maghemite (cf. Cornell & Schwertmann 1996).

During the transformation the corrugated layers of $\text{Fe}(\text{O},\text{OH})_6$ octahedra collapse perpendicular to the *ac*-plane thus inducing more corner- and edge-sharing as is found in the spinel structure of maghemite. This process is accompanied by the formation and release of water molecules (Giovanoli & Brüttsch 1975). The formation of nuclei of maghemite enables the structure to accommodate the strain generated by this process. Increasing the reaction time does not increase the crystallite size, nor does the cation framework order completely. This is because crystallite formation is very rapid and once the lepidocrocite matrix has been disrupted, further diffusion and rearrangement of ions is blocked (cf. Cornell & Schwertmann 1996). The transition temperature of lepidocrocite to maghemite and the size of the resulting particles appear not to be affected by the particle size of the parent lepidocrocite (De Bakker *et al.* 1991).

Inversion to Hematite ($\alpha\text{-Fe}_2\text{O}_3$)

Maghemite is thermodynamically metastable to hematite. The activation energy of the phase transition, however, is relatively high and at normal Earth's surface temperature and pressure $\gamma\text{-Fe}_2\text{O}_3$ is able to persist during geological time. The transformation is thermally activated and compression is also reported to assist the conversion of $\gamma\text{-Fe}_2\text{O}_3$ to $\alpha\text{-Fe}_2\text{O}_3$ (e.g. *Kushiro* 1960). *Adnan & O'Reilly* (1999) studied the inversion of acicular synthetic maghemite particles (ca. 0.5 μm with a length-width ratio of 6:1) and found an energy barrier opposing inversion of 3.7 eV at atmospheric pressure. According to the authors, the energy barrier arises from the combination of a term representing the reduction in lattice energy in an inverted region, and the strain energy associated with the interface between the inverted and non-inverted phases. The height of the energy barrier decreased with increasing pressure, being 0.5 eV at about 100 MPa. The authors argued that the sensitivity of the inversion process to pressure arises from the dependence of the energy barrier terms on interatomic spacing.

The transformation is considered to be topotactic, occurring by restacking of close-packed oxygen ion layers (*ccp* to *hcp*) accompanied by displacement of interstitial ferric ions rather than by wholesale recrystallization (e.g. *Bernal et al.* 1957, 1959; *Kachi et al.* 1963). Hexagonal hematite forms with its (001) planes in the (111) planes of the maghemite, and with the [111] and [110] axes of maghemite corresponding to the [001] and [110] axes of hematite, respectively (see *Fig. 5.4*).

According to *Feitknecht & Mannweiler* (1967), the mechanism of the phase transition appears to depend on crystallite size. Ultrafine maghemite particles (≤ 15 nm) transformed by a chain mechanism involving recrystallization of up to 100 neighbouring particles to large single smooth-edged hematite flakes. With larger crystals of maghemite (ca. 50 nm), there was a one to one transformation with one hematite nucleus forming and growing per crystal (cf. *Cornell & Schwertmann* 1996).

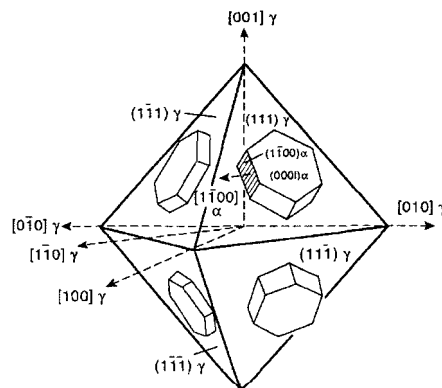


Figure 5.4: Topotactic transformation. Hexagonal hematite crystallites form with their *c*-planes in {111} planes of maghemite (Redrawn from *Kachi et al.* 1963).

The transformation takes place without change in bulk chemical composition but can be monitored by the measurement of structure sensitive physical properties (*cf. Adnan & O'Reilly 1999*). For instance, the progress of inversion can be deduced from X-ray diffractograms or Mössbauer effect spectra (e.g. *Morrish & Sawatzky 1971*). The inversion is also evident during thermomagnetic analyses, because the change in structure is accompanied by a change in the type of magnetism from strong ferrimagnetism for maghemite to the weak spin-canted antiferromagnetism of hematite (see Section 1.4 & 5.4). *Adnan & O'Reilly (1999)*, for instance, used the saturation magnetization and the magnetic susceptibility as a proxy for $\gamma\text{-Fe}_2\text{O}_3$ concentration during the inversion process. Being an exothermic reaction, the transformation can also be monitored by differential thermal analysis (e.g. *Lodding & Hammell 1960*).

Different crystallographic inversion temperatures (T_{inv}) have been reported. On a laboratory time scale, in the dry state and at ambient pressure, T_{inv} may range from $\sim 250^\circ\text{C}$ up to 900°C (e.g. *Bernal et al. 1957; Wilson 1961; Kachi et al. 1963; Özdemir & Banerjee 1984; Özdemir & Dunlop 1988; Özdemir 1990*), depending on the origin of the maghemite, its crystallinity, impurity content, degree of residual Fe^{2+} , and morphological properties such as particle size and shape. It must, however, be understood that the 'high-temperature stability' of various maghemites reported in literature refer to persistence of maghemite against heating rather than to true thermodynamic stability (e.g. *Özdemir & Banerjee 1984*). Because inversion is a thermally activated process, the value of the inversion temperature depends on the time scale over which inversion is allowed to take place, i.e. millions of years in nature (*Adnan & O'Reilly 1999*). Transformation of maghemite to hematite in nature is thus likely to happen at much lower temperatures.

Bando et al. (1965) found T_{inv} to decrease with decreasing particle size and with increasing particle aggregation (*Bando et al. 1965; Özdemir & Dunlop 1988*). In addition, large grains appeared difficult to convert completely to $\alpha\text{-Fe}_2\text{O}_3$. *Feitknecht & Mannweiler (1967)*, reported that hematite nucleation in maghemite crystals $> \sim 70$ nm across was fast, but subsequent hematite growth was slow and a function of the crystal size of the hematite already formed, whereas for smaller sized crystals the hematite nuclei grew rapidly. *Sidhu (1988)* studied the transformation of maghemite with particle diameter of ca. 100 nm. At 500°C , the $\gamma\text{-Fe}_2\text{O}_3$ to $\alpha\text{-Fe}_2\text{O}_3$ transition was completed within 2 h., with no significant alteration of the particle size. However, for temperatures between 320°C and 450°C , the transformation is very slow, and only 10% of the reaction was found to be completed in one week. The same author also showed that small amounts of hematite nuclei already present in the original maghemite crystals before starting the experiment did not enhance the rate of transformation to hematite. Furthermore, the results of *Farell (1972)* indicate that the transformation rate increases with increasing surface area. *Sidhu (1988)* showed that the transformation of maghemite to hematite can be accompanied by a change in the shape of the particles, i.e. reduction in surface area due to sintering of particles on heating. *Morrish & Sawatzky (1971)* reported both size and shape dependencies of T_{inv} . They obtained higher activation energies for spherical particles than for acicular particles. *Imaoka (1968)* found $560^\circ\text{C} \leq T_{\text{inv}} \leq 610^\circ\text{C}$ for acicular but $T_{\text{inv}} \approx 250^\circ\text{C}$ for granular material. *Adnan & O'Reilly (1999)*, however,

argued that variation in concentration and type of internal defects which resulted from different methods of preparation probably play a more important role than the surface of the particle.

Small amounts of impurities such as Mg, Mn, Co and Al in the maghemite lattice are known to raise the inversion temperature (e.g. *Bénard* 1939; *De Boer & Selwood* 1954; *Wilson* 1961; *Morrish & Sawatzky* 1971; *Stacey & Banerjee* 1974). *Wilson* (1961) identified an Al-substituted maghemite in a red-brown laterite baked by a Tertiary lava and reported a T_{inv} between 700°C and 850°C. On the other hand, the most common impurity in nature, Ti^{4+} , is not known to affect the phase transition (*Readman & O'Reilly* 1970). *Sidhu* (1988) found the transformation rate to decrease with slight substitution (≤ 1 mole %) of Co, Ni, Zn, Cu, Mn, Al, V, and Cr for Fe^{3+} ions in the maghemite lattice. The author showed that during the transformation as much as 60% of the Co, Ni, Zn, and Cu present in the crystal structure of maghemite is ejected from the crystals, whereas the Mn, Cr, and Al present in maghemite are redistributed in hematite particles. He argued that the ejection or redistribution of impurity cations requires some additional activation energy and might therefore reduce the transformation rate. *De Bakker et al.* (1991) found the T_{inv} correlated with the amount of excess H_2O molecules present in the original lepidocrocite precursors of the maghemite; the higher this amount of incorporated $(\text{OH})^-$ ions the lower T_{inv} seems to be. *Feitknecht & Mannweiler* (1967) found T_{inv} to increase with increasing amount of residual Cl^- ions in the maghemite lattice.

As mentioned, *Readman & O'Reilly* (1970) argued that Ti^{4+} does not stabilize the metastable cation-deficient structure of maghemite. *O'Donovan & O'Reilly* (1977a & b) and *Özdemir* (1987) studied Mg- and Al-substituted titanomaghemites, respectively. In contrast to their stabilizing effect on the maghemite structure, Mg and Al appear not to have any stabilizing effect on the titanomaghemite structure, i.e. the inversion temperature was almost independent of Mg and Al concentration. In contrast to pure maghemite, the inversion product of titanomaghemite is not a single phase but a multiphase intergrowth of usually magnetite, ilmenite and other minerals (e.g. *Readman & O'Reilly* 1970; *Readman & O'Reilly* 1972; *Özdemir* 1987; *Dunlop & Özdemir* 1997 and references therein).

5.4 Magnetic properties

The magnetic properties of pure maghemite are relatively poorly known compared to those of magnetite, which is the most extensively studied magnetic mineral. Pure and homogeneous maghemite crystals of appreciable size ($>1 \mu\text{m}$) are rarely found in nature and appear hard to synthesize. Hence, so far, no grain-size dependent data for the magnetic properties of maghemite are available. The magnetic properties of maghemite, however, resemble those of magnetite to a large extent as both minerals have fundamentally the same spinel crystal structure. Both minerals are strong ferrimagnets with comparable high saturation magnetizations (σ_s) of ~ 92 and $\sim 74 \text{ Am}^2 \text{ kg}^{-1}$ for magnetite and maghemite respectively (see Subsection 5.4.2), which are two orders of

magnitude higher than those of hematite and goethite (typically $\sim 0.1\text{--}0.6 \text{ Am}^2 \text{ kg}^{-1}$). An important difference between maghemite and magnetite, however, is their composition; $\gamma\text{-Fe}_2\text{O}_3$ is cation deficient compared to Fe_3O_4 and contains only ferric iron instead of a mixture of ferric and ferrous iron, as is the case for magnetite. The ferrimagnetic structure of maghemite and the effect of different cation and vacancy distributions on the saturation magnetization is described in Subsection 5.4.2. Unfortunately, it is not known yet to what extent the various possible cation and vacancy distributions affect the other magnetic properties of maghemite. Hence, some caution must be exercised with conclusions based on a single study, because a review of the existing literature makes it clear that chemically and structurally ‘somewhat different’ samples have been synthesized and investigated.

Several magnetic properties are reported to change upon oxidation, i.e. with a decrease in Fe^{2+} content and an increase in amount of vacancies. Most magnetic changes are usually very subtle (e.g. susceptibility and coercivity). Some changes, however, are so characteristic that they can be used to distinguish between maghemite and magnetite. On oxidation, the Curie temperature, for example, increases from ~ 580 to $\sim 645^\circ\text{C}$ (see Subsection 5.4.4). Since every common impurity causes a decrease of the T_c of magnetite, a $T_c > 580^\circ\text{C}$ points to the presence of non-stoichiometric magnetite, at least when hematite ($T_c \sim 680^\circ\text{C}$) can be excluded. During thermomagnetic analyses, ultrafine maghemite particles, however, will already show a diagnostic drop in magnetization around 350°C reflecting a partial or complete inversion to less magnetic hematite. Even more evident is the disappearance of magnetite's low-temperature Verwey transition on maghemitization (see Subsection 5.4.5). Before discussing these diagnostic magnetic properties of maghemite in more detail, the more general properties are reviewed in Subsection 5.4.1.

5.4.1 General magnetic properties

Magnetic grain sizes: The superparamagnetic (SP) threshold size (d_s) for $\gamma\text{-Fe}_2\text{O}_3$ at room temperature is usually quoted as $25\text{--}30 \text{ nm}$, i.e. similar to that of magnetite and hematite, and relatively insensitive to elongation of the grains (e.g. Berkowitz *et al.* 1968; Dunlop 1973; Dearing *et al.* 1996; Moskowitz *et al.* 1997). Micromagnetic calculations by Lyberatos & Chantrell (1990), however, predicted a slightly higher d_s of 42 nm for maghemite at room temperature. Enkin & Dunlop (1987) found a theoretical upper single-domain threshold size (d_0) for equidimensional maghemite of $\sim 60 \text{ nm}$ at room temperature. This value lies within the range usually reported for equidimensional magnetite, $50\text{--}80 \text{ nm}$ (Dunlop 1973; Enkin & Williams 1994). The room temperature stable single-domain (SD) range is thus very narrow for both maghemite and magnetite. For magnetite it is known, however, that metastable SD states can exist in larger grains, and that elongated grains usually have higher d_0 values (e.g. Dunlop & Özdemir 1997). True multidomain behaviour usually is observed only in grains $> 1 \mu\text{m}$. Consequently, $\gamma\text{-Fe}_2\text{O}_3$ and homogeneous CD magnetites with high z values usually comprise the SP through pseudo-single-domain (PSD) range only, because of their fine-grained nature.

Furthermore, maghemitization can decrease a rock's magnetic grain size by subdividing the original grain into several separate smaller grains. Such behaviour may enhance or reduce the stability of the paleomagnetic signal. The formation of several small SD grains out of a large MD or PSD grain will usually enhance the stability. On the hand, the production of even smaller SP grains will lead to a substantial reduction of the reliability of the paleomagnetic signal (e.g. *Kent & Lowrie 1974; Prevot et al. 1981; Kodama 1982*). Maghemites produced from lepidocrocite usually can carry a remanence, despite the ultrafine size (~10 nm) of their crystallites. The typical SD type behaviour of these maghemites implies that a group of crystallites act together as an uniformly magnetized SD region, typically 30–40 nm in size (e.g. *Hall & Berkowitz 1986; McClelland & Goss 1993; Özdemir & Dunlop 1993*). These SD regions are often divided by so-called antiphase boundaries (APBs), and separate regions in which the vacancies are ordered on different sublattices (e.g. *Hall & Berkowitz 1986*). APBs form at locations where dehydration of γ -FeOOH is first completed (*Bernal et al. 1957*). Neighbouring regions are in exchange contact across the APB and presumably couple negatively so as to reduce the overall magnetic moment (*Özdemir & Dunlop 1993*).

Susceptibility: The low-field mass susceptibility (χ_{lf}) for fine-grained SD γ -Fe₂O₃ generally ranges between $(4.0\text{--}5.5) \times 10^{-4} \text{ m}^3 \text{ kg}^{-1}$, slightly less than the range usually quoted for magnetite, $(5\text{--}10) \times 10^{-4} \text{ m}^3 \text{ kg}^{-1}$. *Porath (1968)* reported an χ_{lf} of $7.4 \times 10^{-4} \text{ m}^3 \text{ kg}^{-1}$ for large acicular maghemite particles with an average size of 0.4 μm and a dimension ratio of 8:1. The susceptibility depends on the magnetic domain state of a sample and thus on its grain size and shape. In the SD through multidomain (MD) size range the susceptibility decreases with decreasing grain size. Below the SP threshold size, however, χ_{lf} increases sharply. Consequently, even a small fraction of SP material in a sample will tend to dominate the induced magnetization. Crushed magnetites in general have lower χ_{lf} values compared to grown crystals (*Hunt et al. 1995* and references therein). The same relation most likely holds for maghemites. Apart from grain size and shape the susceptibility is dependent on concentration and the type of magnetic mineral. The χ_{lf} of hematite and goethite is three orders of magnitude less ($\sim 5 \times 10^{-7} \text{ m}^3 \text{ kg}^{-1}$), and as a results the susceptibility of rocks and soils are strongly dominated by ferrimagnetic magnetite and maghemite particles. This magnetic parameter appears to be particularly sensitive to environmental changes and is often used for correlation purposes (e.g. *Tite & Linington 1975; Stoner et al. 1995*). The susceptibility is also used to characterize soil types. The magnetic enhancement of the soil surface layer, for example, is very easily detected with this parameter. *Graham & Scollar (1976)* heated soils and found that the maghemite produced in this way had a mass susceptibility of $5.4 \times 10^{-4} \text{ m}^3 \text{ kg}^{-1}$.

Hysteresis parameters: As mentioned, the average hysteresis parameters of γ -Fe₂O₃ closely resemble those of magnetite, at least for homogeneous generally fine-grained maghemite particles. Inhomogeneous particles with a maghemite rim around a less or essentially non-oxidized magnetite core, behave differently and will be discussed later on in this Subsection. Just like the susceptibility, the saturation remanence (σ_{rs}), the coercivity (B_c) and the remanent coercivity (B_{cr}) depend on the magnetic domain state of

the particles. Especially the σ_{rs}/σ_s and B_{cr}/B_c ratios have diagnostic values for magnetic grain size (Day *et al.* 1977). Grain-size dependent trends of the hysteresis parameters and their ratios spanning the SD through MD region are not yet available for maghemite. Therefore, we summarize the general trends observed for magnetite supplemented with maghemite data found in literature.

Saturation ratio: Like magnetite, homogeneous $\gamma\text{-Fe}_2\text{O}_3$ particles usually become fully saturated in magnetic fields less than ~ 100 mT. The saturation magnetization ($\sigma_s \sim 74 \text{ Am}^2 \text{ kg}^{-1}$; see Subsection 5.4.2) is a material constant and hence essentially independent on grain size. In contrast, the saturation remanence (σ_{rs}), and the σ_{rs}/σ_s ratio decrease with increasing grain size throughout the SD to MD region. Grown crystals generally have lower values compared to crushed particles for nominally the same grain size (Hunt *et al.* 1995 and references therein). The theoretical ratio of saturation remanence to saturation magnetization is 0.87 for a homogeneous collection of randomly oriented non-interacting SD magnetite particles controlled by magnetocrystalline anisotropy. For grains dominated by shape (uniaxial) anisotropy, $\sigma_{rs}/\sigma_s = 0.5$ (Stoner & Wohlfarth 1948). For pseudo-single-domain (PSD) grains, Dunlop (1972) found values between 0.1 and 0.3. The ratio tends towards zero for MD grains, intergrown grains and grains which are clustered together (Davis & Evans 1976). In a so-called Day-plot (Day *et al.* 1977) the value $\sigma_{rs}/\sigma_s = 0.05$ is used as the lower limit of the ideal MD region. A typical value for σ_{rs}/σ_s for interacting SD grains is 0.3 (*cf.* Dankers 1978). The presence of superparamagnetic particles, commonly encountered in maghemite samples, may bias the σ_{rs}/σ_s Özdemir & Dunlop (1988), for example, found a reduced σ_{rs}/σ_s value of 0.24 for their equidimensional SD maghemite grains dominated by magnetocrystalline anisotropy (median diameter = 24.5 nm), and described the discrepancy with the theoretical value mainly to the existence of a large proportion of additional SP particles.

Coercivity: SD maghemite and magnetite have coercivity (B_c) and remanent coercivity (B_{cr}) values of ~ 10 mT up to several tens of mT. A regular and continuous decrease of both values with increasing grain size is observed for magnetite throughout the SD to MD region (*cf.* Hunt *et al.* 1995 and references therein). Hydrothermally grown magnetite crystals usually have lower values than crushed particles of similar size. At a constant temperature, coercivity is dependent on microstructure, grain size, shape, origin of magnetic anisotropy, applied stress and may depend on particle interactions. For SD maghemite and magnetite particles shape anisotropy dominates over strain and crystal anisotropy. The theoretical coercive force of a dispersion of non-aligned SD grains dominated by magnetocrystalline anisotropy is $0.64|K_1|/\mu_0 M_s$ (*cf.* O'Reilly 1984, page 73) which gives, according to Goss (1988), ~ 19 mT for magnetite, and ~ 15 mT for maghemite at room temperature. Soffel (1991) reported maximum coercive forces of 125, 15, and 30 mT for shape, stress and crystal anisotropy, respectively. For the stress anisotropy the author assumed a strain of 50 MPa. Stacey & Banerjee (1974) reported a theoretical maximum coercivity for very elongated SD grains of 300 mT. In practice, however, both B_c and B_{cr} rarely exceed 100 mT. B_c values for fine-grained $\gamma\text{-Fe}_2\text{O}_3$ found in literature ranged from 23 to 36 mT for elongated SD particles (Morrish & Yu 1955; Eagle & Mallinson 1967; Imaoko 1968; Berkowitz *et al.* 1968; Podolsky 1981; Özdemir 1990) and from 7.5 to 15 mT for equidimensional fine particles (Westmijze 1953; Morrish

& Sawatzky 1971). The minimum coercivity of ~10 mT for SD particles ensures complete stability of SD remanence against changing geomagnetic fields (~0.1 mT) at ordinary temperature, making SD grains the ideal paleomagnetic recorder (Dunlop & Özdemir 1997).

Remanence ratio: Moskowitz *et al.* (1997) found a B_{cr}/B_c value of 1.32 for weakly interacting SD maghemite particles encapsulated by protein shells. Their value is slightly larger than the theoretical value of 1.04–1.09 (Wohlfarth 1958) for a random assembly of uniaxial SD grains, but may be more appropriate for weakly interacting systems commonly found in sediments and soils. A value of $B_{cr}/B_c = 1.5$ and 4 has sometimes been used as a SD limit and as the lower limit for true MD grains, respectively (Day *et al.* 1977); both values, however, are purely arbitrary (*cf.* Dunlop & Özdemir 1997). High values of B_{cr}/B_c , however can also result from an admixture of SP material. For a more detailed description of the hysteresis parameters and other properties of magnetite the reader is referred to O'Reilly (1984), Dunlop & Özdemir (1997) and references therein.

Effect of initial low-temperature maghemitization: Several authors describe the effects of initial stage low-temperature maghemitization on the magnetic properties of SD magnetite (e.g. Knowles 1981; Appel 1987; Housden & O'Reilly 1990; Özdemir *et al.* 1993; Van Velzen & Zijderfeld 1995). Coercive forces of partially oxidized magnetites appear to be significantly higher than those of their non-oxidized monophase equivalents, while a decrease in remanent magnetization is observed. B_{cr} values reported by Van Velzen & Zijderfeld (1995) for slightly oxidized natural SD magnetites are anomalously high exceeding 100 mT up to 188 mT. The enhanced coercivities are attributed to stress developed at the $\gamma\text{-Fe}_2\text{O}_3 - \text{Fe}_3\text{O}_4$ interface during oxidation. The stress in turn has its origin in the different lattice constants of the shell and the core. The more oxidized shell shrinks and is stretched over the core. At low temperature large oxidation gradients can develop between the rim and the core of a particle because of the low diffusion rates of Fe^{2+} (see Subsection 5.3.4); the stresses in the grains are proportional to this gradient. As the diffusion rate is highly temperature-dependent, an increase in temperature will accelerate the diffusion of Fe^{2+} from the core to the rim of the particle and hence reduces the oxidation gradient considerably. Consequently the stresses in the grains will decrease. Van Velzen & Zijderfeld (1995) showed that heating to ~150°C was sufficient to reduce the coercivities from anomalously high values to values normal for homogeneous SD magnetite. Several other rock-magnetic parameters related to the reduction in coercivity also changed after heating to 150°C. The authors observed a decrease in total σ_r (1.5 T) and an increase in χ_{lf} and anhysteretic remanent magnetization. They attributed the decrease in σ_r to the increased number of grains with SP behaviour, which owed their stability before heating only to their enhanced coercivities due to an oxidized shell.

5.4.2 Ferrimagnetic structure and saturation magnetization

The magnetic structure of $\gamma\text{-Fe}_2\text{O}_3$ basically consists of an alternation of two opposed but unequal magnetic sublattices (Néel 1948). The atomic Fe^{3+} moments within each sublattice are coupled parallel, whereas those of the A and B sublattices are coupled

antiparallel through an intervening O^{2-} anion. Because of the non-equivalence of the sublattice magnetizations a strong net ferrimagnetic moment results in maghemite. Per formula unit (*pfu*) $\gamma\text{-Fe}_2\text{O}_3$ an average excess of $\frac{1}{2}\text{Fe}^{3+}$ exists on the B sublattice. This corresponds to a net magnetic moment *pfu* of $2.5\mu_B$, since the spin-only moment per atom for the cation Fe^{3+} is $5\mu_B$ (electron configuration $3d^54s^0$; spin quantum number $S = 5 \times \frac{1}{2} = 2.5$). The magnetic moment can be converted to the macroscopic measure given by the saturation magnetization σ_s (i.e. dipole moment per unit mass) by using the following formula: $\sigma_s = (N_A\beta/M)n_B$ where N_A is Avogadro's number ($6.02 \times 10^{23} \text{ mol}^{-1}$), β is the value of 1 Bohr magneton ($9.27 \times 10^{-24} \text{ Am}^2$), M is the molecular weight (159.7 g mol^{-1}), and n_B is the number of Bohr magnetons ($2.5\mu_B$). Hence, the theoretical saturation magnetization of $\gamma\text{-Fe}_2\text{O}_3$ with a random distribution of octahedral vacancies is $\sim 87 \text{ Am}^2 \text{ kg}^{-1}$, adjusted to zero thermal energy at 0 K. The measured spontaneous moment at 0 K, however, is slightly lower and ranges between 2.36 and $2.43\mu_B$ (Weiss & Forrer 1929; Henry & Boehm 1956; Mollard et al. 1977a).

For magnetite the Fe^{3+} occurs in equal numbers on both sublattices, leaving a net magnetic moment of $4\mu_B$ *pfu* due to the uncompensated Fe^{2+} ($3d^64s^0$; $S = (5 \times \frac{1}{2}) - \frac{1}{2} = 2$) cations on the B lattice. At 0 K, the measured spontaneous magnetic moment *pfu* of Fe_3O_4 is $4.1\text{--}4.2\mu_B$, corresponding to a σ_s of $\sim 96 \text{ Am}^2 \text{ kg}^{-1}$ at this temperature (cf. Dunlop & Özdemir 1997). In the magnetite–maghemite solid-solution series the saturation moment at 0 K decreases steadily with increasing z , from $4.1\mu_B$ for Fe_3O_4 to $\sim 3\mu_B$ when $z = 0.95$ (Readman & O'Reilly 1972).

Typical room temperature values for $\gamma\text{-Fe}_2\text{O}_3$ and Fe_3O_4 are 74 and $92 \text{ Am}^2 \text{ kg}^{-1}$, respectively (e.g. Johnson & Merrill 1974; Bate 1980; Goss 1988; Özdemir & Dunlop 1988; Özdemir 1990; Moskowitz 1993). Maghemites with measured σ_s values slightly higher than $74 \text{ Am}^2 \text{ kg}^{-1}$ most likely contain some residual Fe^{2+} in their lattice, i.e. are not fully oxidized. Takei & Chiba (1966) suggest the presence of some of the vacancies on the A-sublattice to explain higher σ_s values for maghemite. Reduced saturation magnetizations are, however, also often reported for maghemite. Moment reduction due to lattice imperfections and/or due to the substitution of non-magnetic impurity cations with a B-site preference like diamagnetic Al^{3+} ($S = 0$) and Ti^{4+} ($S = 0$) is common for natural maghemites. In addition, particularly the combination grain size and surface effects has been suggested as a cause of the reduced σ_s values (e.g. Berkowitz et al. 1968; Coey 1971; Greaves 1983; Özdemir & Dunlop 1988). Incomplete coordination of the atoms at the surface because of missing bonds leads to a non-collinear spin configuration, i.e. a surface layer (thickness $\sim 1 \text{ nm}$) of randomly orientated spins (Coey 1971). These surface atoms contribute perceptibly to the magnetization of particles in the $0.01 \mu\text{m}$ range. As a result, moment reduction due to a randomly canted surface layer can be significant in these very fine particles (Coey 1971). Berkowitz et al. (1968), for example, reported a decrease in σ_s from 74 to $34 \text{ Am}^2 \text{ kg}^{-1}$ in acicular maghemites as particle width decreased from 70 to 5 nm . Mollard et al. (1977b) found a linear decrease in σ_s with increasing surface area, i.e. decreasing grain size. Batis-Landoulis & Vergon (1983) reported that apart from grain size, the particle morphology might also influence the specific saturation magnetization. Another mechanism for moment reduction that may be relevant for low-temperature maghemites is the presence of structural hydroxyl ions

(e.g. Braun 1952; Van Oosterhout & Rooijmans 1958). Goss (1988) argued that an increase in tetrahedrally coordinated Fe^{3+} ions per unit cell could explain reductions in σ_s of maghemite between 74 and 56 $\text{Am}^2\text{kg}^{-1}$. Özdemir (1990) attributed her observed low σ_s of 65.3 $\text{Am}^2\text{kg}^{-1}$ to the cavities present in her synthetic maghemite.

5.4.3 Magnetocrystalline anisotropy and magnetostriction

Measured and calculated values for the first cubic magnetocrystalline anisotropy constant K_1 of $\gamma\text{-Fe}_2\text{O}_3$ closely agree, being -4.6×10^3 and -4.7×10^3 J m^{-3} respectively (Birks 1950; Takei & Chiba 1966). This is about $1/3$ the value of K_1 reported for magnetite, -13.5×10^3 J m^{-3} (cf. Dunlop & Özdemir 1997). The negative value of K_1 yields a preferred direction of magnetization (*magnetocrystalline easy direction*) along one of the eight [111] cube diagonals, whereas [110] and [100] are respectively the medium and hard directions of magnetization (e.g. Moskowitz 1992). This effect, however, is usually weak compared with the anisotropy associated with the shape of the maghemite grains.

Kaneoke (1980) reported a decrease in measured values of the saturation magnetostriction λ_s with decreasing z throughout the magnetite–maghemite solid-solution series. For $\gamma\text{-Fe}_2\text{O}_3$ and Fe_3O_4 the author obtained $\lambda_s = -8.9 \times 10^{-6}$ and 23×10^{-6} , respectively. Some caution must be exercised with this data however, because his value for magnetite is considerably lower than the generally accepted value of 36×10^{-6} (cf. Dunlop & Özdemir 1997).

5.4.4 Temperature variation of σ_s and the Curie temperature

Gorter (1954) discussed the principal superexchange pathways for the inverse spinel structure. The strength or effectiveness of the superexchange interaction depends on the degree of overlap of the orbitals which in turn depends on the Fe–O distance and, above all, on the Fe–O–Fe angle (e.g. Owen & Taylor 1966). Bond angles between 120–180° are favourable and yield the strongest exchange coupling, whereas angles close to 90° are much weaker. Like in magnetite, the dominating type of interaction is antiferromagnetic coupling via the octahedrally and tetrahedrally coordinated Fe-atoms located on different sublattices having a bond angle of 125.2°. The AA and BB interactions between cations in the same sublattice are much weaker because of the large distances and unfavourable angles, 79.6° and 90° respectively. The strength of coupling, however, is almost identical. Hence, the temperature variation of the sublattice magnetizations $\sigma_A(T)$ and $\sigma_B(T)$ is quite similar (e.g. Stacey & Banerjee 1974), resulting in a so-called Q-type (Néel 1948) σ_s – T curve for ferrimagnets which resembles those of true ferromagnets (cf. O'Reilly 1984; Dunlop & Özdemir 1997). The σ_s – T curve of $\gamma\text{-Fe}_2\text{O}_3$ is similar in shape to that of Fe_3O_4 (Fig. 5.1b). The theoretical best fit for magnetite is $\sigma_s(T) \propto (T_c - T)^{0.43}$ (e.g. Pauthenot 1952). For maghemite, the σ_s – T curve, however, is generally biased (or completely disturbed) by the heating-induced transformation to hematite, causing a characteristic drop in σ_s around ~350°C (see Subsection 5.3.4).

It is generally accepted that T_C increases with increasing z within the magnetite–maghemite series. The true Curie temperature of maghemite, i.e. the temperature at which thermal energy becomes equal to superexchange energy and magnetic order breaks down, is however not known exactly. Direct measuring of the Curie point of maghemite is often not possible, because of its inversion to hematite at lower temperatures, i.e. $T_{inv} < T_C$. The few direct measurements reported in literature indicate a T_C around 640–645°C for γ -Fe₂O₃ compared to a T_C of ~580°C for Fe₃O₄ (Özdemir & Banerjee 1984; Heider & Dunlop 1987; Van Oorschot & Dekkers, 1999; see Fig. 5.1b). The synthetic tetragonal maghemite of Özdemir & Banerjee (1984) contains 1% FeO, is acicular in shape and has a substantial amount of microstructural defects, such as cavities and micropores. The submicron maghemite of Van Oorschot & Dekkers is produced by heating pure synthetic magnetite cubes (0.05–0.2 μ m) at 250°C for 2h. X-ray diffractograms show some indication of tetragonally ordering of the vacancies. Takei & Chiba (1966), on the other hand, reported a T_C of only 470°C for their epitaxially-grown single crystals of maghemite. Dunlop & Özdemir (1997) suggested a film-substrate mismatch or a different vacancy distribution in films compared to particles as the possible cause. Indirect methods, involving addition of impurities to raise the inversion temperatures and extrapolating the observed Curie points to the value corresponding to zero impurity content, or extrapolating Curie temperatures of partially oxidized cation-deficient magnetites to $z = 1$, give about 675–695°C, i.e. similar to the T_C of hematite (Michel & Chaudron 1935; Maxwell *et al.* 1949; Readmann & O'Reilly 1972). The Curie temperature of maghemite can also be calculated using the molecular-field theory for ferrimagnetic substances. Da Costa *et al.* (1995), Frölich & Vollstädt (1967) and O'Reilly (1968) calculated a T_C of ~657°C, 675°C and even of 770°C, respectively. The molecular field model, however, is only a first approximation and the obtained T_C values strongly depend on the used exchange integrals.

Impurity cations like diamagnetic Ti⁴⁺ and Al³⁺ are reported to lower the Curie temperature of maghemite (e.g. Michel *et al.* 1951; Özdemir & O'Reilly 1982; Brown & O'Reilly 1988). Following the molecular-field approximation for ferrimagnetism, Da Costa *et al.* (1995) argued that one expects a close to linear correlation between T_C (in K) and the Al substitution y (in mole %) of $T_C(0) \approx T_C(0)(1-y)$, at least for low y . Their Curie temperatures for Al-substituted maghemites calculated from exchange integrals derived from the measured temperature dependencies of the A- and B-site hyperfine fields of these samples agree reasonably well with this relation when using $T_C(0) = 930$ K for the Al-free sample. The measured T_C of 591°C for a maghemite substituted with 7% Al by Michel *et al.* (1951) supports these findings.

The effect of different ordering of vacancies or cations over the two magnetic sublattices is not yet known exactly. But while σ_s is very sensitive to cation distribution because net magnetization is the difference between A and B sublattice magnetic moments, T_C is determined by the product of the sublattice spin moments. Hence, T_C is less sensitive to cation distribution variations than σ_s (Banerjee 1991).

5.4.5 Low-temperature behaviour

The low-temperature behaviour of $\gamma\text{-Fe}_2\text{O}_3$ and Fe_3O_4 is sufficiently different to be used as a distinction between these two minerals (see *Fig. 5.1a*). The magnetic properties of maghemite which evidently depend on crystalline anisotropy –like the remanent magnetization, the susceptibility and the coercive force– do not show the abrupt change around -155°C characteristic of MD or equidimensional SD magnetite (*cf. Dunlop & Özdemir 1997*). Instead, the magnetic properties of maghemite only slightly change between room temperature and liquid nitrogen temperature (-196°C). On rewarming from -196°C (*Fig. 5.1a*), we measured an almost linear increase in χ_{lf} with about 15% compared to the initial value, using equidimensional SD maghemite. No indication for a low-temperature transition is observed. *Senanayake & McElhinny (1981)* obtained identical low-temperature behaviour of susceptibility for their acicular synthetic SD-maghemite. *Dankers (1978)* described the low-temperature behaviour of induced remanence (SIRM) for a natural Ti-substituted maghemite ($x = 0.07$, $z = 0.9$). The SIRM-intensity hardly changes during cooling to -196°C . On rewarming to room temperature the remanence intensity, however, smoothly decreases with about 20% for 30–25 μm grains and with 13% for the finest grains $<5 \mu\text{m}$. *Özdemir et al. (1993)* reported a gradual decrease of a SIRM (2.5 T, imparted at 5 K) during warming from 5 to 300 K of about 15% for acicular $\gamma\text{-Fe}_2\text{O}_3$ particles (length 0.45 μm , axial ratio 5:1).

On cooling, magnetite successively passes through its magnetic isotropic point (T_i) and the crystallographic Verwey transition (T_v) at ca. -145°C and ca. -155°C , respectively. Both phenomena have the same origin, since both are caused by some sort of electronic ordering. The single-ion anisotropy, one of the sources of the magnetocrystalline anisotropy, is much higher for Fe^{2+} ions than for Fe^{3+} ions due to the unquenched orbital angular momentum in divalent iron (*cf. O'Reilly 1984*). Consequently, the magnetocrystalline anisotropy in spinels should be dominated by the large positive anisotropy displayed by the Fe^{2+} ions. At room temperature, however, rapid electron hopping between randomly arranged octahedral ferrous and ferric ions causes a pure Fe^{2+} contribution to disappear and tetrahedral Fe^{3+} ions are responsible for the dominating negative anisotropy (*cf. Banerjee 1991*). The negative value of the first cubic magnetocrystalline anisotropy constant K_1 confines the magnetic spins to the [111] directions. As mentioned in Subsection 5.3.1, the hopping rate slows down on cooling and as a result the pure Fe^{2+} contribution becomes more and more important. At the isotropic point it dominates the Fe^{3+} contribution; K_1 changes sign and momentarily becomes zero (e.g. *Syono 1965*). The easy axes of magnetization change their orientation from [111] to [100] directions. Although the second anisotropy constant K_2 does not vanish at the same temperature, the net crystalline anisotropy is substantially reduced (*cf. Dunlop & Argyle 1991*), resulting in a maximum χ_{lf} value around T_i for MD magnetite (e.g. *Nagata et al. 1963; Fig. 5.1a*). K_1 increases on further cooling but remains low until magnetite's crystallographic Verwey transition (*Chikazumi 1976*). At T_v complete ordering of the octahedral Fe^{2+} and Fe^{3+} ions prohibits any electron hopping, and consequently a large increase of K_1 is observed below T_v caused by the Fe^{2+} single-ion anisotropy (*Williams et al. 1953*). The ordering of the Fe-ions also causes a very slight distortion of the unit

cell from cubic to monoclinic symmetry. Magnetite now has only a single easy axis of magnetization along one of the former [100] directions, the monoclinic *c*-axis.

Changes at both the isotropic point and the Verwey transition could force domain reorganization and explain the characteristic remanence decrease for magnetite when cooled in zero field (*cf. Hodych et al. 1998*). The change in lattice at T_v , however, is too small to significantly affect the AB interaction and there is hardly any change in σ_s (*cf. Dunlop & Özdemir 1997*). Elongated SD magnetite particles in principle should hardly exhibit any transition in their remanence or susceptibility because their anisotropy is dominantly determined by particle shape (*cf. Dunlop & Özdemir 1997*).

The Verwey transition is depressed, broadened, and eventually eliminated with increasing cation substitution (e.g. Ti^{4+}) and vacancy concentration, i.e. oxidation (e.g. *Özdemir et al. 1993*). As the number of Fe^{2+} ions decreases on oxidation, electron hopping between Fe^{3+} – Fe^{2+} ionic pairs on the octahedral sublattice is inhibited (*Daniels & Rosencwaig 1969*). *Rasmussen & Honig (1988)* found that with a vacancy concentration higher than 0.005 per molecule the transition is second order (*cf. Banerjee 1991*). *Özdemir et al. (1993)* reported that oxidation to $z = 0.3$ essentially suppresses the remanence transition. In pure maghemite, octahedral sites are completely occupied by Fe^{3+} ions and vacancies and no electron hopping and thus no Verwey transition can occur.

5.4.6 Two-phase CRM

A so-called two-phase CRM is a special type of CRM resulting from the formation of a new magnetic mineral through the alteration of an existing magnetic phase. Like *Dunlop & Özdemir (1997)* we prefer the term *crystallization remanent magnetization* for CRM because these authors rightly ascertain that the commonly used term, *chemical remanent magnetization*, is not always strictly accurate, e.g. in the maghemite → hematite transformation, where no chemical change occurs, only a restacking of the lattice. In two-phase transitions the magnetic parent phase might influence the CRM of the crystallizing daughter phase through magnetostatic or exchange coupling across the moving phase boundary. For paleomagnetists it is important to know whether the newly developed CRM ‘remembers’ the NRM direction of the parent phase, tracks the geomagnetic field acting at the time transformation occurs, or lies in an intermediate direction of no paleomagnetic significance (*cf. Heider & Dunlop 1987*).

Magnetite → Maghemite

Magnetite and maghemite have similar crystal lattices and magnetic structures. During oxidation of $Fe_3O_4 \rightarrow \gamma-Fe_2O_3$ the inverse spinel lattice is preserved and the lattice parameter change by less than 1% (see Subsection 5.3.1). It is thus quite acceptable that exchange coupling will be unbroken across the magnetite–maghemite phase boundary (*cf. Dunlop & Özdemir 1997*). The effectiveness of exchange coupling between both ferrimagnetic phases, however, appears to depend on the magnetic grain size of the parent

magnetite and on the oxidation product; i.e. either single-phase maghemite or intergrown maghemite–hematite particles. Laboratory studies performed by *Johnson & Merrill* (1974), *Heider & Dunlop* (1987) and *Özdemir & Dunlop* (1989) in **single-phase** low-temperature oxidation of $\text{SD Fe}_3\text{O}_4 \rightarrow \gamma\text{-Fe}_2\text{O}_3$ indeed indicate that CRM acquired by daughter maghemite always inherits or preserves the remanence direction of the parent magnetite. The CRM only distinguishes from the initial remanence by a decrease in intensity due to the change in σ_s . In contrast, *Johnson & Merrill* (1972) showed that single-phase oxidation of large PSD- to MD-size magnetite results in a field-controlled CRM. *Dunlop & Özdemir* (1997) conclude that only the domains immediately adjacent to the phase boundary are directly exchange coupled, while other more distant domains adjust their sizes and orientations in response to the applied field. *Heider & Dunlop* (1987) showed that for multiphase oxidation of fine-grained magnetite to a mixture of hematite (~90%) and maghemite (~10%), both initial remanence of the parent mineral and the field acting during oxidation influence the CRM direction. The CRM therefore has an intermediate orientation that preserve neither the primary NRM direction nor the geomagnetic field direction during oxidation. A mixture of hexagonal and spinel daughter phases, of which hematite is the most abundant, apparently breaks exchange coupling with the parent mineral. *Johnson & Merrill* (1972), however, did not find intermediate-direction CRMs when they oxidized magnetite to hematite. Their CRMs were all aligned with the field either because their starting material was MD in size or because the field they applied (0.6 mT) was strong enough to dominate the internal field (*cf. Heider & Dunlop* 1987). For a description and a schematic representation of the phase-coupled CRM process occurring during single-phase low-temperature oxidation of SD magnetite to maghemite the reader is referred to *Dunlop & Özdemir* (1997, page 399, Fig. 14.6).

Many studies also tried to simulate the CRM process during maghemitization of titanomagnetite of the seafloor (e.g. *Johnson & Merrill* 1973; *Özdemir & Dunlop* 1985; *Brown & O'Reilly* 1988; *Nishitani & Kono* 1989). *Dunlop* (1995) concludes in his review article that fine SD titanomaghemite grains fortunately can preserve 'TRM' (i.e. their CRM is phase-coupled to the primary TRM during oxidation) and are responsible for the survival of linear magnetic ocean-floor anomalies, while larger PSD ($d \approx \geq 20 \mu\text{m}$) and MD grains acquire growth CRM and lose all memory of the prior TRM. *Özdemir & Dunlop* (1985) and *Brown & O'Reilly* (1988) found that for multiphase oxidation of titanomagnetites (usually occurring only for oxidation parameters $z \geq 0.7$), the CRM direction began to deviate from the TRM toward the applied field direction.

Maghemite \rightarrow Hematite

The inversion of $\gamma\text{-Fe}_2\text{O}_3$ to $\alpha\text{-Fe}_2\text{O}_3$ involves a transformation of crystal structure and the development of a phase-coupled CRM is in this case less evident compared to a two-phase CRM without a change of lattice. In addition, as a consequence of the crystallographic relations between both minerals (see Subsection 5.3.4), the remanence vectors of maghemite and hematite will always make an angle with each other, i.e. exchange coupling should not in any case lead to a CRM parallel to the initial remanence (*cf. Dunlop & Özdemir* 1997). During the inversion of maghemite, hexagonal

(001) planes of hematite grow in (111) planes of maghemite octahedra (see Fig. 5.4). As mentioned in Section 1.4, the magnetization (σ_s) vector of hematite is confined to the basal (001) plane, while the σ_s vector of maghemite is in the $\langle 111 \rangle$ direction, i.e. perpendicular to (111) planes and hematite σ_s vectors in that plane. Because there are four equivalent $\langle 111 \rangle$ axes and (111) planes, the maghemite and hematite σ_s vectors are not always orthogonal. Many different geometrical relationships are possible but in general there will be a substantial angle between them (cf. Özdemir & Dunlop 1993; Dunlop & Özdemir 1997). For example, a $[1\bar{1}0]$ hematite σ_s vector and a $[1\bar{1}1]$ or $[1\bar{1}\bar{1}]$ maghemite σ_s vector are separated by about 40° (cf. Özdemir & Dunlop 1988).

The existence of exchange coupling across the maghemite–hematite phase boundary remains controversial and experimental results appear contradictory. Özdemir & Dunlop (1988), for example, reported that the transformation remanence acquired during the inversion of fine-grained equidimensional maghemite to hematite was univectoral and in the direction of the applied field, i.e. there is no exchange or magnetostatic coupling during inversion. In contrast, both Gustard & Schuele (1966) and Porath (1968) reported anomalously high CRM in partially inverted acicular maghemites which they attributed to positive exchange interaction across the maghemite–hematite interface. Özdemir & Dunlop (1988), however, argued that the magnetic moment of hematite is inadequate to explain the high CRM intensity. They interpreted the remanence peak to be a thermal activation effect of a single mineral species (Hopkinson-type peak in VRM intensity of the shrinking maghemite), and not as phase-coupling of two minerals. Furthermore, both non-vanishing rotational hysteresis at high fields and shifted non-symmetrical hysteresis loops together with unidirectional anisotropy when cooled in a field are observed in the $\gamma\text{-Fe}_2\text{O}_3 - \alpha\text{-Fe}_2\text{O}_3$ system (e.g. Banerjee 1966; Senno & Tawara 1967). These characteristic features are usually regarded as evidence for an exchange-coupled system (e.g. Meiklejohn & Bean 1956; Meiklejohn 1962). Porath (1968), however, clearly shows that the rotational hysteresis increases with the hematite content and attains a maximum for pure $\alpha\text{-Fe}_2\text{O}_3$, indicating that the high anisotropy field (magnetic hardness) of hematite rather than exchange interactions between the two magnetic minerals is primarily responsible for the observed behaviour. So far, the cooling experiments in which induced unidirectional anisotropy and a hysteresis offset were observed for intergrown maghemite–hematite samples are not yet repeated with single-phase $\alpha\text{-Fe}_2\text{O}_3$ samples.

Although phase-coupling seems not to be a general phenomenon in the maghemite–hematite system, some type of phase-coupling seems to occur when polycrystalline $\gamma\text{-Fe}_2\text{O}_3$ produced by dehydrating acicular lepidocrocite crystals inverts towards $\alpha\text{-Fe}_2\text{O}_3$. Antiferromagnetic $\gamma\text{-FeOOH}$ has a Néel temperature of ca. -203°C (Johnson 1969) and thus is paramagnetic at room temperature. Consequently, when dehydration takes place in a magnetic field, the CRM acquired by the produced maghemite will be parallel to the applied field and no magnetic interaction exists between both phases. At temperatures above $\sim 500^\circ\text{C}$, during the final stages of the subsequent inversion of maghemite, Özdemir & Dunlop (1993), however, reported the development of a weak CRM approximately perpendicular to the field and with an internal self-reversal. The crystallographic relations between both phases and the resulting exchange mechanism mentioned above easily explain the observation. Hedley (1968) and

McClelland & Goss (1987, 1993), on the other hand, reported a self-reversal of CRM in almost the same temperature region, which they suggested is caused by a negative exchange coupling between maghemite and hematite. The exact mechanism responsible for these observations is not known yet. *McClelland & Goss* (1993) suggested that the self-reversal of hematite remanence is probably a general feature of the maghemite to hematite transition, and not just a special phenomenon involving a lepidocrocite precursor for maghemite. They suggested that the self-reversal only occurs when the parent maghemite is still blocked at the temperature of its transformation to hematite, i.e. the hematite remanence is controlled by the internal magnetic field of the parent maghemite, otherwise it will be controlled by the external magnetic field and is normally magnetized. To their opinion, the significance of the source lepidocrocite is that it produces maghemite of a suitable grain size, so that much of it remains blocked at the temperature of its transformation to hematite (at the timescale of laboratory experiments). They stated that previous studies which did not find evidence for the existence of exchange coupling or magnetostatic interaction within the maghemite–hematite system did not obey this condition. Their suggestion seems to be supported by a study by *Ellwood et al.* (1986), who reported a self-reversal of CRM during room-temperature oxidation of siderite, involving an intermediate maghemite to hematite transformation step.

Chapter 6

Grain-size dependence of the rock-magnetic properties for a natural maghemite

Cor B. de Boer and Mark J. Dekkers

Paleomagnetic Laboratory 'Fort Hoofddijk', Utrecht University, Faculty of Earth Sciences, Budapestlaan 17, 3584 CD Utrecht, the Netherlands. E-mail: cdeboer@geo.uu.nl

Geophys. Res. Lett. (1996) 23, 2815–2818

SUMMARY

The natural Al-substituted (1.32 ± 0.63 weight per cent) maghemite from the *Robe River* mining district (Australia) is shown to be thermally very stable. The maghemite–hematite inversion occurs at $\sim 650^\circ\text{C}$ for sized fractions ($250 \mu\text{m}$ to $<5 \mu\text{m}$), enabling determination of T_c for maghemite at 610°C . The maghemite is intimately intergrown with hematite and σ_s of the maghemite (corrected for the hematite content) is $64 \text{ Am}^2 \text{ kg}^{-1}$. σ_{rs} , B_{cr} and B_c range between $7.46\text{--}10.18 \text{ Am}^2 \text{ kg}^{-1}$, $16.90\text{--}23.30 \text{ mT}$, and $6.38\text{--}9.00 \text{ mT}$, respectively, indicating PSD maghemite with grain sizes between ~ 1 and $\sim 20 \mu\text{m}$. The grain-size dependence of the rock-magnetic parameters of the maghemite is less prominent than those of magnetite of nominally the same size. It is suggested that the low-temperature behaviour of ARM can be diagnostic of the presence of maghemite: upon cooling to -196°C it shows no change; upon rewarming a gradual decrease in intensity occurs starting at $\sim -120^\circ\text{C}$.

6.1 Introduction

Maghemite, $\gamma\text{-Fe}_2\text{O}_3$, is a strongly ferrimagnetic mineral with the same chemical composition as hematite ($\alpha\text{-Fe}_2\text{O}_3$), but with a structure essentially similar to magnetite (Fe_3O_4). In nature, maghemite is predominantly formed by weathering or low-temperature oxidation of magnetite. Other formation processes, however, such as dehydration of lepidocrocite ($\gamma\text{-FeOOH}$) or heating by fire in the presence of organic matter are also possible (Mullins 1977). Maghemite is thermodynamically metastable with respect to hematite. Variable inversion temperatures (T_i) are reported ($250 < T_i < 900^\circ\text{C}$), depending on conditions during and after formation of the natural sample, synthesis method, crystallinity, impurity content and morphology of the particles (e.g. Bate 1980).

Apart from the relatively common occurrence of Ti-maghemite in ocean-floor basalts, maghemite was long considered to be a rare magnetic mineral in other geological settings. The similarity between the hysteresis properties of maghemite and those of magnetite, often may have led to erroneous magnetite identification. The presence of maghemite, however, is now successfully established in a wide variety of rock types and soils. Hence, its importance for paleomagnetism and other geoscience disciplines like soil- and environmental sciences, and for paleoclimate reconstructions is well recognized. Nevertheless, fundamental rock-magnetic data on maghemites is still scarce, in particular concerning grain-size dependence.

The purpose of this study was to provide more data for natural maghemites in the pseudo-single-domain (PSD) and multidomain (MD) grain-size range. Previous studies on magnetic properties of maghemite concentrated on submicron, synthetic material (e.g. Özdemir 1990). However, synthetic maghemite commonly has an acicular shape and a tetragonal structure which is not likely to occur in nature. To simulate paleomagnetic reality as much as possible, we carried out measurements on a well-defined natural maghemite (intergrown with hematite) which was sieved into 12 grain-size fractions ranging from 250 μm down to $<5 \mu\text{m}$.

6.2 Experimental methods

The maghemite was upgraded from a commercial iron ore concentrate from the *Robe River* mining district (Australia). The *Robe River* (RR) deposits are limonitic fluvialite replacement ores in former river channels. Twelve well-defined grain-size fractions were obtained from the raw ore by a separation procedure described in Dekkers (1988). A JEOL microprobe with SEM facility was used to check the grain-size ranges and to determine the composition of the magnetic particles. For further purity control, X-ray diffractograms were recorded with a Philips PW 1700 diffractometer using Cu-K α radiation and Si as internal standard.

The rock-magnetic measurements were carried out on a set of standard size, cylindrical samples. Ca. 50 mg (~ 0.11 Vol. %) of each grain-size fraction was homogeneously dispersed in non-magnetic matrices. An epoxy-resin matrix was used for

room and low-temperature experiments, and a quartz/bassanite matrix for high-temperature experiments. The low-field mass susceptibility (χ_{lf}) was measured with a Jelinek KLY-2 susceptibility bridge. Remanent coercivities (B_{cr}) and acquisition of isothermal remanent magnetization (IRM) were determined using a PM4 pulse magnetizer. Remanences were measured with a digitized spinner magnetometer, based on a Jelinek JR-3 drive unit. Progressive stepwise alternating field (AF) demagnetization of the IRMs was performed with a laboratory-built AF demagnetizer coil. Afterwards, three-axial IRMs were induced along the orthogonal axes of the specimens (2 T, 150 mT, 30 mT) for subsequent stepwise thermal demagnetization (*cf.* Lowrie 1990). Hysteresis loops in alternating current fields up to 300 mT were determined by measuring the imbalance of a pair of coils, one of which contained the specimen. The σ_{rs}/σ_s and B_{cr}/B_c results were compared and checked with some alternating gradient magnetometer (MicroMag) measurements (up to 500 mT) on small chips taken from the artificial samples. The results were identical. Continuous recordings of the anhysteretic remanent magnetization (ARM) during low-temperature cycling to -196°C were made with a fluxgate spinner magnetometer made suitable for measurements at low temperature. Thermomagnetic analyses were performed with a modified horizontal translation Curie balance which makes use of a cycling field (Mullender *et al.* 1993).

6.3 Experimental results and discussion

6.3.1 Sample characteristics

X-ray diffraction analysis showed that—in addition to maghemite—hematite was present in each fraction. Backscattered electron images of the more or less equidimensional particles revealed that both phases are intimately intergrown, separated by relatively sharp boundaries. In large grains, the maghemite is not finely dispersed throughout the whole grain, but each grain rather consists of two to four distinct maghemite and hematite parts. The maghemite parts are up to $\sim 20\ \mu\text{m}$ in size. Microprobe analyses determined both homogeneous phases as almost pure Fe_2O_3 (95.54 ± 2.18 weight per cent; error refers to standard deviation) with SiO_2 (2.25 ± 1.11) and Al_2O_3 (1.32 ± 0.63) as impurities. Quantitative Rietveld analysis was used to determine the hematite amount in each fraction (Table 6.1), enabling straightforward magnetic corrections. Rietveld refinement indicates that the *RR* maghemite has the face-centered cubic structure (space group: $Fd\bar{3}m$), which implies a random arrangement of the vacancies (Pecharromán *et al.* 1995). The unit cell length a is $8.3350 \pm 0.0005\ \text{\AA}$. This agrees with a pure, fully oxidized maghemite with some Al substitution (e.g. Schwertmann & Fechter 1984). The analyses also show that Si is sorbed onto the maghemite particles rather than isomorphously substituted into the maghemite lattice, like Al.

Table 6.1: Basic rock-magnetic parameters at room temperature for Robe River maghemite.

$\langle d \rangle$ (μm)	$\gamma\text{-Fe}_2\text{O}_3$ (%)	χ_{M} ($\mu\text{m}^3/\text{kg}$)	σ_{rs} (Am^2/kg)	$\sigma_{\text{rs}}/\sigma_{\text{s}}$	B_{c} (mT)	B_{cr} (mT)	$B_{\text{cr}}/B_{\text{c}}$	B_{cr}' (mT)	B_{vH} (mT)	Inv. (%)
200	33	808	7.46	0.12	6.38	17.00	2.67	25.0	8.26	12.7
125	37	802	7.74	0.12	6.44	16.90	2.62	25.5	8.27	14.2
87.5	38	823	8.26	0.13	6.65	17.26	2.59	25.8	8.37	14.8
65	39	839	8.26	0.13	6.81	17.40	2.56	26.2	8.50	15.2
47.5	40	845	8.00	0.13	6.81	17.92	2.63	26.8	8.70	18.9
35	44	798	7.87	0.12	6.81	18.17	2.67	27.7	8.85	20.5
27.5	45	796	8.19	0.13	7.12	18.47	2.59	27.9	9.09	23.5
22.5	47	767	8.00	0.13	7.04	18.73	2.66	28.4	9.25	26.3
12.5	48	751	8.45	0.13	7.43	19.64	2.64	29.7	9.60	31.4
7.5	47	760	9.15	0.14	8.37	21.30	2.54	32.6	10.30	
2.5	48	733	10.18	0.16	9.00	23.30	2.59	35.4	11.30	36.4

All mass specific parameters are corrected for the hematite contribution in each fraction. $\langle d \rangle$ is the mean size of the intergrown particles, Inv. stands for the percentage maghemite inverted to hematite during a thermomagnetic run to 650°C.

6.3.2 Rock-magnetic parameters at room temperature

The rock-magnetic parameters of each grain-size fraction are listed in *Table 6.1*. The mass specific parameters in this table are corrected for the hematite contribution. The saturation magnetization of the maghemite is $\sim 64 \text{ Am}^2 \text{ kg}^{-1}$ at room temperature, which is distinctly lower than the usually quoted value of $74 \text{ Am}^2 \text{ kg}^{-1}$ for pure maghemite (e.g. *Bate* 1980). Reduced values of σ_{s} are often reported for natural maghemites and are here possibly caused by the substitution of diamagnetic Al (*cf. Goss* 1988). The remanence ratios ($\sigma_{\text{rs}}/\sigma_{\text{s}}$) and coercivity ratios ($B_{\text{cr}}/B_{\text{c}}$) range 0.12–0.16 and 2.54–2.67, respectively (*Table 6.1*). All fractions appear within the PSD-area defined by *Day et al.* (1977), rather than the MD-area expected at least for the coarse fractions. Due to the presence of the intergrowths, the actual maghemite grain size is distinctly less than the sieved grain size. The six largest grain-size fractions (250–150 μm , 150–100 μm , 100–75 μm , 75–55 μm , 55–40 μm , 40–30 μm) show only slightly different results, suggesting an equivalent maghemite grain size, which implies that the intergrown hematite resulted in a mean effective maghemite size of $< 30 \mu\text{m}$, estimated to be about 10–20 μm . This agrees with SEM-observations, and also concurs with the onset of truly MD behaviour above 15–20 μm in magnetites (*Dunlop* 1986). Although the maghemite particles fall in a narrow range of sizes ($\sim 1\text{--}20 \mu\text{m}$), the results reported in this paper show weak, but evident grain-size trends.

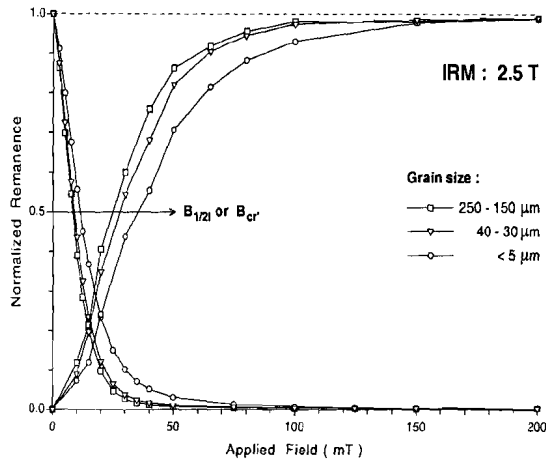


Figure 6.1: The initial part of the IRM acquisition curves normalized to the intensity acquired in a pulse field of 2.5 T, and their subsequent AF demagnetization.

The mass specific initial susceptibility (χ_{if}) of RR maghemite ranges between 733 and 845 $\mu\text{m}^3 \text{kg}^{-1}$; only a slight decrease in χ_{if} with decreasing grain size is observed. The χ_{if} values for RR maghemite are rather high compared to published values for (unannealed) crushed magnetite and maghemitized magnetite of equivalent grain size (e.g. *Dankers* 1978; *Hartstra* 1982; *Dunlop* 1986). Those particles have rather high internal strain resulting in lower χ_{if} . The present particles are grown from solution and the raw material is brittle, so very gently crushing only resulted already in the desired grain-size fractions. There is no indication (wasp-waisted hysteresis loops or high viscosity) for a large contribution of superparamagnetic grains, which also could result in high χ_{if} values.

IRM acquisition curves (*Fig. 6.1*) show that the coarse grain-size fractions virtually saturate (98 %) after application of a 100 mT field only, while the finer grains are slightly harder and saturate in fields of ca. 150 mT. The minute contribution of hematite indicates that the measured hysteresis parameters can be taken as representative for maghemite concurring with the absence of wasp-waisted hysteresis loops (not shown). The saturation IRM intensities range between 7.4 and 10.2 $\text{Am}^2 \text{kg}^{-1}$, and display only a weak trend of increasing σ_{rs} with decreasing grain size. This slight grain-size dependence of σ_{rs} is consistent with data of *Dankers* (1978) on maghemite, but different from data for magnetites, which mostly show a more pronounced variation with grain size in the range ~1–20 μm (e.g. *Dunlop* 1986). The AF stability of the SIRM in all fractions is rather low (*cf.* examples in *Fig. 6.1*). The coarse grains are almost completely demagnetized in peak fields of 50 mT, while the smaller grains need fields up to 80 mT to demagnetize. The cross-over ratio R is considerably less than 0.5 for all fractions, and decreases from ca. 0.24 to 0.21 with increasing grain-size. According to *Cisowski* (1981), this would indicate significant particle interaction. The intergrown grains themselves are sufficiently well

dispersed and diluted (only 0.11 Vol. %) for these effects to be negligible, but each separate grain typically consists of a few maghemite parts. This likely explains the lower R value for the coarser grains. Argyle & Dunlop (1990), however, attributed the differences between acquisition and decay curves to the internal demagnetizing field, which opposes any increase in net magnetization while promoting demagnetization. From Fig. 6.1 the range and the grain-size dependence of B_{cr}' (remanent acquisition coercive force) and $B_{1/2I}$ (median destructive field) values can also be deduced. Like the other coercivity parameters (Table 6.1), B_{cr}' and $B_{1/2I}$ display only a slight, more or less linear increase with decreasing grain size. All coercivity parameters of RR maghemite have lower values than magnetites of equivalent grain size ($\sim 1\text{--}20\ \mu\text{m}$), although the difference is small for the larger grains (e.g. Dankers 1978; Hartstra 1982; Dunlop 1986). The observed small variations with grain size compared to those of magnetites are consistent with measured data of Dankers (1978) on maghemites. Dankers' (1981) empirical relationship $B_{cr}' + B_{1/2I} = 2B_{cr}$ is obeyed for all grain-size fractions, and thus can be extended to natural maghemites.

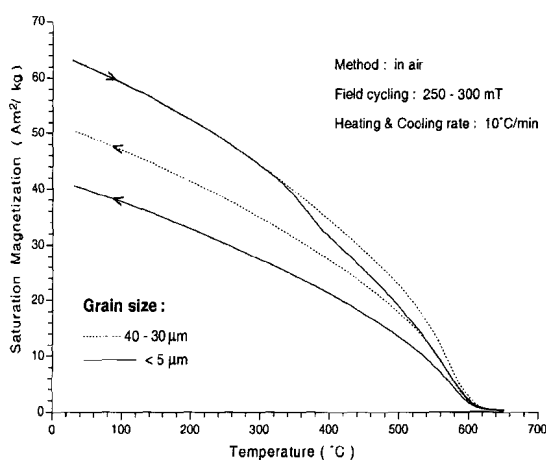


Figure 6.2: Thermomagnetic curves for RR maghemite. Cycling between 250–300 mT corresponds to a steady field of 550 mT.

6.3.3 High- and low-temperature behaviour

Figure 6.2 shows the variation of σ_s (measured in air) with temperature for two different grain-size fractions. σ_s typically decreases smoothly with increasing temperature up to the Curie point (T_c), as illustrated by the behaviour of the 40–30 μm fraction. The three finest fractions (15–10 μm , 10–5 μm , and <5 μm) show an additional inflection point at ca. 350°C. This agrees with inversion temperatures commonly reported in the literature for presumably fine-grained maghemite. All thermomagnetic curves are not completely

reversible upon heating to 650°C: a gradual increase in irreversibility from 13% (250–150 μm) to 36% (<5 μm) is measured (Table 6.1). The extra inflection at 350°C does not disrupt the general trend in irreversibility. This suggests that we are dealing with one maghemite type only and that the different thermomagnetic behaviour is kinetically determined. Despite the presence of intergrown hematite in the samples, which could act as nucleation centers for α-Fe₂O₃ growth, RR maghemite is thermally very stable. This may be related to its relatively coarse grain size. Sidhu (1988) reported a stabilizing effect of Al substitution on the maghemite structure. Therefore, minor substitution of Al in RR maghemite likely also contributes to its thermal stability. The RR maghemite T_c (610°C) is significantly higher than 580°C reported for pure magnetite, but well below the 645°C measured by Özdemir (1990) for a synthetic tetragonal maghemite. The commonly larger strain and higher amount of imperfections in natural samples compared to synthetic samples generally slightly lowers the T_c of the natural samples. Substitution of Fe by diamagnetic Al is also reported to lower the T_c by reducing the exchange interactions (Da Costa et al. 1995). An other suggestion may be that fully ordered tetragonal maghemite (space group: P4₃2₁2) has a different, i.e. higher, T_c as a face-centered cubic maghemite with a random distribution of its vacancies. In this respect, we draw attention to experimental results of Hauptman (1974) obtained for Ti-magnetites, showing a variation in T_c of 70°C for one composition which he related to cation ordering and non-stoichiometry.

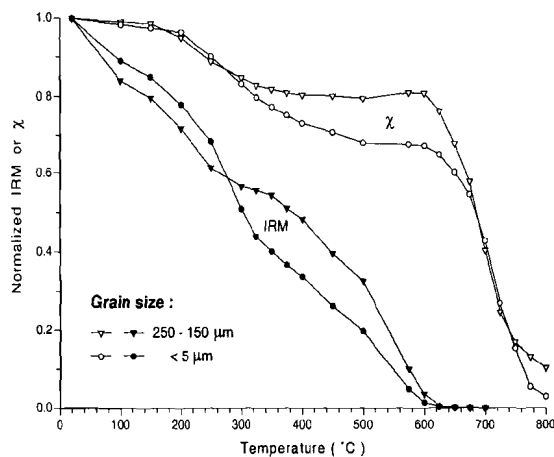


Figure 6.3: Stepwise thermal demagnetization of the SIRM (30–150 mT component) and the low-field bulk susceptibility measured after each temperature increment.

SIRM behaviour of the 30–150 mT component (cf. Lowrie 1990) during thermal demagnetization is shown in Fig. 6.3. In this component, a possible hematite contribution is insignificant. After each demagnetization step χ_{lf} is measured to monitor alterations.

During the first steps of this treatment the remanence carried by the smaller grains is less easily demagnetized by heating than that carried by the coarser grains. However, after the 250°C step the remanence of the smaller grains decays more rapidly. This remanence loss is accompanied by a decrease in χ_{lf} , indicating that an alteration process is the responsible demagnetizing mechanism. A minor (20–33%), and thermally less stable part of the maghemite transforms already to hematite at these lower temperatures. The inversion is evidently more pronounced in the smaller grain-size fractions, suggesting a kinetic relation. The remaining and thermally more stable part of this maghemite, however, unblocks near the Curie point of 610°C. The major inversion to hematite starts after the 600°C step, but still is not fully completed after the 800°C step. The minor as well as the major maghemite inversion is observed ~50°C lower in the stepwise thermal experiments than in thermomagnetic runs. This may be related to a much shorter heating time in the latter case.

The low-temperature behaviour of the saturation ARM (*Fig. 6.4*) is representative of maghemite, because hematite is much harder than 150 mT (peak AC field). The hematite contribution to the measured ARM is therefore negligible. Our observations are basically consistent with preliminary results of *Dankers* (1978). The ARM intensity hardly changes during cooling to –196°C, and –as expected– neither a Morin nor a Verwey transition is observed. With decreasing grain size, however, the cooling curve becomes slightly concave. Upon rewarming to 0°C, initially the heating curve is more or less reversible, but starting from ~ –120°C the remanence intensity smoothly decreases with 4–5% for all fractions. This characteristic low-temperature behaviour with a marked remanence decrease from –120°C during rewarming is suggested to be diagnostic for the presence of maghemite.

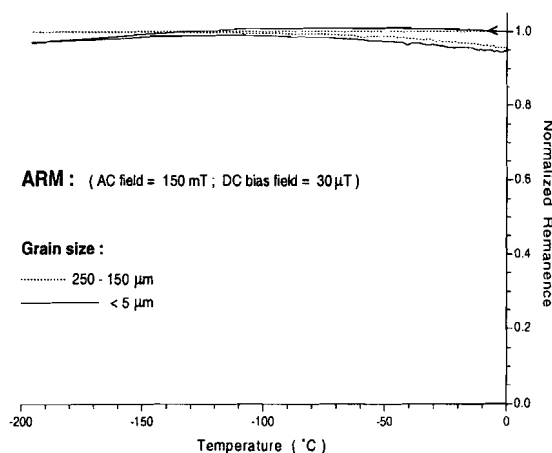


Figure 6.4: Low-temperature behaviour of the saturation ARM during cycling from room temperature to –196°C.

6.4 Conclusions

RR maghemite, which is intergrown with hematite, mainly inverts to hematite after heating at about 650°C, well above its Curie temperature of 610°C. Al substitution presumably stabilizes the maghemite structure. The transformation degree is shown to be grain-size dependent and thus kinetically related. In thermomagnetic runs, the three smallest grain-size fractions show an additional inflection point at ~350°C, a value commonly reported in the literature for inversion of submicron maghemite. This additional inflection, however, does not disrupt the general trend of increasing irreversibility with decreasing grain size. Observed grain-size trends in coercivity and other rock-magnetic parameters of the maghemite are less pronounced than those of magnetite of equivalent grain size (~1 to ~20 µm). A characteristic ARM low-temperature behaviour was observed with no decay upon cooling to -196°C, and upon rewarming a gradual decrease in remanence starting at ~ -120°C.

ACKNOWLEDGEMENTS

The Philips PC-Rietveld plus program package was made available to us by *Prof. dr. R.X. Fischer*. The assistance of *Henk Meijer* with part of the measurements is appreciated. *Mark Dekkers* acknowledges the Royal Netherlands Academy of Sciences and Arts (KNAW) for support in the form of a fellowship. This is Geodynamics Research Institute (Utrecht University) contribution 96.011.

Part III

Combustion- Metamorphic Rocks

*Some men see things as they are and say: "Why?"
I dream things that never were and say: "Why not!"*

(John F. Kennedy)

Chapter 7

Introduction to China's coal fire problem

China's burning problem

Enormous resources of coal are present in China. China is the largest producer, consumer and exporter of coal in the world. In 1996, its production of coal was 1380 million tons and 75% of China's primary energy consumption came from coal (Fan 1997). For the foreseeable future, coal will still remain China's major source of energy. However, its production is seriously affected by subsurface coal fires. Each year coal fires destroy from 10–20 million (Guan *et al.* 1996) to 200 million tons (Rosema *et al.* 1993; Cassels & Van Genderen 1995) of coal resources, a large part being high-quality coal.

Coal fires are a common problem in many coal fields throughout the world. Those in the United States, Australia and India have been extensively studied (Fisher & Kunth 1968; Ellyett & Fleming 1974; and Prakash *et al.* 1995a & b, respectively). However, these coal fires almost fade into insignificance compared to the size, extent, and amount of coal lost by coal fires in Northern China. Remote sensing satellite data studies have shown that coal fires occur from NW to NE China in a belt stretching 5.000 km east-west and 750 km in north-south direction (Guan 1984; 1989). In this large and remote region more than 100 coal fire areas were detected in 55 coal fields (Guan 1984; Kang *et al.* 1993; Van Genderen *et al.* 1996; Guan *et al.* 1996). Some coal fires have been burning for several hundred years and many more have been burning for at least the past four decades.

The large amount of coal lost by spontaneous combustion not only results in a substantial economic loss and safety problems, but also results in adverse environmental impacts. Coal fires pollute the environment by the release of smoke and noxious gases such as CO, NO_x, SO₂ and H₂S. Subsidence of the ground surface, land slides and vegetation degradation are also major consequences of underground coal fires. Apart from a national problem, coal fires of this extent have a global dimension as well. It is estimated that the coal fires in Northern China produce 2–3% of the world's CO₂ emission resulting from the combustion of fossil fuels and thus have a significant effect on global warming (Rosema *et al.* 1993; Cassels & Van Genderen 1995).

Therefore, early detection, monitoring and prevention of coal fires is a high-priority task. At present, the joint research project “*Environmental monitoring of Spontaneous Combustion in the North China Coal Fields*” sponsored by the European Commission, is carried out by the ITC (International Institute for Aerospace Survey and Earth Sciences in Enschede, the Netherlands) and the ARSC (Aerophotogrammetry and Remote Sensing Bureau of China coal in Xi’an, China) in cooperation with other European and Chinese partners. The project aims to set up a methodology for efficient detection, measurement, monitoring and extinguishing of the coal fires by means of remote sensing data and the setting up of a GIS system for regular monitoring of coal fires in the northern part of China. The system will be the basic management tool for the fire prevention and fighting teams.

The Paleomagnetic Laboratory ‘*Fort Hoofddijk*’ in Utrecht, the Netherlands contributes to this project on a minor scale by dating the baked and molten rocks related to extinct coal fires paleomagnetically in order to obtain a better understanding of the evolution and mechanism of the coal fires in this area. It is argued that coal fires are not only caused by human activity but rather are natural phenomena which occurred repeatedly during the recent geological past (*cf.* Chapter 8). Furthermore, rock-magnetic studies showed that these burnt rocks are magnetically anomalous compared to unaffected rocks implying that magnetic anomaly modeling may have potential to delineate the extent and depth of (paleo-) coal fires (*cf.* Chapter 9).

Spontaneous combustion and spreading of coal fires

A coal fire can start wherever a coal layer becomes exposed to the surface by mining activities or by natural processes such as faulting, folding, denudation, or valley incision by streams. There are several ways coal fires can be ignited; these include mining activities itself, forest fires (*Bustin & Mathews* 1982; 1985), lightning (*Guan et al.* 1996), manmade fires, and most importantly, spontaneous combustion.

Spontaneous combustion of coal occurs due to the accumulation of heat liberated from interaction of oxygen in air with coal in ambient temperature. At and beyond some elevated temperature between 50 and 100°C the oxidation rate accelerates greatly due to sustained exothermic reaction and ultimately produces flaming combustion or ignition. The critical threshold temperature, usually 60 to 85°C, depends on the nature of the coal, including its rank (*Zhang & Tang* 1994), content of volatile ash, oxygen (*Banerjee* 1985), moisture (*Schmal* 1987), pyrite, methane (*Vinogradova et al.* 1972), and its porosity. Above the critical temperature the process of oxidation becomes self-sufficient (*Banerjee* 1985). Under natural conditions the threshold temperature can already be exceeded by mere solar heating of favourable exposed coal seams.

Once coal fires ignite at the outcrop, the burning process proceeds along the coal seams to greater depth, i.e. the fires propagate themselves underground (*Kang et al.* 1993; *Shu* 1994). Based on field observations, *Zhang et al.* (1998) developed three general coal fire spreading models, namely the ‘deepening model’, the ‘lateral model’ and the ‘upwards model’. A coal seam of several meters thick with slight or medium dip angles

tends to burn down in the direction of the dip ('deepening model'; Fig. 7.1). The burned coal seam shrinks to an ash layer of only several centimeters in thickness. Therefore, deep cracks develop and eventually the roof of the coal seam collapses. The cracks and the collapsed areas, together with the highly porous burnt overburden rocks then act as a chimney which promotes the access of oxygen further underground. In this way a coal fire that started at the surface outcrop proceeds deeper and deeper underground in the dip direction (cf. Zhang 1998). Subsurface active coal fires down to 125 m are reported by Peng *et al.* (1997), while burnt rock profiles overlaying extinct coal fires of at least 150 m thick are found. When the coal seam is steeply dipping, the coal fires starting at the outcrop move along one or two of the strike directions within a certain depth ('lateral model'). Normally the spreading speed of coal fires is faster in the strike direction (5–15 m/year) (Bustin & Mathews 1982, 1985; Kang *et al.* 1991) than in the dip direction (1–3 m/year) (Ellyett & Fleming 1974; Kang *et al.* 1993), especially when the coal seams are steeply dipping. Where there are several coal layers, coal fires may develop from one lower coal seam to an upper one ('upwards model').

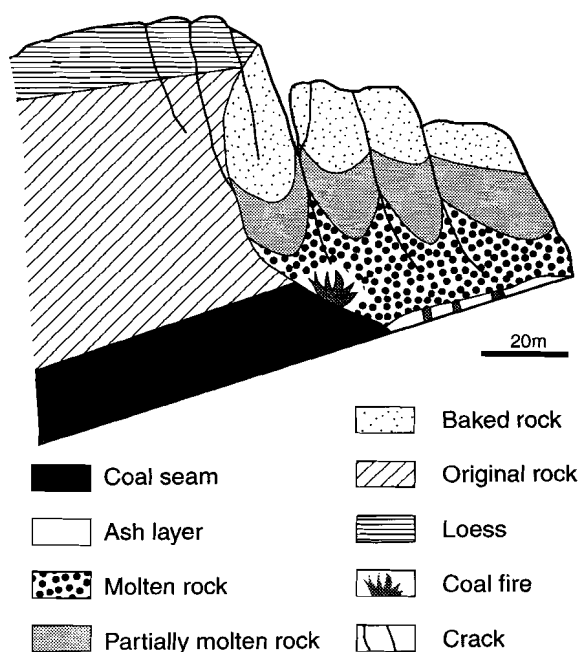


Figure 7.1: Land subsidence caused by a subsurface coal fire ('deepening model').

Detection of subsurface coal fires by remote sensing

The majority of the published literature on the detection of underground coal fires show that several satellite and airborne sensors can successfully detect such fires (e.g. *Kang* 1991; *Kang et al.* 1993, 1996; *Van Genderen et al.* 1996; *Zhang* 1998). This depends, however, on certain conditions such as size and depth of the fire, relief, time of the data acquisition, prevailing weather conditions, time of the year, etc (*Zhang* 1998). Underground mine fires, for instance, are detectable by remote sensing techniques only if they are less than 30 meters in depth (*Greene et al.* 1969) in areas where there are no cracks or fractures to lead the underground heat to the surface.

A diverse series of changes at the surface are used by the various remote sensing platforms and sensors as indicators of subsurface fires, both active and extinct (*cf. Zhang* 1998). These changes include: an increase in temperature, emission of smoke, color changes of caprock, formation and deposition of new materials at the surface (e.g. sulphur, salmiac deposits) and land cracking and subsidence of the surface.

Chapter 8

Pleistocene coal fires in Xinjiang, Northwest China

Xiangmin Zhang⁽¹⁾, Salomon B. Kroonenberg⁽²⁾ and Cor B. de Boer⁽³⁾

1 Dept. of Earth Resources Surveys, ITC, P.O. Box 6, Enschede, the Netherlands,

2 Faculty of Applied Earth Sciences, Delft University of Technology, P.O. Box 5028, 2600 GA Delft, the Netherlands,

3 Paleomagnetic Laboratory 'Fort Hoofddijk', Utrecht University, Faculty of Earth Sciences, Budapestlaan 17, 3584 CD Utrecht, the Netherlands. E-mail: cdeboer@geo.uu.nl

Submitted to Terra Nova

SUMMARY

Coal fires in China are not only an economic but also an environmental threat because of their significant contribution to the global CO₂ budget. This study shows, however, that the environmental impact quantified from mapping burnt rocks might be greatly overestimated, as over 85% of the burnt rocks recognized in remote sensing imagery of NW China is of Pleistocene age. Several age groups of burnt rocks have been recognized based on their intimate relationship with alluvial fan and river terrace deposits of the Toutunhe River and its tributaries: (1) Pliocene–Early Quaternary burnt rocks situated ca. 200 m above present river terrace deposits and overlain by an unbaked alluvial fan; (2) Middle Pleistocene burnt rocks situated above the 90 m terrace deposits; (3) Late Pleistocene burnt rocks situated between the unbaked 90 and 70 m terraces; (4) Holocene baked gravels of the two lowermost terraces; (5) Active coal fires and related burnt rocks. Paleomagnetic data obtained on the burnt rocks seem to support the age estimates but unfortunately could not further constrain them. Although still some uncertainty exists about the precise age of the coal fires, it is evident that they are not only caused by mining activities, but are also common natural phenomena which has occurred repeatedly during the recent geological past. In the studied area, spontaneous combustion of coal fires is related to the creation of favourable outcrops by deformation, uplift and unroofing by erosion in combination with cyclic deposition and dissection related to climate change.

8.1 Introduction

Coal fires are a serious problem for the Chinese coal industry. However, there are conflicting estimates of the annual loss of coal by fires in China, ranging from about 10–20 million tons (*Guan et al.* 1996) to 100–200 million tons (*Schalke et al.* 1993; *Cassells & Van Genderen* 1995; *EARS* 1998). Coal fires have a global impact as well, as the emission of CO₂ might contribute considerably to the increase in greenhouse gases in the atmosphere. If the latter estimate for annual loss of coal is correct, CO₂ emission by coal fires in 1992 would be responsible for 2–3% of the world CO₂ output from combustion of fossil fuels (*Cassell & Van Genderen* 1995).

The discrepancy in the annual output estimates is closely related to the way coal losses are calculated from remote sensing imagery. The best way to detect active coal fires is the use of thermal infrared scanning, which directly detects the temperature anomalies generated by the fire. Especially in night-time thermal infrared imagery active coal fires can be detected easily (*Zhang et al.* 1995, 1997; *Van Genderen et al.* 1996; *Cassells et al.* 1996). Because of the high cost and the difficult availability of the thermal remote sensing data, multispectral scanning in the visible and reflective IR part of the spectrum is often applied instead (*Feng* 1987; *Ma* 1990; *Kang et al.* 1993). In this way no thermal anomalies themselves are detected, but only areas underlain by burnt rocks related to coal fires. The higher estimates for annual loss of coal (100–200 million tons) are essentially based on delineating coal fire boundaries from such multispectral mapping of burnt rocks and extending them underground using dip and thickness of the coal seams.

In this paper we present remote sensing and field data from Xinjiang Autonomous Republic in NW China to demonstrate that the majority of burnt rocks recognized in multispectral imagery is of Pleistocene age. Field relations and paleomagnetic dating show that coal fires have formed by spontaneous combustion of coal seams already more than one million years ago. The annual coal losses and CO₂ output figures based on burnt rock mapping alone are therefore greatly exaggerated. Thermal modeling of the coal fires (*Cassells et al.* 1998) supports this conclusion.

8.2 Geological setting

The Toutunhe study area is situated 30 km southwest of Urumqi (Xinjiang) in the transition zone between the Tian Shan Mountain range and the Junggar Basin, at an altitude between 1000 and 1400 m. It is crossed by the Toutunhe River fed by the glaciers of the Tian Shan Mountains and by its tributaries Qianshuihe, Gangou and Haojiagou (*Figs 8.1 & 8.2*).

The core of the E–W trending Tian Shan Mountain range consists of pre-Mesozoic basement rocks (*Peng & Zhang* 1989; *BGXJ* 1993; *Carroll et al.* 1995). On the northern side of Tian Shan, Mesozoic and Cenozoic sedimentary rocks have been detached from the underlying pre-Mesozoic rocks and folded into three rows of E–W trending anticlines and synclines during the Yanshan orogenic phase at the end of the Cretaceous period. The Kelazha anticline in the study area is situated in the first row, with Jurassic strata

forming the core of the folds. Unfolded Pliocene sediments unconformably cover the Jurassic and Cretaceous rocks. The main coal-bearing strata that have been burnt belong to the Middle Jurassic Xishanyao Group, which consists of fresh-water deltaic sediments including mudstone, siltstone, sandstone and coal layers (BGXJ 1993; Schneider 1996). The coal layers are concentrated in the lower parts of the Xishanyao Group with thicknesses varying from 1 to 27 m. The lowest mineable layer is called Dacao coal layer with a constant thickness of 15–17 m.

The Toutunhe River dissects the folded Jurassic coal-bearing strata and shows a flight of at least six river terraces (Figs 8.2 & 8.3; Qiao 1981; Hung & Zhao 1981; Molnar *et al.* 1994). The uppermost ones are situated about 90 m above the river, the lowermost one about 15 m above present river level. The other terraces are situated between these, with a regular space interval of about 10–15 m. Most of the terraces are cut into bedrock and capped by 1–3 m of coarse gravel.

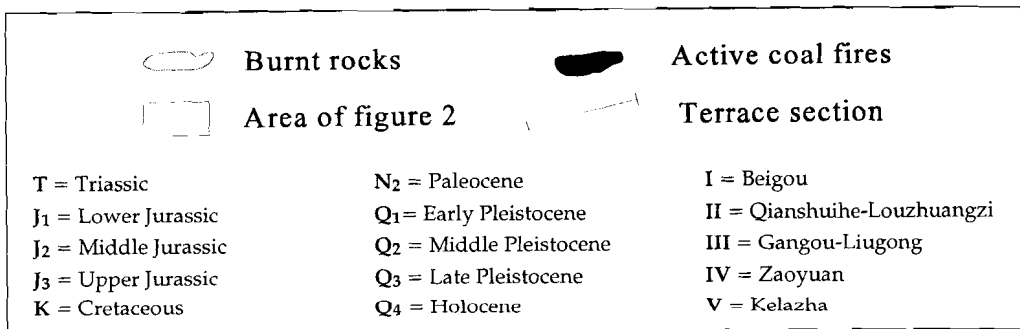
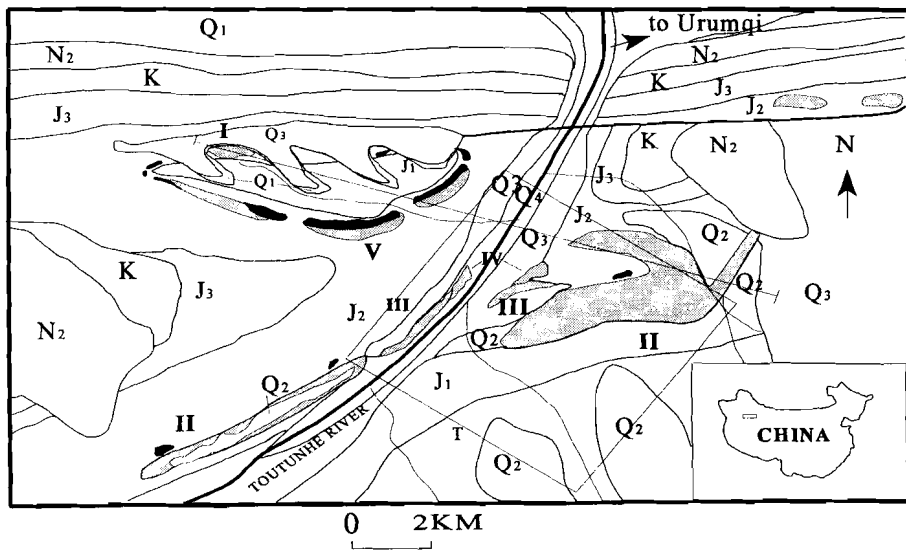


Figure 8.1: Geological map of the study area with distribution of burnt rocks and active coal fires.

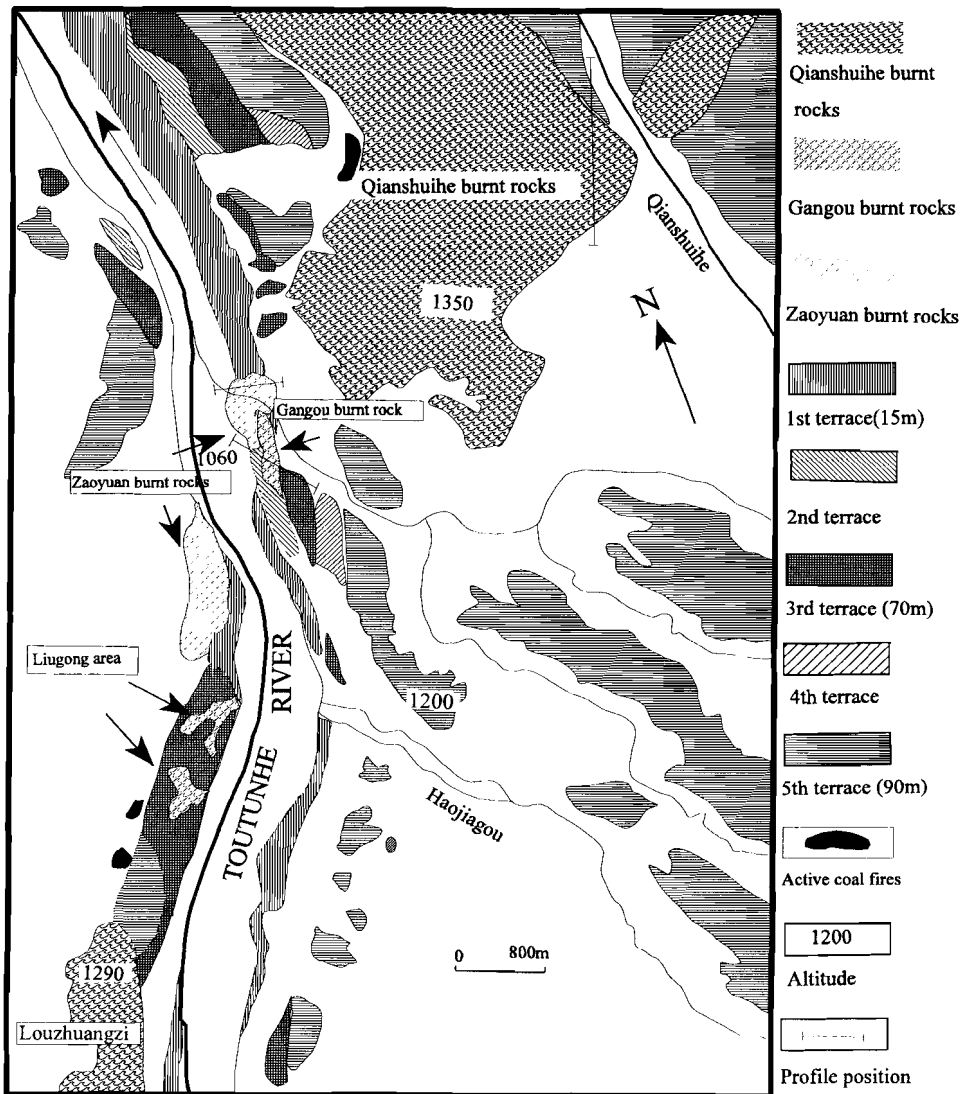


Figure 8.2: Distribution of burnt rocks and river terraces.

8.3 Remote sensing data

Airborne thermal data acquired on July 30, 1992 (night-time), at a wavelength of 8–12 μm were used to delineate the areal extent of active coal fires in the study area. Airborne multispectral data (band 1: 0.45–0.51 μm ; band 2: 0.53–0.61 μm ; band 3: 0.61–0.69 μm ; band 4: 0.69–0.77 μm), LANDSAT TM within the visible and infrared wavebands, SPOT data and colour infrared stereo photographs, acquired on the 7th of August 1992 at a scale of 1:25,000, have been used to map burnt rocks and their outcrop conditions (*cf. Zhang 1998, Fig. 7.1*). Combining the thermal data with the other types of imagery shows that only ~10.4% (*Fig. 8.2*) of the burnt rock area corresponds with active coal fires; the remaining burnt-rock surface shows no thermal anomalies and is therefore extinct: Zaoyan burnt rocks (4.7%), Gangou–Liugong burnt rocks (8.2%), Qianshuihe–Louzhuangzi burnt rocks (76.2%), and Beigou burnt rocks (0.5%).

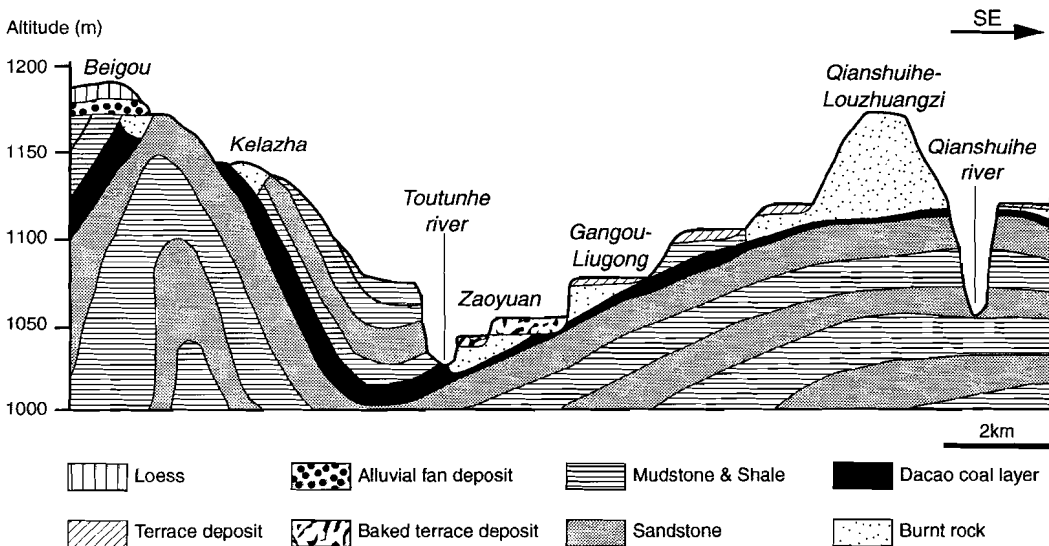


Figure 8.3: Cross-section of Toutunhe River terraces and burnt rock occurrences.

8.4 Field characteristics of burnt rocks

Burnt rocks (pyrometamorphosed rocks) is a general term for thermally metamorphosed rocks originating from heating by burning coal seams. Burnt rocks can be classified according to characteristics such as colour, texture and structure and metamorphic temperatures (Guan 1963). In a face-slope exposure of slightly dipping burnt rocks in a cuesta a characteristic three-layer profile is developed (*cf.* Fig. 8.4). (1) At the bottom, there are the unburnt rocks underlying the coal seams. Nearing the contact with the burnt coal seam, the rocks gradually get a baked appearance, as is obvious in mudstones from the brick-red colour, ceramic character and sound, and sometimes a characteristic mm-sized six-sided columnar structure (chop-stick rock) caused by shrinkage joints disposed in a sheaf-like fashion, not unlike jointing in basaltic lava flows. These have been baked at temperatures between 500–800°C (H. Guan, pers. comm.). Locally, the presence of a characteristic hardened kaolin layer (baked underclay) seems to have acted as an insulator, thus protecting the underlying rocks from baking. Sandstones appear less affected by baking alone. (2) The coal seam itself has been reduced to a thin ash layer of only a few centimeters in thickness, often rich in gypsum. (3) Above the ash layer the roof of the coal seam has usually collapsed, resulting in a breccia-like structure. As the temperature of coal fires usually increases upwards as a result of oxygen supply, these rocks are also partially molten. Between the partially molten fragments of collapsed roof rocks, often a dark vesicular glassy matrix is found, sometimes with micro-flow structures as in ropy lavas. These rocks have attained temperatures between 1000–1200°C, based on mineralogical evidence. Locally occurring completely molten scoria-like rocks may even have attained temperatures between 1500–2100°C (H. Guan, pers. comm.). Loess overlying burnt rock may have been baked to brick-like substances. The maximum thickness of the burnt rocks in the study area is about 100–150 m. The reddish-yellowish colour enables unequivocal identification of burnt rocks in the remote sensing imagery acquired from visible and infrared bands.

8.5 Age of the paleo-coal fires

8.5.1 Quaternary stratigraphy

The outcrop conditions of the paleo-coal fires in the Toutunhe area are intimately related to the development of river terraces (Fig. 8.3), which in turn is closely related to glaciation and deglaciation in the adjacent Tianshan Mountains. A general age classification of the terrace deposits spanning the whole Quaternary has been obtained mainly by correlation with morainic stages in the Tianshan Mountains in the upper reaches of the Toutunhe River (Bo 1981; Qiao 1981; BGXJ 1993). Five age groups of burnt rocks have been recognized in this area based on their relationship with the terraces.

(1) *The Beigou burnt rocks*

The Beigou burnt rocks occur at an unconformity between steeply dipping Jurassic coals and black shales and unbaked deposits of a dissected alluvial fan, ca. 200 m above the level of the Beigou tributary of the Toutunhe River. The alluvial fan could be Late Pliocene or Early Pleistocene (Q1 high terrace, in Chinese terminology, 0.7–2 Ma). These deposits might correspond to the Xiyu formation in which elsewhere abundant Late Pliocene fauna has been found, and which is generally associated with the inception of glaciation (Qiao 1981; Molnar *et al.* 1994).

(2) *The Qianshuihe and Louzhuangzi burnt rocks*

In the Qianshuihe area a classic profile of burnt rocks (Fig. 8.4) shows 20 m of molten scoriaceous breccias on top of the burnt Dacao coal layer, in turn underlain by a baked kaolin ('porcellanite') layer. Their position in the field suggests them to be older than the 90 m terrace nearby. A similar situation is found in the southwestern part of the area near Louzhuangzi along the western side of the Toutunhe River. The Qianshuihe and Louzhuangzi 90 m terraces are fluvio-glacial, and of Middle Pleistocene age (Q2, 0.7–0.1 Ma). The only published age 'control' is the find of *Palaeoloxodon*, a fossil elephant (now generally included in the genus *Elephas*; Nilsson 1983) in the Middle Pleistocene gravels at Yaomuoshan about 15 km east of the study area (Qiao 1981).

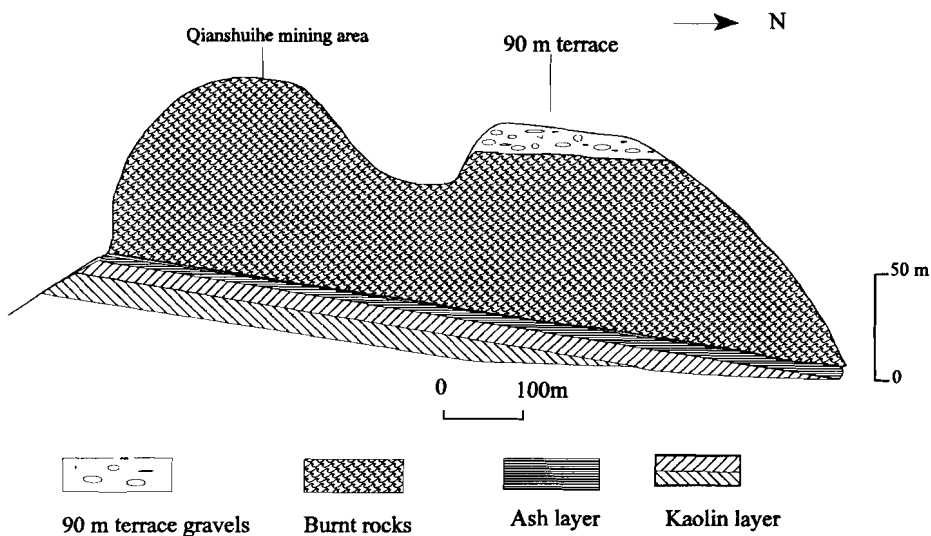


Figure 8.4: Qianshuihe burnt rock profile.

(3) *The Gangou and Liugong burnt rocks*

Along the lowermost reach of the Gangou tributary of the Toutunhe River, 15–20 m of burnt rocks, molten breccias and small lava-like glassy flows are overlain by unbaked gravel of the 70 m terrace of the Toutunhe River (Figs 8.2 & 8.5). The burnt rocks contain strongly deformed, molten and baked pebbles derived from an older cover of terrace gravel deposited prior to the coal fire, probably from the collapsed roof of the 90 m terrace. Similar burnt rocks are found at the Liugong area at the west side of the Toutunhe River (Fig. 8.2). The Gangou 70 m fluvio-glacial terrace is estimated by Qiao (1981) to be Late Pleistocene (Q3, 100–10 ka).

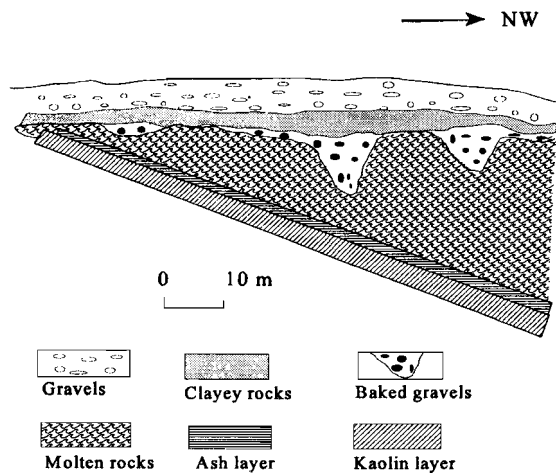


Figure 8.5: *Gangou burnt rock profile.*

(4) *The Zaoyuan burnt rocks*

The Zaoyuan burnt rocks lie on the first and second terrace of the Toutunhe River (Figs 8.1–8.3). Pebbles on top of the burnt rocks were completely baked, and even partially molten. No unbaked sediments are present on top of these terrace deposits. The Zaoyuan coal fires are probably Holocene (Q4, <10 ka).

(5) *The Kelazha burnt rocks*

The Kelazha burnt rocks are directly related to the active coal fires. These burnt rocks occur above, around or close to the active coal fires. These are the only burnt rocks that show up in thermal IR imagery. In the field they differ in a number of aspects from the paleo-coal fires. No complete sections can be seen, as most fires are raging underground. Most characteristic are differences in surface mineralogy as related to temperatures at the

vents, as measured with the thermal radiometer in the field (Zhang *et al.* 1995). On a horizontal surface, coal fire vents below 80–90°C have a halo around them consisting of tarry substances mixed with sulfur. Between 90–120°C the halo consists of native sulfur alone, while above 120°C, i.e. above the sublimation point of sulfur, white linings of salmiac can be found. None of these materials have been found so far in paleo-coal fires.

8.5.2 Paleomagnetism

Paleomagnetic measurements were carried out on rock samples collected in the field to constrain the age estimates of the coal fires magnetostratigraphically. The characteristic remanent magnetization (ChRM) of the samples was determined to obtain their magnetic polarity. The magnetic polarity pattern of the burnt rocks can then be correlated to the geomagnetic polarity time scale (Fig. 8.6), which is constructed based on irregular reversals of the Earth's magnetic field. This method has been used successfully in dating porcellanites from North Bohemian coal basins (Tyráček 1994).

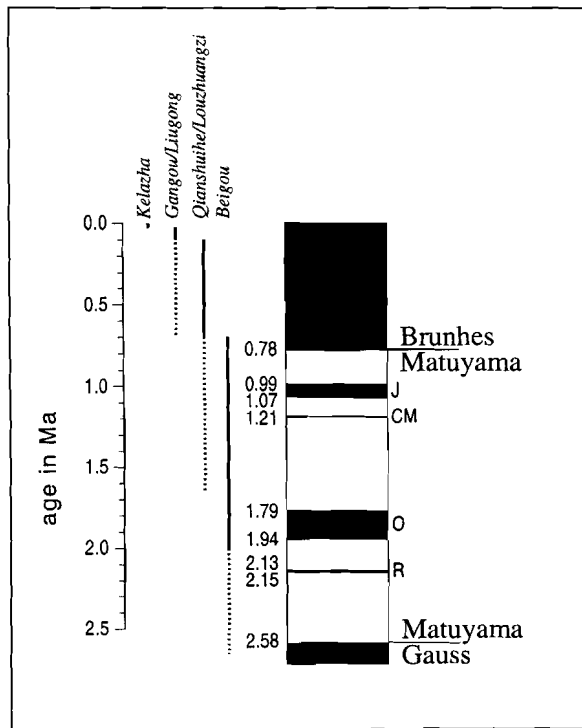


Figure 8.6: Geomagnetic polarity time scale of the Late Pliocene to Holocene according to Lourens *et al.* (1996). Black (white) blocks denote periods with normal (reversed) directions of the geomagnetic field. J: Jaramillo; CM: Cobb Mountain; O: Olduvai; R: Reunion. Vertical lines represent the age estimates based on Quaternary stratigraphy.

Ten oriented hand samples were taken in the field. Two samples from each of the Beigou, Qianshuihe–Louzhuangzi and Kelazha groups, and four samples from the Gangou–Liugong group were processed. From each hand sample, one core (diameter of 25 mm) was drilled in the laboratory; several specimens with a length of 22 mm were cut from each core. At least one of the specimens was stepwise demagnetized with alternating fields.

The different burnt rocks give good paleomagnetic results (*Fig. 8.7*). They show relatively high initial NRM intensities ranging 0.002–5.79 A/m. After the decay of a small viscous NRM component at 10–20 mT peak alternating field, they show univectorial decay to the origin. All cores showed stable normal ChRM directions. Measured inclinations conform to expected values for the site latitude.

The directions of the ChRM in these burnt rocks could well be caused by a thermoremanent magnetization (TRM) acquired at the time of final cooling. The pyrometamorphic rocks of the Xinjiang region, in particular the breccious types on top of the burnt coal seams show field evidence of having reached temperatures well above 765°C, i.e. higher than the Curie points (T_c) of all magnetic minerals. On cooling below their T_c , magnetic minerals acquire a magnetization parallel to the ambient geomagnetic field. If the measured remanence is indeed a primary TRM, it implies that the sampled rocks all cooled during a normal period of the geomagnetic field.

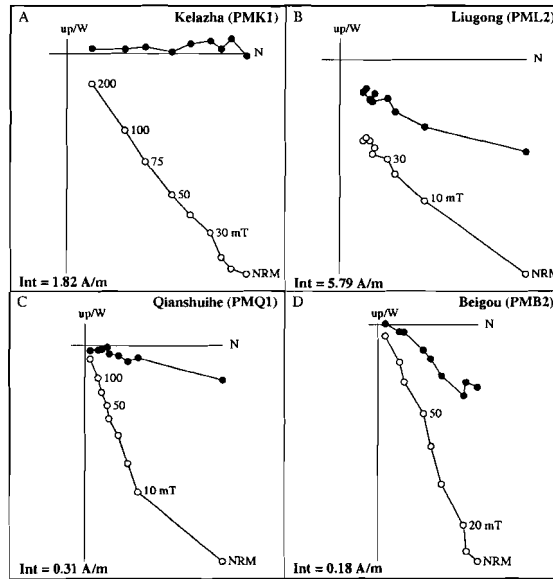


Figure 8.7: Examples of alternating field demagnetization diagrams for samples of the burnt rock groups from the Xinjiang region, showing their normal polarity. Closed (open) symbols represent the projection of the NRM vector end-points on the horizontal (vertical) plane, respectively; values represent alternating fields in mT. Int = initial NRM intensity.

On the basis of the general stratigraphy outlined above, normal directions of the ChRM are expected for the samples from the Holocene (<10 ka) Kelazha and Zaoyuan groups and the Middle to Late Pleistocene (0.7–0.01 Ma) Gangou-Liugong group, because these groups of burnt rocks are younger than the beginning of the last normal polarity interval (Brunhes/Matuyama boundary: 780 ka). The normal polarities of the older Qianshuihe–Louzhuangzi and Beigou groups yield various options for their paleomagnetic age: slightly younger than 0.780 Ma (beginning of the normal Brunhes Chron), between 0.990 and 1.070 Ma (Jaramillo subchron) or, rather coincidentally at 1.21 Ma (Cobb Mountain cryptochron). Older options for the burnt rocks from the Beigou group are the normal polarity intervals during the Late Pliocene: Olduvai subchron (1.785–1.942 Ma); Reunion subchron (2.129–2.149, also rather coincidentally) and the end of the normal Gauss Chron ≥ 2.582 Ma (ages by *Lourens et al.* 1996).

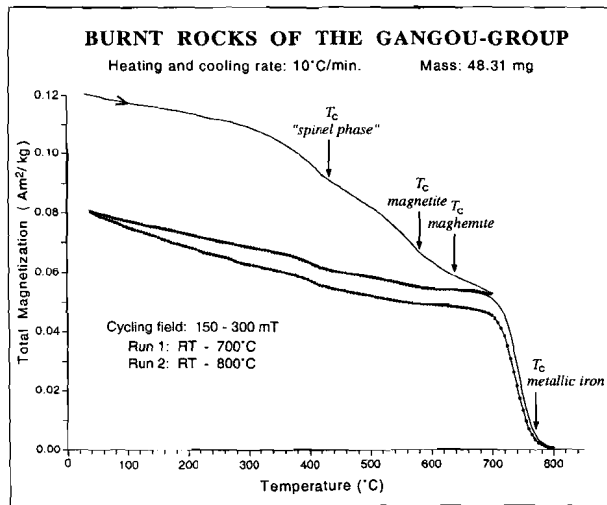


Figure 8.8: Example showing a typical in air thermomagnetic analysis of burnt rocks from the Gangou group, clearly indicating the presence of metallic iron ($T_c = 770^\circ\text{C}$). Minor inflection points around 440°C , 580°C and 640°C suggest the presence of a magnetic spinel phase, magnetite, and maghemite, respectively.

Various rock-magnetic analyses were carried out to identify the carriers of the NRM and to investigate the significance of the paleomagnetic datings of the end of the coal fires (see Chapter 9). Most burnt rocks appear to contain more than one magnetic mineral. The dominant magnetic carriers are stable single-domain to pseudo-single-domain magnetites (Fe_3O_4) of varying oxidation and/or isomorphous substitution degree. Near pure maghemite ($\gamma\text{-Fe}_2\text{O}_3$) and hematite ($\alpha\text{-Fe}_2\text{O}_3$) are the remanence carriers in the Beigou burnt rocks. In addition, amounts of rare native iron ($\alpha\text{-Fe}$; $T_c = 770^\circ\text{C}$; *Bozorth* 1961) were detected during thermomagnetic runs (*Fig. 8.8*). The presence of $\alpha\text{-Fe}$ implies

extremely reducing conditions during the formation of the burnt rocks, similar to those encountered in a blast furnace.

The traces of metallic iron were detected in the younger Kelazha and Gangou samples. Since the ChRM of the older Qianshuihe–Louzhuangzi and Beigou groups is carried by iron oxides, one might suggest that they have recorded oxidation during a normal polarity interval any time after burning, rather than expressing a primary TRM. Also, a primary remanence carried by metallic iron particles may be magnetically not very stable, and thus the observed magnetization would more likely be caused by viscous resetting. This would imply that the measured normal directions of the ChRM were acquired recently instead of representing a primary TRM. These options, however, appear rather unlikely. Thermomagnetic analyses (*Fig. 8.8*), for instance, showed that the metallic iron survives heating in air up to 800°C, whereas magnetite was almost completely oxidized to hematite during the same experiment. First this suggests that both magnetic minerals exist as separate phases and second that the α -Fe particles are likely incorporated as tiny inclusions in host minerals. In this form they likely may persist during geological time. Furthermore, progressive stepwise thermal demagnetization of an imparted triaxial IRM revealed that the α -Fe particles belong to the high coercivity fraction (>120 mT). The native iron present in burnt rocks thus can carry a magnetically stable remanence, implying that the particles are single domain ranging between ~ 0.008 – 0.02 μm . In addition, they likely have an acicular shape, since magnetic domain theory predicts coercivities (B_c) of ~ 25 mT for equant grains and up to 1 T for long needles (e.g. *Tagawa et al. 1986; Dunlop & Özdemir 1997*).

8.6 Discussion

The combined remote sensing and field data show that coal fires have occurred in the area during a large part of the Pleistocene. Under natural conditions, a coal fire can start wherever a coal seam crops out near the surface. Processes as faulting, folding and denudation or valley incision by streams can cause natural exposure of coal seams. Once exposed, spontaneous combustion can start, as this is an exothermic oxidation process as soon as a certain threshold temperature is passed (*Banerjee 1985*). The threshold temperature for specific types of coal can be exceeded by forest fires, lightning, and even by solar heating for favourably exposed coal seams.

In the Toutunhe area, the process that led to exposure of the coal seams is intimately related to the formation of river terraces starting from the Pliocene onward. Using ^{10}Be exposure age dating of deformed river terraces in the uplifting Kuitun He and Qiuergou He valleys nearby, *Molnar et al. (1994)* concluded that cyclicity in terrace deposition and dissection is probably tuned to the 100 kyr cyclicity of global climate change. This is consistent with modeling studies on terrace formation (*Boll et al. 1988; Veldkamp & Vermeulen 1989; Veldkamp 1992*).

Taking this into account, and based on the Plio-Pleistocene age (~2 Ma) of the Beigou alluvial fan deposit at 200 m, terrace steps at 10 m intervals would indeed coincide with the major 100 kyr global climate cycles. It would imply as well that the 70 m Gangou/Liugong terraces are around 700 ka old, i.e. considerably older than traditionally considered in Chinese Quaternary stratigraphy (Qiao 1981). Uplift rates here are a factor 10 lower than in the area studied by Molnar *et al.* (1994), and more in line with the uplift rate of 10 cm/kyr considered optimal for river terrace formation and preservation (Veldkamp & Van Dijke 1998).

Terrace deposition probably took place during arid glacial periods and early deglaciation, while dissection predominated in the interglacials. Exposure of coal seams and concomitant spontaneous combustion of coal seams therefore must be largely an interglacial phenomenon.

8.7 Conclusions

Spontaneous combustion of coal seams is a natural phenomenon which has occurred repeatedly during the recent geological past. It can occur at any site where deformation, uplift and dissection lead to exposure of coal to the air. Spontaneous coal fires are especially likely to occur during interglacial dissection of river valleys at moderate uplift rates.

A large part of burnt rocks identified in remote sensing imagery and field data in NW China appears to be of Pleistocene age, although still considerable uncertainty exists about the precise age of the coal fires. Establishing the contribution of coal fires to the global CO₂ budget should be done on the base of a combination of remote sensing imagery including thermal IR data, and field data, not on the base of the occurrence of burnt rocks alone.

ACKNOWLEDGMENTS

This project is funded by Commission of The European Communities under the contract No. CII*-CT93-0008. The authors would like to thank *Prof. J.L van Genderen* and *Prof. Guan Haiyan* for kindly organizing the field work. The authors also wish thank *Dr. Tan Yongjie*, *Dr. P. van Dijk*, *Mr. Zhang Jianzhong*, *Mr. Kang Gaofeng* and *Mrs Yang Hong* for their help during the field work. *Dr. Hogne Jungner* of Helsinki University is thanked for his cooperation in trying to date the burnt rocks with TL, and the late *ir. Christiaan Maugelest* for literature research on *Palaeoloxodon*. *Ton van Hoof* is acknowledged for performing the AF demagnetizations of the NRM and for measuring the hysteresis parameters.

Chapter 9

Rock-magnetic properties of baked and molten rocks overlying burnt coal seams in Northwest China

C. B. de Boer⁽¹⁾, M.J. Dekkers⁽¹⁾, X. Zhang⁽²⁾ and S.B. Kroonenberg⁽³⁾

1 Paleomagnetic Laboratory 'Fort Hoofddijk', Utrecht University, Faculty of Earth Sciences, Budapestlaan 17, 3584 CD Utrecht, the Netherlands. E-mail: cdeboer@geo.uu.nl

2 Dept of Earth Resources Surveys, ITC, P.O. Box 6, Enschede, the Netherlands,

3 Faculty of Applied Earth Sciences, Delft University of Technology, P.O. Box 5028, 2600 GA Delft, the Netherlands,

SUMMARY

The subsurface spontaneous combustion of coal seams in Xinjiang (NW China) during Pleistocene to Recent times produced large areas of thermally altered sedimentary rocks that have become highly magnetic. The NRM intensities and low-field susceptibilities of such combustion-metamorphic rocks typically range 0.1–10 A/m and $100\text{--}1000 \times 10^{-4}$ SI, respectively, which is two to three orders of magnitude higher than values generally reported for their sedimentary protoliths. The dominant magnetic carriers in the burnt rocks appear to include relatively pure forms of magnetite, maghemite and hematite as well as spinel phases with various amounts of isomorphous substitution. These magnetic phases dominantly occur as stable pseudo-single-domain particles. Conspicuous is the presence of pure metallic iron (α Fe) in some samples. This highly magnetic phase most likely appears as more or less elongated superparamagnetic and single-domain (SD) inclusions in host minerals, which prevent them from oxidizing. The SD α Fe particles can carry a highly stable remanence, having remanent coercivities ranging 70–140 mT. The ARM and IRM stability of all burnt rock samples to alternating fields appears to be relatively high; median destructive fields, $B_{\frac{1}{2}A}$ and $B_{\frac{1}{2}I}$, range 25–46 and ~20–30 mT for dominant spinel-bearing samples, 34–36 and 47–53 for maghemite-hematite-bearing samples, and 48–89 and 64–84 for metallic iron-bearing samples. Consequently, burnt rocks are high-quality geomagnetic field recorders. Their very nature makes them useful

for paleointensity determinations although age determination might be a limiting factor. Furthermore, remanence intensities and susceptibilities of these magnetically enhanced rocks are sufficient to produce observable magnetic anomalies. This property illustrates the potential to delineate the areal extent and depth of (extinct) coal fires with magnetic anomaly methodology. Such information is necessary to refine estimates of hazardous CO₂ emission and furthers our understanding of the evolution and mechanism of coal fires. In addition, magnetic anomaly modelling on burnt rocks also has potential for coal exploration.

Key Words: *combustion-metamorphic rocks, coal fires, metallic iron, rock magnetism*

9.1 Introduction

Baked and fused rocks produced by the subsurface spontaneous combustion of coal seams are fairly common geological features in many countries throughout the world: e.g. United States (Foit *et al.* 1987; Cosca *et al.* 1989), India (Prakash *et al.* 1997), Romania (Rădan & Rădan 1998), Czech Republic (Tyráček 1994), Australia (Ellyett & Fleming 1974), New Zealand (Lindqvist *et al.* 1985) and China (Zhang 1998). In Northern China, these so-called pyrometamorphic or combustion-metamorphic rocks are scattered over an enormous area stretching 5.000 km EW and 750 km NS (Guan 1984, 1989). In this region alone, already more than 100 active coal fire areas were detected in 55 coal fields, some of which have been burning for several hundreds of years (Guan 1984; Kang *et al.* 1993; Van Genderen *et al.* 1996; Guan *et al.* 1996). The combustion-metamorphic rocks, however, are not restricted to active coal fires only. In Xinjiang (NW China), for instance, it was shown (Zhang 1998; Chapter 8) that spontaneous combustion of coal seams has occurred repeatedly during the recent geological past; over 90% of the burnt rocks recognized in remote sensing imagery were associated with extinct coal fires and mainly of Pleistocene age.

Combustion-metamorphism generally occurs at high (>600°C) to ultra-high (>1000°C) temperatures and low pressures (≤100 MPa). However, the degree of thermal alteration produced by burning coal beds is variable, and a single outcrop may contain altered rocks ranging from slightly baked to entirely fused (*cf.* Cosca *et al.* 1989). In close proximity to the burning coal seam and especially near vents and cracks in the overlying rocks (fresh oxygen supply) extreme temperatures up to 1500–2100°C can be reached (e.g. Bentor *et al.* 1981; H. Guan, pers. comm.). The subsurface coal fire now operates as a natural blast furnace. Indeed, the (partially) fused and often highly vesicular rocks resemble blast furnace slags to a large extent, both in appearance and mineralogy.

The few paleomagnetic studies on these thermally affected rocks indicate that they can be high-fidelity geomagnetic field recorders (Jones *et al.* 1984; Krsová *et al.* 1989; Tyráček 1994; Rădan & Rădan 1998) possessing a stable (partial) thermoremanent and/or thermochemical remanent magnetization. Because of the substantial heating, the rocks generally become magnetically enhanced resulting in high remanence intensities resembling those of regular extrusive rocks. In addition, results by Jones *et al.* (1984) on

baked rocks from Wyoming –although of preliminary nature– suggest that combustion-metamorphic rocks have potential to provide a high-resolution recording of the geomagnetic field, at least for much of the Quaternary, since the baked rocks show secular variation. Because of a favourable coal-seam/topography relationship, the combustion-metamorphic rocks would represent a long duration. The fires have started at the original outcrop and with propagation rates that are nowadays reasonably well known (e.g. Kang *et al.* 1993) the duration of a burning event can be estimated from the depth of the burnt rocks. Jones *et al.* argue that intermittent burning events (also in different coal seams) would be correlatable by fission-track dating on zircons that also would provide absolute ages for (part of) the records, although the rather large errors inherent to the fission-track method are acknowledged. In the ideal situation a more or less continuous composite record would be constructable. Although being interesting from a paleomagnetic point of view, so far very little is known of the magnetic minerals which carry the remanence in these conspicuous rocks.

In this contribution we report on the rock-magnetic properties of various burnt rock samples taken from outcrops exposed in the Toutunhe River area located in the foothills of the Tian Shan Mountains SW of Urumqi, the capital city of the Xinjiang Uygur Autonomous Region in NW China. The samples were collected to constrain their age paleomagnetically. Their NRM characteristics were published in an earlier paper together with a brief description of the appearance of the burnt rocks at the sample sites (Zhang *et al.* 1999; Chapter 8). In the study area, spontaneous combustion of folded coal seams –varying in thickness from 1 to 27 m– has thermally altered the overlying Jurassic deltaic sequences of siltstones, mudstones, and sandstones (Schneider 1996) as well as Holocene river terraces. Typical thickness of the burnt rock deposits in the study area is 10–30 m, whereas the maximum thickness is approximately 100–150 m.

9.2 Samples and equipment

Ten oriented hand samples were collected from four different age-groups of burnt rocks spanning the Quaternary (Table 9.1). Because of their original paleomagnetic purpose, sampling was confined to areas where the burnt rocks had a hard and coherent appearance, were least deformed and showed evidence of high baking temperatures, i.e. total removal of any pre-existing remanence. Furthermore, the samples were taken as much as possible from the bottom of the collapsed layer to avoid reorientation after TRM acquisition. The NRM intensities, age estimates, and texture and colour descriptions are summarized in Table 9.1. The oldest burnt rocks from the Beigou-group (PMB1 & PMB2) are compact reddish-brown samples that are slightly breccious. The dark grey samples of Middle Pleistocene age, PMQ1 and PML3, respectively, are slightly and highly vesicular with a ‘sugary’ appearance. PMQ1 weathers pale brownish. The Late Pleistocene Gangou (PMG1 & PMG2) samples are (pale) grey vesicular with a variable breccious character. Sample PMG1 has a brownish weathering colour, whereas PMG2 has a pale yellowish-brown surface layer. The Liugong burnt rock samples (PML1 & PML2) belong to the same age-group as Gangou: they are pale grey vesicular and black

Table 9.1: *NRM intensities, ages estimates and some colour and texture characteristics of the different burnt rock samples collected in the Toutunhe River area in NW China.*

Sample site	code	colour	texture	NRM (A/m)	estimated age
BEIGOU	PMB1	reddish-brown	compact/breccious	0.189	Late Pliocene/Early Pleistocene
„	PMB2	reddish-brown	compact/breccious	0.178	Late Pliocene/Early Pleistocene
QIANSHUIHE	PMQ1	dark grey	slightly vesicular	0.314	Middle Pleistocene
LOUZHUANGZI	PML3	dark grey/black	highly vesicular	0.741	Middle Pleistocene
GANGOU	PMG1	pale grey	vesicular	0.002	Late Pleistocene
„	PMG2	pale grey	vesicular	0.002	Late Pleistocene
LIUGONG	PML1	pale grey	slightly vesicular	0.879	Late Pleistocene
„	PML2	purple-black	compact/fine-grained	5.789	Late Pleistocene
KELAZHA	PMK1	brownish-grey	vesicular/breccious	1.824	Holocene/ active fires
„	PMK2	tiger-striped	relict structure/vesicular	0.779	Holocene/ active fires

fine-grained compact rocks with a purple shade, respectively. PML1 has a brownish weathering colour. The youngest burnt rocks which are associated with active coal fires, are labeled PMK1 & PMK2. PMK1 is a brownish-grey vesicular breccia with an orange-brown weathering colour, whereas the slightly vesicular PMK2 sample is the only rock in which remnants of a relict bedding structure are still recognizable by a reddish tigerstripe pattern (mm scale). Apart from the Gangou samples, the NRM intensities appear to be very high (0.2–5.8 A/m) when compared to the NRM intensities generally reported for their sedimentary protoliths (~0.01–1 mA/m). Heating-induced mineral transformation thus magnetically enhanced these rocks, although there is a fundamental difference between the NRM acquisition mechanisms: TRM for the burnt rocks versus a DRM for their protoliths. The acquisition of a TRM would have resulted in a (several) orders of magnitude higher intensity, regardless of enhancement in magnetic minerals

The alternating field (AF) demagnetization diagrams of the NRM of all burnt rock samples were of high quality. The determination of the ChRM directions was straightforward, all samples show univectorial decay to the origin (*cf.* Chapter 8). Only stable normal ChRM directions were detected. Rock-magnetic investigations, reported on here and performed to characterize the carriers of the remanence, comprised acquisition of anhysteretic (ARM) and isothermal (IRM) remanent magnetization, AF and thermal demagnetization, susceptibility measurements, and Curie temperature analysis. ARM and IRM measurements were performed on standard cylindrical samples that were sister specimens of samples on which the NRM has previously been analyzed (Chapter 8). Unfortunately, no sister specimen of sample PML2 was available or could be obtained from the hand sample by additional drilling. Before imparting the ARM, the samples were AF demagnetized in a 0.3 T peak field to remove the high intensity NRMs. Anhysteretic remanences were progressively imparted using a laboratory-built AF demagnetizer coil with a maximum peak AF field of 0.3 T and a steady DC biasing field of ~16 μ T which

was parallel to the axis of the alternating field. An uniaxial (1 T) as well as a triaxial composite IRM (1 T, 120 mT and 20 mT), were acquired with a PM4 pulse magnetizer. The acquired remanences were measured on a digitized spinner magnetometer based on a Jelinek JR3 drive unit. After acquisition was completed, the ARM and the single-axis IRM were stepwise AF demagnetized in peak fields up to 0.3 T, whereas the triaxial IRMs were progressively demagnetized by applying stepwise thermal demagnetization with 50° or 100°C temperature increments below 500°C and with 20°C intervals up to 750°C. Thermal demagnetizations were performed in a magnetically shielded laboratory-built furnace. After each temperature step, the low-field bulk susceptibility was measured with a KLY-2 susceptibility bridge (AGICO, Brno) by averaging measurements along three orthogonal sample axes. Thermomagnetic runs of crushed samples were recorded in air with a modified horizontal translation Curie balance making use of a cycling field (Mullender *et al.* 1993). Hysteresis loops and remanent coercivity curves were obtained on rock chips of a few milligram using an alternating gradient magnetometer (MicroMag Model 2900).

9.3 Experimental results

9.3.1 Thermomagnetic analysis

Apart from samples PMQ1, PML1, and PMK1, the strong-field thermomagnetic behaviour in air of the burnt rocks is characterized by more than one magnetic mineral (Figs 9.1a-j). The heating curves of the reddish-brown Beigou samples (Figs 9.1a & b), for instance, exhibit Curie points (T_c) at ~630°C and ~675°C, typical of nearly pure maghemite ($\gamma\text{-Fe}_2\text{O}_3$) and pure hematite ($\alpha\text{-Fe}_2\text{O}_3$), respectively. The inflection at 410–420°C might represent the T_c of a spinel-type phase (substituted magnetite) or the irreversible transformation of the most fine-grained portion of the maghemite phase to less magnetic hematite. The latter option is favoured as the cooling curve does not show the break in slope at 410–420°C. Most of the thermodynamically metastable maghemite, however, survives heating up to 700°C. Such ‘high-temperature stability’ is reported for relatively coarse-grained maghemite and slightly Al- and/or Ti-substituted maghemite varieties (e.g. Wilson 1961; De Boer & Dekkers 1996). Although both samples are magnetically dominated by highly magnetic maghemite, chemically they are fully dominated by hematite, since the spontaneous magnetization (σ_s) of $\gamma\text{-Fe}_2\text{O}_3$ is higher than that of $\alpha\text{-Fe}_2\text{O}_3$ by two orders of magnitude. Estimated weight percentages of hematite and maghemite based on the curves measured and their commonly reported σ_s values of 0.4 and 74 Am² kg⁻¹, are 10–20% and <1%, respectively.

Similarly-shaped irreversible thermomagnetic curves with a single 550–600°C near magnetite (Fe_3O_4) T_c characterize the samples PMQ1, PML1, and PMK1 of the Quianshuihe, the Liugong, and the Kalazha group, respectively (Figs 9.1c, g & i). The differences in Curie point are likely caused by slightly different degrees of isomorphous substitution and/or oxidation: impurities such as Ti, Al, and Mg are reported

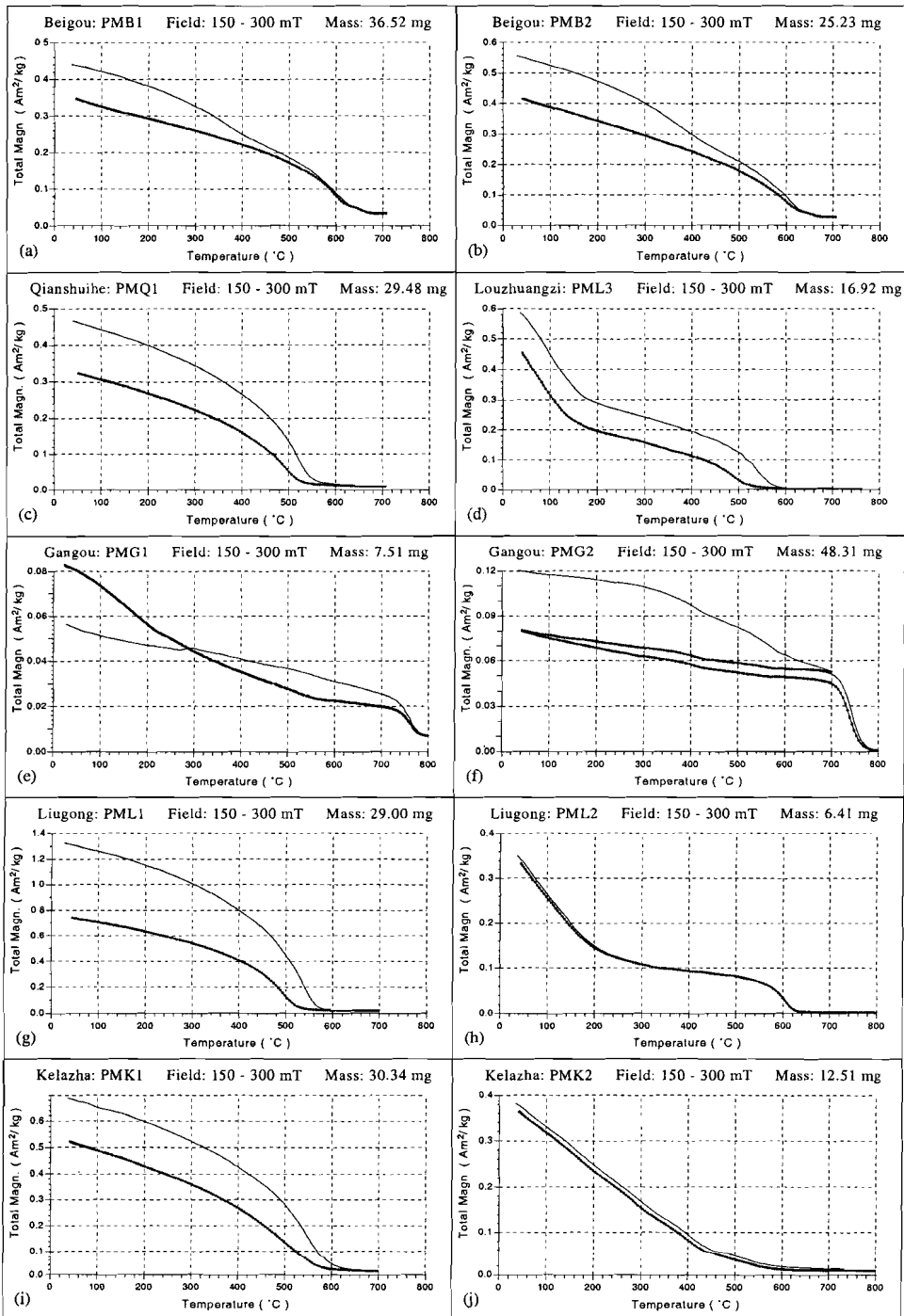


Figure 9.1 (left): Typical thermomagnetic curves measured in air of various combustion-metamorphic rocks. Thin solid lines and thick dotted lines denote heating and cooling runs, respectively.

to lower the T_c , while T_c increases with oxidation degree within the Fe_3O_4 – $\gamma\text{Fe}_2\text{O}_3$ solid-solution series (cf. Dunlop & Özdemir 1997). Curie temperatures for pure magnetite and maghemite are $\sim 580^\circ\text{C}$ and ~ 640 – 645°C , respectively (cf. Dunlop & Özdemir 1997). Noteworthy is the 30 – 50°C shift of the Curie points to lower temperatures on cooling from 700°C . This shift cannot be explained by experimental error, because temperature lag ($\leq 1^\circ$) is insignificant (see Figs 9.1a, b & h). This typical behaviour, however, could be caused by a heating-induced change of cation ordering. It appears that the Curie temperature of spinel-phases can be very sensitive to the intracrystalline distribution of Fe and ‘foreign’ cations between tetrahedral and octahedral sites of the spinel crystal structure: Harrison & Putnis (1999), for instance, showed that T_c appears to decrease with increasing disordering. For near-stoichiometric magnesioferrite (MgFe_2O_4), the authors obtained differences up to 60°C between the equilibrium ordered phase ($T_c = 364^\circ\text{C}$) and more disordered phases. In our case, this could imply that heating induced some degree of disordering of the cations which remains on cooling, resulting in the observed decrease in T_c . In this view, the decrease in magnetization observed on cycling might be explained by a lower spontaneous magnetization of the disordered phase compared to the initial ordered phase, rather than by heating-induced oxidation. The latter process also reduces the magnetization but normally increases the Curie temperature. Weight percentages of the magnetic phase in these burnt rock types ranges between ~ 0.5 and $\sim 1.5\%$ based on $\sigma_s = 92 \text{ Am}^2 \text{ kg}^{-1}$ at room-temperature for pure magnetite.

Samples PML3 of the Louzhuangzi-group (Fig. 9.2d) and PML2 of the Liugong-group (Fig. 9.2h) are both characterized by a low- T_c (180 – 220°C) and a high- T_c (570 – 620°C) magnetic mineral, likely representing members of the magnetite–maghemite series with a high and a low degree of isomorphous substitution, respectively. The thermomagnetic behaviour of both samples, however, differ from each other by their behaviour on cooling. The high- T_c phase of sample PML3 shows the afore-mentioned shift in T_c and decrease in magnetization on cooling, whereas the high- T_c phase of sample PML2 shows reversible heating and cooling behaviour. The difference is likely explained by a different type and/or valence state of the substituting atom. The low- T_c phases of both samples show identical heating and cooling curves. Evidently, these phases are not susceptible to heating-induced changes in cationic ordering over the two magnetic sublattices of the spinel structure.

The Gangou-group burnt rocks (Figs 9.1e & f), which are significantly less magnetic (σ_s values: ~ 0.06 and $\sim 0.12 \text{ Am}^2 \text{ kg}^{-1}$) than the other samples (σ_s values: ~ 0.36 – $1.3 \text{ Am}^2 \text{ kg}^{-1}$), show the most conspicuous thermomagnetic behaviour. The samples are characterized by traces of highly magnetic pure native iron (αFe ; $T_c = 770^\circ\text{C}$; Bozorth 1961) which remarkably (partly) survives thermal cycling in air up to 800°C . This latter observation suggests that the αFe particles are present as tiny inclusions trapped in host minerals which prevent them from being oxidized. This suggestion is supported by a

study of *Haggerty & Toft* (1985) who observed metallic iron inclusions in altered garnet and ilmenite grains from lower crustal granulite xenoliths using reflected light microscopy. The detection of αFe in the burnt rocks is noteworthy because native iron is very rare in terrestrial rocks. Pure αFe has been described from only a few localities (e.g. *Verma & Prasad* 1975; *Deutsch et al.* 1977; *Haggerty & Toft* 1985) of which the most famous is Disko Island on West Greenland where huge iron boulders were formed after the incorporation of carbon-rich sediments into basalts during the extrusion (cf. *Ulf-Møller* 1990). Strongly reducing conditions and increased temperatures are required to produce native iron. In our setting, similarity to blast furnace conditions is highly conceivable.

The strong-field thermomagnetic behaviour of sample PMG1 seems to be dominated by ferromagnetic native iron, because no other Curie points are observed on the heating curve. The peculiar small break in slope at $\sim 270^\circ\text{C}$ is reproducible in other subsamples; its cause, however, is not known. The estimated weight percentage of αFe in this sample, based on the initial magnetization of $\sim 0.057 \text{ Am}^2 \text{ kg}^{-1}$ and a σ_s of $217.75 \text{ Am}^2 \text{ kg}^{-1}$ (*Bozorth* 1961), is only 0.026%. Sample PMG2 contains a comparable amount of metallic iron and additional traces of magnetite and a magnetic spinel phase with a T_c of ca. 440°C . Sample PMK2 of the Kelazha-group (*Fig. 9.1j*) seems to contain the same magnetic mineralogy as sample PMG2, but in different quantities and different relative amounts. The thermomagnetic curves of this sample are strongly dominated by the spinel phase with the T_c of ca. 440°C , whereas the Curie point of metallic iron is hardly visible.

9.3.2 Hysteresis parameters

Figure 9.2(a-c) shows some typical hysteresis curves for combustion-metamorphic rocks, whereas the hysteresis parameters of all samples are listed in *Table 9.2*. Panel (a)-type hysteresis loops were obtained on the maghemite-hematite-bearing Beigou samples. Such constricted or wasp-waisted hysteresis loops are produced by a mixture of magnetically soft (maghemite) and hard (hematite) minerals only when the two phases contribute comparable amounts of magnetization (e.g. *Roberts et al.* 1995). Like the thermomagnetic curves, this observation implies that hematite must be about 100 times as abundant in these rocks as maghemite to rival the latter's contribution to magnetization (cf. *Dunlop & Özdemir* 1997). The coercive force (B_c) of $\sim 30 \text{ mT}$ and the remanent coercive force (B_{cr}) of $\sim 100 \text{ mT}$ —dominated by the maghemite and the hematite phase, respectively—point to stable single-domain (SD) to pseudo-single-domain (PSD) particles for both minerals.

Ramp-like hysteresis curves, as shown in panel (b), are characteristic of the native iron-bearing Gangou samples. Such typical loops can be produced by large multidomain (MD) particles or by a mixture of superparamagnetic (SP) and SD particles. The relatively high B_{cr} values of 71 and 141 mT measured on these samples, however, appear to reject the first option. The high B_{cr} values imply that the SD part of the αFe particles is able to carry a highly stable remanent magnetization.

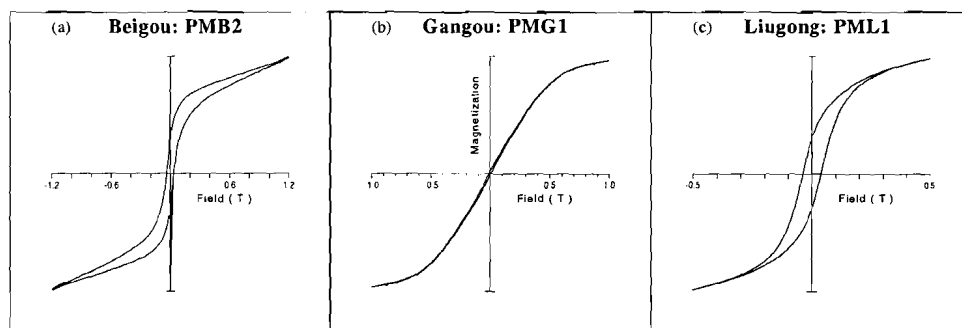


Figure 9.2: Room temperature hysteresis loops typical of (a) magnetite-hematite-bearing samples, (b) native iron-bearing samples and (c) spinel-bearing samples of combustion-metamorphic rocks. Magnetization (y -axis) is in arbitrary units.

The hysteresis loops of the remaining samples resemble more or less that shown in Fig. 9.2(c). According to their thermomagnetic analysis, samples PMQ1, PML1 and PMK1 may contain only one magnetic phase of near-magnetite composition and thus their hysteresis parameters can be interpreted in terms of magnetic grain size. The remanence (M_{rs}/M_s) and coercivity (B_{cr}/B_c) ratios for the three samples are characteristic of PSD grains implying that they can carry a stable NRM. The absence of meaningful viscosity makes the alternative possibility of superposed SD and SP grains (*cf. Tauxe et al. 1996*) rather unlikely. Although the hysteresis parameters obtained for the other samples cannot directly be interpreted in terms of magnetic grain size because their hysteresis loops are superimposed curves of various magnetically soft minerals, they probably fall also in the stable PSD range.

9.3.3 Acquisition and AF stability of ARM and uniaxial IRM

Figure 9.3 shows the weak-field ARM (a-c) and high-field IRM (d-f) characteristics of the various burnt rock samples. Table 9.2 lists the ARM (300 mT; 16 μ T) and IRM (1T) intensities together with the rock-magnetic parameters derived by intersecting the normalized acquisition and AF demagnetization curves with a horizontal line through 0.5. The remanent acquisition coercive force (B_{cr}') is defined as the strength of the DC field required to produce half of the IRM (1T), whereas the median destructive field of the ARM and IRM ($B_{1/2A}$ and $B_{1/2I}$, respectively) is defined as the AF field required to eliminate half of the remanent magnetization.

Apart from the relative low-intensity (~ 10 mA/m) α Fe-bearing Gangou samples, the ARM_(300 mT) intensities of the burnt rocks show a tight range of ~ 0.5 – 2.9 A/m. ARM_(300 mT) intensities induced in 16 μ T DC bias fields are of similar magnitude as the initial NRM intensities (*cf. Table 9.1*) measured on sister specimens. The fine-grained nature of the rocks as well as their mode of formation makes large changes in magnetic mineralogy on

Table 9.2: Basic rock-magnetic parameters at room temperature for various burnt rocks.

code	χ_{lf} (10^{-4} SI)	ARM (A/m)	$B_{1/2A}$ (mT)	IRM (A/m)	$B_{1/2I}$ (mT)	B_{cr}' (mT)	B_c (mT)	B_{cr} (mT)	B_{cr}/B_c	M_{rs}/M_s
PMB1	120	1.256	36	478	53	95	27.9	113.0	4.1	0.38
PMB2	111	1.120	34	406	47	77	33.1	86.8	2.6	0.51
PMQ1	151	0.497	25	492	23	58	14.2	44.5	3.1	0.14
PML3	329	1.198	33	>1000	*20	*43	29.9	57.5	1.9	0.32
PMG1	6.5	0.013	89	3	84	143	8.2	141.0	17.2	0.03
PMG2	6.5	0.008	48	8	64	144	4.7	71.2	15.2	0.08
PML1	113	0.815	45	616	30	64	39.1	64.0	1.6	0.42
PML2	955	nd	nd	nd	nd	nd	11.2	16.4	1.5	0.42
PMK1	604	2.948	46	>1000	*28	*33	26.1	65.1	2.5	0.36
PMK2	35	0.686	45	86	30	51	9.4	36.4	3.9	0.23

Meanings of the parameters are explained in the text. Susceptibility and the ARM and IRM parameters were measured on standard 2.5 cm cylindrical samples, whereas the latter four hysteresis parameters were measured on small rock chips of a few milligrams using an alternating-gradient force magnetometer. nd = not determined. * B_{cr}' and * $B_{1/2I}$ are too low and too high, respectively, because the IRM intensity of these samples lies beyond the measurable range already after applying ~100 mT DC fields.

a centimeter scale unlikely. Therefore, we may compare sister specimens from drill cores. The $ARM_{(300\text{ mT})}/NRM_{(int)}$ ratio ranges 0.9 to 6.6; the higher values (4–6.6) are obtained on samples which contain a mixture of magnetically soft and hard minerals (i.e. the maghemite-hematite-bearing Beigou samples and the α Fe-bearing Gangou samples), whereas the lower values (0.9–1.6) belong to samples which only contain relatively soft spinels. This observation shows that, compared to the NRM, the ARM favours the contribution of the soft minerals to the signal, hinting at possibly different grain-size trends for TRM and ARM (cf. Dunlop & Xu 1993).

$IRM_{(1T)}$ intensities are ~5 A/m for the α Fe-bearing samples and range between 86 and ~1200 A/m for the other samples. Samples PML3 and PMK1 have intensities above the highest measurable intensity of 1000 A/m; visual extrapolation of their acquisition curves to 1 T yields values near ~1200 A/m. The $IRM_{(1T)}/ARM_{(300\text{ mT})}$ ratio is highly variable, ranging ~125 to ~1000, likely implying that the two remanent magnetizations are dominated by different coercivity fractions.

ARM acquisition shows that the burnt rock samples appear hard to saturate in the maximum available alternating current (AC) field (Figs 9.3b & c). PMQ1 is the only sample that fully saturates in a 300 mT AC field, while the other samples still show a more or less gradual increase in ARM values, implying the presence of magnetically relatively hard components. At 100 mT, the AC field commonly used to induce an ARM, the ARM reaches ~45 to ~90% of the intensity obtained with 300 mT AC fields. For sample PMG1, the presence of two magnetic phases with contrasting coercivities can clearly be deduced from the shape of the ARM acquisition and AF demagnetization curves. Based on their thermomagnetic curves and hysteresis parameters, the high-coerci-

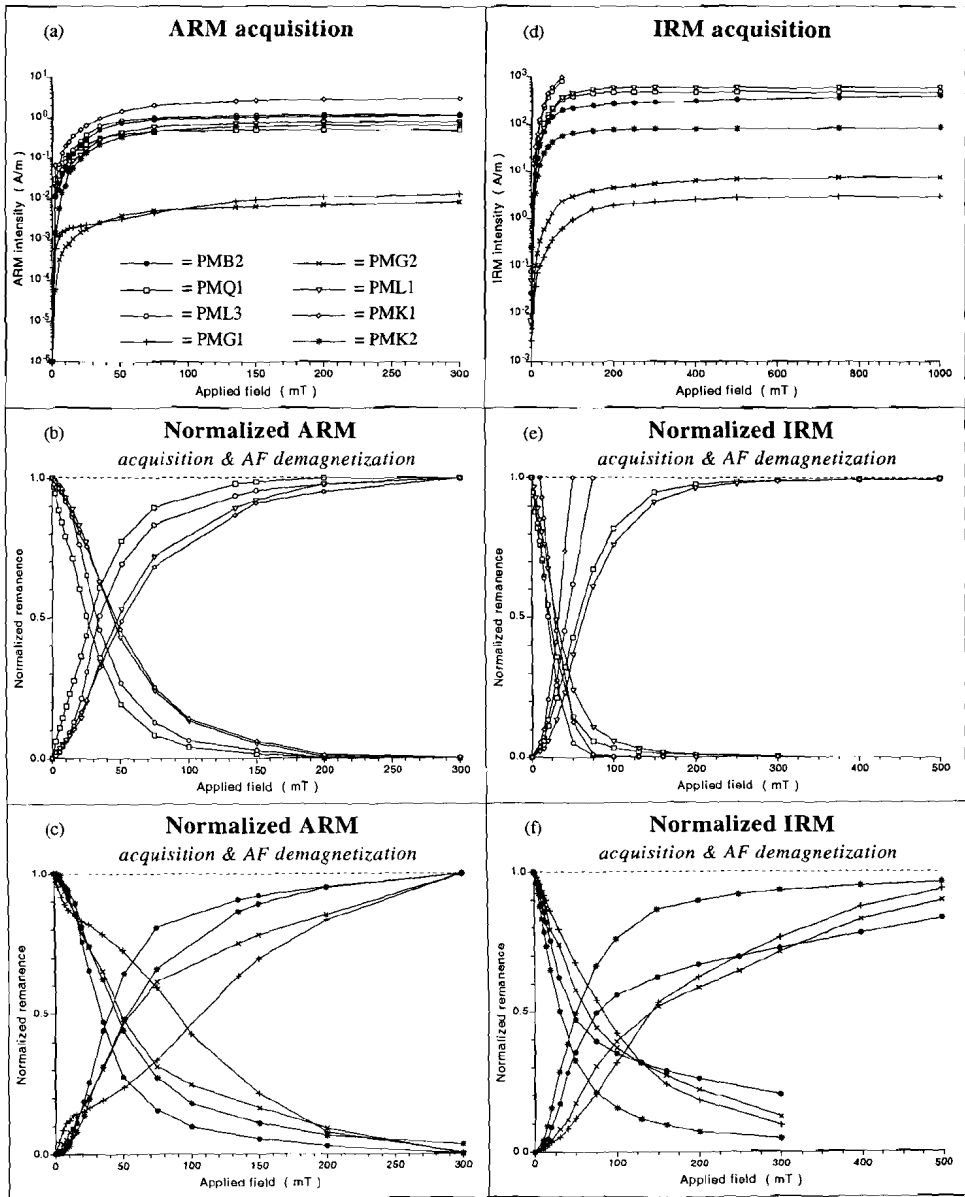


Figure 9.3: Typical acquisition and AF demagnetization curves of ARM and IRM for various burnt rocks. Sample PMB1 and PMB2 show identical behaviour. Therefore, only the results of sample PMB2 are plotted. The ARM DC bias field was 16 μ T. IRM acquisition and AF demagnetization curves of panels (e) & (f) are normalized to the intensity acquired at 1 T. The IRM intensity of samples PML3 and PMK1 exceeds already the highest measurable intensity in DC fields smaller than 100 mT.

vity mineral likely is SD native iron, whereas the low-coercivity component that almost saturates and demagnetizes in AF fields of ca. 20 mT might represent large MD or very small SD particles of α -Fe and/or spinel.

The resistance of the induced weak-field ARM against AC demagnetizing fields is relatively high for all burnt rock samples. The ARM median destructive fields range 25–89 mT. For the spinel-bearing samples (*Fig. 9.3b*) these values may be interpreted in terms of grain size and point to stable PSD particles. Their slightly S-shaped demagnetization curves support this suggestion; true SD grains show strongly sigmoid curves (i.e. S-shaped, with an initial plateau of no or hardly any demagnetization and an inflection point at intermediate fields), while true MD grains show a more exponential decrease (e.g. *Argyle et al.* 1994). The ARM of sample PMQ1 is carried by relatively large spinel particles which lie close to the MD side of the PSD range, while the particles of the other spinel-bearing samples lie closer to the SD side. The ARM of these samples (*Fig. 9.3b*) becomes fully demagnetized in 200 mT AC fields, while samples shown in *Fig. 9.3(c)* are relatively harder, needing fields up to 300 mT. The ARM of sample PMK2 could even not be fully demagnetized in the maximum available AC field.

The crossover ratio R between the ARM acquisition and demagnetization curves lies close to 0.5 for all samples. This observation implies that the ARM carrying particles are well-separated and do not magnetically interact (*Cisowski* 1981).

The normalized IRM acquisition curves show that the IRM of samples PMQ1 and PML1 (*Fig. 9.3e*) is already close to saturation (>97%) in 300 mT fields and fully saturates after applying 500 mT fields. B_{cr}' values are 58 and 64, respectively, implying PSD-type remanence carriers. Spinel-bearing samples PML3 and PMK1 likely exhibit similar behaviour. On the other hand, the magnetically harder samples shown in *Fig. 9.3(f)* not even fully saturate in 1 T DC fields. Their B_{cr}' values range 51 to 144 mT. In general, the B_{cr}' and B_{cr} values of all samples match each other quite well, implying that the small rock chips on which the hysteresis parameters were determined contain magnetic minerals similar in grain size and type as those present in the larger cylindrical samples.

Samples with the highest final $IRM_{(1T)}$ intensities, PML3 and PMK1, show the lowest resistance with respect to AC demagnetizing fields and are already fully demagnetized in fields of 50–75 mT. Note that their $IRM_{(1T)}$ intensities lie beyond the measuring range of the magnetometer; their demagnetization curves are normalized to the first measurable values after applying AC fields. The other spinel-bearing samples (*Fig. 9.3e*) have $B_{\frac{1}{2}I}$ values of 23 and 30 mT, but are only fully demagnetized after applying 0.3 T AC fields. The ratio $B_{\frac{1}{2}A}/B_{\frac{1}{2}I}$ exceeds 1 for these two samples, which supports their suggested PSD size, according to the Lowrie-Fuller test (1971). Samples shown in *Fig. 9.3(f)* again exhibit a much higher AF stability than the aforementioned spinel-bearing samples. Their $B_{\frac{1}{2}I}$ values range 30 to 84 mT, and the IRM induced in 1 T DC fields of neither sample becomes fully demagnetized after applying AC fields up to 0.3 T.

The crossover ratio R between the IRM acquisition and demagnetization curves ranges ~0.3 – ~0.4 which is considerably lower than for the ARM experiment. The acquisition of weak-field ARM and strong-field IRM and their respective

AF demagnetization are dominated by slightly different factors. The observed difference might imply that, unlike ARM carrying minerals, magnetic interaction exists between IRM carrying minerals. Another, more plausible, explanation might be that internal demagnetizing fields of the remanence carrying minerals are more important in IRM than in ARM experiments (*cf. Argyle & Dunlop 1990*). The low value of the ARM would correspond to a lower internal demagnetizing field than the high value of the IRM. Small grains are also more susceptible to ARM than IRM (*cf. Jackson 1991*).

9.3.4 Susceptibility and thermal stability of composite IRMs

Thermal demagnetization of the three orthogonal components of the composite IRMs (*Figs 9.4a-g*) yields information on the identification of the remanence carrying phases and their relative quantities to the signal. Heating, however, may induce alterations in magnetic mineralogy which may interfere with the demagnetization process. For this reason, the low-field susceptibility was measured at room temperature after each heating step (*Fig. 9.4h*). The unheated samples exhibit high initial χ_{lf} values varying between 6 and 604×10^{-4} SI; variation in three orthogonal direction was insignificant for all samples. For most samples, no major changes in χ_{lf} were observed during heating in air to 750°C. This indicates that their magnetic mineralogy was stabilized, chemically and physically, at high temperatures. The χ_{lf} of α Fe-bearing Gangou and maghemite-hematite-bearing Beigou samples hardly changes up to 600°C. Heating the samples above this temperature, however, results in an increase of susceptibility which continues up to the final heating step of 750°C. This χ_{lf} increase not necessarily implies the creation of a new magnetic mineral, it may also be caused by a reduction in grain size of the existing minerals transforming PSD and/or SD particles to highly magnetic unstable SP particles.

For the Beigou samples (*Figs 9.4a & b*) the intermediate- and high-coercivity components contribute equally to the initial IRM. A magnetic phase with an unblocking temperature of ~630°C contributes to all three coercivity fractions, but mainly dominates the intermediate component. This phase likely is near-pure maghemite of dominantly PSD size. The high-coercivity component is dominated by 680°C unblocking temperature implying the presence of PSD to SD hematite.

Samples PMQ1, PML1, and PMK2 (*Figs 9.4c, d & g*) are characterized by only one remanence carrying phase of mainly intermediate coercivity and with an unblocking temperature of ~580–600°C indicating the presence of a spinel-phase of near-magnetite composition. The contribution of the high-coercivity fraction to the signal is equal to or higher than the low-coercivity fraction suggesting that most particles lie on the near-SD side of the PSD range.

The IRM of the Gangou-samples (*Figs 9.4e & f*) is dominated by high- and intermediate-coercivity minerals. The intermediate-coercivity component unblocks at ~580°C and ~300–350°C for sample PMG1 and PMG2, respectively. The latter unblocking temperatures indicate the presence of a spinel phase with considerable isomorphous substitution. Identical spinel phases also dominate the high-coercivity com-

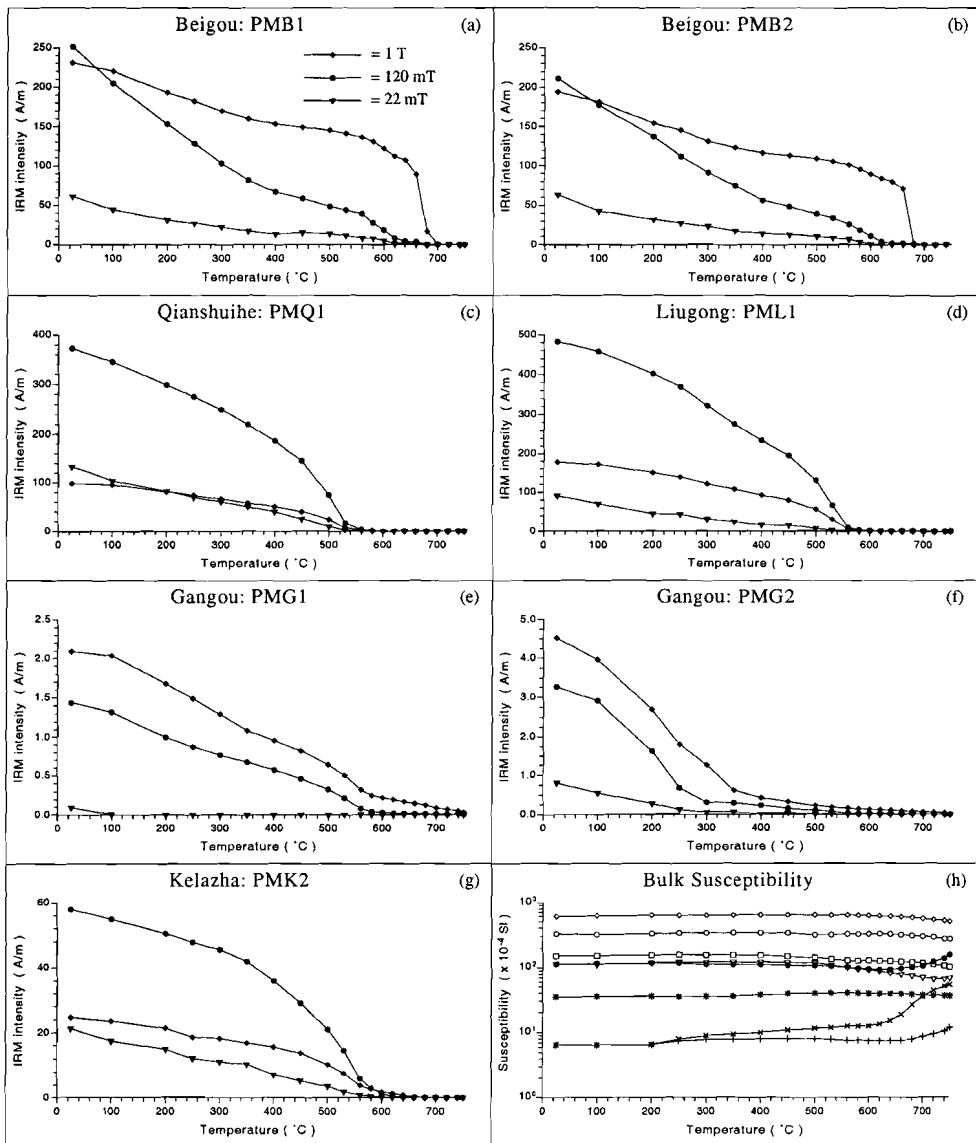


Figure 9.4: (a-g) Stepwise thermal demagnetization of composite IRMs (cf. Lowrie 1990) showing the different remanence carrying minerals in combustion-metamorphic rock samples. The high- (1 T), intermediate- (120 mT), and low-coercivity (22 mT) fractions are denoted with diamonds, circles, and triangles, respectively. (h) Bulk susceptibility measured at room temperature after each temperature step. Symbols as in Fig. 9.1.

ponent of both samples. A significant remanence, however, remains for these components, which only completely demagnetizes after heating at temperatures up to 750°C indicating the presence of metallic iron. The high remanent coercivities of the spinel phases and especially that of metallic iron suggests that these phases are present as more or less elongated SD particles.

9.4 Discussion: implications and applications

9.4.1 Magnetic minerals and their appearance

The intense heat generated by the spontaneous subsurface combustion of coal seams completely metamorphosed the overlying sediments to multi-coloured burnt rocks varying in appearance from dense to vesicular or scoriaceous. The substantial susceptibility enhancement of these thermally-altered rocks compared to their sedimentary protoliths indicates that additional magnetic minerals were created during metamorphism. Indeed, the formation of abundant magnetic accessory phases is a phenomenon commonly associated with the thermal alteration of various non-magnetic Fe-bearing minerals. Thermomagnetic analyses and stepwise thermal demagnetization of composite IRMs showed that burnt rocks produced from mudstones, siltstones and sandstones may contain a wide variety of magnetic minerals including pure forms of metallic iron, magnetite, maghemite and hematite as well as impure magnetite phases with various amounts and/or types of isomorphous substitution and/or different oxidation degree. The paleomagnetic samples may contain only one single magnetic mineral, but often show multiple magnetic phases.

The magnetic mineral assemblage encountered in burnt rocks depends on many physical and chemical parameters including the original sediment bulk composition, temperature, degree of melting, and oxidation state (*cf. Costa et al. 1989*). The extreme differences in oxidation degree between the magnetic mineralogy of the maghemite-hematite-bearing Beigou samples and the native iron-bearing Gangou samples indicate that the conditions during combustion may range from highly oxidizing to effectively reducing. In this context, the supply of fresh air to the rocks and their permeability are important factors. Oxidizing conditions may prevail during initial ignition of the coal layer at the outcrop or in the vicinity of cracks and vents in the overlying rocks after the coal fire propagated itself subsurface. *Gleason & Kyser (1984)* recognized that groundwater may be involved as an oxidant. The high amount of hematite (10–20 mass %) in the Beigou burnt rocks may indicate that they are produced from 'red bed'-like sediments already rich in α -Fe₂O₃ and/or goethite (α -FeOOH). The native iron-bearing burnt rocks are the least magnetic samples. Their protoliths likely are compact 'clean' sandstones relatively low in Fe-bearing minerals and highly impermeable to oxygen. Additional oxidation of minor incorporated organic matter during heating may have caused the extremely low oxygen fugacity required.

The Fe-bearing precursor minerals of the magnetic phases, based on their sedimentary protoliths, likely are various clay minerals, ferromagnesian silicates and pyrites. Consequently, the most abundant 'foreign' cations substituting for Fe in magnetic iron oxides will be Al, Mg and Ti. Indeed, in petrographic studies on glass-bearing burnt rocks from Wyoming *Foit et al.* (1987) and *Cosca et al.* (1989) recognized members of the magnetite-hercynite(FeAl_2O_4)-ulvöspinel(Fe_2TiO_4) solid-solution series, the hematite-ilmenite(FeTiO_3) solid-solutions series, and solid-solution series from magnesioferrite along the spinel(MgAl_2O_4)-magnesioferrite(MgFe_2O_4) join to $\text{Sp}_{80}\text{Mf}_{20}$ and along the magnesioferrite-hematite join to $\text{Mf}_{60}\text{Hm}_{40}$. Most compositions of the latter two solid solution series lie in the Al-rich field and have formulas that are slightly cation deficient. Typical high-temperature non-magnetic minerals encountered in combustion-metamorphic rocks appear to include several Fe and Al-rich clinopyroxenes, melilite solid solutions, cristobalite, tridymite, mullite, cordierite and fayalitic olivine as well as minor glass (e.g. *Foit et al.* 1987; *Cosca et al.* 1989; *Rádan et al.* 1994).

Various rock-magnetic properties indicated that most magnetic iron oxide particles grew to PSD size during metamorphism. For equidimensional magnetite and maghemite this implies grain sizes between ~ 0.12 and ca. $10\text{--}15\ \mu\text{m}$ (cf. *Heider & Williams* 1988; *Dunlop & Özdemir* 1997). For elongated grains and substituted spinel phases the PSD grain-size range is considerably broader. Native iron, on the other hand, occurs as tiny SP and SD particles. For equidimensional αFe -particles the lower and upper limits for SD behaviour are ~ 0.008 and $\sim 0.023\ \mu\text{m}$, respectively (*Kneller & Luborsky* 1963). Based on their high remanent coercivities, SD native iron, however, more likely is present as (slightly) elongated grains of which the SD range is broader compared to equant grains. The αFe -particles survive heating in air indicating that they occur as inclusions encased in host minerals largely impermeable to oxygen. Furthermore, the crossover ratio R appeared to be < 0.5 for IRM carrying minerals which might indicate some degree of magnetic interaction between these particles. Consequently, a portion of individual magnetic grains lies close together or magnetic interaction exists between different parts of inhomogenous grains.

The characteristics of the magnetic minerals deduced from their rock-magnetic properties concurs well with the few available descriptions of iron oxides observed in thin sections of burnt rocks. *Foit et al.* (1987) and *Cosca et al.* (1989), reported that the iron oxides range in size from tiny euhedral crystals to large irregular masses and stringers hundreds of micrometers long. Most iron oxide masses and euhedra have been unmixed upon cooling to produce more or less complex two-phase intergrowths reminiscent of the Fe-Ti oxide intergrowths described by *Haggerty* (1976). Consequently, relatively pure magnetite or hematite phases are abundantly present as numerous geometrically arranged blebs or lamellae (sometimes in typical boxwork patterns) encased in iron oxide host minerals with substantial isomorphous substitution. These latter minerals represent the magnetic phases with relatively low Curie points.

9.4.2 Application of the magnetic properties of combustion-metamorphic rocks

Geomagnetic field recording

The very nature of the combustion-metamorphic rocks, especially those in the vicinity to the remaining ash layer of the coal seam, implies that they, in principle, are high-fidelity geomagnetic field recorders allowing reliable determinations of absolute paleointensities and recording of magnetic reversals. Indeed, the rocks are strongly magnetized and the minerals likely have been stabilized, physically and chemically, well above their Curie temperatures before or during final cooling. The NRM is a pure TRM and/or TCRM which appears to reside mainly in small PSD grains capable of carrying a hard and stable remanence. Furthermore, for the majority of burnt rock samples no or hardly any chemical changes occur during laboratory heating up to $\sim 750^{\circ}\text{C}$, even when highly reduced magnetic minerals (αFe) are involved.

On the other hand, the normal polarity obtained on all our samples might be alarming in view of the time they are expected to represent based on stratigraphic dating of overlying river deposits (Late Pliocene / Early Pleistocene to Recent; *Table 9.1*). Consequently, the possibility that the NRM of burnt rocks represents a secondary VRM or CRM due to weathering may, although unlikely, not be excluded. After removal of a small viscous component, the NRM of all samples, however, show univectorial decay to the origin. The lack of directional change suggests that the various remanence-carrying minerals present in a single sample were formed simultaneously. Moreover, other authors (*Jones et al. 1984; Krsová et al. 1989; Tyráček 1994*) found reversed directions for several burnt rocks of Quaternary age, excluding the VRM option. Virtually all thermal demagnetization diagrams by *Jones et al. (1984)* and *Krsová et al. (1989)* showed univectorial decay to the origin, similar to our AF demagnetization diagrams.

Like lavas, cooling rates involved are a few years at most, and thus burnt rocks record a 'snapshot' of the ancient geomagnetic field. Furthermore, a particular burnt rock deposit produced by a coal fire lasting a few hundreds of years may contain a more or less continuous geomagnetic field record for that time interval. In addition, individual burning events often occur intermittently, for instance because the exposure of new coal seams is controlled by the downcutting erosion or valley incision by rivers (*cf. Tyráček 1994; Zhang et al. 1999*). This again may yield a record of directional and intensity change of the geomagnetic field. Studies by *Jones et al. (1984)* and *Krsová et al. (1989)* yielded promising results, but age determination of the burnt rocks appears to be a limiting factor of the use of burnt rocks for paleointensity and paleosecular variation determinations. Dating by fission-track, thermoluminescence and/or by means of stratigraphic correlation is possible but generally yields considerable errors. In addition, one must be aware that additional field evidence is necessary to exclude the possibility that reorientation of the sampled rock took place after TRM acquisition, for instance, caused by overburden collapse after cooling.

Magnetic anomaly modelling

The high NRM intensities and susceptibility values measured on the burnt rocks of the Xinjiang region concur well with data obtained on similar rocks from other localities (e.g. *Lindqvist et al.* 1985; *Krsová et al.* 1989; *Rădan & Rădan* 1998). For combustion-metamorphic rocks, the two parameters appear to range typically 0.1–10 A/m and 100–1000 × 10⁻⁴ SI, respectively. The αFe-bearing Gangou-samples clearly fall outside these ranges and can be considered as anomalously low. Burnt rocks thus possess NRM intensities and χ_{lf} values that in general are two to three orders of magnitude higher than values usually reported for their sedimentary protoliths. As a consequence, the magnetic contrast between burnt rocks and the surrounding unaffected sedimentary rocks will likely be sufficient to produce observable magnetic anomalies. Indeed, *Watson* (1979), *Lindqvist et al.* (1985) and *Rădan & Rădan* (1998) observed strong magnetic anomalies of ca. 500–2000 nT over exposed and unexposed burnt rock deposits by surface magnetic measurements, whereas *Parker Gay & Hawley* (1991) showed that anomalies associated with burnt rocks were strong enough to be recognized by aeromagnetic survey.

This property of burnt rocks has potential for coal exploration and, more importantly from China's point of view, it can be used to delineate the areal extent and depth of (extinct) coal fires. In China, the spontaneous combustion of coal not only results in a substantial economic loss –estimated annual loss ~10–20 million tons (*Guan et al.* 1996)–, but also results in adverse environmental impacts by the release of smoke and noxious gases such as CO_x, NO_x, SO₂ and H₂S. Magnetic anomaly modelling of burnt rock deposits may yield valuable information necessary to further our understanding of the (subsurface) evolution and mechanism of coal fires. Comprehensive knowledge on this burning problem is badly needed to fight the extensive coal fires in China more efficiently and to prevent the start of new fires. In addition, combining magnetic anomaly data with remote sensing and field data can refine estimates of the actual and paleo release of CO₂ by spontaneous combustion of coal in China.

9.5 Conclusions

Thermally altered sediments associated with burnt coal seams are high-fidelity geomagnetic field recorders, especially those in close vicinity to the remaining ash layer. They are suitable for paleointensity and paleosecular variation studies, although age determination will often be a limiting factor. The high NRMs and susceptibility values of these magnetically enhanced rocks approach those of extrusive rocks and generally range 0.1–10 A/m and 100–1000 × 10⁻⁴ SI, respectively. The dominant remanence carriers in combustion-metamorphic rocks are relatively pure magnetite particles. In addition, relatively pure forms of maghemite, hematite and native iron as wells as complex spinel phases can be present. The majority of the magnetic phases show rock-magnetic properties characteristic of small PSD particles. Native iron is likely present as SD more or less elongated particles capable of carrying a hard remanence. All magnetic phases show a high chemical and physical stability during heating in air. They likely are present

as exsolution phases encased in host minerals. The extremes in oxidation degree of the iron phases indicate that conditions during combustion can vary between highly oxidizing to effectively reducing.

ACKNOWLEDGEMENTS

We gratefully acknowledge *Ton van Hoof* for performing the AF demagnetizations of the NRM and for measuring the hysteresis parameters. *Piet-Jan Verplak* measured some of the thermomagnetic runs. *Tom Mullender* upgraded the JR3 spinner magnetometer. This work was conducted under the programme of the Vening Meinesz Research School of Geodynamics (VMSG).

References

- Abreu, M.M. & Robert, M., 1985. Characterization of maghemite in B-horizons of three soils from S. Portugal. *Geoderma*, **36**, 97–108.
- Ade-Hall, J.M., Palmer, H.C. & Hubbard, T.P., 1971. The magnetic and opaque petrological response of basalts to regional hydrothermal alteration. *Geophys. J. R. astr. Soc.*, **24**, 137–174.
- Adetoy, F., 1970. Maghemite in Sydney duricrusts. *Am. Mineral.*, **55**, 925–933.
- Adnan, J. & O'Reilly, W., 1999. The transformation of $\gamma\text{Fe}_2\text{O}_3$ to $\alpha\text{Fe}_2\text{O}_3$: thermal activation and the effect of elevated pressure. *Phys. Earth Planet. Inter.*, **110**, 43–50.
- Aharoni, A., Frei, E.H. & Schieber, M., 1963. Curie point and origin of weak ferromagnetism in hematite. *Phys. Rev.*, **131**, 1478–1482.
- Anand, R.R. & Gilkes, R.J., 1987a. Iron oxides in laterite soils from Western Australia. *J. Soil Sci.*, **38**, 607–622.
- Anand, R.R. & Gilkes, R.J., 1987b. The association of maghemite and corundum in Darling Range laterites, Western Australia. *Austr. J. Soil Res.*, **25**, 303–311.
- Anderson, P.W., Merritt, F.R., Remeika, J.P. & Yager, W.A., 1954. Magnetic resonance in $\alpha\text{-Fe}_2\text{O}_3$. *Phys. Rev.*, **93**, 717–718.
- Annersten, H. & Hafner, S.S., 1973. Vacancy distribution in synthetic spinels of the serie $\text{Fe}_3\text{O}_4 - \gamma\text{-Fe}_2\text{O}_3$. *Z. Kristallogr.*, **137**, 321–340.
- Appel, E., 1987. Stress anisotropy in Ti-rich titanomagnetites. *Phys. Earth Planet. Inter.*, **46**, 233–240.
- Argyle, K.S. & Dunlop, D.J., 1990. Low-temperature and high-temperature hysteresis of small multidomain magnetites (215–540 nm). *J. Geophys. Res.*, **95**, 7069–7083.
- Argyle, K.S., Dunlop, D.J. & Xu, S., 1994. Single-domain behaviour of multidomain magnetite grains (abstract). *Eos (Trans. Am. Geophys. Un.)*, **75**, Fall Meeting suppl., 196.
- Armstrong, R.J., Morrish, A.M. & Sawatzky, G.A., 1966. Mössbauer study of ferric ions in the tetrahedral and octahedral sites of a spinel. *Phys. Lett.*, **23**, 414–416.
- Artman, J.O., Murphy, J.C. & Foner, S., 1965. Magnetic anisotropy in antiferromagnetic corundum-type sesquioxides. *Phys. Rev.*, **138**, A912–917.
- Baag, C. & Helsley, C.E., 1974. Evidence for penecontemporaneous magnetization of the Moenkopi Formation. *J. Geophys. Res.*, **79**, 3308–3320.
- Bagin, V.I., Gendler, T.S., Kuz'min, R.N., Rybak, R.S. & Urazayeva, T.K., 1976. The weak ferromagnetism of natural hydrogoethites. *Izv. Acad. Sci. USSR, Phys. Solid Earth, Engl. Trans.*, **12**, 328–333.
- Bando, Y., Kiyama, M., Takada, T. & Kachi, S., 1965. The effect of particle size of $\gamma\text{-Fe}_2\text{O}_3$ on the transformation from γ -form to α -form. *Jpn. J. Appl. Phys.*, **4**, 240–241.
- Bando Y., Kiyama, M., Yamamoto, N., Takada, T., Shinjo, T. & Takaki, H., 1965. The magnetic properties of $\alpha\text{-Fe}_2\text{O}_3$ fine particles. *J. Phys. Soc. Japan*, **20**, 2086.
- Banerjee, S.C., 1985. *Spontaneous combustion of coal and mine fires*. Balkema, Rotterdam, pp. 167.
- Banerjee, S.K., 1966. Exchange anisotropy in intergrown maghemite and hematite. *Geophys. J. R. astr. Soc.*, **10**, 449–450.
- Banerjee, S.K., 1970. Origin of thermoremanence in goethite. *Earth Planet. Sci. Lett.*, **8**, 197–201.
- Banerjee, S.K., 1971. New grain size limits for paleomagnetic stability in haematite. *Nature Phys. Sci.*, **232**, 15–16.
- Banerjee, S.K., 1991. Magnetic properties of Fe-Ti oxides. In: D.H. Lindsley (ed.), *Oxide Minerals, Reviews in Mineralogy* **25**, Min. Soc. Am., Washington D.C., 107–128.
- Barrón, V. & Torrent, J., 1984. Influence of aluminum substitution on the color of synthetic hematites. *Clays Clay Miner.*, **32**, 157–158.
- Barrón, V., Gálvez, N., Hochella, M.F. Jr. & Torrent, J., 1997. Epitaxial overgrowth of goethite on hematite synthesized in phosphate media: A scanning force and transmission electron microscopy study. *Am. Mineral.*, **82**, 1091–1100.
- Bate, G., 1980. Recording materials. In: E.P. Wohlfarth (ed.), *Ferromagnetic Materials*, Vol. 2, North-Holland, New York, 381–507.
-

- Batis-Landoulis, H. & Vergnon, P., 1983. Magnetic moment of γ -Fe₂O₃ microcrystals, morphological and size effects. *J. Mat. Sci.*, **18**, 3399–3403.
- Bentor, Y.K., Kastner, M., Perlman, I. & Yellin, Y., 1981. Combustion metamorphism of bituminous sediments and the formation of melts of granitic and sedimentary composition. *Geoch. Cosmoch. Acta*, **45**, 2229–2255.
- Berkowitz, A.E., Schuele, W.J. & Flanders, P.J., 1968. Influence of crystallite size on the magnetic properties of acicular γ -Fe₂O₃ particles. *J. Appl. Phys.*, **39**, 1261–1263.
- Berkowitz, A.E., Goehler, R.P., Hall, E.L. & Flanders, P.J., 1985. Microstructure, relaxation and print-through in γ -Fe₂O₃ particles. *J. Appl. Phys.*, **57**, 3928–3930.
- Bernal, J.D., Dasgupta, D.R. & Mackay, A.L., 1957. Oriented transformation in iron oxides and hydroxides. *Nature*, **180**, 645–647.
- Bernal, J.D., Dasgupta, D.R. & Mackay, A.L., 1959. The oxides and hydroxides of iron and their structural interrelationships. *Clay Min. Bull.*, **4**, 15–30.
- Bérnard, J., 1939. Étude de la décomposition du protoxyde de fer et de solutions solides. *Ann. Chim. (Paris)*, **12**, 5–92.
- Besser, P.J., Morrish, A.H. & Scarle, C.W., 1967. Magnetocrystalline anisotropy of pure and doped hematite. *Phys. Rev.*, **153**, 632–640.
- Birks, J.B., 1950. The properties of ferromagnetic compounds at centimetre wavelengths. *Proc. Phys. Soc. (London)*, **B63**, 65–74.
- Blackman, M. & Kaye, G., 1960. An electron diffraction study of the effects of heat treatment on α -Fe₂O₃ (haematite) single crystals. *Proc. Phys. Soc. London*, **75**, 364–368.
- Blake, R.L., Hessevick, R.E., Zoltai, T. & Finger, L.W., 1966. Refinement of the hematite structure. *Am. Mineral.*, **51**, 123–129.
- Blodgett, R.H., Crabaugh, J.P. & McBride, E.F., 1993. The color of red beds – A geologic perspective. In: J.M. Bigham and E.J. Coilkosz (eds), Soil Sci. Soc. Am., *Spec. Publ. No. 31*, 127–159.
- Bo, M., 1981. Study on Quaternary System in Xinjiang. *Collection of Papers on Quaternary and Glacial Geology in Xinjiang*, 159–162 (in Chinese).
- Bocquet, S. & Hill, A.J., 1995. Correlation of Néel temperature and vacancy defects in fine-particle goethites. *Phys. Chem. Minerals*, **22**, 524–528.
- Boll, J., Thewessen, T.J.W., Meijer E.L. & Kroonenberg, S.B., 1988. A simulation of the development of river terraces. *Z. Geomorphologie*, **32**, 31–45.
- Borradaile G.J., 1994. Low-temperature demagnetization and ice-pressure demagnetization in magnetite and haematite. *Geophys. J. Int.*, **116**, 571–584.
- Boudeulle, M., Batis-Landoulis, H., Leclercq, C-H. & Vergnon, P., 1983. Structure of γ -Fe₂O₃ microcrystals: vacancy distribution and structure. *J. Solid State Chem.*, **48**, 21–32.
- Bowen, L.H., De Grave, E. & Bryan, A.M., 1994. Mössbauer studies in external field of well crystallized Al-maghemites made from hematite. *Hyperfine Int.*, **94**, 1977–1982.
- Boyd, J.R., Fuller, M. & Halgedahl, S., 1984. Domain wall nucleation as a controlling factor in the behaviour of fine magnetic particles in rocks. *Geophys. Res. Lett.*, **11**, 193–196.
- Bozorth, R.M., 1961. *Ferromagnetism*. D. Van Nostrand Company, Inc., New York, pp. 968.
- Bragg, W.H., 1915. The structure of magnetite and the spinels. *Nature*, **95**, 561.
- Bragg, W.H. & Bragg, W.L., 1918. *X-rays and Crystal Structure*, Third Edition. G. Bell and Sons, London.
- Bragg, W.L., Gottfried, C. & West, J., 1931. *Z. Kristallogr.*, **77**, 255.
- Braun, P.B., 1952. A superstructure in spinels. *Nature*, **27**, 1123.
- Brown, K. & O'Reilly, W., 1988. The effect of low-temperature oxidation on the remanence of TRM-carrying titanomagnetite Fe_{2.4}Ti_{0.6}O₄. *Phys. Earth Planet. Int.*, **52**, 108–116.
- Brown, N.E., Navrotsky, A., Nord, G.L. Jr. & Banerjee, S.K., 1993. Hematite-ilmenite (Fe₂O₃–FeTiO₃) solid solutions: Determination of Fe-Ti order from magnetic properties. *Am. Mineral.*, **78**, 941–951.
- Bucur, I., 1978. Experimental study of the origin and properties of the defect moment in single domain hematite. *Geophys. J. R. astr. Soc.*, **55**, 589–604.
- Bureau of Geology and Mineral Resources of Xinjiang-Uygur Autonomous Region (BGXJ), 1993. *Regional Geology of Xinjiang Uygur Autonomous Region, Geol. Mem. Series I, Number 32*, pp. 783–841.
- Burton, J.W. & Godwin, R.P., 1967. *Phys. Rev.*, **158**, 218.

- Bustin, R.M. & Mathews, W.H., 1982. In situ gasification of coal, a natural example: history, petrology, and mechanics of combustion. *Canadian J. Earth Sci.*, **19**, 514–523.
- Bustin, R.M. & Mathews, W.H., 1985. In situ gasification of coal, a natural example: additional data on the Aldridge Creek coal fire, South-eastern British Columbia. *Canadian J. Earth Sci.*, **22**, 1858–1864.
- Butler, R.F., 1992. *Paleomagnetism: magnetic domains to geological terranes*. Blackwell Sci. Publ., Boston, pp. 319.
- Callen, H.B. & Callen, E.R., 1966. The present status of the temperature dependence of magnetocrystalline anisotropy, and the $l(l+1)/2$ power law. *J. Phys. Chem. Solids*, **27**, 1271–1285.
- Carroll, A.R., Graham, S.A., Hendrix, M.S., Ying, D. & Zhou, D., 1995. Late Paleozoic tectonic amalgamation of northwestern China: sedimentary record of the northern Tarim, northwest Turpan and southern Junggar basin. *Bull. Geol. Soc. Amer.*, **107**, 571–594.
- Cassells, C.J.S. & Van Genderen, J.L., 1995. Thermal modeling of underground coal fires in northern China, *Proceedings of the 21st Annual Conference of the Remote Sensing Society*, 11–14 Sept. 1995, University of Southampton, 544–551.
- Cassells, C.J.S., Van Genderen, J.L. & Zhang, X.M., 1996. Detecting and measuring underground coal fires by remote sensing. *Proc. 8th Australian Remote Sensing Conference*, Canberra, March 1996, Vol 2, 90–101.
- Cassells, C.J.S., Zhang, X.M. & Thamm, H.P., 1998. Estimating the CO₂ output of coal fires by thermal modelling, 9th Global Warming International Conference & Expo, 8–11 June 1998, HongKong.
- Chadwick, J.C., Jones, D.H., Thomas, M.F., Tatlock, C.J. & Devenish, M., 1968. *Hyperfine Int.*, **28**, 541.
- Channell, J.E.T., McCabe, C. & Woodcock, N.H., 1992. Early Devonian (pre-Acadian) magnetisation directions in Lower Old Red Sandstone of south Wales (UK). *Geophys. J. Int.*, **108**, 883–894.
- Charlesworth, G. & Long, F.A., 1939. *Proc. Leeds. Phil. Lit. Soc., Sci. Sect.*, **3**, 315.
- Chaudron, G. & Forestier, H., 1924. *Compt. Rend. Acad. Sci. Paris*, **179**, 763.
- Chevallier, R. & Mathieu, S., 1943. Propriétés magnétiques des poudres d'hématites; influence des dimensions des grains. *Ann. Phys.*, **18**, 258–288.
- Chevallier, R., 1951. Propriétés magnétiques de l'oxyde ferrique rhomboédrique (Fe₂O₃-α). *J. Phys. Radium*, **12**, 178–188.
- Chevallier, R.J., Bolfa, J. & Mathieu, S., 1955. Titanomagnetites et ilmenites ferromagnétiques (1). Étude optique, radiocristallographique, chimique. *Bull. Soc. Français Miner. Cristall.*, **78**, 307–346.
- Chikazumi, S., 1976. Current understanding of low temperature phase transition of magnetite, particularly in relation to the behaviour of magnetocrystalline anisotropy. In: J.J. Becker, G.H. Lander and J.J. Rhyne (eds), *Magnetism and Magnetic Materials*, Am. Inst. Phys., New York, 382–387.
- Christensen, H. & Nørland-Christensen, A., 1978. Hydrogen bonds of γ-FeOOH. *Acta Chem. Scand.*, **32**, 87–88.
- Cisowski, S., 1981. Interacting vs. non-interacting single domain behaviour in natural and synthetic samples. *Phys. Earth Planet. Int.*, **26**, 56–62.
- Coey, J.M.D., 1971. Non-collinear spin arrangement in ultrafine ferrimagnetic crystallites. *Phys. Rev. Lett.*, **27**, 1140–1142.
- Coey, J.M.D., 1987. Noncollinear spin structures. *Can. J. Phys.*, **65**, 1210–1232.
- Collinson, D.W., 1966. Carrier of remanent magnetization in certain red sandstones. *Nature*, **210**, 516–517.
- Collinson, D.W., 1969. Investigations into the stable remanent magnetization of sediments. *Geophys. J. R. astr. Soc.*, **18**, 211–222.
- Collinson, D.W., 1974. The role of pigment and specularite in the remanent magnetization of red sandstones. *Geophys. J. R. astr. Soc.*, **38**, 253–264.
- Collinson, D.W., 1983. *Methods in Rock Magnetism and Palaeomagnetism: Techniques and Instrumentation*. Chapman and Hall, London & New York, pp. 503.
- Collyer, S., Grimes, N.W., Vaughan, D.J. & Longworth, G., 1988. Studies of the crystal structure and chemistry of titanomaghemite. *Am. Mineral.*, **73**, 153–160.
- Colombo, U., Fagherazzi, G., Gazzarrini, F., Lanzavecchia, G. & Sironi, G., 1964. Mechanisms in the first stage of oxidation of magnetites. *Nature*, **202**, 175–176.
- Cornell, R.M. & Schwertmann, U., 1996. *The Iron Oxides*, VCH, New York, pp. 573.
- Cosca, M.A., Essene, E.J., Geissman, J.W., Simmons, W.B. & Coates, D.A., 1989. Pyrometamorphic rocks associated with naturally burned coal beds, Powder River Basin, Wyoming. *Am. Mineral.*, **74**, 85–100.
-

- Coventry, R.J., Taylor, R.M. & Fitzpatrick, R.W., 1983. Pedological significance of the gravel in some red and grey earth of central North Queensland. *Aust. J. Soil Res.*, **21**, 219–240.
- Creer, K.M., 1961. Superparamagnetism in red sandstones. *Geophys. J. R. astr. Soc.*, **5**, 16–28.
- Creer, K.M., 1962a. On the origin of remanent magnetisation of red beds. *J. Geomag. Geoelect.*, **13**, 86–100.
- Creer, K.M., 1962b. A statistical enquiry into the partial remagnetization of folded Old Red Sandstone rocks. *J. Geophys. Res.*, **67**, 1899–1906.
- Creer, K.M., 1967. Rock magnetic investigations at low temperatures. In: D.W. Collinson, K.M. Creer and S.K. Runcorn (eds), *Methods in Paleomagnetism*, Elsevier, Amsterdam, 514–528.
- Curi, N. & Franzmeier, D.P., 1984. A toposequence of oxisols from the Central Plateau of Brazil. *Soil Sci. Soc. Am. J.*, **48**, 341–346.
- Curry, N.A., Johnston, G.B., Besser, P.J. & Morrish, A.H., 1965. Neutron diffraction measurements on pure and doped synthetic hematite crystals. *Phil. Mag.*, **12**, 221–228.
- Da Costa, G.M., De Grave, E., Bowen, L.H., de Bakker, P.M.A. & Vandenberghe, R.E., 1994a. The center shift in Mössbauer spectra of maghemite and aluminum maghemites. *Clays Clay Minerals*, **42**, 628–633.
- Da Costa, G.M., De Grave, E., Bryan, A.M. & Bowen, L.H., 1994b. Mössbauer studies of nanosized aluminum-substituted maghemites. *Hyp. Inter.*, **94**, 1983–1987.
- Da Costa, G.M., De Grave, E., Bowen, L.H., de Bakker, P.M.A. & Vandenberghe, R.E., 1995. Temperature dependence of the hyperfine parameters of maghemite and Al-substituted maghemites. *Phys. Chem. Minerals*, **22**, 178–185.
- Dalan, R.A. & Banerjee, S.K., 1996. Soil magnetism, an approach for examining archaeological landscapes. *Geophys. Res. Lett.*, **23**, 185–188.
- Daniels, J.M. & Rosencwaig, A., 1969. Mössbauer spectroscopy of stoichiometric and non-stoichiometric magnetite. *J. Phys. Chem. Solids*, **30**, 1561–1571.
- Dankers, P.H.M., 1978. *Magnetic properties of dispersed natural iron-oxides of known grain-size*, PhD thesis, Utrecht University, Utrecht, The Netherlands, pp. 142.
- Dankers, P.H.M., 1981. Relationship between the median destructive field and remanent coercive forces for dispersed magnetite, titanomagnetite and hematite. *Geophys. J. R. astr. Soc.*, **64**, 447–461.
- David, I. & Welch, A.J.E., 1956. The oxidation of magnetite and related spinels. *Trans. Farad. Soc.*, **52**, 1642–1650.
- Davis, P.M. & Evans, M.E., 1976. Interacting single-domain properties of magnetite intergrowths. *J. Geophys. Res.*, **81**, 989–994.
- Day, R., 1975. Some curious thermomagnetic curves and their interpretation. *Earth Planet. Sci. Lett.*, **27**, 95–100.
- Day, R., Fuller, M. & Schmidt, V.A., 1977. Hysteresis properties of titanomagnetites: Grain size and compositional dependence. *Phys. Earth Planet. Inter.*, **13**, 260–267.
- Dearing, J.A., Dann, R.J.L., Hay, K., Lees, J.A., Loveland, P.J., Maher, B.A. & O'Grady, K., 1996. Frequency-dependent susceptibility measurements of environmental materials. *Geophys. J. Int.*, **124**, 228–240.
- De Bakker, P.M.A., de Grave, E., Vandenberghe, R.E., Bowen, L.H., Pollard, R.J. & Persoons, R.M., 1991. Mössbauer study of the thermal decomposition of lepidocrocite and characterization of the decomposition products. *Phys. Chem. Minerals*, **18**, 131–143.
- De Boer, C.B. & Dekkers, M.J., 1996. Grain-size dependence of the rock magnetic properties for a natural maghemite. *Geophys. Res. Lett.*, **23**, 2815–2818.
- De Boer, C.B., Van Hoof, A.A.M., Zhang, X.M., Kroonenberg, S.B. & Dekkers M.J., 1997. Native iron in baked sediments due to spontaneous underground combustion of coal seams. ESG Congress, Vienna, *Annales Geophysicae*, 1997, Suppl. I to Vol 15, C111.
- De Boer, C.B. & Dekkers, M.J., 1998. Thermomagnetic behaviour of hematite and goethite as a function of grain size in various non-saturating magnetic fields. *Geophys. J. Int.*, **133**, 541–552.
- De Boer, F. & Selwood, P.W., 1954. The activation energy for the solid state reaction $\gamma\text{-Fe}_2\text{O}_3 \rightarrow \alpha\text{-Fe}_2\text{O}_3$. *J. Am. Chem. Soc.*, **76**, 3365.
- Deer, W.A., Howie, R.A. & Zussman, J., 1980. *An introduction to the rock-forming minerals*. Longman, London, pp. 528.
- De Grave, E., Bowen, L.H. & Weed, S.B., 1982. Mössbauer study of aluminum-substituted hematites. *J. Magn. Mat.*, **27**, 98–108.

- De Grave, E., Chambaerc, D. & Bowen, L.H., 1983. Nature of the Morin transition in Al-substituted hematite. *J. Magn. Magn. Mat.*, **30**, 349–354.
- Dekkers, M.J., 1988. *Some rock magnetic parameters for natural goethite, pyrrhotite and fine-grained hematite*. PhD thesis, Utrecht University, Utrecht, The Netherlands, pp. 231.
- Dekkers, M.J., 1989a. Magnetic properties of natural goethite-I. Grain-size dependence of some low- and high-field related rockmagnetic parameters measured at room temperature, *Geophys. J.*, **97**, 323–340.
- Dekkers, M.J., 1989b. Magnetic properties of natural goethite-II. TRM behaviour during thermal and alternating field demagnetisation and low-temperature treatment, *Geophys. J.*, **97**, 341–355.
- Dekkers, M.J. & Linssen, J.H., 1989. Rock magnetic properties of fine-grained natural low-temperature haematite with reference to remanence acquisition mechanisms in red beds. *Geophys. J. Int.*, **99**, 1–18.
- Dekkers, M.J. & Pietersen, H.S., 1992. Magnetic properties of low-Ca fly ash: A rapid tool for Fe-assessment and a survey for potentially hazardous elements. In: F.P. Glasser, G.J. McCarthy, J.F. Young, T.O. Mason and P.L. Pratt (eds), *Advanced cementitious systems – Materials Res. Soc. Proc.*, **245**, 37–47.
- Dekkers, M.J. & Rochette, P., 1992. Magnetic properties of chemical magnetisation in synthetic and natural goethite: Prospects for a natural remanent magnetisation/thermoremanent magnetisation ratio paleomagnetic stability test? *J. Geophys. Res.*, **97**, 17,291–17,307.
- DeMenocal, P.B., Ruddiman, W.F. & Kent, D.V., 1990. Depth of post-depositional remanence acquisition in deep-sea sediments: A case study of the Brunhes-Matuyama reversal and oxygen isotopic stage 19.1. *Earth Planet. Sci. Lett.*, **99**, 1–13.
- Deutsch, E.R., Rao, K.V., Laurent, R. & Sequin, S.K., 1977. New evidence and possible origin of native iron in ophiolites of eastern Canada. *Nature*, **269**, 684–685.
- Dougllass, D.N., 1988. Paleomagnetism of Roingerike Old Red Sandstone and related rocks, southern Norway: implications for pre-Carboniferous separation of Baltica and British terranes. *Tectonophysics*, **148**, 11–27.
- Duff, B.A., 1979. Peaked thermomagnetic curves for hematite-bearing rocks and concentrates. *Phys. Earth Planet. Int.*, **19**, P1–4.
- Dunlop, D. J., 1971. Magnetic properties of fine-particle hematite. *Ann. Geophys.*, **27**, 269–293.
- Dunlop, D.J., 1972. Magnetic mineralogy of unheated and heated red sediments by coercivity spectrum analysis. *Geophys. J. R. astr. Soc.*, **27**, 37–55.
- Dunlop, D.J., 1973. Superparamagnetic and single-domain threshold sizes in magnetite. *J. Geophys. Res.*, **78**, 1780–1793.
- Dunlop, D.J., 1986. Hysteresis properties of magnetite and their dependence on particle size: a test of PSD remanence models. *J. Geophys. Res.*, **91**, 9569–9584.
- Dunlop, D.J., 1990. Developments in rock magnetism. *Rep. Prog. Phys.*, **53**, 707–792.
- Dunlop, D.J. & Argyle, K.S., 1991. Separating multidomain and single-domain-like remanences in pseudo-single-domain magnetites (215–540 nm) by low-temperature demagnetization. *J. Geophys. Res.*, **96**, 2007–2017.
- Dunlop, D.J. & Xu, S., 1993. A comparison of methods of granulometry and domain structure determination (abstract). *Eos (Trans. Am. Geophys. Un.)*, **74**, Fall Meeting suppl., 203.
- Dunlop, D.J., 1995. Magnetism in rocks. *J. Geophys. Res.*, **100**, 2161–2174.
- Dunlop, D.J. & Özdemir, Ö., 1997. *Rock Magnetism - Fundamentals and Frontiers*, Cambridge University Press, Cambridge, pp. 592.
- Dzyaloshinsky, I.E., 1958. A thermodynamic theory of “weak” ferromagnetism of antiferromagnetics, *J. Phys. Chem. Solids*, **4**, 241–255.
- Eagle, D.F. & Mallinson, J.C., 1967. On the coercivity of γ -Fe₂O₃ particles. *J. Appl. Phys.*, **38**, 995–997.
- EARS, 1998. <http://biz.inter.nl.net/ears/projects/txtco.htm>
- Eaton, J.A. & Morrish, A.H., 1969. Magnetic domains in hematite at and above the Morin transition. *J. Appl. Phys.*, **40**, 3180–3185.
- Eggleton, R.A., Schulze, D.G. & Stucki, J.W., 1988. Introduction to crystal structures of iron-containing minerals. In: J.W. Stucki, B.A. Goodman and U. Schwertmann (eds), *Iron in Soils and Clay Minerals*, D. Riedel Publ. Co., Dordrecht, NATO ASI Series C217, 141–164.
- Elder, T., 1965. Particle-size effect in oxidation of natural magnetites. *J. Appl. Phys.*, **36**, 1012–1013.
- Ellwood, B.B., Balsam, W., Burkart, B., Long, G.J. & Buhl, M.L., 1986. Anomalous magnetic properties in rocks containing the mineral siderite: Paleomagnetic implications. *J. Geophys. Res.*, **91**, 12,779–12,790.
-

- Ellyett, C.D. & Fleming, A.W., 1974. Thermal infrared imagery of the burning mountain coal fire. *Remote Sensing of Environment*, **3**, 79–86.
- Ellyett, C.D. & Fleming, A.W., 1974. Thermal infrared imagery of the burning mountain coal fire. *Remote Sensing of Environment*, **11**, 221–229.
- Elmore, R.D. & Van der Voo, R., 1982. Origin of hematite and its associated remanence in the Copper Harbor conglomerate (Keweenaw), Upper Michigan. *J. Geophys. Res.*, **B 87**, 10918–10928.
- Elston, D.P. & Purucker, M.E., 1979. Detrital magnetization in red beds of the Moenkopi Formation (Triassic), Gray Mountain, Arizona. *J. Geophys. Res.*, **84**, 1653–1665.
- Enkin, R.J. & Dunlop, D.J., 1987. A micromagnetic study of pseudo-single-domain remanence in magnetite. *J. Geophys. Res.*, **92**, 12,726–12,740.
- Enkin, R.J. & Williams, W., 1994. Three-dimensional micromagnetic analysis of stability in fine magnetic grains. *J. Geophys. Res.*, **99**, 611–618.
- Evans, M.E. & Heller, F., 1994. Magnetic enhancement and paleoclimate: study of a loess/paleosol couplet across the Loess Plateau of China. *Geophys. J. Int.*, **117**, 257–264.
- Ewing, F.G., 1935. The crystal structure of lepidocrocite. *J. Chem. Phys.*, **3**, 420–424.
- Eyre, J.K. & Shaw, J., 1994. Magnetic enhancement of Chinese loess - The role of γ -Fe₂O₃? *Geophys. J. Int.*, **117**, 265–271.
- Fan, W.T., 1997. *Coal Geology Newspaper*, 2 July 1997, No. 559 (in Chinese).
- Farell, D.M., 1972. A study of the infrared absorption in the oxidation of magnetite to maghemite and hematite. **Mines Branch Inv. Rept. 72-118**, Dept. Energy Mines Res., Ottawa, Ontario, Canada, pp. 44.
- Fasiska, E.J., 1967. Structural aspects of the oxides and oxidehydrates of iron. *Corrosion Sci.*, **7**, 833–839.
- Feitknecht, W., 1964. Einfluß der Teilchengröße auf den Mechanismus von Festkörperreaktionen. *Rev. Pure Appl. Chem.*, 423–440.
- Feitknecht, W., 1965. Die Oxidation von feinteiligem Fe₃O₄ und Eisen. *Mem. Sci. Rev. Metallurg.*, **42**, 121–126.
- Feitknecht, W. & Mannweiler, U., 1967. Der Mechanismus der Umwandlung von γ - zu α -Eisensesquioxid. *Helv. Chim. Acta*, **50**, 570–581.
- Feitknecht, W. & Gallagher, K.J., 1970. Mechanisms for the oxidation of Fe₃O₄. *Nature*, **228**, 548–549.
- Feng, F.C., 1987. Delineation of the boundaries of the burnt rocks in Xinmin coal field, Shaanxi, China using black-white aerophotos, *ARSC internal report*, Xian, China, (in Chinese).
- Fey, M.V. & Dixon, J.B., 1981. Synthesis and properties of poorly crystalline hydrated aluminous goethites. *Clays Clay Miner.*, **29**, 91–100.
- Finch, G.I. & Sinha, K.P., 1957. An electron-diffraction study of the transformation α -Fe₂O₃ to γ -Fe₂O₃. *Proc. Roy. Soc. (London)*, **A241**, 1–8.
- Fine, P., Singer, M.J., La Ven, R., Verosub, K.L. & Southard, R.J., 1989. Role of pedogenesis in distribution of magnetic susceptibility in two California chronosequences. *Geoderma*, **44**, 287–306.
- Fisher, W.J. & Knuth, W.M. 1968. Detection and delineation of subsurface coal fires by aerial infrared scanning. *Geol. Soc. Am.*, **Special Paper 115**, 67–68.
- Fitzpatrick, R.W., 1978. *Occurrence and properties of iron and titanium oxides in soils along the eastern seaboard of South Africa*. PhD. thesis, University of Natal.
- Fitzpatrick, R.W., 1988. Iron compounds as indicators of pedogenic processes: Examples from the southern hemisphere. In: J.W. Stucki, B.A. Goodman and U. Schwertmann (eds), *Iron in Soils and Clay Minerals*, D. Riedel Publ. Co., Dordrecht, **NATO ASI Series C217**, 351–396.
- Flanders, P.J. & Schuele, W.J., 1964. Temperature-dependent magnetic properties of hematite single crystals. *Proc. Int'l Conf. Magnetism*, Nottingham, U.K., 594–596.
- Flanders, P.J. & Schuele, W.J., 1964. Anisotropy in the basal plane of hematite single crystals. *Phil. Mag.*, **9**, 485–490.
- Flanders, P.J. & Remeika J.P., 1965. Magnetic properties of hematite single crystals. *Phil. Mag.*, **11**, 1271–1288.
- Foit, F.F., Jr., Hooper, R.L. & Rosenberg, P.E., 1987. An unusual pyroxene, melilite, and iron oxide mineral assemblage in a coal-fire buchite from Buffalo, Wyoming. *Am. Mineral.*, **72**, 137–147.
- Fontes, M.P.F. & Weed, S.B., 1991. Iron oxides in selected Brazilian oxisols: I. Mineralogy. *Soil Sci. Soc. Am. J.*, **55**, 1143–1149.

- Francombe, M.H. & Rooksby, H.P., 1959. Structure transformations effected by the dehydration of diaspore, goethite and delta ferric oxide. *Clay Min. Bull.*, **21**, 1–14.
- Freeman, R., 1986. Magnetic mineralogy of pelagic limestones. *Geophys. J. R. astr. Soc.*, **85**, 433–452.
- Freier, S., Greenspan, M., Hillman, P. & Schechter, H., 1962. The antiferromagnetic Curie point in α -Fe₂O₃. *Phys. Lett.*, **2**, 191–193.
- Frölich, F. & Vollstädt, H., 1967. Untersuchungen zur Bestimmung der Curietemperatur von Maghemit (γ -Fe₂O₃). *Monatsber. Deutsch. Akad. Wiss., Berlin*, **9**, 180–186.
- Fuller, M.D. & Kobayashi, K., 1964. Identification of the magnetic phases carrying natural remanent magnetization in certain rocks. *J. Geophys. Res.*, **69**, 4409–4413.
- Fuller, M.D., 1970. Geophysical aspects of paleomagnetism, *C.R.C. Crit. Rev. Solid State Sci.*, **1**, 137–219.
- Furnas, X., 1926. *Trans. Amer. Inst. Chem. Eng.*, **18**, 309.
- Fysh, S.A. & Clark, P.E., 1982. Aluminous Hematite: A Mössbauer Study. *Phys. Chem. Minerals*, **8**, 257–267.
- Gallagher, K., Feitknecht, W. & Mannweiler, U., 1968. Mechanism of oxidation of magnetite to γ -Fe₂O₃. *Nature*, **217**, 1118–1121.
- Gallagher, P.K. & Gyorgy, E.M., 1969. *Phys. Rev.*, **180**, 622.
- Gallon, T.E., 1968a. The remanent magnetisation of haematite singly crystals. *Proc. Roy. Soc. (London)*, **A 303**, 511–524.
- Gallon, T.E., 1968b. The ferromagnetic domain structure of haematite. *Proc. Roy. Soc. (London)*, **A 303**, 525–529.
- Gardner, R.F.G., Sweett, F. & Tanner, D.W., 1963. *J. Phys. Chem. Solids*, **24**, 1175–1183.
- Ge, J. & Kent, D.V., 1994. Variations in Layer 2A thickness and the origin of the central anomaly magnetic high. *Geophys. Res. Lett.*, **21**, 297–300.
- Gillot, B., Rousset, A. & Dupre, G., 1978. Influence of crystallite size on the oxidation kinetics of magnetite. *J. Solid State Chem.*, **25**, 263–271.
- Giovanoli, R. & Brüttsch, R., 1975. Kinetics and mechanism of the dehydration of γ -FeOOH. *Thermochem. Acta*, **13**, 15–36.
- Gleason, J.D. & Kyser, T.K., 1984. Stable isotope compositions of gases and vegetation near naturally burning coal. *Nature*, **307**, 254–257.
- Gorter, E.W., 1954. Saturation magnetization and crystal chemistry of ferrimagnetic oxides. *Philips Res. Rep.*, **9**, 295–320 & 321–355.
- Goss, C.J., 1988. Saturation magnetisation, coercivity and lattice parameter changes in the system Fe₃O₄ – γ -Fe₂O₃, and their relationship to structure. *Phys. Chem. Minerals*, **16**, 164–171.
- Graham, I.D.G. & Scollar, I., 1976. Limitations on magnetic prospecting in Archaeology imposed by soil properties. *Archaeo-Physika*, **6**, 1–124. Bonn: Rheinland Verlag.
- Greaves, C., 1983. A powder neutron diffraction investigation of vacancy ordering and covalency in γ -Fe₂O₃. *J. Solid State Chem.*, **49**, 325–333.
- Greene, G.W., Moxham, R.M. & Harvey, A.H., 1969. Aerial infrared surveys and borehole temperature measurements of coal mine fires in Pennsylvania. *Proc. of the Sixth Intern. Symp. on Remote sensing of Environment, Michigan*, **13–16 Oct.**, 517–525.
- Grønvold, F. & Samuelsen, E.J., 1975. Heat capacity and thermodynamic properties of α -Fe₂O₃ in the region 300–1050 K. Antiferromagnetic transition. *J. Phys. Chem. Solids*, **36**, 249–256.
- Guan, H.Y., 1963. On Yaojie burnt rocks. *Proc. of Shaanxi Young Scientists Conference*, China, 212–226
- Guan, H.Y., 1984. The research of coal bed thermal IR radiation. *Proc. of the Seminars on Remote Sensing for Geological Applications*, 535–547.
- Guan, H.Y., 1989. Applications of remote sensing techniques in coal geology. *Acta Geologica Sinica*, **2**, 254–269.
- Guan, H.Y., Van Genderen, J.L. & Schalke, H.J.W.G., 1996. Study and survey on the geological hazards of coal fire in North China. *30th International Geological Congress Abstracts, Beijing, China*, **Vol 1**, 458.
- Gustard, B. & Schuele, W.J., 1966. Anomalously high remanence in (γ -Fe₂O₃)_{1-x}(α -Fe₂O₃)_x particles. *J. Appl. Phys.*, **37**, 1168–1169.
- Haggerty, S.E., 1976. Oxidation of opaque mineral oxides in basalts, and opaque mineral oxides in terrestrial igneous rocks. In: D. Rumble III (ed.), *Oxide Minerals, Reviews in Mineralogy* **3**, Min. Soc. Am., Washington D.C., Hg1–177.

- Haggerty, S.E. & Toft, P.B., 1985. Native iron in the continental lower crust: Petrological and geophysical implications. *Science*, **229**, 647–649.
- Haigh, G., 1957a. Observations on the magnetic transition in hematite at -15°C . *Phil. Mag.*, **2**, 887–890.
- Haigh, G., 1957b. The effect of added titanium and aluminium on the magnetic behaviour of α -ferric oxide. *Phil. Mag.*, **2**, 505–520.
- Halgedahl, S.L., 1995. Bitter pattern versus hysteresis behavior in small single particles of hematite. *J. Geophys. Res.*, **100**, 353–364.
- Halgedahl, S.L. & Jarrard, R.D., 1995. Low temperature behavior of single-domain through multidomain magnetite. *Earth Planet. Sci. Lett.*, **130**, 127–139.
- Hall, E.L. & Berkowitz, A.E., 1986. Microstructural defects in γ - Fe_2O_3 particles. *J. Mater. Res.*, **2**, 836–844.
- Haneda, K. & Morrish, A.H., 1977. Vacancy ordering in γ - Fe_2O_3 small particles. *Solid State Commun.*, **22**, 779–782.
- Hargraves, R.B., Collinson, D.W., Arvidson, R.E. & Spitzer, C.R., 1977. The Viking magnetic properties experiment; primary mission results. *J. Geophys. Res.*, **82**, 4547–4558.
- Harms, J.E. & Morgan, B.D., 1964. Pisolithic limonite deposits in northwest Australia. *Proc. Australas. Inst. Min. Metall.*, **212**, 91–124.
- Harrison, R.J. & Putnis, A., 1999. Determination of the mechanism of cation ordering in magnesioferrite (MgFe_2O_4) from the time- and temperature-dependence of magnetic susceptibility. *Phys. Chem. Minerals*, **26**, 322–332.
- Hartman, P., 1980. The attachment energy as a habit controlling factor: III Application to corundum. *J. Crystal Growth*, **49**, 166–170.
- Hartman, P. & Bennema, P., 1980. *J. Crystal Growth*, **49**, 145–1??.
- Hartstra, R.L., 1982. *Some rockmagnetic parameters for natural iron-titanium oxides*. PhD thesis, Utrecht University, Utrecht, The Netherlands, pp. 145.
- Hauptman, Z., 1974. High temperature oxidation, range of non-stoichiometry and Curie point variation of cation deficient titanomagnetite $\text{Fe}_{2.4}\text{Ti}_{0.6}\text{O}_{4+x}$. *Geophys. J. R. astr. Soc.*, **38**, 29–47.
- Hedley, I.G., 1968. Chemical remanent magnetisation of the FeOOH , Fe_2O_3 system. *Phys. Earth Planet. Int.*, **1**, 103–121.
- Hedley, I.G., 1971. The weak ferromagnetism of goethite (α - FeOOH). *Z. Geophys.*, **37**, 409–420. *Earth Planet. Inter.*, **63**, 41–57.
- Heider, F. & Williams, W., 1988. Note on temperature dependence of exchange constant in magnetite. *Geophys. Res. Lett.*, **15**, 184–187.
- Heider, F. & Dunlop, D.J., 1987. Two types of chemical remanent magnetization during oxidation of magnetite. *Phys. Earth Planet. Int.*, **46**, 24–45.
- Hejda, P., Kropáček, V., Petrovský, E., Zelinka, T. & Žatecký, J., 1992. Some magnetic properties of synthetic and natural hematite of different grain size. *Phys. Earth Planet. Inter.*, **70**, 261–272.
- Heller, F., Carracedo, J.C. & Soler, V., 1986. Reversed magnetization in pyroclastics from the 1985 eruption of Nevado del Ruiz, Colombia. *Nature*, **324**, 241–242.
- Heller, F., Shen, C.D., Beer, J., Liu, X.M., Liu, T.S., Bronger, A., Suter, M. & Bonani, G., 1993. Quantitative estimates of pedogenic ferromagnetic mineral formation in Chinese loess and paleoclimatic implications. *Earth Planet. Sci. Lett.*, **114**, 385–390.
- Heller, F., Strzyszczyk, Z. & Magiera, T., 1998. Magnetic record of industrial pollution in forest soils of Upper Silesia, Poland. *J. Geophys. Res.*, **103**, 17,767–17,774.
- Henry, W.E. & Boehm, M.J., 1956. Intradomain magnetic saturation and magnetic structure of γ - Fe_2O_3 . *Phys. Rev.*, **101**, 1253–1254.
- Henshaw, P.C. & Merrill, R.T., 1980. Magnetic and chemical changes in marine sediments. *Rev. Geophys. Space Phys.*, **18**, 483–504.
- Herrero-Bervera, E. & Helsen, C.E., 1983. Paleomagnetism of a polarity transition in the Lower(?) Triassic Chugwater Formation, Wyoming. *J. Geophys. Res.*, **88**, 3506–3522.
- Hodych, J.P., Mackay, R.I. & English, G.M., 1998. Low-temperature demagnetization of saturation remanence in magnetite-bearing dolerites of high coercivity. *Geophys. J. Int.*, **132**, 401–411.
- Hoffman, K.A., 1992. Self-reversal of thermoremanent magnetization in the ilmenite-hematite system: Order-disorder, symmetry, and spin alignment. *J. Geophys. Res.*, **97**, 10,883–10,895.

- Hoffmann, V. & Fehr, K.Th., 1996. (Micro-)magnetic and mineralogical studies on dacitic pumice from the Pinatubo eruption (1991, Phillipines) showing self-reversed TRM. *Geophys. Res. Lett.*, **23**, 2835–2838.
- Honda, K. & Soné, T., 1914. *Sci. Rept. Tohoku Imp. Univ. Ser. I*, **3**, 223.
- Housden, J. & O'Reilly, W., 1990. On the intensity and stability of the natural remanent magnetization of ocean floor basalts. *Phys. Earth Planet. Inter.*, **64**, 261–278.
- Huang, H. & Zhao, Z., 1981. Classification and Characteristics of Quaternary in Xinjiang, *Collection of Papers on Quaternary and Glacial Geology in Xinjiang*, 166–169 (in Chinese).
- Hunt, C.P., Moskowitz, B.M. & Banerjee, S.K., 1995. Magnetic properties of rocks and minerals. In: T.J. Ahrens (ed.) *Rock Physics and Phase Relations – A Handbook of Physical Constants*, **AGU Reference Shelf 3**, 189–204.
- Hus, J.J., 1990. The magnetic properties of siderite concretions and the CRM of their oxidation products. *Phys. Hendricks, S.B. & Pauling, L.*, 1926. *Z. Kristallogr.*, **64**, 303.
- Hutchings, M.T., 1964. Point-charge calculations of energy levels of magnetic ions in crystalline electric fields. *Solid State Phys.*, **16**, 227–273.
- Iida, S. & Mizushima, K., 1966. Effective in-plane anisotropy and trigonal magnetostriction in α -Fe₂O₃. *J. Phys. Soc. Japan*, **21**, 401–402.
- Imaoka, Y., 1968. On the coercive force of magnetic iron oxides. *J. Electrochem. Soc. Japan.*, **36**, 15–22.
- Irving, E., 1970. The Mid-Atlantic Ridge at 45°N. XVI. Oxidation and magnetic properties of basalts; review and discussion. *Can. J. Earth Sci.*, **7**, 1528–1538.
- Ishikawa, Y. & Akimoto, S., 1957. Magnetic properties of the FeTiO₃–Fe₂O₃ solid solution series. *J. Phys. Soc. Japan*, **12**, 1083–1098.
- Ishikawa, Y., Sato, S. & Syono, Y., 1971. Neutron and magnetic studies of a single crystal of Fe₂TiO₄. *J. Phys. Soc. Japan*, **31**, 452–460.
- Jackson, M., 1991. Anisotropy of magnetic remanence: a brief review of mineralogical sources, physical origins, geological applications and comparison with susceptibility anisotropy. *Pure Appl. Geophys.*, **136**, 1–28.
- Janot, C. & Gilbert, H., 1970. Les constituants du fer dans certaines bauxites naturelles étudiées par effect Mössbauer. *Bull. Soc. Franç. Minér. Cristall.*, **93**, 213–223.
- Johnson, H.P. & Merrill, R.T., 1973. Low-temperature oxidation of a titanomagnetite and the implications for paleomagnetism. *J. Geophys. Res.*, **78**, 4938–4949.
- Johnson, H.P. & Merrill, R.T., 1974. Low-temperature oxidation of a single-domain magnetite. *J. Geophys. Res.*, **79**, 5533–5534.
- Johnson, H.P., Lowrie, W. & Kent, D.V., 1975. Stability of anhysteretic remanent magnetization in fine and coarse magnetite and maghemite particles. *Geophys. J. R. astr. Soc.*, **41**, 1–10.
- Johnson, H.P. & Hall, J.M., 1978. A detailed rock magnetic and opaque mineralogy study of the basalts from the Nazca Plate. *Geophys. J. R. astr. Soc.*, **52**, 45–64.
- Johnson, H.P. & Pariso, J.E., 1993. Variations in oceanic crustal magnetization: Systematic changes in the last 160 million years. *J. Geophys. Res.*, **98**, 435–445.
- Jones, A.H., Geissman, J.W. & Coates, D.A., 1984. Clunker deposits, Powder River Basin, Wyoming and Montana: A new source of high-fidelity paleomagnetic data for the Quarternary. *Geophys. Res. Lett.*, **11**, 1231–1234.
- Kachi, S., Momiyama, K. & Shimizu, S., 1963. An electron diffraction study and a theory of the transformation from γ -Fe₂O₃ to α -Fe₂O₃. *J. Phys. Soc. Japan*, **18**, 106–116.
- Kachi, S., Nakanishi, N., Kosuge, K. & Hiramatsu, H., 1971. Electron microscopic observations on the transformation of α -Fe₂O₃. In: Y. Hoshino, S. Iida, and M. Sugimoto (eds), *Ferrites: Proceedings of the International Conference*, University of Tokyo Press, Tokyo, 141–143.
- Kaneoke, M., 1980. Change in coercive force of γ -Fe₂O₃ – Fe₃O₄ solid solutions with magnetostrictive anisotropy. *IEEE Trans. Magn.*, **MAG16**, 1319–1322.
- Kang, G.F., Zhang, Q.S. & Lei, X.W., 1993. Coal fire investigation report of northern part of China (Northwest Area), *ARSC internal report*. Xian, China, 93 p. (in Chinese).
- Kawai, N. & Ono, F., 1966. *Phys. Lett.*, **21**, 279.
- Kawai, N., Ono, F. & Hirooka, K., 1968. *J. Appl. Phys.*, **39**, 712.
- Kent, D.V. & Lowrie, W., 1974. Origin of magnetic instability in sediment cores from the central North Pacific. *J. Geophys. Res.*, **79**, 2987–3000.

- Kneller, E. & Luborsky, F.E., 1963. Particle size dependence of coercivity and remanence of single-domain particles. *J. Appl. Phys.*, **34**, 656–658.
- Knowles, J.E., 1981. The properties of acicular particles of $(\gamma\text{-Fe}_2\text{O}_3)_x(\text{Fe}_3\text{O}_4)_{1-x}$. *J. Magn. Magn. Mat.*, **22**, 263–266.
- Kodama, P., 1982. Magnetic effects of magnetization of Plio-Pleistocene marine sediments, northern California. *J. Geophys. Res.*, **87**, 7113–7125.
- Kojima, M., 1964. The free iron minerals contained in Kanto loam. *J. Soil Sci. Tokyo*, **35**, 174–180.
- Kostov, I., 1968. *Mineralogy*, Oliver and Boyd, Edinburgh, London, pp. 587.
- Krén, E., Molnár, B., Sváb, E. & Zsoldos, E., 1974. Neutron diffraction study of the $(1-x)\alpha\text{-Fe}_2\text{O}_3 - \alpha\text{-Al}_2\text{O}_3$ system. *Solid State Commun.*, **15**, 1707–1710.
- Krsová, M., Krs, M., Pruner, P. & Chvojka, R., 1989. Palaeointensity of the geomagnetic field during Upper Cainozoic derived from placo-slugs and porcellanites in North Bohemia. *Studia Geophys. et Geod.*, **33**, 338–361.
- Kumagai, H., Abe, H., Ono, K., Hayashi, I., Shimada, J. & Iwanaga, K., 1955. Frequency dependence of magnetic resonance in $\alpha\text{-Fe}_2\text{O}_3$. *Phys. Rev.*, **99**, 1116–1118.
- Kündig, W., Bömmel, H., Constabaris, G. & Lindquist, R.H., 1966. Some properties of supported small $\alpha\text{-Fe}_2\text{O}_3$ particles determined with the Mössbauer effect. *Phys. Rev.*, **142**, 327–333.
- Kündig, W., Ando, K.J., Lindquist, R.H. & Constabaris, G., 1967. *Czech. J. Phys.*, **B17**, 467.
- Kushiro, I., 1960. $\gamma \rightarrow \alpha$ transition in Fe_2O_3 with pressure. *J. Geomag. Geoelectr.*, **11**, 148–151.
- Le Borgne, E., 1955. Abnormal magnetic susceptibility of the top soil. *Ann. Geophys.*, **11**, 399–419.
- Lee, Y.S., Nishimura, S. & Min, K.D., 1996. High-unblocking-temperature haematite magnetizations of Late Palaeozoic red beds from the Okcheon zone, southern part of the Korean Peninsula. *Geophys. J. Int.*, **125**, 266–284.
- Lin, S.T., 1960. Magnetic behaviour in the transition region of a hematite single crystal. *J. Appl. Phys.*, **31**, 2735–2745.
- Lindqvist, J.K., Hatherton, T. & Mumme, T.C., 1985. Magnetic anomalies resulting from baked sediments over burnt coal seams in southern New Zealand. *New Zealand J. Geol. and Geophys.*, **28**, 405–412.
- Lindsley, D.H., 1976a. The crystal chemistry and structure of oxide minerals as exemplified by the Fe-Ti oxides. In: D. Rumble III (ed.), *Oxide Minerals, Reviews in Mineralogy 3*, Min. Soc. Am., Washington D.C., L1–60.
- Lindsley, D.H., 1976b. Experimental studies of iron oxide minerals. In: D. Rumble III (ed.), *Oxide Minerals, Reviews in Mineralogy 3*, Min. Soc. Am., Washington D.C., L61–88.
- Lindsley, D.H., 1991. Experimental studies of oxide minerals. In: D.H. Lindsley (ed.), *Oxide minerals, Reviews in Mineralogy 25*, Min. Soc. Am., Washington, D.C., 69–106.
- Lodding, W. & Hammell, L., 1960. DTA of hydroxides in a reducing atmosphere. *Anal. Chem.*, **32**, 657–662.
- Lourens, L.J., Antoarakou, A., Hilgen, F.J., Van Hoof, A.A.M., Vergnaud-Grazzini, C. & Zachariasse, W.J., 1996. Evaluation of the Plio-Pleistocene astronomical time scale. *Paleoceanography*, **11**, 391–413.
- Løvlie, R., 1976. The intensity pattern of post-depositional remanence acquired in some marine sediments deposited during a reversal of the external magnetic field. *Earth Planet. Sci. Lett.*, **30**, 209–214.
- Lowrie, W. & Fuller, M., 1971. On the alternating field demagnetisation characteristics of multidomain thermoremanent magnetisation in magnetite. *J. Geophys. Res.*, **76**, 6339–6349.
- Lowrie, W., 1990. Identification of ferromagnetic minerals in a rock by coercivity and unblocking temperature properties. *Geophys. Res. Lett.*, **17**, 159–162.
- Lyberatos, A. & Chantrell, R.W., 1990. Calculation of the size dependence of the coercive force in fine particles. *IEEE Trans. Magn.*, **26**, 2119–2121.
- Ma, J.W., 1990. Investigation of coal fires in Xinjiang by remote sensing, *ARSC internal report*, Xian, China, (in Chinese).
- Maeda, Y., 1978. High coercive $\gamma\text{-Fe}_2\text{O}_3$ fine particles. *The electronics and tele-communications laboratories, NNT. E.C.L. Techn. Publ.*, **179**, 1–7.
- Maher, B.A., 1986. Characterization of soils by mineral magnetic measurements. *Phys. Earth Planet. Inter.*, **42**, 76–92.
- Maher, B.A. & Thompson, R., 1992. Paleoclimatic significance of the minerals magnetic record of the Chinese loess and paleosols. *Quat. Res.*, **37**, 155–170.

- Maher, B.A., 1998. Magnetic properties of modern soils and Quaternary loessic paleosols: paleoclimatic implications. *Paleogeogr. Paleoclim. Paleoc.*, **137**, 25–54.
- Maxwell, L.R., Smart, J.S. & Brunaver, S., 1949. Dependence of the intensity of magnetization and the Curie point of certain iron oxides upon ratio of $\text{Fe}^{2+} / \text{Fe}^{3+}$. *Phys. Rev.*, **76**, 459–460.
- McClelland, E. & Goss, C., 1987. Self-reversal of CRM due to the maghemite-hematite transition; natural and laboratory examples. Paper presented at XIX General Assembly, IUGG, Vancouver, B.C. (*abstract*).
- McClelland, E. & Goss, C., 1993. Self reversal of chemical remanent magnetisation on the transformation of maghemite to haematite. *Geophys. J. Int.*, **112**, 517–532.
- McClelland, E. & Shcherbakov, V.P., 1995. Metastability of domain state in multidomain magnetite: Consequences for remanence acquisition. *J. Geophys. Res.*, **100**, 3841–3857.
- McClelland, E., Muxworthy, A.R. & Thomas, R.M., 1996. Magnetic properties of the stable fraction of remanence in large multidomain (MD) magnetite grains: single-domain or MD? *Geophys. Res. Lett.*, **23**, 2831–2834.
- Meiklejohn, W.H. & Bean, C.P., 1956. New magnetic anisotropy. *Phys. Rev.*, **102**, 1413–1414.
- Meiklejohn, W.H., 1962. Exchange anisotropy - A review. *J. Appl. Phys.*, **33S**, 1328–1335.
- Meillon, S., Dammak, H., Flavin, E. & Pascard, H., 1995. Existence of a direct phase transformation from haemite to maghemite. *Phil. Mag. Lett.*, **72**, 105–110.
- Michel, A. & Chaudron, G., 1935. Étude du sesquioxide de fer cubique stabilisé. *C. R. Acad. Sci. Paris*, **201**, 1191–1193.
- Michel, A., Chaudron, G. & Bénard, J., 1951. Propriétés des composés ferromagnétiques non métalliques. *J. Physique*, **12**, 189–201.
- Miyamoto, Y. & Chikazumi, S., 1988. Crystal symmetry of magnetite in low temperature phase deduced from magneto electric measurements. *J. Phys. Soc. Japan*, **57**, 2040–2050.
- Mollard, P., Rousset, A. & Dupré, G., 1977a. Moment à saturation du sesquioxyde de fer cubique. *Mat. Res. Bull.*, **12**, 797–801.
- Mollard, P., Germi, P. & Rousset, A., 1977b. Surface effects of saturation magnetization of fine spinel ferrite particles. *Physica*, **86–88 B+C**, 1393–1394.
- Molnar, P., Brown, E.T., Burchfiel, B.C., Deng, Q.D., Feng, X.Y., Li, J., Raisbeck, G.M., Shi, J.B., Wu, Z.M., Yiou, F. & You, H.C., 1994. Quaternary climate change and the formation of river terraces across growing anticlines on the North Flank of the Tien Shan, China. *Amer. J. Geology*, **102**, 583–602.
- Morales, J., Tirado, J.L. & Valera, C., 1989. Preferential X-ray broadening and thermal behaviour of $\gamma\text{-Fe}_2\text{O}_3$. *J. Am. Ceram. Soc.*, **72**, 1244–1246.
- Morin, J., 1950. Magnetic susceptibility of $\alpha\text{-Fe}_2\text{O}_3$ and Fe_2O_3 with added titanium. *Phys. Rev.*, **78**, 819–820.
- Moriya, T., 1960. Anisotropic superexchange interaction and weak ferromagnetism. *Phys. Rev.*, **120**, 91–98.
- Morris, R.V., Lauer, H.V., Lawson, C.A., Gibson, E.K., Nace, G.A. & Stewart, C., 1985. Spectral and other physico-chemical properties of submicron powders of hematite ($\alpha\text{-Fe}_2\text{O}_3$), maghemite ($\gamma\text{-Fe}_2\text{O}_3$), magnetite (Fe_3O_4), goethite ($\alpha\text{-FeOOH}$) and lepidocrocite ($\gamma\text{-FeOOH}$). *J. Geophys. Res.*, **B90**, 3126–3144.
- Morrish, A.H. & Yu, S.P., 1955. Dependence of the coercive force on the density of some iron oxide powders. *J. Appl. Phys.*, **26**, 1049–1055.
- Morrish, A.H., Johnston, G.B. & Curry, N.A., 1963. Magnetic transition in pure and Ga doped $\alpha\text{-Fe}_2\text{O}_3$. *Phys. Lett.*, **77**, 177–178.
- Morrish, A.H. & Sawatzky, G.A., 1971. Mössbauer study of the $\gamma \rightarrow \alpha$ transformation in pure and cobalt-doped ferric oxide. In: Y. Hoshino, S. Iida and M. Sugimoto (eds), *Ferrites: Proceedings of the Intern. Conference*, University of Tokyo Press, Tokyo, 144–147.
- Morrish, A.H., 1994. *Canted antiferromagnetism: Hematite*, World Scientific, London, pp. 192.
- Moskowitz, B.M. & Banerjee, S.K., 1981. A comparison of the magnetic properties of synthetic titanomaghemites and some oceanic basalts. *J. Geophys. Res.*, **86**, 11,869–11,882.
- Moskowitz, B.M., 1992. *Rock Magnetism Laboratory Notes*. University of Minnesota, Minneapolis, MN, pp. 40.
- Moskowitz, B.M., 1993. High-temperature magnetostriction of magnetite and titanomagnetites. *J. Geophys. Res.*, **98**, 359–372.
-

- Moskowitz, B.M., Frankel, R.B., Walton, S.A., Dickson, D.P.E., Wong, K.K.W., Douglas, T. & Mann, S., 1997. Determination of the preexponential frequency factor for superparamagnetic maghemite particles in magnetoferritin. *J. Geophys. Res.*, **102**, 22,671–22,680.
- Mullender, T.A.T., van Velzen, A.J. & Dekkers, M.J., 1993. Continuous drift correction and separate identification of ferrimagnetic and paramagnetic contribution in thermomagnetic runs. *Geophys. J. Int.*, **114**, 663–672.
- Mullins, C.E., 1977. Magnetic susceptibility of the soil and its significance in soil science – a review. *J. Soil Sci.*, **28**, 223–246.
- Murad, E. & Schwertmann, U., 1993. The influence of aluminium substitution and crystallinity on the Mössbauer spectra of goethite. *Clay Min.*, **18**, 301–312.
- Murray, J.W., 1979. Iron oxides, Marine minerals. *Short Course Notes Mineral. Soc. Am.*, **6**, 47–98.
- Nagata, T. & Akimoto, S., 1956. Magnetic properties of ferromagnetic ilmenites. *Geofis. Pure e Appl.*, **34**, 36–50.
- Nagata, T., Yama-ai, M. & Akimoto, S., 1961. 'Memory' of initial remanent magnetisation and number of repeating heat treatments in low-temperature behaviour of hemaematite. *Nature*, **190**, 620–621.
- Nagata, T., 1961. *Rock Magnetism*, 2nd edition, Maruzen, Tokyo, pp. 350.
- Nagata, T. Ozima, M. & Yamai-ai, M. 1963. Demonstration of the production of a new type of remanent magnetization: Inversed type of thermoremanent magnetization. *Nature*, **197**, 444–445.
- Naono, H. & Fujiwara, R., 1980. Micropore formation due to thermal decomposition of acicular microcrystals of α -FeOOH. *J. Colloid Interface Sci.*, **73**, 406–415.
- Néel, L., 1948. Propriétés magnétiques des ferrites: ferrimagnétisme et antiferromagnétisme. *Annales Phys.*, **3**, 137–198.
- Néel, L. & Pauthenet, R., 1952. Étude thermomagnétique d'un monocristal de $\text{Fe}_2\text{O}_3\alpha$. *C.R. Acad. Sci. (Paris)*, **234**, 2172–2174.
- Néel, L., 1953. Some new results on antiferromagnetism and ferromagnetism, *Rev. Mod. Phys.*, **25**, 58–63.
- Néel, L., 1955. Some theoretical aspects of rock magnetism. *Adv. Phys.*, **4**, 191–243.
- Nilsson, T., 1983. *The Pleistocene*. Reidel, Dordrecht, pp. 651.
- Nininger, R.C. & Schroerer, D., 1978. Mössbauer studies of the Morin transition in bulk and microcrystalline α - Fe_2O_3 . *J. Phys. Chem. Solids*, **39**, 137–144.
- Nishikawa, S., 1915. Structure of some crystals of the spinel group. *Proc. Math. Phys. Soc. Tokyo*, **8**, 199–209.
- Nishitani, T. & Kono, M., 1982. Grainsize effect on the low-temperature oxidation of titanomagnetite. *J. Geophys.*, **50**, 137–142.
- Nishitani, T. & Kono, M., 1983. Curie temperature and lattice constant of oxidized titanomagnetite. *Geophys. J. R. astr. Soc.*, **74**, 585–600.
- Nishitani, T. & Kono, M., 1989. Effect of low-temperature oxidation on the remanence properties of titanomagnetites. *J. Geomagn. Geoelectr.*, **41**, 19–38.
- O'Donovan, J.B. & O'Reilly, W., 1977a. Mondomain behaviour in multiphase oxidized titanomagnetite. *Earth Planet. Sci. Lett.*, **34**, 396–402.
- O'Donovan, J.B. & O'Reilly, W., 1977b. The preparation, characterization and magnetic properties of synthetic analogues of some carriers of the paleomagnetic record. *J. Geomagn. Geoelectr.*, **29**, 331–344.
- Oles, A., Szytula, A. & Wanic, A., 1970. Neutron diffraction study of γ -FeOOH. *Phys. Stat. Sol.*, **41**, 173–177.
- Ono, K. & Ito, A., 1962. A Mössbauer study of the internal field at Fe^{57} in α - Fe_2O_3 . *J. Phys. Soc. Japan*, **17**, 1012–1017.
- O'Reilly, W. & Banerjee, S.K., 1965. Cation distribution in titanomagnetites $(1-x)\text{Fe}_3\text{O}_4-x\text{Fe}_2\text{TiO}_4$. *Phys. Lett.*, **17**, 237–238.
- O'Reilly, W. & Banerjee, S.K., 1967. The mechanism of oxidation in titanomagnetites: A magnetic study. *Mineral Magazine*, **36**, 29–37.
- O'Reilly, W., 1968. Estimation of the Curie temperatures of maghemite and oxidized titanomagnetites. *J. Geomag. Geoelectr.*, **20**, 381–386.
- O'Reilly, W., 1984. *Rock and Mineral Magnetism*, Blackie, Glasgow, pp. 220.
- Owen, J. & Taylor, D.R., 1966. Zero-spin deviation in antiferromagnets. *Phys. Rev. Lett.*, **16**, 1164–1166.
- Ozaki, M. & Matijevic, E., 1990. Preparation and magnetic properties of monodispersed, spindle type γ - Fe_2O_3 particles. *J. Colloid Interface Sci.*, **107**, 199–203.

- Özdemir, Ö. & O'Reilly, W., 1981. High-temperature hysteresis and other magnetic properties of synthetic monodomain titanomagnetites. *Phys. Earth Planet. Inter.*, **25**, 406–418.
- Özdemir, Ö. & O'Reilly, W., 1982. Magnetic hysteresis properties of synthetic monodomain titanomaghemites. *Earth Planet. Sci. Lett.*, **57**, 437–447.
- Özdemir, Ö. & Banerjee, S.K., 1984. High-temperature stability of maghemite. *Geophys. Res. Lett.*, **11**, 161–164.
- Özdemir, Ö. & Dunlop, D.J., 1985. An experimental study of chemical remanent magnetizations of synthetic monodomain titanomaghemites with initial thermoremanent magnetizations. *J. Geophys. Res.*, **90**, 11,513–11,523.
- Özdemir, Ö., 1987. Inversion of titanomaghemites. *Phys. Earth Planet. Inter.*, **46**, 184–196.
- Özdemir, Ö. & Dunlop, D.J., 1988. Crystallization remanent magnetisation during the transformation of maghemite to hematite. *J. Geophys. Res.*, **93**, 6530–6544.
- Özdemir, Ö. & Dunlop, D.J., 1989. Chemico-viscous remanent magnetization in the Fe_3O_4 – $\gamma\text{Fe}_2\text{O}_3$ system. *Science*, **243**, 1043–1047.
- Özdemir, Ö., 1990. High-temperature hysteresis and thermoremanence of single-domain maghemite. *Phys. Earth Planet. Inter.*, **65**, 125–136.
- Özdemir, Ö. & Moskowitz, B.M., 1992. Magnetostriction in aluminium-substituted titanomagnetites. *Geophys. Res. Lett.*, **19**, 2361–2364.
- Özdemir, Ö. & Dunlop, D.J., 1993. Chemical remanent magnetization during γFeOOH phase transformations. *J. Geophys. Res.*, **98**, 4191–4198.
- Özdemir, Ö., Dunlop, D.J. & Moskowitz, B.M., 1993. The effect of oxidation on the Verwey transition in magnetite. *Geophys. Res. Lett.*, **20**, 1671–1674.
- Özdemir, Ö. & Dunlop, D.J., 1996. Thermoremanence and Néel temperature of goethite. *Geophys. Res. Lett.*, **23**, 921–924.
- Özdemir, Ö., 1998. (abstract) Chemical remanent magnetization during the transformation of goethite to hematite: possible formation of intermediate spinel product. *Geologica Carpathica*, **49**, 225.
- Ozima, M., Ozima, M. & Akimoto, S., 1964. Low temperature characteristics of remanent magnetization of magnetite. *J. Geomag. Geoelectr.*, **16**, 165–177.
- Ozima, M., 1971. Magnetic processes in oceanic ridge. *Earth Planet. Sci. Lett.*, **13**, 1–5.
- Parker Gay, S., Jr. & Hawley, B.W., 1991. Syngenetic magnetic anomaly sources: Three examples. *Geophysics*, **56**, 902–913.
- Pastrana, J.M. & Hopstock, D.M., 1977. Magnetic properties of natural hematite and goethite. *Transactions, SME/AIME*, Vol. **262**, 1–5.
- Pauthenet, R., 1952. Aimantation spontanée des ferrites. *Ann. Phys.*, **7**, 710–747.
- Pawluck, S., 1971. Characteristics of ferra eluviated gleysols developed from acidic shale in north-western Alberta. *Can. J. Soil Sci.*, **51**, 113–124.
- Pecharromás, C., González-Carreño, T. & Iglesias, J.E., 1995. The infrared dielectric properties of maghemite, $\gamma\text{-Fe}_2\text{O}_3$, from reflectance measurement on pressed powders. *Phys. Chem. Minerals*, **22**, 21–29.
- Peng, X. & Zhang G., 1989. Tectonic features of the Junggar basin and their relation with oil and gas distribution. In: K.J. Hsü (ed.), *Chinese sedimentary basins*, Elsevier, 17–31.
- Peng, W.X., van Genderen, J.L., Kang, G.F., Guan, H.Y. & Tan, Y.J., 1997. Estimating the depth of underground coal fires using data integration techniques. *Terra Nova*, **9**, 180–183.
- Petersen, N. & Vali, H., 1987. Observation of shrinkage cracks in ocean floor titanomagnetites. *Phys. Earth Planet. Inter.*, **46**, 197–205.
- Petrovský, E., Dekkers, M.J., Kropáček, V., Hejda, P. & Zelinka, T., 1994. Incompatible magnetic behaviour of fine-grained natural hematite samples prepared in similar ways. *Studia Geoph. Geod.*, **38**, 46–56.
- Petrovský, E., Kropáček, V., Dekkers, M.J., de Boer, C.B., Hoffmann, V. & Ambatiello, A., 1996. Transformation of hematite to maghemite as observed by changes in magnetic parameters: Effects of mechanical activation? *Geophys. Res. Lett.*, **23**, 1477–1480.
- Podolsky, G., 1981. Relationship of $\gamma\text{-Fe}_2\text{O}_3$ audio tape properties to particle size. *IEEE Trans. Magn.*, **MAG-17**, 3032–3034.
- Porath, H., 1968a. Stress-induced magnetic anisotropy in natural single crystals of hematite. *Phil. Mag.*, **17**, 603–608.
-

- Porath, H., 1968b. Magnetic studies on specimens of intergrown maghemite and hematite. *J. Geophys. Res.*, **73**, 5959–5965.
- Prakash, A., Saraf, A.K., Gupta, R.P., Dutta, M. & Sundaram, R.M., 1995a. Surface thermal anomalies with underground fires in Jhahra coal mine, India. *Int. J. Remote Sensing*, **16**(12), 2105–2109.
- Prakash, A., Sastry, R.G.S., Gupta, R.P. & Saraf, A.K., 1995b. Estimating the depth of burned hot feature from thermal IR remote sensing data, a conceptual approach. *Int. J. Remote Sensing*, **16**(13), 2503–2510.
- Prakash, A., Gupta, R.P. & Saraf, A.K., 1997. A Landsat TM based comparative study of surface and subsurface fires in the Jharia coalfield, India. *Internat. J. Remote Sensing*, **18**, 2463–2469.
- Prevot, M., Lecaille, A. & Mankinen, E.A., 1981. Magnetic effects of maghemitization of oceanic crust. *J. Geophys. Res.*, **86**, 4009–4020.
- Pullaiah, G., Irving, E., Buchan, K.L. & Dunlop, D.J., 1975. Magnetization changes caused by burial and uplift. *Earth Planet. Sci. Lett.*, **28**, 133–143.
- Purucker, M.E., Elston, D.P. & Shoemaker, E.M., 1980. Early acquisition of characteristic magnetisation in red beds of the Moenkopi Formation (Triassic), Gray Mountain, Arizona. *J. Geophys. Res.*, **85**, 997–1012.
- Putnis, A., 1992. *Introduction to mineral sciences*. Cambridge University Press
- Qiao, Z., 1981. Quaternary Strata in Urumqi and Toutunhe River Area, *Collection of Papers on Quaternary and Glacial Geology in Xinjiang*, 176–183.
- Rădan, S.C., Rădan, M. & Rădan, S., 1994. Magnetic properties of sediments associated with coal seams: applications and implications. New Trends in Geomagnetism, Třešt, Czech Republic. (abstract).
- Rădan, S.C. & Rădan, M., 1998. Rock magnetism and paleomagnetism of porcelanites/clinkers from the western Dacic Basin (Romania). *Geologica Carpathica*, **49**, 209–211.
- Ramdeani, A., Steinmetz, J., Gleitzer, C., Coey, J.M.D. & Freidt, J.M., 1987. Perturbation de l'échange électronique rapide par les lacunes cationique dans $\text{Fe}_{3-x}\text{O}_4$ ($x \leq 0.09$). *J. Phys. Chem. Solids*, 217–228.
- Rao, V., Shashiomohan, A.L. & Biswas, A.B., 1974. Studies on the formation of $\gamma\text{-Fe}_2\text{O}_3$ by thermal decomposition of ferrous oxalate dihydrate. *J. Mater. Sci.*, **9**, 430–433.
- Rasmussen, R.J. & Honig, J.M., 1988. Ac electrical transport properties of magnetite. *J. Appl. Phys.*, **64**, 5666.
- Readman, P.W. & O'Reilly, W., 1970. The synthesis and inversion of non-stoichiometric titanomagnetites. *Phys. Earth Planet. Int.*, **4**, 121–128.
- Readman, P.W. & O'Reilly, W., 1972. Magnetic properties of oxidized (cation-deficient) titanomaghemite. $(\text{Fe, Ti, } \square)_3\text{O}_4$. *J. Geomagn. Geoelectr.*, **24**, 69–90.
- Reeves, N.J. & Mann, S., 1991. Influence of inorganic and organic additives on the tailored synthesis of iron oxides. *J. Chem. Soc. Faraday Trans. I*, **87**, 3875–3880.
- Rendon, J.L., Cornejo, J., De Arambarri, P. & Serna, C.J., 1983. Pore structure of thermally treated goethite ($\alpha\text{-FeOOH}$). *J. Colloid Interface Sci.*, **92**, 508–516.
- Roberts, A.P., Cui, Y. & Verosub, K.L., 1995. Wasp-waisted hysteresis loops: Mineral magnetic characteristics and discrimination of components in mixed magnetic systems. *J. Geophys. Res.*, **100**, 17,909–17,924.
- Rochette, P. & Fillion, G., 1989. Field and temperature dependence of remanence in synthetic goethite: paleomagnetic implications. *Geophys. Res. Lett.*, **16**, 851–854.
- Rosema, A., van Genderen, J.L. & Schalke, H.J.W.G., 1993. Environmental monitoring of coal fires in north China. *Project Identification Mission Report, BCRS 93-29 (ISBN 90-5411-1054)*, pp. 24.
- Roy, J.L. & Park, J.K., 1972. Red beds: DRM or CRM? *Earth Planet. Sci. Lett.*, **17**, 211–216.
- Ruan, H.D. & Gilkes, R.J., 1995. Dehydroxylation of aluminous goethite: unit cell dimensions, crystal size and surface area. *Clays Clay Minerals*, **43**, 196–211.
- Ryall, P.J.C. & Ade-Hall, J.M., 1975. Radical variation of magnetic properties in submarine pillow basalts. *Can. J. Earth Sci.*, **12**, 1959–1969.
- Sadiq, M. & Lindsay, W.L., 1988. The solubility product of soil maghemite. *Soil Sci.*, **146**, 1–5.
- Schalke, H.J.W.G., Rosema, A. & van Genderen, J.L., 1993. Environmental monitoring of coal fires in North China. *Project identification mission report*. Netherlands Remote Sensing Board Report, 93–29.
- Schmal, D., 1987. *A model for the spontaneous heating of stored coal*. PhD thesis, Technology University of Delft, Delft, The Netherlands.
- Schmidt, V.A., 1970. Basal plane susceptibility anisotropy in hematite. *EOS Trans. Am. Geophys. Union*, **52**, 277 (abstract).
- Schneider, W., 1996. The coal-bearing Jurassic at the southern margin of the Junggar basin, Xinjiang. *Geowissenschaften*, **14**, 285–287.

- Schroerer, D. & Nininger, R.C., 1967. *Phys. Rev. Lett.*, **19**, 632- .
- Schulze, D.G., 1982. *The identification of soil iron oxides by differential X-ray diffraction and the influence of aluminum substitution on the structure of goethite*. PhD thesis, Technische Universität, München, Germany.
- Schulze, D.G., 1984. The influence of aluminum on iron oxides. VIII. Unit-cell dimensions of Al-substituted goethites and estimation of Al from them. *Clay Clay Miner.*, **32**, 36-44.
- Schulze, D.G. & Schwertmann, U., 1984. The influence of aluminium on iron oxides: X. Properties of Al-substituted goethites. *Clay Miner.*, **19**, 521-539.
- Schwertmann, U. & Heinemann, B., 1959. The occurrence and formation of maghemite in soils of N.W. Germany. *Neues Jahrb. Mineral., Monatsh.*, **8**, 174-181.
- Schwertmann, U. & Taylor, R.M., 1977. Iron oxides. In: J.B. Dixon and S.B. Weed (eds), *Minerals in Soil Environments*. Soil Sci. Soc. Am., Madison, Wisc., 145-180.
- Schwertmann, U., Fitzpatrick, R.W., Taylor, R.M. & Lewis, D.G., 1979. The influence of aluminium on iron oxides. Part II. Preparation and properties of Al-substituted hematites. *Clays Clay Minerals*, **27**, 105-112.
- Schwertmann, U., & Murad, E., 1983. The effect of pH on the formation of goethite and hematite from ferrihydrate. *Clays Clay Miner.*, **31**, 277-284.
- Schwertmann, U. & Fechter, H., 1984. The influence of aluminum on iron oxides. XI. Aluminum-substituted maghemite in soils and its formation. *Soil Sci. Soc. Am. J.*, **48**, 1462-1463.
- Schwertmann, U., 1985. The effect of pedogenic environments on iron oxide minerals. *Adv. Soil Sci.*, **1**, 172-200.
- Schwertmann, U. & Latham, M., 1986. Properties of iron oxides in some New Caledonian soils. *Geoderma*, **39**, 105-123.
- Schwertmann, U., 1988a. Some properties of soil and synthetic iron oxides. In: J.W. Stucki, B.A. Goodman, and U. Schwertmann (eds), *Iron in Soils and Clay Minerals*, D. Riedel Publ. Co., Dordrecht, NATO ASI Series C217, 203-250.
- Schwertmann, U., 1988b. Occurrence and formation of iron oxides in various pedoenvironments. In: J.W. Stucki, B.A. Goodman, and U. Schwertmann (eds), *Iron in Soils and Clay Minerals*, D. Riedel Publ. Co., Dordrecht, NATO ASI Series C217, 267-308.
- Schwertmann, U. & Murad, E., 1990. The influence of aluminium on iron oxides: XIV. Al-substituted magnetite synthesized at ambient temperatures. *Clays Clay Min.*, **38**, 196-202.
- Schwertmann, U & Cornell, R.M., 1991. *Iron oxides in the laboratory*, VCH, Weinheim, pp. 236.
- Schwertmann, U. & Stanjek, H., 1998. Stirring effects on properties of Al goethite formed from ferrihydrate. *Clays Clay Minerals*, **46**, 317-321.
- Searle, C.W. & Wang, S.T., 1968. Magnetic resonance properties of pure and titanium-doped hematite. *J. Appl. Phys.*, **39**, 1025-1026.
- Senanayake, W.E. & McElhinney, M.W., 1981. Hysteresis and susceptibility characteristics of magnetite and titanomagnetites: interpretation of results from basaltic rocks. *Phys. Earth Planet. Inter.*, **26**, 47-55.
- Senno, H. & Tawara, Y., 1967. Exchange anisotropy in the mixed phase of $\gamma\text{Fe}_2\text{O}_3$ and $\alpha\text{Fe}_2\text{O}_3$. *J. Jpn. Appl. Phys.*, **6**, 509-511.
- Shannon, R.D. & Prewitt, C.T., 1969. Effective ionic radii in oxides and fluorides. *Acta Cryst.*, **B25**, 925-946.
- Shive, P.N., Steiner, M.B. & Huycke, D.T., 1984. Magnetostratigraphy, paleomagnetism, and remanence acquisition in the Triassic Chugwater Formation of Wyoming. *J. Geophys. Res.*, **89**, 1801-1815.
- Shu, X., 1994. Thermal analysis of spontaneous combustion of coal. *Coal Geol. China*, **6**, 25-29.
- Shull, C.G., Strauser, W.A. & Wollan, E.O., 1951. Neutron diffraction by paramagnetic and antiferromagnetic substances. *Phys. Rev.*, **83**, 333-345.
- Sidhu, P.S., Gilkes, R.J. & Posner, A.M., 1977. Mechanism of the low-temperature oxidation of synthetic magnetites. *J. Inorg. Nucl. Chem.*, **39**, 1953-1958.
- Sidhu, P.S., Gilkes, R.J. & Posner, A.M., 1980. The behavior of Co, Ni, Zn, Cu, Mn, and Cr in magnetite during alteration to maghemite and hematite. *Soil Sci. Soc. Am. J.*, **44**, 135-138.
- Sidhu, P.S., 1988. Transformation of trace element substituted maghemite to hematite. *Clays Clay Minerals*, **36**, 31-38.
- Singer, M.J. & Fine, P., 1989. Pedogenic factors affecting magnetic susceptibility of northern California soils. *Soil Sci. Soc. Am. J.*, **53**, 1119-1127.
-

- Singh, B. & Gilkes R.J., 1995. The natural occurrence of χ -alumina in lateritic pisolites. *Clay Minerals*, **30**, 39–44.
- Smit, J. & Wijn, H.P.J., 1959. *Ferrites*, Philips' Technical Library, pp. 369.
- Smith, P.K.K., 1979. The observation of enantiomorphous domains in a natural maghemite. *Contrib. Mineral. Petrol.*, **69**, 249–254.
- Smith, R.W. & Fuller, M., 1967. Alpha-hematite: stable remanence and memory. *Science*, **156**, 1130–1133.
- Soffel, H., 1991. *Paläomagnetismus und Archäomagnetismus*. Springer, Berlin, pp. 276.
- Sosman, R.B. & Posnjak, E., 1925. Ferromagnetic ferric oxide, artificial and natural. *J. Washington Ac. Sci.*, **15**, 329–342.
- Srivastava, J.J. & Sharma, R.P., 1972. Magnetic dilution effects on Morin phase transition in hematite. *Phys. Status Solidi*, **B 49**, 135–146.
- Stacey, F.D. & Banerjee, S.K., 1974. *The physical principles of rock magnetism*, Elsevier, Amsterdam, pp. 195.
- Stanjek, H. & Schwertmann, U., 1992. The influence of aluminum on iron oxides. Part XVI: Hydroxyl and aluminium substitution in synthetic hematites. *Clay Clay Min.*, **40**, 347–354.
- Stephenson, A., 1969. The temperature-dependent cation distribution in titanomagnetites. *Geophys. J. R. astr. Soc.*, **18**, 199–210.
- Steiner, M.B., 1983. Detrital remanent magnetization in hematite. *J. Geophys. Res.*, **88**, 6523–6539.
- Stocking, L.B. & Tauxe, L., 1990. Properties of chemical remanence in synthetic hematite: Testing theoretical predictions. *J. Geophys. Res.*, **95**, 12,639–12,652.
- Stoner, E.C. & Wohlfarth, E.P., 1948. A mechanism of magnetic hysteresis in heterogeneous alloys. *Phil. Trans Roy. Soc. (London)*, **A 240**, 599–642.
- Stoner, J.S., Channell, J.E.T. & Hillaire-Marcel, C., 1995. Magnetic properties of deep-sea sediments off southwest Greenland: Evidence for major differences between the last two deglaciations. *Geology*, **23**, 241–244.
- Strangway, D.W., McMahon, B.E. & Honea, R.M., 1967a. Stable magnetic remanence in antiferromagnetic goethite. *Science*, **158**, 785–787.
- Strangway, D.W., McMahon, B.E., Honea, R.M. & Larson, E.E., 1967b. Superparamagnetism in hematite. *Earth Planet. Sci. Lett.*, **2**, 367–371.
- Strangway, D.W., Honea, R.M., McMahon, B.E. & Larson, E.E., 1968. The magnetic properties of naturally occurring goethite. *Geophys. J. R. astr. Soc.*, **15**, 345–359.
- Strzyszczyk, Z., 1993. Magnetic susceptibility of soils in the areas influenced by industrial emission. In: R. Schullin et al. (eds), *Soil Monitoring: Early Detection and Surveying of soils Contamination and Degradation*, Birkhäuser Verlag, Basel, 255–269.
- Šubrt, J., Šolcavá, A., Hanousek, F., Petrina, A. & Zapletal, V., 1984. Preparation of α -Fe₂O₃ (hematite) by oxidation precipitation of aqueous solutions of iron(II) sulphate. *Collection Czechoslovak Chem. Commun.*, **49**, 2478–2485.
- Sunagawa, I., 1987. The morphology of minerals. In: I. Sunagawa (ed) *The morphology of crystals*, Terra Sci. Publ. Co., Tokyo, 509–588.
- Sváb, E. & Krén, E., 1979. Neutron diffraction study of substituted hematite. *J. Magn. Magn. Mat.*, **14**, 184–186.
- Swaddle, T.W. & Oltmann, P., 1980. Kinetics of the magnetite-maghemite-hematite transformation, with special reference to hydrothermal systems. *Can. J. Chem.*, **58**, 1763–1772.
- Syono, Y., 1965. Magnetocrystalline anisotropy and magnetostriction of Fe₃O₄-Fe₂TiO₄ series – With special application to rock magnetism. *Jpn. J. Geophys.*, **4**, 71–143.
- Tagawa, K., Matsunaga, M., Ohshiwa, K., Hirawatsu, M., Ishibashi, T. & Mikami, J., 1986. Annealing effect of oxidized α -Fe particles. *I.E.E.E. Trans. Magn.*, **Vol. MAG-22, NO. 5**, 729–731.
- Takei, H. & Chiba, S., 1966. Vacancy ordering in epitaxially-grown single crystals of γ -Fe₂O₃. *J. Phys. Soc. Japan*, **21**, 1255–1263.
- Tauxe, L., Kent, D.V. & Opdyke, N.D., 1980. Magnetic components contributing to the NRM of Middle Siwalik red beds. *Earth Planet. Sci. Lett.*, **47**, 279–284.
- Tauxe, L., Mullender, T.A.T. & Pickett, T., 1996. Potbellies, wasp-waists and superparamagnetism in magnetic hysteresis. *J. Geophys. Res.*, **101**, 571–583.
- Taylor, R.M., 1980. Formation and properties of Fe(II) Fe(III) hydroxy-carbonate and its possible significance in soil formation. *Clay Minerals*, **15**, 369–382.

- Taylor, R.M. & Schwertmann, U., 1974a. Maghemite in soils and its origin. I. Properties and observations on soil maghemites. *Clay Minerals*, **10**, 289–298.
- Taylor, R.M. & Schwertmann, U., 1974b. Maghemite in soils and its origin. II. Maghemite synthesis at ambient temperature and pH 7. *Clay Minerals*, **10**, 299–310.
- Thompson, R. & Oldfield, F., 1986. *Environmental Magnetism*. Allen & Unwin, London, pp. 227.
- Tice, A.R. & Oliphant, J.L., 1984. The effects of magnetic particles on the unfrozen water content of frozen soils determined by nuclear magnetic resonance. *Soil Sci.*, **138**, 63–73.
- Tite, M.S. & Linington, R.E., 1975. Effect of climate on the magnetic susceptibility of soils. *Nature*, **256**, 565–566.
- Trolard, F., Bourrie, G., Jeanroy, E., Herbillon, A. & Martin, E., 1995. Trace metals in natural iron oxides from laterites: A study using selective kinetic extraction. *Geochim. Cosmochim. Acta*, **59**, 1285–1297.
- Turner, P., 1980. *Continental Red Beds, Developments in Sedimentology*, Vol 29, Elsevier, Amsterdam, pp. 562.
- Tyráček, J., 1994. Stratigraphical interpretation of the paleomagnetic measurements of the porcellanites of the Most basin, Czech Republic. *Vestník Českého geologického ústavu* **69**, 2, 83–87.
- Ulf-Møller, F., 1990. Formation of native iron in sediment-contaminated magma: I. A case study of the Hanekammen Complex on Disko Island, West-Greenland. *Geochim. Cosmochim. Acta*, **54**, 57–70.
- Umehayashi, H., Frazer, B.C., Shirane, G. & Daniels, W.B., 1966. *Phys. Lett.*, **22**, 407–.
- Umeorah, E.M., 1987. Depositional environment and facies relationships of the Cretaceous ironstone of the Agbaja Plateau, Nigeria. *J. African Earth Sci.*, **6**, 385–390.
- Urquhart, H.M.A. & Goldman, J.E., 1956. Magnetostrictive effects in an antiferromagnetic haematite crystal. *Phys. Rev.*, **101**, 1443–1450.
- Uyeda, S., 1958. Thermo-remanent magnetism as a medium of paleomagnetism, with special reference to reverse thermo-remanent magnetism. *Jpn. J. Geophys.*, **2**, 1–123.
- Van den Ende, C., 1977. *Paleomagnetism of Permian red beds of the Dôme de Barrot (S. France)*, PhD thesis, University of Utrecht, Utrecht, The Netherlands, pp. 171.
- Van der Horst, A.A., van der Kraan, A.M., van Loef, J.J., Lieftink, D.J. & Joosten, C., 1994. Mössbauer spectroscopic study of core and mantle of rattle stones. *Hyp. Int.*, **91**, 613–618.
- Van der Woude, F., 1966. Mössbauer effect in α -Fe₂O₃. *Phys. Staus Solidi*, **17**, 417–432.
- Van der Marel, H.W., 1951. γ -ferric oxide in sediments. *J. Sedim. Petrol.*, **21**, 12–21.
- Van Genderen, J.L., Cassells, C.J.S. & Zhang, X.M., 1996. The synergistic use of remotely sensed data for the detection of underground coal fires. *International Archives of Photogrammetry and Remote sensing*, 9-19 July, Vienna, Vol. **31-B7**, 722–727.
- Van Oorschot, I.H.M. & Dekkers, M.J., 1999. Dissolution behaviour of fine-grained magnetite and maghemite in the citrate-bicarbonate-dithionite extraction method. *Earth Planet. Sci. Lett.*, **167**, 283–295.
- Van Oosterhout, G.W. & Rooijmans, C.J.M., 1958. A new superstructure in gamma-ferric oxide. *Nature*, **181**, 44.
- Van Oosterhout, G.W., 1960. Morphology of synthetic submicroscopic crystals of α - and γ -FeOOH and of γ -Fe₂O₃ prepared from FeOOH. *Acta Cryst.*, **13**, 932–935.
- Van Oosterhout, G.W., 1965. The structure of goethite. *Proc. Int. Conf. Magnetism, Nottingham (Institute of Physics, London)*, 529–532.
- Van Velzen, A.J. & Zijdeveld, J.D.A., 1995. Effects of weathering on single-domain magnetite in Early Pliocene marine marls. *Geophys. J. Int.*, **121**, 267–278.
- Vegard, L., 1921. Die Konstitution der Mischkristalle und die Raumerfüllung der Atome. *Z. Kristallogr.*, **67**, 148–162.
- Veldkamp, A. & Vermeulen, S.E.J.W., 1989. River terrace formation, modelling and 3-D graphical simulation. *Earth Surface Processes and Landforms*, **14**, 641–654.
- Veldkamp, A., 1992. A 3-D model of Quaternary terrace development, simulations of terrace stratigraphy and valley asymmetry: a case study in the Allier terraces (Limagne, France). *Earth Surface processes and Landforms*, **17**, 487–500.
- Verbeeck, A.E., de Grave, E. & Vandenbergh. R.E., 1986. *Hyp. Int.*, **28**, 639–.
- Verma, R.K. & Prasad, S.N., 1975. Probable existence of native iron in newer dolerites from Singbhum, Bihar, India. *J. Geophys. Res.*, **80**, 3755–3756.
-

- Verosub, K.L., Fine, P., Singer, M.J. & TenPas, J., 1993. Pedogenesis and paleoclimate: Interpretation of the magnetic susceptibility record of Chinese loess-paleosol sequences. *Geology*, **21**, 1011–1014.
- Vincenz, S.A., 1975. Unusually high Curie temperatures of some natural hematites. In: R.M. Fisher, M.D. Fuller, V.A. Schmidt and P.J. Wasilewski (eds) *Proc. Takesi Nagata Conference 1974*, University of Pittsburgh, Goddard Space Flight Center, Greenbelt, MD, 106–111.
- Vinogradova, L.P., Surnatchev, B.A. & Terpigorava, E.A., 1972. How gas in seams affects heating and susceptibility to spontaneous combustion. *Ugol* 1972, No. 9.
- Walker, T.R., Larson, E.E. & Hoblitt, R.P., 1981. Nature and origin of hematite in the Moenkopi Formation (Triassic), Colorado Plateau: A contribution to the origin of magnetism in red beds. *J. Geophys. Res.*, **86**, 317–333.
- Watari, F., Delavignette, P., van Landuyt, J. & Amelinckx, S., 1983. Electron microscopic study of dehydration transformations. Part III: High resolution observation of the reaction process FeOOH to Fe_2O_3 . *J. Solid State Chem.*, **48**, 49–64.
- Watkins, N.D. & Haggerty, S.E., 1967. Primary oxidation variation and petrogenesis in a single lava. *Contrib. Miner. Petrol.*, **15**, 251–271.
- Watson, D.E., 1979. Magnetic properties of clinkers (Abs.). *Geophysics*, **44**, 376–377.
- Waychunas, G.A., 1991. Crystal chemistry of oxides and oxyhydroxides. In: D.H. Lindsley (ed.) *Oxide Minerals Review in Mineralogy* **25**, Min. Soc. Am., Washington D.C., 11–68.
- Weber, H.P. & Hafner, S.S., 1971. Vacancy distribution in nonstoichiometric magnetites. *Z. Kristallogr.*, **133**, 327–340.
- Weidler, P.G. & Stanjek, H., 1998. The effect of dry heating on synthetic 2-line and 6-line ferrihydrite: II. Surface area, porosity and fractal dimension. *Clay Minerals*, **33**, 277–284.
- Weiss, P. & Forrer, R., 1929. Saturation absolue des ferromagnétiques et loi d'approche en fonction d'H et de T. *Annales Phys.*, **12**, 279–324.
- Westcott-Lewis, M.F. & Parry, L.G., 1971. Magnetism in rhombohedral iron-titanium oxides. *Australian J. Phys.*, **24**, 719–734.
- Westmijze, W.K., 1953. Studies on magnetic recording. *Philips Res. Rep.*, **8**, 245–269.
- White, A.F., Peterson, M.L. & Hochella, M.F., 1994. Electrochemistry and dissolution kinetics of magnetite and ilmenite. *Geoch. Cosm. Acta*, Vol. **58**, No. **8**, 1859–1875.
- Williams, H.J., Bozorth, R.M. & Goertz, M., 1953. Mechanism of transition in magnetite at low temperatures. *Phys. Rev.*, **91**, 1107–1115.
- Wilson, R.L., 1961. Paleomagnetism in Northern Ireland, I: The thermal demagnetization of natural magnetic moments in rocks. *Geophys. J. R. astr. Soc.*, **5**, 45–58.
- Wilson, R.L. & Watkins, N.D., 1967. Correlation of petrology and natural magnetic polarity in Columbia Plateau basalts. *Geophys. J. R. astr. Soc.*, **12**, 405–424.
- Wohlfarth, E.P., 1958. Relations between different modes of acquisition of the remanent magnetization of ferromagnetic particles. *J. Appl. Phys.*, **29**, 595–596.
- Wolska, E., 1981. The structure of hydrohematite. *Z. Kristallogr.*, **154**, 69–75.
- Wolska, E. & Baszynski, J., 1986. Pre-reactional transformations in the topotactic conversion $\gamma\text{-FeOOH} \rightarrow \gamma\text{-Fe}_2\text{O}_3$. *Phys. Status Solidi (a)*, **95**, 87–92.
- Wolska, E. & Schwertmann, U., 1989. The vacancy ordering and distribution of aluminium ions in $\gamma\text{-(Fe,Al)}_2\text{O}_3$. *Solid State Ionics*, **32/33**, 214–218.
- Wolska, E. & Schwertmann, U., 1989. Nonstoichiometric structures during dehydroxylation of goethite. *Z. Kristallogr.*, **189**, 223–237.
- Xu, W., Peacor, D.R., Dollase, W.A., van der Voo, R. & Beaubouef, R., 1997. Transformation of titanomagnetite to titanomaghemite: A slow, two-step, oxidation-ordering process in MORB. *Am. Mineral.*, **82**, 1101–1110.
- Yamamoto, N., 1968. The shift of the spin flip temperature of $\alpha\text{-Fe}_2\text{O}_3$ fine particles. *J. Phys. Soc. Japan*, **24**, 23–28.
- Yamazaki, T., 1995. Rock magnetism of Pacific pelagic red clay. *The IRM Quarterly*, Vol. **4**, No. **4**.
- Zdujic, M., Jovalekic, C., Karanovic, Lj., Mitric, M., Poleti, D. & Skala, D., 1998. *Materials Sci. Engineering*, **A245**, 109–117.
- Zhang, Y. & Tang, X., 1994. Coal petrology application for liability of coal to spontaneous combustion. *Coal Geology and Exploration*, **22**, 21–24.

- Zhang, X., Koopmans, B.N. & Wan, Y., 1995. Detection of spontaneous combustion of coal in northern China, using thermal remote sensing data. in: *Proceedings Environmental assessment of Geological hazards*. Space Congress, Bremen, May 24-25, European Space Report, 2-8.
- Zhang, X., van Genderen, J.L. & Kroonenberg, S.B., 1997. A method to evaluate the capability of Landsat-5 TM band 6 data for sub-pixel coal fire detection. *Int. J. Remote Sensing*, **Vol. 18, No. 15**, 3279-3288.
- Zhang, X., 1998. *Coal Fires in Northwest China: Detection, monitoring, and prediction using remote sensing data*. PhD thesis, Technology University of Delft, Delft, The Netherlands, pp. 135.
- Zhang, X., van Genderen, J.L. & Kroonenberg, S.B., 1998. Spatial analysis of thermal anomalies from airborne multi-spectral data. *Int. J. Remote Sensing* (submitted).
- Zhang, X., Kroonenberg, S.B. & de Boer, C.B., 1999. Pleistocene coal fires in Xinjiang, Northwest China. *Submitted to Terra Nova*.
- Zhetbaev, A.K., Donbaev, K.M. & Ablonov, M.B., 1990. *Phys Stat. Solidi*, **B 157**, K55.
- Zhetbaev, A.K., Donbaev, K.M., Ule, M.H. & Mukusheva, M.K., 1992. *Hyp. Int.*, **70**, 893.
- Zoltai, T. & Stout, J.H., 1984. *Mineralogy, Concepts and Principles*. Burgess Publishing Co., Minneapolis, MN., pp. 505.

Samenvatting

Gesteentemagnetisme: een korte introductie

In dit proefschrift komen diverse gesteente- en mineraalmagnetische onderzoeken aan de orde. Daartoe is het nuttig eerst een kort overzicht te geven van het vakgebied gesteentemagnetisme zelf. Gesteentemagnetisme is de geofysische discipline die zich bezig houdt met de magnetische eigenschappen van gesteenten en van in de natuur voorkomende mineralen, alsmede van hun synthetische equivalenten. Deze zogeheten 'magnetische mineralen' onderscheiden zich doordat zij een permanent of remanent magnetisch signaal miljarden jaren kunnen bewaren. Gesteenten, waarin magnetische mineralen in spore-hoeveelheden kunnen voorkomen, zijn dus als het ware de oudste magnetische opname-apparaten ter wereld. De meest voorkomende magnetische mineralen zijn de oxides, de oxyhydroxides en enkele sulfides van ijzer. Gesteentemagnетици onderzoeken hoe de magnetische eigenschappen van deze mineralen afhangen van factoren als korrelgrootte, korrelvorm, kristalliniteit, chemische samenstelling, temperatuur en druk. Tevens bestudeert deze discipline de oorsprong en de karakteristieken van de verschillende soorten remanente magnetisatie die gesteenten en mineralen onder natuurlijke omstandigheden kunnen verwerven. Dit bestudeert men aan de hand van de analyse van natuurlijke monsters, door experimenten uit te voeren in het laboratorium of met behulp van modelmatige computersimulaties. Het soms miljarden jaren oude magnetische signaal dat de magnetische mineralen bevatten kan met behulp van speciale demagnetisatie-technieken in het laboratorium gedecodeerd worden. De natuurlijke 'opname'- en 'afspeel'-condities verschillen echter aanzienlijk van de condities die gangbaar zijn in de magnetische opname-technologie, zoals bijvoorbeeld toegepast in videorecorders en computers. Desalniettemin berusten deze twee disciplines op dezelfde fundamentele fysische wetten zoals ferromagnetisme en het concept van magnetische domeinen. Gesteentemagnetisme is naast een fundamentele ook een toegepaste wetenschappelijke discipline. De studie van de magnetische eigenschappen van gesteenten en mineralen heeft reeds een aanzienlijke bijdrage geleverd aan verschillende aardwetenschappelijke disciplines en nog steeds blijken er mogelijkheden te zijn voor nieuwe toepassingen.

Historisch gezien is gesteentemagnetisme voortgekomen uit twee andere disciplines: de fysica van de vaste stof en paleomagnetisme. Het hoofddoel van paleomagnetisch onderzoek is het verkrijgen van een zo continu en gedetailleerd mogelijke opname van de configuraties van het aardmagneetveld gedurende de geologische geschiedenis met als doel tektonische bewegingen te achterhalen en gesteente-series te correleren en te dateren. Tevens worden de tijdsafhankelijke eigenschappen van het magneetveld gebruikt om een beter begrip te krijgen van de processen die zich in het binnenste van de aarde afspeelen. Gesteentemagnetisme is dus ontwikkeld om het fysische begrip van het magnetische geheugen van gesteenten gedurende geologische tijd te leveren, en om de betrouwbaarheid van de natuurlijke remanente magnetisatie (NRM) aan te tonen.

Het vormt een directe verbinding tussen theoretische aspecten van de fysica van het magnetisme en paleomagnetische toepassingen. Tegenwoordig is het gebruik van gesteente- en mineraalmagnetische meettechnieken niet langer beperkt tot paleomagnetisme alleen, maar worden de technieken toegepast in een grote variëteit aan (aard)wetenschappelijke disciplines. De studie van de magnetische eigenschappen van gesteenten en mineralen speelt nu een belangrijke rol in het vergroten van ons begrip van geologische, geofysische, geochemische en klimatologische processen, vooral wanneer ze gecombineerd worden met andere multidisciplinaire informatie.

Dit proefschrift

De onderzoekingen beschreven in dit proefschrift zijn onderverdeeld in drie hoofddelen. *Deel I* en *II* bevatten fundamenteel onderzoek naar de gesteente- en mineraalmagnetische eigenschappen van respectievelijk hematiet (α - Fe_2O_3) en maghemiet (γ - Fe_2O_3). Het doel van deze studies was het opstellen van diagnostische magnetische parameters voor α - Fe_2O_3 en γ - Fe_2O_3 en het verkrijgen van meer inzicht in de oorzaken van hun variabiliteit. Hematiet en maghemiet zijn na magnetiet (Fe_3O_4) de meest voorkomende magnetische mineralen in een grote variëteit aan sedimentaire gesteenten en bodems. Sedimenten worden steeds vaker gebruikt voor paleomagnetisch onderzoek vanwege hun continue karakter en hun wereldwijde verspreiding. Tevens is er in de regel een goede tijdscontrole door hun fossielinhoud en/of ingeschakelde vulkanische aslagen. Bovendien is de gesteentemagnetische waarde van sedimenten enorm toegenomen vanwege de wereldwijde inspanningen om paleoklimatologische informatie uit sedimenten te verkrijgen. Gesteentemagnetische gegevens blijken steeds vaker van nut bij de interpretatie van deze zogeheten geologische 'proxy records'. De variatie in type, hoeveelheid en korrelgrootte van de magnetische mineralen in een opeenvolging van sedimentaire lagen is namelijk vaak gerelateerd aan klimatologische veranderingen in het brongebied. Tevens worden gesteentemagnetische technieken met steeds meer succes gebruikt om diagenetische processen in sedimenten te traceren en beter te leren begrijpen. Ondanks het onderkende belang van beide magnetische mineralen voor paleomagnetische interpretaties en andere aardwetenschappelijke disciplines is ons begrip van hun magnetische eigenschappen nog verre van compleet.

Deel III omvat gesteentemagnetisch onderzoek aan verbrandings-metamorfe gesteenten. Deze opmerkelijke gesteenten zijn gerelateerd aan ondergrondse steenkoolbranden. De oorspronkelijke sedimenten zijn geheel gemetamorfiseerd door de enorme hitte die vrijkomt bij de spontane ontbranding van nabije steenkoollagen. De magnetische eigenschappen van deze gemetamorfiseerde gesteenten zijn gebruikt om de evolutie van de uitgebreide ondergrondse steenkoolbranden in een gedeelte van China te ontrafelen. Tevens worden andere potentiële toepassingen van de magnetische eigenschappen van de verbrandings-metamorfe gesteenten bediscussieerd.

Deel I: Hematiet

Hoofdstuk 1 bevat een uitgebreid literatuuroverzicht van de huidige kennis van de magnetische eigenschappen van hematiet en hun relatie ten opzichte van variaties in temperatuur, magnetische veldsterkte, druk, korrelgrootte en chemische samenstelling. Het overzicht bouwt voort op eerdere overzichten uit de jaren 70 en 80 (*Fuller 1970; O'Reilly 1984*), en is aangevuld met gedetailleerde informatie over relevante chemische en fysische eigenschappen noodzakelijk voor een goed begrip van de zeer complexe magnetische eigenschappen van hematiet. Het overzicht benadrukt de buitengewoon grote invloed van roosterdefecten op de magnetische eigenschappen van hematiet in vergelijking tot hun invloed bij veel sterker magnetische mineralen zoals magnetiet en maghemiet. Tevens wordt beargumenteerd dat waargenomen veranderingen in de magnetische eigenschappen binnen een gesynthetiseerde hematietreeks vaak abusievelijk zijn toegeschreven aan de variatie van één enkele parameter. In het algemeen, echter, vertonen parameters als korrelgrootte, mate van isomorfe vervanging, interne stress, alsmede de hoeveelheid en het type defecten enige relatie met elkaar. Het is daarom niet correct om alle waargenomen variatie trachten terug te voeren op één enkele oorzaak.

In **Hoofdstuk 2** wordt het thermomagnetische gedrag van hematiet en goethiet (α -FeOOH) beschreven als functie van korrelgrootte in verschillende niet-verzadigende magnetische velden. Deze studie heeft de interpretatieve waarde van thermomagnetische analyses van niet-verzadigde magnetische mineralen aanzienlijk verhoogd. De temperatuursafhankelijkheid van het magnetisch moment van niet-verzadigde mineralen blijkt afhankelijk te zijn van het samenspel tussen de temperatuursvariatie van de 'exchange'-energie en die van de coërciviteitskracht, beide met betrekking tot het aangelegde magnetische veld. Het is aangetoond dat het herdispargeren van het monster in de monsterhouder tussen opeenvolgende thermomagnetische metingen een goed middel is om onderscheid te kunnen maken tussen chemische of structurele veranderingen die niet-omkeerbaar zijn, en magnetische veranderingen waarbij na herdispersie de uitgangssituatie wel opnieuw verkregen wordt. Verder was het mogelijk om verschillende typen hematiet te onderscheiden, gebaseerd op hun specifieke thermomagnetische gedrag. De zogeheten 'defect-arme' types waarvan het magnetische moment veroorzaakt wordt doordat de twee magnetische subroosters niet volledig antiparallel zijn, vertonen een langzaam oplopende initiële magnetisatie tijdens het opwarmen en een karakteristieke irreversibele blokvormige afkoelcurve. De zogeheten 'defect-rijke types' waarvan de magnetische eigenschappen mede bepaald worden door een extra magnetisch moment veroorzaakt door een onbalans tussen de magnetische subroosters, vertonen daarentegen een langzaam dalende initiële magnetisatie tijdens het opwarmen. De afkoelcurve krijgt pas de karakteristieke blokvorm nadat het merendeel van de roosterdefecten uit het mineraal is gediffundeerd.

In **Hoofdstuk 3** is het onderzoek naar het lage-temperatuur gedrag van verschillende types hematiet beschreven. We hebben aangetoond dat de lage-veld susceptibiliteit en de magnetisatie geïnduceerd in niet-verzadigende magnetische velden van grofkorrelige hematiet ($>1\mu\text{m}$) verhoogd kan worden door middel van een thermische cyclus door de Morin transitie. Deze observaties zijn geïnterpreteerd in termen van transdomeine overgangen (de toename van het aantal magnetische domeinen in eenzelfde mineraalkorrel als functie van de magnetische geschiedenis). Deze worden mogelijk gemaakt door de lage magnetische anisotropie gedurende het temperatuursinterval van de Morin transitie. Op deze manier kan dus de magnetische toestand van grote metastabiele 'single domain' en 'pseudo-single-domain' deeltjes worden veranderd. Onze bevindingen kunnen serieuze implicaties hebben voor paleomagnetische resultaten verkregen uit hematiet-rijke sedimenten, vooral wanneer de dominante remanentie door relatief pure zogeheten speculariet deeltjes wordt gedragen. Het temperatuurtraject van de Morin transitie ($\sim -10^\circ\text{C}$) van zulke deeltjes ligt namelijk binnen het bereik van temperaturen aan het aardoppervlak.

In **Hoofdstuk 4** wordt een nieuwe, sterk magnetische fase met een Curie punt van $470\text{--}475^\circ\text{C}$ beschreven. Gedurende verhitting in lucht tot tenminste 400°C , vormt deze fase dunne epitaxische vergroeiingen op de basale (001) vlakken van bepaalde hematiet types zonder isomorfe substitutie. De nieuwe fase heeft een kubische spinelstructuur met een lengte voor de eenheidscel gelijk aan die van maghemiet. De voorgestelde structuur is gelijk aan die van pure maghemiet, maar nu met een deel van de lege roosterplaatsen op tetraëdrische holten in plaats van de gebruikelijke verdeling van de lege roosterplaatsen over alleen de octaëdrische holten. Het thermisch geactiveerde verlies van structureel gebonden water in hematiet zou tot de vorming van deze nieuwe fase geleid hebben waarbij het noodzakelijk is dat de hexagonale dichtste bolstapeling van hematiet lokaal overgaat in een kubische dichtste bolstapeling, karakteristiek voor maghemiet.

Deel II: Maghemiet

Hoofdstuk 5 geeft een synopsis van de huidige kennis van de magnetische eigenschappen van maghemiet, aangevuld met relevante chemische en fysisch-kristallografische data. Tevens wordt een overzicht gegeven van de belangrijkste omstandigheden waaronder maghemiet geologisch voorkomt en van de algemene vormingsprocessen onder deze omstandigheden. Tot nu toe was er geen uitgebreid overzicht in de literatuur voorhanden waarin de magnetische eigenschappen van maghemiet zijn gerelateerd aan de herkomst en manier van vorming. Het blijkt dat wat met 'maghemiet' wordt aangeduid eigenlijk meerdere verschillende fases zijn, gekarakteriseerd door een verschillende verdeling van de lege roosterplaatsen over de octaëdrische en tetraëdrische holtes in het spinelrooster. De precieze invloed van deze verschillende rangschikkingen van lege roosterplaatsen op de magnetische eigenschappen is nog niet geheel duidelijk.

De korrelgrootte-afhankelijkheid van de gesteentemagnetische eigenschappen van een natuurlijke maghemiet vormt het onderwerp van **Hoofdstuk 6**. Ze blijkt minder prominent te zijn dan die van magnetiet van gelijke korrelgrootte. De maghemiet overleeft gedeeltelijk verhitting tot 700°C zodat een directe bepaling van de Curie temperatuur van 610°C mogelijk was. Substitutie van aluminium voor ijzer heeft de maghemietstructuur waarschijnlijk gestabiliseerd. De mate van transformatie van maghemiet naar hematiet tijdens een thermomagnetische cyclus blijkt tevens korrelgrootte-afhankelijk te zijn, een sterke aanwijzing dat deze kinetisch is bepaald. Verder vormt mogelijk het waargenomen lage-temperatuur gedrag van de zogeheten anhysteretische remanente magnetisatie een diagnostische eigenschap voor de aanwezigheid van maghemiet.

Deel III: Verbrandings-metamorfe gesteenten

In 1997 raakte het Paleomagnetisch Laboratorium 'Fort Hoofddijk' betrokken bij het onderzoek naar de omvangrijke ondergrondse steenkoolbranden in China. De grote hoeveelheden steenkool die verloren gaan door spontane ontbranding resulteren niet alleen in een aanzienlijke economische schadepost maar hebben ook een kwalijke invloed op het milieu. Naast inzakkingen van het aardoppervlak, het optreden van aardverschuivingen en de vernietiging van de vegetatie hebben de steenkoolbranden de uitstoot van rook en schadelijke gassen tot gevolg. Steenkoolbranden van deze omvang hebben naast een nationale echter ook een mondiale dimensie. Het is bepaald dat de koolbranden in Noord-China maar liefst 2 tot 3 procent van de totale CO₂ emissie op aarde als gevolg van de verbranding van fossiele brandstoffen zouden produceren en dus een significante invloed op het broeikas effect zouden hebben. **Hoofdstuk 7** schetst de omvang van het steenkoolbranden probleem in China en geeft een overzicht van de mogelijke oorzaken van de spontane ontbranding. Tevens passeren de verschillende verspreidingsmodellen voor ondergrondse koolbranden de revue.

De hoogste schattingen van het jaarlijkse verlies aan steenkool en de CO₂ uitstoot zijn in essentie gebaseerd op het karteren van verbrandings-metamorfe gesteenten met behulp van remote sensing technieken waarbij met behulp van dagzoomconstructies het ondergrondse verloop is gereconstrueerd gebruikmakende van de helling en de dikte van de koollagen. Gecombineerde stratigrafische en paleomagnetische resultaten, besproken in **Hoofdstuk 8**, laten zien dat de eerder genoemde schattingen sterk overdreven zijn, omdat meer dan 85% van de verbrandings-metamorfe gesteentes in een onderzoeksgebied gevormd blijken te zijn tijdens verschillende perioden gedurende het Pleistoceen. De totale CO₂-uitstoot heeft dus plaatsgevonden over een lange tijd. De spontane ontbranding van koollagen blijkt gerelateerd aan het voorkomen van gunstig gelegen dagzomen gevormd door deformatie en opheffing van het gebied met de daarmee gepaard gaande insnijding door rivieren. Klimaatsveranderingen hebben geresulteerd in een cyclisch patroon van opeenvolgende afzetting van rivierterrassen en insnijdingen.

Hoofdstuk 9 richt zich op de specifieke magnetische eigenschappen van de verbrandings-metamorfe gesteenten. Het aardmagneetveld blijkt uitstekend geregistreerd te worden in dit type gesteente; derhalve zijn er mogelijkheden voor de studie van de paleointensiteit en paleoseculaire variatie. Behalve de meer gangbare ijzeroxides zijn ook sporen van metallisch ijzer aangetoond. Dit geeft aan dat de omstandigheden gedurende de verbranding kunnen variëren tussen sterk reducerend en sterk oxiderend. Verder blijken de thermisch veranderde gesteenten aanzienlijk magnetischer in vergelijking tot hun sedimentaire voorgangers. Modelleren van magnetische anomalieën veroorzaakt door de verbrandings-metamorfe gesteenten kan dan ook mogelijk aangewend worden voor exploratie van steenkool en zeker voor het afbakenen van de uitgebreidheid en diepte van (uitgedoofde) steenkoolbranden. Deze informatie kan weer worden gebruikt om schattingen van de CO₂ uitstoot te verbeteren en om de evolutie en het mechanisme van steenkoolbranden beter te begrijpen.

Dankwoord

Nu mijn interessante ontdekkingsstocht naar de ‘verborgen aantrekkingskracht’ van gesteenten en mineralen beëindigd is, wil ik van de gelegenheid gebruik maken om iedereen te bedanken die heeft geholpen bij het tot stand komen van dit proefschrift.

Mijn co-promotor Mark Dekkers en de technicus Tom Mullender zijn door hun wetenschappelijke en technische ondersteuning van groot belang geweest tijdens mijn onderzoek. Beiden hebben mij wegwijs gemaakt in de wereld van het gesteentemagnetisme. Ik denk met veel plezier terug aan onze gezamenlijke discussies en inspanningen om één van ’s werelds meest opzienbarende fenomenen te begrijpen. Mark ben ik verder zeer erkentelijk voor de gegeven vrijheid bij het uitvoeren van het onderzoek en de constructieve opmerkingen en waardevolle aanvullingen op dit proefschrift. Tom wil ik speciaal bedanken voor zijn inventieve hulp bij de meest uiteenlopende technische en elektronische problemen.

Mijn promotor Cor Langereis ben ik dank verschuldigd voor het verzorgen van de uitstekende computerfaciliteiten op ‘Fort Hoofddijk’. Zijn visie, dat elke promovendus zijn eigen computer moet hebben, heeft mij veel kostbare tijd opgeleverd. Ook de gestage uitbreiding van het arsenaal aan gesteentemagnetische analyse-apparatuur onder zijn en Marks leiding heeft de kwaliteit en diversiteit van mijn onderzoek positief beïnvloed.

My co-authors, Xiangmin Zhang and Salomon Kroonenberg, are indebted for involving me in China’s coal fire problem and for providing the various combustion-metamorphic rocks.

I enjoyed the co-operation with my foreign colleague and co-author, Eduard Petrovský. He is thanked for helpful discussions about hematite and for providing the Kadaň hematite sample.

Veel plezier heb ik beleefd aan de samenwerking met mijn collega’s op het ‘Fort Hoofddijk’. In het bijzonder bedank ik mijn goede vriend Wout Krijgsman. Door mij na mijn diensttijd op de promotieplaats te attenderen kreeg onze plezierige relatie als studie- en huisgenoot een onverwachte verlenging. Zijn gevoel voor humor en positieve levensinstelling zijn in vele opzichten een stimulans geweest. Ton van Hoof wil ik bedanken voor zijn enthousiasme en het geduldig uitleggen van de vele computerprogramma’s. Adry van Velzen bedank ik voor de waardevolle discussies en zijn hulp met de lage-temperatuur metingen op de MicroMag. Nicole van Vugt ben ik dan verschuldigd voor haar hulp bij de opmaak van enkele figuren. Mijn kamergenoten van de laatste jaren: Jaume Dinarés, Ingeborg van Oorschot, Hilde Passier en Michael Urbat bedank ik voor de gezellige werksfeer. Willy van BEEK bedank ik voor de secretariële ondersteuning en het kopiëren van de ontelbare wetenschappelijke artikelen. Henk Meijer wordt bedankt voor het zetten van enorme aantallen straffe bakjes koffie die

mij 's middags op de been hielden. Tevens bedank ik hem voor zijn relativiserende kijk op de wetenschap en het opluisteren van saaie meetsessies met zijn opmerkelijke kijk op de wereld en met passionele verhalen over malt whiskey, motorsport en vrouwen. Piet-Jan Verplak wil ik bedanken voor zijn vriendschap en voor het mogen genieten van zijn culinaire hoogstandjes. Verder bedank ik naast de eerder genoemde collega's de andere leden van het hechte Fort-team: Charon Duermeijer, Teresa Juárez, Yvo Kok, Pauline Kruiver, Thomas Pick, Hans Wensink en Tanja Zegers. Gesteentemagneticus en voormalig Fort-medewerker, Pieter Vlag, bedank ik voor de gezellige tijd tijdens verschillende congressen en voor de fijne samenwerking die resulteerde in een gezamenlijk artikel.

Mijn goede vrienden en paranimfen, Bastiaan van der List en Hendrik-Jan Visser, wil ik bedanken voor hun getoonde interesse in mij en mijn werk en voor de vele gezellige en mooie momenten die ik met hen beleefd heb.

Dit proefschrift is opgedragen aan de vier meest belangrijke personen in mijn leven: mijn ouders, mijn zus Anneke Tea en mijn vriendin Janny van Zutphen. *'Happiness is hard to come by in this life, but you giving me more than my share.'* Mijn ouders wil ik bedanken voor hun stimulerende vertrouwen in mij en voor de mogelijkheden die ze mij hebben geboden in mijn leven. De onvoorwaardelijke liefde, de morele steun en het getoonde begrip van Janny waren van onschatbare waarde, vooral tijdens de moeilijke perioden die elke promotie kent. Tevens wil ik haar bedanken voor het geloof dat zij altijd in mij heeft gehad, juist wanneer ik dat zelf dreigde te verliezen. Verder kan ik mij niet aan de indruk onttrekken dat mijn beschermengeltje, Anneke, mij meer dan eens op het juiste spoor naar de oplossing van een probleem heeft gezet.

*Cor,
augustus 1999*

Curriculum vitae

Cor de Boer werd geboren op 18 november 1966 te Leeuwarden. In mei 1985 behaalde hij het diploma ongedeeld VWO aan het Lienward College te Leeuwarden. In datzelfde jaar begon hij met een studie Geologie aan de Universiteit van Utrecht. In augustus 1991 rondde hij deze studie af met als hoofdvak Exogene Geochemie en als keuzevakken Milieukunde en Milieugeochemie. Zijn afstudeeronderzoek verrichtte hij in opdracht van de KEMA (Arnhem) en had als onderwerp de uitloogbaarheid van zware metalen uit vliegias. In de jaren 1992 en 1993 vervulde hij zijn dienstplicht in het Nederlandse leger. In november 1993 trad hij als assistent in opleiding (AIO) in dienst bij de vakgroep Geofysica van de faculteit voor Aardwetenschappen te Utrecht. Het promotie onderzoek werd uitgevoerd op het Paleomagnetisch Laboratorium 'Fort Hoofddijk' onder begeleiding van Dr. Mark Dekkers.

Notes

The magnetic force is animate, or imitates a soul; in many respects it surpasses the human soul while it is united to an organic body.

(William Gilbert, *De Magnete*)

The nation that controls magnetism controls the universe

(Dick Tracey)

*All animals feel Wonder, and many exhibit Curiosity.
They sometimes suffer from this latter quality*

(Charles Darwin, *The Descent of Man*)